IMPERIAL COLLEGE OF SCIENCE, TECHNOLOGY & MEDICINE

University of London

PREDICTION OF TURBOMACHINERY AEROELASTICITY EFFECTS USING A 3D NON-LINEAR INTEGRATED METHOD

by

J.G.Marshall

A thesis submitted to the University of London
for the degree of Doctor of Philosophy

Centre of Vibration Engineering
Department of Mechanical Engineering
Imperial College of Science, Technology & Medicine
Exhibition Road, London SW7 2BX

April 1996

For my wife, my father, and my grandfather.

Acknowledgements

I would like to express my deepest appreciation to Dr. Mehmet Imregun for his supervision and guidance in all matters, but especially those relating to this thesis. I would like to thank Professor D.J. Ewins and all the staff of the Dynamics section for many enjoyable years. I would also like to thank my colleagues, especially Dr. A.S. Nobari, Dr. R. Mostofi, Mr. H. Yiu and Miss M.L.M. Duarte for many useful discussions.

I would like to thank the Engineering and Physical Science Research Council (EPSRC) and Rolls-Royce plc. for jointly funding this work through an Industrial Studentship. I would also like to thank those at Rolls-Royce who have helped me, particularly Dr. P. Stow for many helpful discussions and much guidance, and also Dr. A. Suddhoo, the late Dr. A. Cargill, and Dr. J. Chew for their invaluable contributions.

I would especially like to thank Dr. M. Vahdati for the use of the UV2D code and many fruitful late-night discussions, and Dr. L. He for providing the VIB3D code.

Finally, I would like to thank my brother, Robert, for putting up with me for four years, and my wife, Jane, for many sacrifices in order that this work may be completed.

ABSTRACT

Turbomachinery blade vibration caused by the aeroelastic phenomena of flutter and forced response resonance are limiting factors in the design of modern, high-performance gas turbines. There are few established prediction methods, and problems in rigs and engines are often brought to light only at the testing stage, leading to setbacks and increased development costs. With the trend towards lighter, more highly loaded designs, these problems are set to continue unless reliable prediction methods can be developed: such is the aim of this thesis.

The method presented in this work involves solving the governing equations of fluid and structural motion alternately in the time-domain, with information being passed as a boundary condition between the two domains at each time step. This method is general in that any combinations of fluid- and structural-dynamic time-domain solvers may be implemented, depending of the requirements of the case. Here, two computational fluid dynamic codes have been used: the first is an inviscid Euler solver in 2D, using a totally unstructured grid methodology. The second employs a structured grid methodology solving the 3D thin-layer Reynolds-averaged Navier-Stokes equations using cell-vertex finite volume scheme with 4-stage Runge-Kutta time-marching. This explicit method is accelerated by the use of a time-consistent two grid method. The structural model, used in both cases, is formulated via the assumed modes method, with the modeshapes having been determined from a previous finite element calculation, including the effects such as temperature and rotation. The aeroelastic equation of motion is formulated in the modal domain, and advanced in time using the Newmark-β scheme.

These models are first applied to the case of transonic wing flutter in 2- and 3D, which is a well known non-linear problem. The results are compared to each other, and to the work of previous researchers. The rest of the case studies relate to 3D transonic compressor blade aeroelasticity. The steady flow and static aeroelastic effects are dealt with first, and the results are compared to classical methods, and experimental data, where available. Finally the flutter analysis of a whole turbomachinery rotor is attempted, and the advantages of the new method are demonstrated.

TABLE OF CONTENTS

Section	Title	Page
Chapter 1	**Introduction**	1
1.0	About this Chapter	1
1.1	Problem Definition	2
1.1.1	Static Aeroelasticity	4
1.1.2	Dynamic Aeroelasticity	4
1.1.3	Forced Response	6
1.1.4	Acoustic Resonance	6
1.1.5	Rotating Stall	7
1.1.6	Particular Problems of Interest	7
1.2	Research Objectives	12
1.3	Scope of this Thesis	14
1.4	Preview of the Thesis	15
Chapter 2	**A Review of the Literature**	17
2.0	About this Chapter	17
2.1	Introduction	18
2.2	Computational Methods for Unsteady Flows	19
2.2.1	Classical Methods	21
2.2.2	Linearised Potential and Euler Methods	22
2.2.3	Non-Linear Potential and Euler Methods	23
2.2.4	Reynolds Averaged Navier-Stokes Methods	23
2.3	Numerical Structural Dynamics Methods	24
2.3.1	Equations of Motion	25
2.3.2	Models	25
2.3.3	Methods of Solution	27
2.4	Aeroelasticity Methods	30
2.4.1	Classical Methods	30
2.4.2	Integrated Aerelasticity Methods	34
2.4.2.1	Partially-Integrated Methods	35
2.4.2.2	Fully-Integrated Methods	38
2.4.3	Methods for Forced Response Prediction	39
2.5	Experimental Data	39
2.6	Critical Review of the State-of-the-Art	41
Chapter 3	**Mathematical Formulation**	44
3.0	About this Chapter	44
3.1	Introduction	45
3.2	Aeroelastic Equations of Motion for the Structure	45
3.2.1	Arbitrary Geometry	45
3.2.2	Properties of the Equations of Motion	47
3.2.3	Formulation for 3D Engineering Structures	49
3.2.4	Formulation for 2D Sections	51
3.3	Unsteady Aerodynamic Analysis	52
3.3.1	Navier-Stokes Equations	52

3.3.2	Methods of Solution	58
3.3.3	Boundary Conditions	61
3.4	Numerical Solutions for Aeroelasticity	63
3.4.1	Time-Marching Solution of Global Equations	63
3.4.2	Local Assembly Time-Marching Solution	63
3.4.3	Time Integration Methods	64
3.5	Numerical Issues and Implementation	69
Chapter 4	**Aeroelasticity Analysis of 2D Aerofoils**	74
4.0	About this Chapter	74
4.1	Introduction	75
4.2	Formulation	76
4.2.1	Structural Models	76
4.2.2	Fluid Model	80
4.2.3	PI Aeroelastic Method	83
4.3	Case Study - NACA006 Aerofoil	83
4.3.1	Steady Flow	84
4.3.2	Fluid Mesh Kinematics	84
4.3.3	Uncoupled Unsteady Calculations	84
4.3.4	Aeroelastic Calculations	85
4.4	Conclusions	89
Chapter 5	**Aeroelasticity Analysis of 3D Wings**	99
5.0	About this Chapter	99
5.1	Introduction	100
5.2	Formulation	100
5.2.1	Structural Model	100
5.2.2	Inviscid Fluid Modelling	101
5.2.3	Partially-Integrated Method of Solution	103
5.3	Case Study - NACA006 Wing	104
5.4	Conclusion	109
Chapter 6	**An Example of Static Aeroelasticity: 3D Blade Untwist**	115
6.0	About this Chapter	115
6.1	Introduction	116
6.1.1	Iterative Approach	116
6.1.2	Direct Approach	118
6.2	Formulation	119
6.2.1	Structural Model	119
6.2.2	Aerodynamic Model	119
6.3	Case Study - Transonic Fan Untwist	122
6.3.1	Static Non-Linear Predictions (100% Speed)	123
6.3.2	FE Solution	124
6.3.3	Interpolation onto the Aerodynamic Mesh	125
6.3.4	Steady Flow Results	125
6.3.5	Untwist Results	129
6.3.6	Effect of the Number of Structural Modes	133
6.4	Conclusions	134

Chapter 7	**3D Blade Flutter**	151
7.0	About this Chapter	151
7.1	Introduction	152
7.2	Formulation	152
7.2.1	Energy Analysis of Flutter	153
7.2.2	Inter-Blade Phase Angle Considerations	154
7.3	Case Study - NASA Rotor 67 Fanblade	156
7.3.1	Steady Flow	156
7.3.2	Static Aeroelasticity Calculations	158
7.3.3	Dynamic Aeroelasticity Calculations	159
7.3.4	Results	161
7.4	Conclusions	164
Chapter 8	**3D Bladed Assembly Flutter**	180
8.0	About this Chapter	180
8.1	Introduction	181
8.2	Aeroelastic Model	181
8.3	Case Study - Transonic Fanblade Flutter	183
8.3.1	Structural Model	184
8.3.2	Interpolation onto the Aerodynamic Mesh	185
8.3.3	Steady Flow Results	186
8.3.4	Single Blade Passage Uncoupled Flutter Analysis	186
8.3.5	Single Blade Passage Coupled Flutter Analysis	188
8.3.6	Multiple Blade Passage Coupled Flutter Analysis	190
8.4	Concluding Remarks	191
8.4.1	Flutter Prediction Methods	192
8.4.2	Flutter Behaviour of this Fan Blade	193
Chapter 9	**Conclusions & Recommendations**	206
9.0	About this Chapter	206
9.1	Integrated Aeroelastic Coupling	207
9.2	Importance of Non-linearities	208
9.3	Multiple Passages for Handling the IBPA	210
9.4	An Inviscid Mechanism for Flutter?	211
9.5	Overall Recommendations for Flutter Prediction	212
9.6	Future Directions	213
9.6.1	Improved Structural Model	213
9.6.2	Mistuning	214
9.6.3	Aerodynamic Features	215
9.6.4	Forced Response	215
9.6.5	Acoustic Interactions	216
9.7	Recommendations for Further Research	216
References		218

Figures	Caption	Page
1.1	Possible Modes of Compressor Flutter	9
1.2	Campbell Diagram for a Typical Rotor Blade	11
2.1	Breakdown of Aeroelasticity Prediction Methodologies	43
4.1	2D 2-DOF Standard Aerofoil Section	76
4.2	Unstructured Fluid Mesh	91
4.3	Steady Flow Pressure Coefficients	91
4.4	Steady Flow Mach Number Contours	91
4.5	Fluid Mesh Motion Detail	91
4.6(a&b)	Uncoupled Pitch Motion Time Histories	92
4.6(c&d)	Uncoupled Pitch/Plunge Motion Time Histories	93
4.7(a&b)	Uncoupled Motion Phase Plane	94
4.8	Unsteady Flow Mach Number Snapshot	95
4.9(a&b)	Flutter Time History (M=0.87)	96
4.10	Flutter Time History (M=0.92)	97
4.11	Flutter Time History -Effect of Starting Conditions	97
4.12	Bifurcation Diagram	98
4.13	Flutter Boundary	98
5.1(a-c)	FE Vibration Modeshapes	110
5.2	Aerodynamic Mesh	111
5.3	Steady Flow Pressure Coefficients	111
5.4	Steady Flow Mach Number Contours	111
5.5	Fluid Mesh Motion Detail	111
5.6(a-c)	Flutter Time History (M=0.80)	112
5.7	Flutter Time History (M=0.87)	113
5.8	Flutter Time History (M=0.92)	113
5.9	Effect of Starting Conditions	114
5.10	Bifurcation Diagram	114
6.1	FE Mesh	136
6.2	CF Displacements (High Speed)	136
6.3	Mode 1 (1st Flap) Contours (High Speed)	136
6.4	Mode 3 (1st Torsion) Contours (High Speed)	136
6.5	Aerodynamic Surface Mesh	137
6.6	Interpolated CF Displacements	137
6.7	Interpolated Mode 1	137
6.8	Interpolated Mode 3	137
6.9(a&b)	Pressure Surface Pressure Contours	138
6.10(a&b)	Suction Surface Pressure Contours	138
6.11(a-d)	Blade to Blade Mach Number Contours	139
6.12	Blade Surface Static Pressure (70% Height)	140
6.13(a&b)	Mass-Averaged Radial Profiles (High Speed)	140
6.14(a-d)	Suction Surface Pressure Contours (Low Speed)	141
6.15(a-d)	Blade to Blade Mach Number Contours (70% Height)	142
6.16	Blade Surface Static Pressure (70% Height)	143

6.17	Cumulative Blade Loading along Chord	143
6.18	Mass-Averaged Radial Profiles (Low Speed, NS)	144
6.19(a&b)	Untwist Time History (High Speed)	145
6.20(a&b)	Effect of Structural Damping on Untwist	146
6.21	Blade Tip Location before & after Untwist (High Speed)	147
6.22	Gas Untwist Displacement Contours (High Speed)	147
6.23	Untwist Time History (Low Speed)	148
6.24	Blade Tip Location for 3 Flow Conditions (Low Speed)	148
6.25(a&b)	Time History of Modal Quantities (Low Speed)	149
6.26(a&b)	Performance Characteristics (Low Speed)	150
7.1(a-c)	FE Mesh and Vibration Modeshapes 1 & 3	167
7.2a	Meridional Aerodynamic Mesh	168
7.2b	Blade-toBlade Aerodynamic Mesh (70% Height)	168
7.3(a&b)	Mach Number Contours near PE (70% Height)	169
7.4(a&b)	Mach Number Contours near stall (70% Height)	169
7.5(a-d)	Circumferentially Averaged Radial Profiles (PE)	170
7.6(a-d)	Circumferentially Averaged Radial Profiles (NS)	170
7.7	Untwist Modal Displacement Time History (PE)	171
7.8(a)	Untwist Modal Displacement Time History (NS)	171
7.8(b)	Untwist Real Displacement Time History (NS)	172
7.9	Untwist Tip Stagger Tip History	172
7.10(a&b)	Blade Static Pressure Profile (70% Height)	173
7.11(a&b)	Coupled Flutter Time History (Mode 3)	174
7.12	Uncoupled Flutter Phase Plane (0° & 180° IBPA)	175
7.13	Uncoupled Flutter Energy Time History (0° & 180° IBPA)	175
7.14	Uncoupled Flutter Phase Plane (90° IBPA)	175
7.15	Uncoupled Flutter Energy Time History (90° IBPA)	175
7.16(a&b)	Coupled Flutter Time History (Mode 1, 0° IBPA)	176
7.17(a&b)	Coupled Flutter Time History (Mode 1, 180° IBPA)	177
7.18(a&b)	Coupled Flutter Time History (Mode 1, 90° IBPA)	178
7.19	Stability (logdec) against IBPA (PE)	179
7.20	Stability (logdec) against IBPA (NS)	179
7.21	Frequency Shift against IBPA (PE)	179
7.22	Frequency Shift against IBPA (PE)	179
8.1	FE Cyclic Symmetry Model Mesh	194
8.2(a&b)	Fan Performance Characteristics (80% Speed, new points)	195
8.3(a-d)	Blade-to-blade Mach Number Contours (Points A, B & C)	196
8.4(a&b)	Surface Static Pressure (70% Height)	197
8.5	Flutter Stability (logdec), Points '1', '0' & '2'	198
8.6	Flutter Frequency Shift, Points '1', '0' & '2'	198
8.7(a&b)	Flutter Time History (80% Speed, 0 IBPA, Point '0')	199
8.8	Flutter Stability (logdec) - along 80% Speed Characteristic	200
8.9	Flutter Frequency Shift - along 80% Speed Characteristic	200
8.10	Flutter Time History - 5 modes, 80% Speed, 0 IBPA	201
8.11	AV3D Multiple Blade Passage Aerodynamic Mesh	201
8.12(a&b)	Multi-passage Flutter Time History - Points 'A' & 'B'	202

8.12(c)	Multi-passage Flutter Time History - Point 'C'	203
8.13	Multi-passage Flutter Energy History - Point 'A'	203
8.14(a-d)	Multi-passage Flutter Displacement History - Point 'B'	204
8.15	Flutter Stability (logdec) Points 'B' & 'C'	205
8.16	Flutter Frequency Shift Points 'B' & 'C'	205

Tables	**Caption**	**Page**
4.1	Non-Dimensional Variables	83
4.2	Uncoupled Unsteady Calculations	85
4.3	Aeroelastic Calculations	87
4.4	Parameter Variation Cases	88
5.1	Finite Element Modes	105
5.2	Reduced Speeds	106
5.3	Change in Reduced Speeds for New Frequencies	107
5.4	Aeroelastic Calculations	107
6.1	FE Calculated Natural Frequencies (80 & 100% Speeds)	124
6.2	Performance After Untwist along 80% Speed Characteristic	127
6.3	Tip Untwist Displacements and Angles (100%, Design)	130
6.4	Tip Untwist Displacements and Angles (80% Speed)	132
6.5	Tip Gas Untwist Displacements (80% Speed)	132
6.6	Blade Untwist - Effect of Number of Modes	133
6.7	Contribution of Each Mode to Blade Untwist	134
7.1	Relationship between Nodal Diameters, IBPA & Passages	155
7.2	FE Modeshapes	156
7.3	Results from the 3 Analysis Methods near PE	162
7.4	Results from the 3 Analysis Methods near stall	162
8.1	FE Sector Model Natural Frequencies	185
8.2	Performance Along 80% Speed Characteristic	186
8.3	Uncoupled Flutter Stability, 80% Speed Point '1'	187
8.4	Uncoupled Flutter Stability, 80% Speed Point '0'	187
8.5	Uncoupled Flutter Stability, 80% Speed Point '2'	187
8.6	Coupled Flutter Stability, 80% Speed IBPA = 0°	188

NOMENCLATURE

Latin

a	velocity of sound
a_h	elastic axis (EA) location (non-dimensionalised by b)
A	surface area
b	semi-chord
c	chord
C_L	section lift coefficient
C_M	section moment coefficient
C_p	pressure coefficient
c_h	translational viscous damping of section
c_α	torsional viscous damping of section
c_r	modal (proportional) damping
c_p	gas specific heat coefficient at constant pressure
c_v	gas specific heat coefficient at constant volume
$\mathbf{C}$	damping matrix
$\mathbf{D}$	fluid numerical damping terms
E	fluid total energy
E_{tot}	total structural energy
E_k	structural kinetic energy
E_p	structural potential energy
E_d	structural damping energy
$\mathcal{E}$	Young's modulus
f	frequency (Hz)
$\mathbf{f}$	body force vector (components $f_x f_y f_z$)
F	generalised force
$\mathbf{F,G,H}$	fluid flux vectors
h	plunging co-ordinate (+ve down)
H	fluid enthalpy
I	fluid internal energy
I_α	section moment of inertia about EA
$\mathbf{I}$	identity matrix
k	heat conduction coefficient
k	elemental stiffness
k_r	modal stiffness
k_h	translational stiffness of section
k_α	torsional stiffness of section
$\mathbf{K}$	stiffness matrix
l	aerofoil span / blade height
L	aerofoil lift (+ve upwards)
$\mathcal{L}$	Lagrangian variable
$\overline{m}$	section mass per unit span
m	elemental mass
m_r	modal mass
$\dot{m}$	mass rate of flow
m	reduced / retained number of degrees of freedom (DOF)
$\mathbf{M}$	mass matrix
M	Mach number

$\mathcal{M}$	aerofoil moment (+ve nose up)
$\mathbf{n}$	normal vector (components n_x, n_y, n_z)
N	total number of DOF; passage number
N	rotational speed (rpm)
p	fluid pressure
$\mathbf{p}(t)$	aerodynamic load vector
Pr	Prandtl number
$\mathbf{q}$	generalised co-ordinate vector
$\mathbf{q}_k$	heat conduction vector
r	radius
r_α	radius of gyration about EA (non-dimensionalised by b)
R	gas constant
$\mathbf{R}_i$, $\mathbf{R}_v$	fluid inviscid and viscous residual vectors
Re	Reynolds number
s	blade pitch (rad)
S	face surface area
$\mathbf{S}_i$, $\mathbf{S}_v$	fluid inviscid & viscous source vectors
S_α	section static moment about EA
t	time
T	periodic time
T	temperature
U	fluid flow speed
U^*	reduced speed (or with bar)
$\mathbf{U}$	fluid state vector
v_x, v_y, v_z	fluid cartesian velocities (vector, $\mathbf{v}$)
v_x, v_θ, v_r	fluid cylindrical polar absolute velocities
V	cell volume
w_x, w_y, w_z	fluid cartesian relative velocities
w_x, w_θ, w_r	fluid cylindrical polar relative velocities
W	work done by fluid
x, y, z	cartesian co-ordinates
x, θ, r	cylindrical polar co-ordinates
x_α	non-dimensional offset of centre of gravity from EA

Greek

α	pitching co-ordinate (+ve nose up)
α	absolute flow angle
β	relative flow angle
β	Newmark constant
γ	ratio of fluid specific heats
γ	Newmark damping coefficient
γ	blade stagger angle
δ	logarithmic decrement
δ_{ij}	Krondeker delta function
δ	flow deviation angle
Δt	time-step
ε	eddy viscosity

θ	blade camber angle
η	efficiency
η	principal co-ordinate vector
ι	flow incidence angle
κ_c	reduced frequency
λ_r	eigenvalue ($=\omega_r^2$)
Λ	eigenvalue matrix
μ_r	mass ratio
μ	fluid dynamic viscosity
ν	Poisson's ratio
Π	aerodynamic load vector (modal force)
ρ	density
σ	Inter-blade phase angle
τ	fluid viscous shear stress (or stress components)
τ	non-dimensional time, ωt
ω	natural frequency (rad/s)
$\overline{\omega}$	frequency ratio (plunge/pitch)
ω	angular velocity
ψ	modeshape vector (eigenvector)
Ψ	matrix of modeshapes (eigenvectors)
ϕ	mass-normalised modeshape vector
Φ	matrix of mass-normalised modeshapes
χ	blade inlet / exit angle
ξ	non-dimensional plunging co-ordinate
ζ	critical damping ratio (c/c_0)
Ω	rotational speed (rad/s)

Sub/Superscripts

0	fluid stagnation condition
1,2...	station number
f, s	fluid / structure (solid)
hub	hub / inner casing / blade root
i	node number
i,j,k	grid counters in x,y,z directions
le	leading edge
m, s	master / slave co-ordinates
n	time step number
p, s	pressure / suction surface
r	mode number
te	trailing edge
tip	tip / outer casing / shroud
w	conditions on the wall
∞	conditions far upstream, at infinity
T	transpose matrix/vector
dot	differentiate w.r.t. time (t)
dash	differentiate w.r.t. non-dimensional time (τ)

Abbreviations

ADI	alternating direction implicit
AV3D	Aeroelastic VIB3D (the aeroelasticity code)
CF	centrifugal
CFD	computational fluid dynamics
CFL	Courant-Freidrichs-Lewy
CPU	central processing unit (time)
DOF(s)	degree(s)-of-freedom
EOM	equation of motion
EO	engine order(s)
FE	finite element (method)
FI	fully-integrated
IBPA	inter-blade phase angle
LE	leading edge
LES	large eddy simulation
LU	lower/upper (decomposition)
MF	max flow (choke)
NS	near stall
PE	peak efficiency
PI	partially-integrated
RANS	Reynolds-averaged Navier-Stokes (equations) - or just 'N-S'
TE	trailing edge
UV2D	2D unsteady Euler code
2/3D	2/3-dimensional

Chapter 1

Introduction

1.0 About this Chapter

This chapter introduces the subject area of aeroelasticity, and the challenging problems it poses to designers of modern turbomachines. The major topics of practical importance, namely static and dynamic aeroelasticity are introduced, and these will be looked at in detail in this thesis. Also the related areas of forced response, rotating stall, and acoustic resonance are described briefly, to which the methods presented herein are equally applicable, but are beyond the limits of the current work. Next the scope of the work presented here is stated, and finally there is a short preview of what is contained in the following chapters.

1.1 PROBLEM DEFINITION

In general terms, *aeroelasticity* may be defined as the physical science involving the interaction of fluid, elastic and inertial forces, that determine the response of a non-rigid body to the fluid flow in which it is immersed. This definition is attributable to Collar (1947) who drew up his triangle of forces to describe the problem; he also noted that the consideration of how aeroelasticity affects design is the most important issue, as normally aeroelastic effects are to be avoided. Aeroelasticity affects a wide range of engineering applications from fluid-structure interaction problems (usually with incompressible fluids) such as sloshing of fluids in containers and pipe flow problems, to wave and wind excitation problems for civil engineering structures. However, this work is primarily concerned with high-speed (compressible) flows that are normally associated with aerospace structures. Here the fundamental problem arises from the fact that minimisation of weight is of the utmost importance, thus any structure has to be optimised with this factor in mind, as well as its aerodynamic performance. Over time, as designs improve and develop, this approach tends to lead to lighter structures, which are more highly loaded by fluid forces. Thus the relative importance of aeroelasticity in all aerospace structures is set to increase in the future.

The inclusion of thermal loads changes the triangle of forces into a tetrahedron - hence the term *aerothermoelasticity*. However, although parts of turbomachines operate at high temperature, fluctuating thermal loads are not normally too high, so this subject will not be touched on here. Finally, with the advent of high speed digital control systems, the idea of active control for aeroelastic phenomenon has become a real possibility, and the subject of *aeroservoelasticity* is born. However most of the research in this field is focused on fixed and rotary wing aircraft, although some work has been done on the active control of surge and rotating stall in axial compressors.

As is intimated by its title, this thesis is not primarily aimed at flight vehicle (external flow) applications such as rotary wing and fixed wing aircraft. However wing flutter is looked at in some detail in two chapters; this is because a large body of data exists for these cases, and the physics are generally much better understood. Also, any method capable of predicting turbomachinery blade flutter, will almost certainly be able to calculate fixed and rotary wing problems.

Turbomachines in general can be defined as fluid-dynamic rotating machines where the objective is to extract energy from the fluid flow (turbine), or add energy to it by raising the fluid pressure (compressor). In most common designs of these devices, the two components are used together, with heat addition to the working fluid in-between

the compressor and turbine, usually by burning fuel in the working fluid (combustion chamber). This device is known as a gas turbine, and the working fluid is usually air. Gas turbines have seen widespread use as propulsion systems, since their first successful implementation in the 1930's (Whittle). This is primarily because of their high power to weight ratio, but also due to their high reliability, and the fact that they may make use of the kinetic energy of the fluid leaving the turbine (which ground based applications usually cannot). Also, by optimising the thermodynamic cycle, and by using the components in different configurations, the gas turbine has application to all flight speeds from low subsonic (turbo-prop, and turbo-shaft for helicopters), through high subsonic (turbofan, unducted fan), to supersonic (turbojet, ramjet). This is not to say that gas turbines have not made major impacts in other areas such as electricity generation, pumping, and sea propulsion systems. However due to the high development cost of these machines, it has often made economic sense to base industrial designs on existing aeroengine designs, by derating the engine and strengthening it to provide longer life, with appropriate modifications for different fuel and load conditions.

There are two basic types of compressor and turbine: the axial and radial (or centrifugal) flow types. The radial devices provide a high pressure rise for each compressor stage, but their efficiency is low, and mass-flow capacity is limited. Thus for a modern large civil aeroengine application, the centrifugal compressor required would be too heavy, and use up too much frontal area (thus increasing the overall drag), to be of any use. So radial turbomachines will be ignored in this work, although they are widely used in small engine (e.g. turboshaft) designs, as their rugged design means they rarely suffer from aeroelasticity problems. However the axial flow machines are ideal for aeroengine applications, offering high component efficiency, large mass flow, and light weight. But due to their relatively thin blading, with high aerodynamic loads, they are particularly susceptible to aeroelastic instability problems, and they will provide the main thrust of this work.

Turbomachinery aeroelastic phenomena are characterised by the interaction of two physical domains, the describing equations of which are non-linear. These are the fluid and structural domains where the dynamic equations of motion cannot be solved analytically for generalised geometries. However, methods of solution for Lagrange's equation for structural dynamics, and the Navier-Stokes equations for fluid dynamics have become possible using numerical techniques in conjunction with modern digital computers. Numerical techniques have also been applied to the aeroelasticity problem, but a large number of assumptions have had to be made in order to render the problem

solvable. As these existing methods have generally proved inadequate, especially for the specific case of flutter, it is now appropriate to re-examine the validity of the assumptions made, bearing in mind the continuing improvement in available computer power. The main areas of interest in this field, which will be looked at in detail in the next section, are: static aeroelasticity, dynamic aeroelasticity, forced response, acoustic resonance and rotating stall.

1.1.1 Static Aeroelasticity

Static aeroelasticity deals with the calculation of the blade running shape from knowledge of the design geometry and flow conditions. Turbomachinery blades deform elastically under both centrifugal and gas loads as they tend to deform in a torsional fashion from their original manufactured shape, hence the colloquial name of untwist for this phenomenon. However, it should be noted that the blades do not just untwist about a fixed axis, the section profiles being also affected - known as uncambering.

The engineering problem is in effect an inverse one: the blade geometry is designed to give optimum aerodynamic efficiency at some working condition - but this is not the shape that must be manufactured. The manufactured or 'cold' blade shape must be calculated by taking off the effect of centrifugal and pressure loads from this optimum geometry, a procedure known as blade unrunning. An incorrect manufactured shape will thus not yield the desired shape at the design speed and a loss of efficiency will ensue. Although this procedure is routinely used at the design condition in order to obtain the manufactured blade shape, off-design calculations are not widely reported, and yet constitute an important first stage to the prediction of dynamic aeroelasticity and other unsteady effects.

The other important effect in static aeroelasticity is divergence. Simply, if the structure is not stiff enough, it will deflect beyond the limits of elastic behaviour of the structure under the gas loads, and will ultimately break. This phenomenon is of importance in flight vehicles, particularly historically, but is not normally an issue in modern turbomachinery blading. This is because the stiffness of materials used is more than adequate for the gas loads encountered, and usually the designer is left with the dynamic aeroelastic effects to worry about.

1.1.2 Dynamic Aeroelasticity

Although most aeroelastic phenomena (other than those mentioned above) are of dynamic origin aeroelasticity, only purely self-excited effects (usually termed *flutter*)

will be studied under this heading. Flutter is defined as an unstable and self-excited vibration of a body in an airstream and it results from a continuous interaction between the fluid and the structure, either or both of which may be non-linear in nature. Thus it differs from other aeroelastic effects in that there are no unsteady forces or perturbations coming in through the boundary of the fluid-structure domain.

In turbomachinery blade rows, the (structure to fluid) mass ratio tends to be high while the same parameter is much lower for wings. Thus, whereas the wing flutter usually occurs as a result of coupling between the (bending and torsional) modes, turbomachinery blade flutter tends to be a single mode phenomenon as the aerodynamic forces, which remain much smaller than the inertial and stiffness ones, cannot cause modal coupling. In the former case, the aeroelastic mode can be significantly different from the structural one, in both frequency and mode shape, while this is usually not the situation in the latter case where there is little difference between the aeroelastic mode and the corresponding structural mode. However, coupled (blade) mode turbomachinery flutter cannot be ruled out, and may occur in modern designs where blading tends to become thinner and more highly loaded to improve aerodynamic efficiency. Where coupling more often occurs, however, is through the disc, or part- and full-span shrouds, if present. So, it is important to realise the effect that having many interacting blades on flutter.

The most important parameter used in describing flutter is the reduced frequency. This is defined as the ratio of the vibration mode frequency (in which flutter occurs or is expected to occur) to the (relative) flow speed over blade chord. In external flow applications semichord, rather than chord is used, and sometimes reduced velocity (the reciprocal of reduced frequency) is quoted. The physical significance of this parameter is how quickly the blade vibrates compared to how quickly flow information convects (to the next blade for instance). A low reduced frequency implies a quasi-steady flow, and a high value implies the flow may be 'frozen'. In the early days of aeroelasticity the reduced frequency was used as a design parameter developed from a set of empirical correlations to avoid flutter (e.g. k_c>0.35 for first. flap, and k_c >1.5 for first torsion to avoid flutter (AGARD, 1985)). Some of 'rules' are still used today as a first guess as to whether flutter is likely to occur.

In any case, flutter is a particularly difficult problem in turbomachinery cases since there are many additional features with not fully-understood consequences: flow distortions due to up and downstream blade-rows, coupling of assembly modes, and

loss of spatial periodicity of vibration due to aerodynamic effects and blade-to-blade manufacturing differences - known as mistuning.

1.1.3 Forced Response

When the rotating blades pass through flow defects created by the interaction of upstream and downstream bladerows, the ensuing large unsteady aerodynamic forces can cause excessive vibration levels, hence the term forced response. One of the first design steps for minimising the response levels is the Campbell diagram (see **Fig.1.2**), which can only indicate the possibility of a mode being excited at a particular rotational speed. However, what is of real interest to the designer is the prediction of the vibration amplitude under unsteady aerodynamic loading which can be due to wake passing from upstream blade-rows (wake-rotor interaction), the potential field of upstream and downstream blade-rows (potential-rotor interaction), or due to fluctuating back pressures. Because of the numerous unknown factors such as structural damping, non-linear damping in the blade roots, and the forcing itself, forced response analyses usually aim at ranking potential designs rather than predicting actual vibration levels. Such analyses are also used to explain failure mechanisms and to evaluate the effects of possible remedial modifications.

1.1.4 Acoustic Resonance

Acoustic resonance is probably one of the least understood aeroelastic phenomena but it is usually accepted to be of aerodynamic origin. For an infinite cascade of flat plates, most linearised theories will tend to predict acoustic resonance when the interblade phase angle coincides with the propagation time of a perturbation between two adjacent blades. It can be shown that acoustic resonances correspond to the singular terms in the infinite series expression for the unsteady pressure field. Further discussion can be found in Samolovich (1967) and Verdon (1977).

In turbomachinery cases, acoustic resonances, or fluid vibration modes as they are sometimes called, are also believed to be excited by vortex shedding from a (usually stalled) blade row. Such resonances are not always initially accompanied by structural vibration but the resulting unsteady forces can become large enough to cause structural failure. This is an area of research in its own right, but what is of interest here is whether acoustic resonance can affect flutter modes, especially in front stage fans, where there is a large duct directly in front of the fan, which has the possibility of resonating in sympathy with the unsteady pressures due to the vibrating blades.

1.1.5 Rotating Stall

Another related area to aeroelasticity is other instabilities which may occur in the turbomachine (usually the compressor) which are often though of as pure aerodynamic instabilities. When the compressor moves off the design working line, and the incidence on the blades increases (above the working line), then the blades may reach a stalling condition. When this occurs at least three different instabilities may occur: the first is stall flutter, described below; the second is surge, where the pressure downstream of the stalling stage being higher than upstream of it, causes the whole flow to suddenly and violently reverse - this results either in structural damage or the machine recovering to the correct flow direction; the third is rotating stall. This occurs when due to differences in the flow around the annulus (e.g. due to an inlet distortion or upstream obstruction) only some of the blades stall. The stalled 'cell' then causes a higher incidence onto the blades nearest in the opposite direction to the rotation (causing those to stall), and a lower incidence onto the blades nearest in the rotation direction (causing those to recover). Thus the stalled cell rotates around the annulus in the same direction as the rotor rotation (usually at about 1/3 of the rotor speed), and typically there is more than one cell in the annulus (usually 3-4).

This phenomenon obviously causes large unsteady forces on the blades, so at least some forced vibration would be expected to accompany rotating stall. In the past, it has been difficult to distinguish between rotating stall and stall flutter, some researchers arguing that they were in fact one and the same. However the difference can be seen in the fact that due to the high mass-ratio in turbomachines, flutter occurs at frequencies close to the blade natural frequencies, and may occur with no significant annular flow distortion. Rotating stall, on the other hand, may occur at a frequency which has no bearing on the blade frequencies. The difficulty may come when the rotating stall frequency happens to be close to the blade frequency, and due to small non-linearities and scatter of frequencies, the rotating stall wave becomes locked into the blade frequency.

1.1.6 Particular Problems of Interest

There are a number of particular problems, prevalent in contemporary designs of axial-flow turbomachines, that the work presented here is primarily aimed at:

- Blade Untwist (calculation of the deflected shape of blades particularly at off-design conditions)
- Flutter (prediction of vibration instabilities in the operating range of bladerows)

- Forced or Gust Response (calculation of the amplitude of blade response due to unsteady loading from up- and downstream flow distortions)

Untwist

The accurate prediction of the deflection of blades under running conditions in turbomachinery is a long standing problem. The problem for classical calculations, where the fluid- and structural domain are calculated separately, is that small changes may change the aerodynamic loading considerably. Thus, calculations are routinely performed at design conditions, where the blades are 'unrun' - the cold (as manufactured) shape is determined from the desired aerodynamic shape at running conditions using a static analysis. Here the aerodynamic loads are known a priori, as they are those at the final (desired) position.

However, calculations are not often performed at off-design conditions, where the final gas loads are not known, even though this is a vital first step towards determining off-design performance, as well as surge and flutter margins. Here, the classical static analysis would have to be iterated, to update the flow solution each time the blade moved, and there would be no guarantee of convergence. Thus, new tools that could easily calculate untwist would be useful to the turbomachinery blade designer.

Stall Flutter

The second important area that classical methods have failed to predict with any accuracy is stall flutter. It is known that an isolated aerofoil in pure bending is stable, unless either the aerofoil stalls, or there is a torsion mode coupled to the bending mode. The former has proved difficult to predict as classical methods tend to split the fluid and structural domains into two separate parts, and often use linearised analyses, whereas flutter (and particularly stall-flutter) is believed to be a phenomenon where the coupling between the flow and blade is strong, and non-linear effects (such as shock boundary-layer interaction) exist. The aerodynamic conditions at which stall flutter tends to occur, which is at part-speed, high working line conditions, where the incidence onto the blades is high, which tends to thicken the boundary layer still remain difficult to model even for steady flow conditions. At transonic flow conditions (which is typical for the tip sections of front stage fans) there is a shock wave, which at these conditions stands outside the blade passage (i.e. misses the leading edge of the next blade). This tends to lead to a strong shock / boundary-layer interaction, which may be an important part of the stall flutter mechanism.

Sisto (1987) has shown the areas on the compressor map where it is possible for flutter to occur (not necessarily at all places in any one design) as shown in **Fig.1.1.**

Figure 1.1 Possible Modes of Compressor Flutter

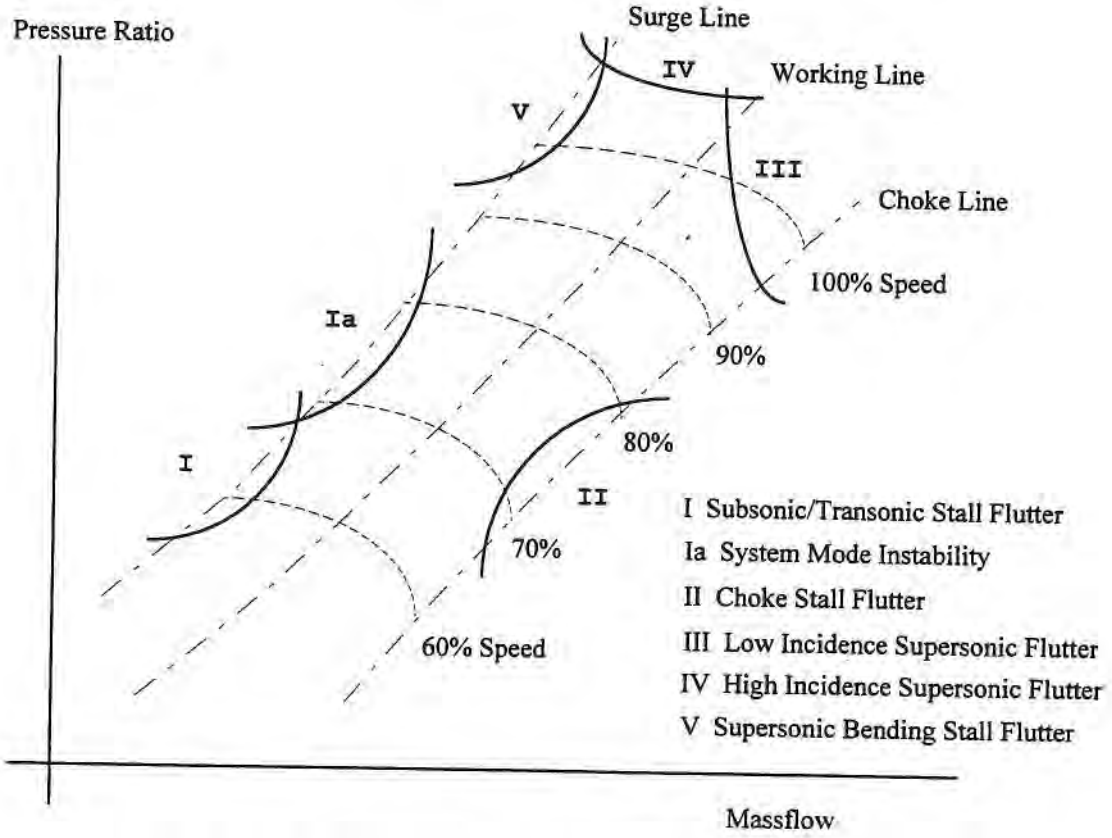

Classical stall flutter is shown to occur in regions I and V above the working line, and can be characterised by whether the flow is subsonic / transonic or supersonic, and / or whether bending or torsion motion is involved in the flutter mode. Also in this region of the compressor map, a different type of instability is identified as a system mode instability (Ia). This usually occurs where, due to the large hub/tip ratio of modern front stage compressors, part span shrouds (clappers / snubbers) have been introduced to increase the rigidity of the bladed disc structure. But this tends to couple the bending and torsion modes together (via the structure) with a phase lag between them, and it is well known from wing aeroelasticity that the flutter mode is usually a coupled bending / torsion mode (albeit with coupling via the fluid in that case).

However, with the advent of wide-chord fan blades that do not require clappers, there is still some question as to whether such instabilities can arise in a purely inviscid system i.e. not involving stall in the classic sense. It may be possible that 'stall' flutter is possible where the blades are near stall, but its mechanism is inviscid coupled with

particular nodal diameter modes of the bladed disc - this is given further consideration in later chapters.

Other Types of Flutter

The other possible types of flutter, as shown above, are choke flutter, and various types of supersonic flutter. Choke flutter can occur at the opposite end of the compressor characteristic to stall. Here the incidence onto the blades decreases and becomes negative. At subsonic flow conditions this may lead to the separation of the boundary layer from the pressure surface, and the flutter mechanism is similar to that of stall flutter (Fleeter (1979) has termed this negative incidence stall flutter). At transonic flow conditions choke will normally occur before stall whereupon the flow cannot change further, and flutter may occur due to large unsteady pressure from oscillatory shocks.

Regions III, IV, and V occur at supersonic relative flow conditions (turbomachinery flows being always axially subsonic), usually above the normal operating conditions of compressors. Region III may be a potential design limitation as this is the only one to occur on the normal operating line of the compressor, however this is usually only at an overspeed condition. Some success has been reported in the prediction of these phenomena using the classical linearised approaches (Whitehead 1966a&b, Verdon 1977, Adamczyk 1978).

Flutter is by no means confined to compressor blades; flutter has been reported in turbines, particularly in low pressure blades of high aspect ratio. The types and mechanisms of flutter broadly fit into the same categories, described above, with high / low incidence types, involving flexural and torsional modes. The possibility arises of bending and torsion modes being coupled together to form the flutter modes, particularly as turbine blades are usually shrouded although the blades would not normally be designed with frequencies close enough to be coupled by the fluid (as this would very likely cause forced response problems as well).

Forced Response

In forced response calculations we are interested in the prediction of the amplitude of vibration due to a given unsteady aerodynamic loading. This can be due to wake passing from upstream blade-rows (wake-rotor interaction), the potential field of up/downstream blade-rows (potential-rotor interaction), or due to fluctuating back pressures.

These unsteady loadings occur at synchronous speeds - i.e. frequencies of vibration modes that coincide with multiples of the engine rotation frequencies (known as engine orders, EO). The strength of the forcing in different engine orders depends on many things, but a useful tool which can indicate the possibility of modes being excited is the Campbell diagram. This is a plot of the bladed disc mode family frequencies against rotor speed, onto which the engine order lines are superimposed - see **Fig.1.2.**

Figure 1.2 Campbell Diagram for a typical rotor blade

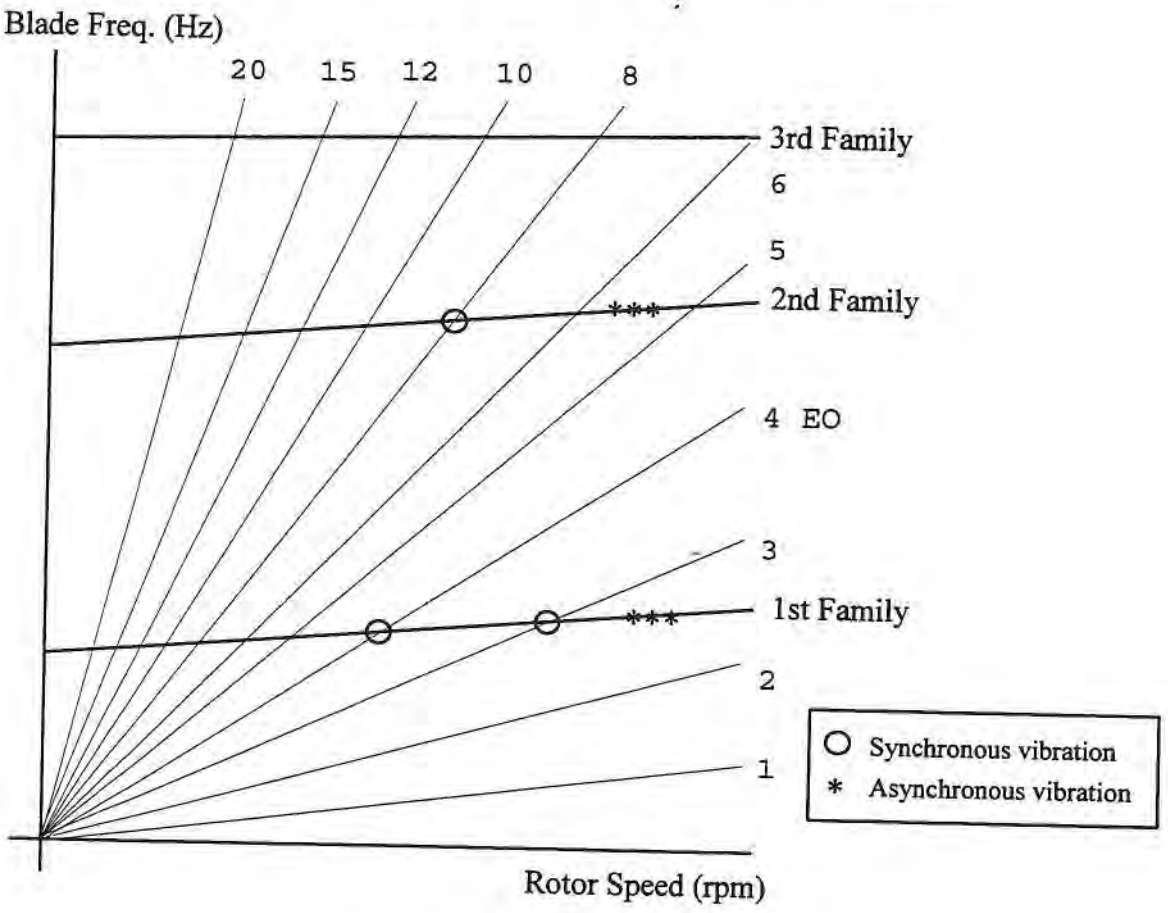

Forced response occurs where engine order lines coincide with nodal diameter mode frequencies - thus termed a synchronous vibration as it occurs where frequencies match. Thus forced response problems may be alleviated by reducing the forcing (by modifying the aerodynamics), or by controlling the resulting vibration (e.g. using under platform dampers), or it may be removed entirely by moving coincident frequencies out of the running range. It is not usually so easy to move resonances out of the running range for aeroengines as it is for industrial applications, as the aeroengine operates over a wide range of speeds and aerodynamic conditions. So it is important to be able to calculate the magnitude of vibration responses, for fatigue life

predictions. This problem is usually greatest in high pressure turbines, where the blades are already under large thermal and centrifugal loading. Conversely, flutter and flow instabilities such as rotating stall occur at non-synchronous speeds, so they cannot simply be avoided by changing blade frequencies or numbers.

Predictive models are currently available that calculate the unsteady pressures acting on the blade due to forced response effects. However these codes currently take no account of the effect of the blade motion - simply the unsteady forces resulting from the external forcing are separately used to calculate the amplitude of response. The justification for this assumption is that the stability of the blade under consideration is either considered separately, or ignored. If aerodynamic damping contribution is ignored, the calculation will be conservative, as normally the unsteady force due to the blade motion contributes positively to the stability, as otherwise the problem would be that of flutter, and not forced response. However it is not known whether this may change under the unsteady forcing, and in any case it will be computationally expensive to perform two unsteady calculations, rather than one.

Forced response predictions could be improved by using an integrated model, such as that which will be tested on flutter cases. Then the fluid and structure are allowed to freely interact as they do in reality, as well as obtaining the effect of the change in the unsteady forcing due to the blade motion. Also such an approach would allow the incorporation of non-linear structural effects such as friction damping in the blade roots. This subject is a new research area in its own right, so detailed analysis is not attempted here. The future possibilities for forced response are also examined in Chapter 9.

1.2 RESEARCH OBJECTIVES

The objective of this research is to improve aeroelasticity analysis capabilities by using a new generation of integrated non-linear analysis methods. The integrated method involves solving both fluid and structural domains simultaneously, rather than treating them separately. This approach has also been termed coupled, as distinct from classical uncoupled techniques. It can be assumed that in this work time-domain solvers are implied by the integrated approach, although there is no inherent reason why other types of integrated models could not be formulated, if required.

The need for more integrated time-marching approaches arises from the non-linear response of fluid flow to the motion of solid boundaries, especially at transonic flow speeds, and the existence of non-linear structural effects such as damping in the blade

roots. By solving fluid and structural equations together in a time accurate fashion, the fluid forces affect the motion of the blade and vice-versa, as occurs in reality, rather than assuming a forced harmonic motion.

A number of integrated methods have been identified - they have broadly been split into two groups: fully-integrated (FI) and partially-integrated (PI). In the former the same numerical solver is used over the entire fluid/structural domain, thus ensuring a close coupling with virtually no assumptions. However this approach may place undesirable restrictions on the modelling of the two domains (e.g. mesh density compatibility on the blade surface). The latter (PI) approach allows independent fluid- and structural-dynamic time-marching codes to be used. The exchange of information occurs at the boundary between the two domains, as the equations of motion are solved alternately in real-time. This approach for this work is chosen as it offers significant improvements over traditional uncoupled approaches, while at the same time the method can make use of existing codes as the computational fluid dynamics (CFD) and transient structural-dynamics (TSD) solvers.

Thus integrated aeroelastic analysis methods would allow stability problems to be detected at an early stage, and avoid expensive redesigns and retests. With computer power still increasing rapidly, and likely to continue to do so for the foreseeable future, it is important to research the different possibilities for turbomachinery aeroelasticity to take advantage of modern computers in order to reduce risk and cost. This research will also open avenues for prediction of similar effects in other applications. New methods should be able to provide:

- Improvement in calculation of loaded blade deflections at off-design conditions
- Improvement in prediction of blade flutter stability
- Prediction of fully dynamic aeroelasticity features (divergence, limit cycles, stresses, deflections)

There are a number of complex and non-linear features associated with turbomachinery blading that will require modelling in order for a new aeroelastic method to be successful:

- 3-D Flows: tip clearance flows; lambda shocks, secondary flows
- Viscous effects: separation, shock boundary layer interaction
- Compressibility: strong and unsteady shocks

- Turbulence: transition, Reynolds-averaging
- Interaction with distortions from upstream and downstream blade rows
- Structural non-linearities
- Mechanical effects such as disc coupling, friction damping, and mistuning.

These phenomena should be considered when deciding which approach to use, so that their inclusion is not precluded by the formulation of the model. It is the modelling of such features (or the lack of it) that has resulted in the poor performance of existing flutter prediction methods, as well as not coupling the fluid and structure together.

1.3 SCOPE OF THIS THESIS

As stated above this work is primarily aimed at time-domain, integrated analysis methods for aeroelasticity in axial flow turbomachinery blade rows at high flow speeds (i.e. compressible flow). However, due to the complex nature of this problem, the methods have first been applied to 2-dimensional isolated aerofoils, and also to 3-dimensional wings. The later chapters are aimed at turbomachinery calculations, although forced response predictions are not included. However, many of the techniques developed for flutter, can be used directly for forced response, with appropriate models of the unsteady forcing. The methods described herein are also applicable to many other areas, such as wind turbines, rotorcraft, propellers, and missile fins, with suitable modelling of the aerodynamics and structural dynamics involved.

This work is concentrated on the so-called partially-integrated method, and not on methods where the equations of the fluid and structure are solved simultaneously by the same solver (fully-integrated methods). This is because of the considerably greater flexibility offered by the former, and that any advances in the differing fields of CFD and structural dynamics can immediately be taken advantage of.

There are two emerging avenues in which improvements in analysis would bring benefits to the design of modern gas turbines. One is what could be termed a full flutter analysis - this would be a state-of-the-art three-dimensional non-linear integrated analysis which could be used for research into mechanisms of flutter, and for the final analysis of critical designs before rig/engine testing. However, these analyses are likely to be expensive computationally and to take large elapsed times to run, although what is considered expensive today may be routine in 5 years. Another important method would be one that can be used by a designer in an iterative manner whilst refining a design. Such a method would need to run quickly on low-cost

workstations and would need to be a simplified version of the full analysis while retaining the physics of the problem. This is likely to be a linearised analysis, to be fast enough to be repeated many times over for many different designs and operating conditions.

This work is aimed at the first type of analysis, in the hope that this would be applicable to a wide range of aeroelastic problems, and that it should help to improve the understanding of the flutter mechanisms. Then, with a greater knowledge of the phenomena involved, it may be possible to identify what is important to have in the model, and what can be left out. Armed with this knowledge, the second type of analysis may be developed.

1.4 PREVIEW OF THE THESIS

This thesis is divided into nine chapters, including this one. Chapter 2 surveys the literature of existing methods for aeroelasticity prediction with emphasis on turbomachinery, but also covers wings, as a large body of the existing techniques have been pioneered for external flow. This chapter also includes brief reviews on unsteady CFD and transient structural dynamics models. Chapter 3 sets out the mathematical formulation for the combined fluid/structural analysis in the form of a partially-integrated method. Chapters 4 and 5 cover the aeroelastic analysis of isolated aerofoils using the proposed method, in 2D and 3D respectively.

The rest of the thesis is concerned with 3D turbomachinery blading. 2D models are not included, as it is difficult to get realistic flutter data that is 2-dimensional (most of the experimental data comes from 2D linear cascades with prescribed rigid motion). The test cases used are modern designs of front stage compressors (fans) - these are chosen as they offer most of the features that have proved difficult in the past, namely transonic / supersonic flow, strong shocks, separated boundary layers, bladed disc structural modes, mistuning etc. Chapter 6 presents untwist predictions at design conditions, and includes comparisons with static (non-linear) calculations and experimental data. Off-design untwist data are also presented, showing the reasons why the static methods have not been unable to calculate these conditions accurately. Chapters 7 and 8 present analyses of the flutter behaviour for two different fans. The first analysis is at design speed, comparing the results of the new approach against the classical methods (using the same aerodynamic code and computational mesh). The second is at part-speed near the stall boundary. This chapter includes an experimental flutter point with analysis, using the classical single-passage uncoupled method as a

benchmark and finally demonstrating a multi-passage simulation of the entire bladed disc annulus.

The ninth and final chapter draws together the findings of this work. Discussion of the mechanisms that may be involved in the flutter cases examined is given. The relative advantages and shortcomings of the different levels of modelling that have been used are discussed, including an attempt to determine which approaches may be best used in different circumstances. Finally, some discussions of future directions, and recommendations for further work are made.

Chapter 2

A Review of the Literature

2.0 About this Chapter

This chapter is a review of current aeroelasticity methods with particular emphasis on turbomachinery applications. It also includes a survey of the computational fluid dynamics procedures that can be used for the modelling of unsteady flows in such environments, and a brief survey of the structural dynamics techniques used to model bladed discs. The aeroelasticity phenomena encountered in turbomachinery are introduced from an industrial perspective and the predictive methods are divided into two classes: classical and integrated. The former combine the fluid and structural equations in an uncoupled fashion while the latter attempt to solve the equations together by either exchanging information at each time step or by formulating the aeroelasticity problem in a single unified fluid/structure medium. Further topics, such as the availability of experimental data for model validation, non-linear structural behaviour, general inter-blade phase angle, and blade mistuning are also discussed in some detail.

This chapter has been published in the paper '*A Review of Aeroelasticity Methods With Emphasis on Turbomachinery Applications*' in the April 1996 volume of the Journal of Fluids and Structures.

2.1 INTRODUCTION

Aeroelasticity is the study of the mutual interaction that takes place within the triangle of the inertial, elastic, and aerodynamic forces acting on structural members exposed to an airstream, and the influence of this study on design (Collar 1947). In a turbomachinery environment, these forces act on various blade rows and can cause excessive blade vibration, a feature that continues to limit the design and performance of gas turbines. Turbomachinery aeroelasticity phenomena are characterised by the interaction of two physical domains, the describing equations of which are non-linear. These are the fluid and structural domains where the dynamic equations of motion cannot be solved analytically for generalised geometries. A number of extra complications stem from the existence of large numbers of complex-shaped blades, arranged in alternate stator and rotor rows with relative motion between them. The flow therefore exhibits a number of non-linear aerodynamic effects (e.g. shock/ boundary-layer interaction, flow separation, turbulence) that are very difficult to model representatively. The structure may also bring additional non-linear features such as friction damping in blade roots and/or shroud interfaces, and large deformations under centrifugal effects.

Reviews of advances in the field of aeroelasticity have been made by Collar (1947, 1978), Sisto (1953), Platzer (1975, 1978 & 1982), Fleeter (1979), Garrick (1976), Garrick and Reed (1981), Kaza (1988), Bendiksen (1988, 1993), and a summary can be found in the AGARD Manual (1985). The textbooks on the subject include works by Bisplinghoff, Ashley & Halfman (1955), Bisplinghoff & Ashley (1962), Forsching (1974), and Curtiss, Scanlan & Sisto, Ed. Dowell (1989). The particular area of stall flutter has been surveyed by Chi and Srinivasan (1985) while rotary wing aeroelasticity has been discussed by Friedmann (1987). The structural dynamics aspects of the turbomachinery environment have also been the subject of many review articles: Ewins (1973), Srinivasan (1976), Rao (1977, 1980, 1983a, 1983b, 1987), Lalanne (1985) and Irretier (1988).

As the existing aeroelasticity methods have generally proved inadequate, especially for the specific case of flutter, it is now appropriate to re-examine the validity of the assumptions made, bearing in mind the continuing improvement in the available computing power. The purpose of this Chapter is thus threefold:

(i) to summarise the range of aeroelastic problems encountered in turbomachinery and to highlight the difficulties associated with such applications,
(ii) to critically review and classify existing prediction methods, and

(iii) to discuss current trends and to suggest new avenues for further research.

The aeroelasticity phenomena that are of interest to turbomachinery designers have already been described in Chapter 1. It is now appropriate to review aeroelasticity methods that have been tried in the past, for fixed and rotary wing flight vehicles, as well as for turbomachinery blade rows. However the building blocks necessary for any aeroelasticity method, fluid dynamics and structural dynamics method will be reviewed first.

2.2 COMPUTATIONAL METHODS FOR UNSTEADY FLOWS

With dramatic increases in computing power and advances in computational fluid dynamics (CFD) methods, it is now possible to obtain solutions for both inviscid (hyperbolic Euler equations) and viscous (parabolic Navier-Stokes equations) steady flows, including a reasonable representation of viscous losses. The usual approach is to use time integration, starting from known initial conditions. Unsteady flows are much more complex in nature because of temporal variations but representative solutions can still be obtained if the time-dependent terms are discretised in a time-accurate fashion. Over the last two decades, time domain solutions have progressed through full-potential, linearised-Euler, Euler and, most recently, Reynolds-averaged Navier-Stokes equations. The numerical modelling of aerodynamics has been reviewed by Jameson (1983a) while Sharma et al. (1992) and Verdon (1993) have assessed the unsteady flow modelling for turbomachinery applications.

Two distinct methods have been adopted to discretise the fluid domain. The first one, known as finite-difference, is based on the differential form of the governing equations. However, it is not of primary interest in turbomachinery aeroelasticity, its main application area being external aerodynamics. The physical grid on which the calculation is to be performed is transformed to a rectangular computational grid with equal spacings in each direction, onto which the equations are discretised. In the case of commonly used structures (such as wings, fins, etc.), the required transformations and their associated grids are well known so that these can be handled routinely. Both steady and unsteady solutions have been obtained using explicit (MacCormack, 1976) and implicit (Beam and Warming (1978) ADI scheme) time-marching schemes.

The second method, known as finite-volume, uses the integral form of the governing equations which are discretised as fluxes through control volumes of known shape but arbitrary size. No grid transformations are required and the calculation takes place in the physical domain. The technique was first developed by Jameson et al. (1974,

1981) and adapted to turbomachinery applications by Denton (1975, 1983). To accelerate the computation of these methods the multiple grid method can be used (Ni, 1981) with local time-stepping. More recent formulations include the use of semi-implicit residual smoothing (Jameson & Baker 1983b) or fully implicit schemes which use ADI or LU decomposition to solve the resulting block tri-diagonal matrix equations.

Of the two formulations, the finite-volume one has proved popular for turbomachinery applications with complex 3D geometries since there are no grid transformations. Furthermore, considerable research has been devoted to unstructured adaptive meshing techniques that are applicable to finite-volume codes since the combination is very well-suited to turbomachinery cases. Further differences between the CFD methods lie in the integration schemes adopted (explicit or implicit) for solving the discretised equations (cell vertex or cell centred schemes), the meshing strategy used (structured - O, C, or H meshes; unstructured - adaptative, dynamic meshes) and the implementation of the boundary conditions (non-reflecting, periodic, moving boundaries).

One of the major problems associated with 3D unsteady flow modelling is the amount of CPU time required to obtain fully-converged solutions. Although both finite-volume and finite-difference methods can be accelerated by implicit schemes and numerical techniques such as multigrid and local time-stepping as described above, these schemes do not usually preserve time-accuracy throughout the fluid domain. So these acceleration techniques are usually restricted to steady flows, notable exceptions being the time-accurate multiple grid scheme of He (1993a), and the implicit schemes using multi-grid to solve each time level of Batina (1990).

The modelling of turbulence is probably one of the most significant challenges to the accuracy of modern CFD methods, especially in the case of turbomachinery applications. For the foreseeable future, it is impractical to contemplate a direct application of the Navier-Stokes equations to turbulence as an unrealistically fine mesh would be required to capture the smallest eddies, an approximate size of which being provided by Kolmagorov scale. Therefore, turbulence can only be represented using simplified models which are usually based on equivalent local turbulent viscosities given by the averaged effect of the eddies at some point in the flow. There is a hierarchy of such methods which range from the fully-empirical mixing length model (zero-equation eddy viscosity model, Baldwin & Lomax (1978)), the one-equation k-l model (Cebeci & Smith (1974), Johnson & King (1985), and Baldwin &

Barth (1990)), the two-equation k-ε model (Jones & Launder (1973)), and ultimately the Reynolds stress model with 3 equations in 2D, and 6 equations in 3D. All of these methods rely on an accurate modelling of the transition point from laminar to turbulent flow. One possible route would be to assume turbulent flow throughout but the latest design techniques allow the blades to be designed specifically to maintain laminar flow for as long as possible. So accurate models of transition are essential to viscous analyses.

All turbulence and transition models have their limitations, a feature that must be borne in mind when attempting flutter predictions, especially if the viscous effects are known to be significant from the experimental evidence. In any case, there is a lack of consensus as to which model one should use with unsteady flows, the simpler models being capable of producing at least as good agreement with measurements as their computationally more expensive counterparts.

Since unsteady flow solutions require much more CPU power than steady flow ones, it is desirable to be able to use simplified implementations wherever possible. Some of the established simple aerodynamics theories and their modern equivalents are discussed below.

2.2.1 Classical Methods

Theodorsen (1933) and later Whitehead (1960) produced tables of data from measurements, with which flow coefficients could be derived for standard geometries. With the advent of the digital computer in the 1950s, it became possible to solve Laplace's equation using singularity methods. Simplifying assumptions such as inviscid, incompressible, irrotational flow were the norm and the general trend was to seek semi-analytical formulations. Although such restrictions were widely acknowledged to be unrealistic for turbomachinery aeroelasticity, these simplified methods were nevertheless used as no real alternatives were available. Although they were perhaps useful in the aerodynamic design, they were of little use for the prediction of flutter and other aeroelastic effects, especially for transonic flow speeds where the equations are highly non-linear, and the flow is no longer incompressible. Such methods include linearised cascade theories (Whitehead (1970, 1977), Namba (1972), Friedmann and Yuan (1977), Atassi and Akai (1978), Adamczyk and Goldstein (1978b), Tadros and Botman (1981), Dunn and Dugundji (1992), Z. Yang (1988)), singularity methods such as doublet lattice (Brase and Eversman (1988)) or vortex techniques (Sisto et al. (1989, 1991)), and frequency domain panel method (Lee (1986), Williams et al. (1991), Cebeci et al. (1992), and Su (1992)).

The classical methods have also been used to predict stall flutter but it was soon realised that cascades stalled differently from single aerofoils (Sisto and Ni, 1972). A widespread practice has been the calibration of inviscid methods using experimental evidence for the prediction of stall flutter. The most effective approach has been the use of actuator disc theory which will be discussed later.

Some of the classical methods are still in use and may provide acceptable results for preliminary design purposes where computational speed is particularly important. However, in the aerospace industry, these methods seem to have an established history of not being able to provide reliable predictions such as the ranking of various designs for flutter stability.

2.2.2 Linearised Potential and Euler Methods

The linearised potential and Euler equations describe inviscid, compressible and rotational flows. The Euler equations conserve the mass, momentum, and energy but neglect viscous terms. The potential equations further assume that the flow velocity components can be written as spatial derivatives of a scalar function (irrotational flow). Both the Euler and potential equations can be used to calculate time-dependent inviscid flows if the unsteady terms (involving time derivatives) are discretised to the desired order of accuracy. However, the equations are non-linear in nature and their full solution can be computationally expensive so that a further simplification is made to speed up the solution. This involves *linearising* the equations whereby each variable is expressed as a mean value (obtained from a non-linear steady flow calculation) plus a small perturbation about that value (Chow et al. (1984)). Such an approach provides a good compromise between the computational efficiency and the flow physics but its applicability to a detailed flutter analysis is questionable since linearisation will prevent the observation of limit cycle behaviour. Some well-established linearised methods and their application to aeroelasticity problems are listed below:

- 2-D linear potential codes: Ni & Sisto (1976); LTRAN2, Ballhaus & Goorjian (1977,78); LINFLO, Verdon & Caspar (1984); Surampudi & Adamczyk (1986); Usab & Verdon (1986,91); FINSUP, Whitehead (1990)
- 3-D linear potential codes: XTRAN3S, Guruswamy & Goorjian (1984); CAP-TSD, Batina (1988); Henke et al. (1991)
- 2-D linear Euler Codes: Hall & Crawley (1989); Hall & Clark (1991); Holmes & Chuang (1991)

- 3-D linear Euler Codes: Hall & Lorence (1992); Giles (1992)

2.2.3 Non-Linear Potential and Euler Methods

The models are identical to those of the previous section but no linearisation is made during the unsteady calculations which are solved in time using a time-accurate discretisation of the time-dependent terms. It is also possible to include boundary layer effects by a process known as viscous-inviscid interaction (He & Denton (1991a)). Regions far from the structure are modelled using inviscid equations while extra equations to model the turbulence are used near the structure since the viscous effects are much more important near the boundary. Thus viscous effects can be modelled without resorting to the full Navier-Stokes equations, a feature that reduces the computational effort significantly. Unless viscous effects are particularly significant, Euler equations probably offer the best compromise for aeroelasticity analyses, especially when there is a need to model a whole annulus in 3D. Although the location and the strength of shocks may not be necessarily predicted with good accuracy, equivalent viscous solutions can be found by changing some of the flow parameters such as the exit pressure. Some well-established full unsteady methods and their application to aeroelasticity problems are listed below:

- 2-D full potential codes: Malone & Sankar (1984); Bakhle, Reddy, & Keith (1992); Korakianitis (1992)
- 3-D full potential codes: Tatum & Giles (1988); Gea, Chow, & Chang (1992)
- 2-D Euler codes: Erdos, Alzner, & McNally (1977); Fransson & Pandolfi (1986); Sankar, Wake & Lekoudis (1986); Venatakrishnan & Jameson (1988); Gerolymos (1988); Giles (1988, 90, 91); Batina (1990); He (1990, 91a); Huff, Swafford & Reddy (1991); Trepanier et al. (1991)
- 3-D Euler codes: Guruswamy (1990); Brenneis & Eberle (1990); Robinson, Batina and Yang (1991); Gerolymos (1992a,b); Obayashi, Guruswamy & Goorjian (1991); He (1993b)

2.2.4 Reynolds-Averaged Navier-Stokes Methods

The state-of-the-art CFD methods use the full Reynolds-averaged Navier-Stokes (RANS) equations where all the viscous terms are retained, the only simplification being the time-averaging of the turbulence quantities which are modelled by semi-empirical formulae. Such techniques are now well established for steady flows but

there is little evidence to indicate that they are directly applicable to unsteady flows. As mentioned earlier, there are a variety of turbulence models available but the RANS formulation is usually used with the one- or two-equation models as the Reynolds stress equations tend to be computationally very expensive and results seem to indicate that they present little improvement over the much simpler models. Although RANS methods are ideally-suited for non-linear aeroelasticity analyses, the computational requirements for 3D unsteady flow calculations are very substantial. Relatively few cases are reported in the literature. 2D work is published by Sankar and Tang (1985), Scott and Hankley (1986), Wu et al. (1987) and Siden (1991) while 3D examples have been studied by Hirt et al. (1974), and Chaderjian and Guruswamy (1992). More recently methods have also been presented by Ferrand and Aubert (1994), Ekaterinaris and Platzer (1994), and Aso and Kumamoto (1994).

Two further avenues may be explored with the availability of increasing computational power. One is large eddy simulation (LES) where the larger eddies are calculated directly and only the smallest ones are computed using Reynolds-averaging and turbulence modelling. This approach should reduce the error produced in calculating blockage and losses due to poor turbulence modelling. Although this method has been tried for research purposes, it is beyond the scope of routine calculations. The second possibility, which is probably one of the ultimate goals in CFD, is the direct solution of the full Navier-Stokes equations without any averaging. However, this approach obviously requires grids fine enough to capture the smallest eddies and probably requires around a 10^9 fold increase in computational power than is currently available from the fastest machines for high Reynolds number flows.

2.3 NUMERICAL STRUCTURAL DYNAMICS METHODS

In 1924 Campbell (1924) presented his landmark study of vibration in steam turbine bladed discs. He identified three different modes in which discs may vibrate: these are lateral waves around the disc edge with nodal contours forming diametral lines (nodal diameters); concentric circles (nodal circles); or hybrid modes which have both nodal diameters and circles. These mode families are strongly affected by the rotational speed in the case of rotor discs. Real turbomachinery bladed discs are complex structures with variations in material properties (due to temperature effects), joints between the blade and disc, and possibly between blades (which leads to non-linear damping at these interfaces), and small imperfections in the manufacturing (which lead to 'mistuning').

Mathematical models of structural dynamics in general, and bladed discs in particular can be divided into two areas, continuous and discrete models. Also, for a given model, there are different ways of solving the equations of motion, using various numerical techniques. This section outlines some of the most popular models that have been used in this application.

2.3.1 Equations of Motion

The equations of motion for structural dynamics can be written in two basic ways: these are by resolution of dynamic forces and moments (Newtons Laws, D'Alembert's principle), or by balancing the different forms of energy present in the system (virtual work, Lagrange's Equation, Hamilton's principle). However, for a particular model, no matter how the equations are derived, the same equation of motion should result, given the same assumptions. The most widely used models, split into their two categories as described above, are described in turn.

2.3.2 Models

Continuous Models

Continuous models are useful for particular cases, where an analytical solution may be derived. Thus these special cases can be used to check the validity of numerical models, whereas for more complex cases, approximate solutions may be available. Continuous systems are not inherently different to discrete models, described below, other than that they possess an infinite number of degrees-of-freedom, and the same techniques may be applied. One of the first methods to be applied to bladed disc vibration was closed-form receptance coupling, by Armstrong (1967), and Bishop & Johnson (1960). This method uses Euler or Timosenko beam theory (Bernoulli beam) to model the blades, which are then coupled to the disc through their receptances. This model, although simple, has proved useful, and has been further improved by Ewins (1973), and Cottney & Ewins (1975). These models were useful principally for obtaining the dynamic behaviour of blades.

Conservation of energy principles can be applied to continuous models; for example the same case as above (Bernoulli-Euler beam with a circular disc) can be formulated using the Rayleigh-Ritz method instead of receptance coupling as above. The complete energy equation cannot be solved, however an approximate solution can be obtained by substituting trial functions based on modal synthesis (this is the essence of the Rayleigh-Ritz method). In this way the equations of motion are formed, and can be solved in the standard ways, as described below. Thus the models are capable of

being extended to model bladed discs. With advances in computer power, there models have largely been superseded, but they are still useful for basic studies.

Discrete Models

Discrete models are formed by splitting a structure into small elements, which consist of lumped masses connected by massless elastic elements. Thus the equations of motion could be derived by writing down all the compatibility and dynamic relations for all the degrees-of-freedom. However this would involve an unnecessary amount of algebra; a much neater way is to use the transfer matrix method, originally used for bladed-discs by Thomson (1950). This method expresses the properties of each section in matrix form , whereupon they can be related to each other. This method has not been widely used for bladed discs in itself (although it has been used in rotor dynamics), but it is important in that it showed what could be achieved by discretising techniques. Also the model was relatively compact, so it could be computed with the limited power then available.

A most useful, and yet simple discrete model has been the mass-spring-damper model (lumped parameter model). This method uses relatively few degrees-of-freedom to describe the system (e.g. one mass per disc sector, and one per blade). However the parameters in the model are usually chosen by identifying modal parameters in the real structure, and choosing the values of mass and stiffness so as to arrive at the correct bladed disc natural frequencies. Due to its simplicity, it has been used in studies where other aspects of the calculation are computationally expensive e.g. aeroelasticity (Ballhaus & Goorjian (1978), Abdel-Rahim et al. (1991)) or mistuning studies (Dye & Henry (1969), Afolabi (1988)).

The finite element technique is a class of Rayleigh-Ritz method, where the trial functions (or shape functions as they are known) are piecewise continuous. The structure is first discretised into a large number of small cells (known as finite elements - FE). The shape functions are polynomials, with their order usually depending on the number of nodes per element. The equations of motion are derived using matrix methods, which then can be solved by methods outlined below. The advantage of this method is that libraries of standard elements have now been developed for a wide range of problems, and numerical methods of solution have been highly developed for solution on modern digital computers. However, for bladed discs, it is still not usual to solve the entire 3D assembly, as this would require a large amount of computational power. Instead, the technique that can be used for bladed discs is that of cyclic symmetry (which is usually the case) which involves taking

advantage of the rotational symmetry, and only solve one disc sector, with its blade attached. Then the bladed disc modes can be calculated by specifying each nodal diameter number in turn.

For non cyclically symmetrical structures, the technique of sub-structuring can be used. Here the model is split into two or more parts, which are solve for separately using the FE method. Then the characteristics of the whole structure can be determined by using component mode synthesis. Fuller descriptions of the Finite Element method are given in Zienkiewicz and Taylor (1989) and Meirovitch (1980).

2.3.3 Methods of Solution

Structural dynamic equations of motion are usually solved in the frequency domain. Such methods are fundamentally linear, although non-linear terms can be accommodated by considering them as a source term on the right hand side of the equation. The solution proceeds by assuming that the response is harmonic (i.e. consists of linear combination of sinusoidal motions at fixed frequencies). Then the second order differential equations reduce to a first order eigenvalue problem which can be solved by well known matrix methods such as Gauss-Seidel, Cholesky decomposition etc. A second type of frequency domain method is known as the harmonic balance method. This can be used to determine the response of a structure due to an external loading even in the case of non-linearity. It is based on finding linear coefficients which are representative of the dynamics of the structure, and in general depend on amplitude and frequency (known as describing functions). This method has seen quite widespread use, but depends on knowing the forcing explicitly.

A second possible approach is to convert the N second order equations into $2N$ first order equations - this is known as the state-space method. Instead of finding the solution as a function of the displacements alone, a state-space vector is defined in terms of the displacements and velocities. Then the equations can be solved by using a convolution integral. This method is described in more detail in section 3.4.

The third common approach to the solution to the equations of motion is time-marching. This is usually only used when there are significant non-linearities, or the frequency response of an external load is hard to determine (whereas its time-varying value is not). This is due to the fact that time-domain solution methods are considerably more expensive in computer time than their frequency domain counterparts. There are many possible time-marching schemes, and they will be covered in great detail in section 3.4.

However, due to the size of problems encountered, it is not uncommon to have models with many tens of thousands of degrees-of-freedom. Due to this fact various reduction techniques have been established to facilitate the solution of large problems. One that has already been mentioned above is substructure coupling. This involves splitting the model into its different sub-assemblies (if this is possible), and obtaining a dynamic model for each in turn (e.g. Craig & Bampton 1968). Then the model for the entire assembly can be obtained by techniques such as receptance coupling. The next possibility comes from the fact that the modeshapes of a structure are orthogonal - thus they uncouple the equations of motion into N uncoupled equations. Thus it is possible to neglect modes that are of no interest, or that are not excited in the problem under consideration - this is known as the assumed modes method and will be described in more detail in section 3.2. Finally, another possible alternative is to select a number of master co-ordinates from the full model of the structure - the rest becoming slaves. Then the dynamic response of the structure can be obtained in terms of the master co-ordinates only (e.g. Guyan (1965)). A number of reduction techniques will be discussed further in section 3.2.

This brief survey of structural dynamics would not be complete without mentioning Modal Testing. This is the process whereby a mathematical model is derived from the actual test data by extracting the system parameters from the measured response functions. The main testing procedures used are hammer testing and shaker testing. In the former the structure is excited by an impulse at a point, and the response at other points is measured as a frequency response function; in the latter the input force is usually sinusoidal such that its frequency can be varied. After the vibration testing, the results can be post-processed to identify the modeshapes and the natural frequencies of the structure. Then these data can be correlated with the FE model (a stage facilitated if the same co-ordinates are used both in testing and in modelling). Finally, as the FE predictions invariably differ from the experimentally-derived results, new techniques, known as model updating, are being used to correct the FE model in the light of the measured data.

Non-linear Structural Effects

In a turbomachinery environment, the existence of non-linear structural effects cannot always be ignored. These may come about due to friction damping in joints and blade roots, high temperature effects, centrifugal forces due to rotation (which in mathematical terms is geometrically non-linear), or advanced materials which have non-linear and anisotropic properties. Non-linear contributions which are large enough not to be neglected, must be incorporated into the structural model. Research

has been conducted into some of these areas, especially friction damping which is important for controlling blade forced response.

Mistuning

During the 1970s, the understanding of the dynamics of cyclic symmetric structures was further advanced by Ewins (1973), Srinivasan (1976), and Ford and Foord (1979). Substantial work was also done to understand the effects of small differences between the nominally-identical blades of a same stage, or mistuning (Ewins, 1976, 1991). Mistuning destroys the cyclic symmetry and hence no constant inter-blade phase angle can any longer exist between the blades. Mistuning is of particular importance in aeroelasticity analyses since it is believed that it has a stabilising effect on flutter stability. Investigations by Whitehead (1966b & c), Imregun and Ewins (1984) and Kaza and Kielb (1982, 1985) indicate that mistuning has an overall stabilising effect. However, in these studies, the aerodynamic part of the cascade model assumes a fixed inter-blade phase angle, the mistuning being introduced into the structural part of the model only. An accurate analysis of this stabilising effect will require both a non-linear aeroelasticity model and the modelling of a whole annulus.

Although the conjecture of the stabilising effect of mistuning is supported by both experimental and anecdotal evidence, the idea of using deliberate mistuning as part of the standard design process was not pursued by the aeroengine manufacturers. However, in other industries there are situations where prescribed mistuning was used, mainly to cure a specific problem. One such reported case is the so-called mix-tuning, the use of alternate mistuning, by Westinghouse in a steam turbine (Scalzo et al. 1986).

In any case, all bladed-disks possess a certain amount of inherent mistuning and hence the introduction of further deliberate mistuning may be questionable as an optimum pattern would need to be found. Such a prescribed mistuning pattern is likely to create serious production problems, and, more alarmingly, a significant loss of cyclic symmetry may well cause increases in blade forced response levels and hence blade stresses, as well as aerodynamic losses. The traditional way of investigating such effects of mistuning is via a deterministic approach in which predetermined configurations of mistuned assemblies are studied directly (Dye and Henry 1969, Ewins and Han 1984). More recent research is focused on statistical analyses (Sinha 1986, Wei and Pierre 1990, Sanliturk et al. 1992, and Yiu 1995).

2.4 AEROELASTICITY METHODS

The potentially disastrous effects of fluid/structure interaction are not new problems in the field of aerospace engineering. The problem of wing divergence was obvious to early aircraft designers in that it caused a number of unexpected crashes. However, early attempts to cure the problem usually involved structural stiffening with little understanding of the aeroelastic nature of the problem. A history of aircraft flutter can be found in the review article by Garrick and Reed (1981). The development of aeroelasticity methods for specific turbomachinery applications started in the early 1950s but the scale of the problem is such that after some forty years of focused and innovative research, there are still no established numerical methods that can routinely predict flutter stability.

Broadly speaking, aeroelasticity analyses can be divided into classical and integrated methods, the former ignoring the interaction between the fluid and the structure, and the latter attempting to model it (**Figure 2.1**). It is now proposed to examine these techniques in more detail.

2.4.1 Classical Methods

Classical aeroelasticity methods are those where the fluid and structural domains remain uncoupled in such a way that the fluid flow does not effect the structural response, and a prescribed (often rigid) blade motion is used. Such methods thus split an inherently coupled non-linear phenomenon into two separate linear and uncoupled analyses.

One of the key developments in early turbomachinery aeroelasticity is due to Lane (1956) who introduced the concept of inter-blade phase angle: the individual blades in a cascade can be assumed to vibrate with the same amplitude but the maximum is reached with a constant phase lag, the so-called inter-blade phase angle. Armed with Lane's assumption, some of the first cascade aeroelasticity methods were formulated by Whitehead (1966a, b). The structure and the fluid were decoupled so that a free vibration problem (taking no account of the aerodynamic loads) could be solved first. Then the predicted modeshapes were used with an arbitrary amplitude to calculate the unsteady aerodynamic forces, from which a measure of stability was inferred.

Such methods became popular for three main reasons. Firstly, assumptions had to be made in order to solve the otherwise intractable governing differential equations with limited computing power. Secondly, some aeroelasticity problems, especially those involving low speed external flows, may not require coupled solutions, as the motion

of structure is well defined by a particular mode of vibration that remains almost unchanged by the fluid. Thirdly, there has been relatively little cross-fertilisation across structural dynamics and aerodynamics and the tendency has been to use existing aerodynamic or structural codes with minimum changes in order to accommodate one another. However, the methods were found to be of limited use when applied to turbomachinery cases where a number of non-linear effects and strong structure/fluid coupling may exist. Designers thus tended to rely on existing empirical correlations (AGARD Manual (1985)), and remedial actions were taken in the light of test rig data.

Although most of the earlier uncoupled methods rely on simplified aerodynamic theories for incompressible inviscid flows, the more recent ones use linearised flow equations, a simplification that is not guaranteed to capture some important features such as shocks and flow separation. This is especially a problem in turbomachinery blade-rows where an accurate representation of the shock strength and position is crucial for flutter predictions. However, some of the methods have been successful for certain applications and it is worth reviewing some of the major techniques.

Actuator Disc Theory

Actuator disk representations are simplified forms of linearised aerofoil and cascade theories, based on the fundamental assumptions of low reduced frequency and small interblade phase angle (Whitehead 1959). An important variant is the semi-actuator disk theory where the restriction to small frequencies is relaxed (Tanida and Okazaki 1963). The method was improved and adapted for 2D unsteady compressible flow by Adamczyk and his co-researchers (Adamczyk (1978a), Adamczyk et al. (1982)). The actuator disk model predicts the unsteady aerodynamic forces as a function of the steady flow field and the dynamic response of the cascade. The field equations used in this case are the linearised potential equations, and viscous and stalling effects are included via experimentally derived quasi-steady loss coefficients. Thus different values should be derived for each new geometry, however, it is not unusual to use the original coefficients for a wide range of blades. For this method, as with other classical methods, the inter-blade phase angle must be assumed for each calculation. In any case, best results are obtained when both the inter-blade phase angle and the frequency parameter are small. In the absence of viable alternatives, the method has seen quite widespread use in the turbomachinery field and, reportedly, gives acceptable predictions for supersonic types of flutter. However, the main drawback is that the method requires 'tuning' to each particular type of problem, and its

performance would be poorer for transonic stall-flutter, for example, where viscous effects are known to be important.

Indicial Method

The indicial method was proposed by Ballhaus and Goorjian (1978), and further explored by Ueda and Dowell (1984) and Stark (1984). It uses transonic small disturbance (TSD), or linearised potential equations to compute the unsteady forces acting on an airfoil in transonic flow. The fluid response due to a step change in the airfoil position is computed first and the response to any other prescribed motion is obtained via the convolution integral using this initial result. The airfoil motion is assumed to be simple harmonic so that the aeroelastic equation of motion can be solved by standard matrix techniques once the aerodynamic forcing terms are known. The method has the advantage of predicting the flutter boundary over a range of conditions from only one set of time-marching fluid calculations. Since it is assumed that the fluid equations are linear so that the superposition of responses is valid, the applicability to turbomachinery calculations is questionable, though Ueda and Dowell (1984) extended the method to include the non-linear effects in an approximate manner.

Aeroelastic Eigensolution Method

The aeroelastic eigensolution method has been by far the most popular of the classical flutter stability analyses. It is based on obtaining the linearised harmonic unsteady aerodynamic coefficients for the motion of a freely vibrating structure. The unsteady aerodynamics can be provided by anything from empirically-determined section lift and moment coefficients, through various cascade theories, to linearised potential methods. The structural model is often restricted to a two-degree-of-freedom typical (rigid) section representation but the formulation is general so that three-dimensional descriptions can also be accommodated. Once determined, the aeroelastic forces are expressed in the frequency domain, either directly if analytical theories are used, or by Fourier analysis if the forces were first calculated in the time domain. However, the resulting system matrices may well become a function of the frequency, in which case the eigenproblem is no longer mathematically linear. In this case an engineering solution can be found using iterative techniques. Thus, the stability of the system is assessed by considering the amount of damping in each mode or by calculating the overall damping in the system.

Wing flutter cases were studied by Yang et al. (1980, 1982), Guruswamy and Goorjian (1984, 1985), Lee (1986), and Dunn et al. (1992) while a rotor blade case is

presented by Friedmann (1977). One of the main advantages of the method lies in its simplified representation of the structural dynamics (usually a lumped parameter model), which allows parametric studies to be conducted with minimum computational effort. Various cascade cases were studied by Tadros and Botman (1981), Bendiksen and Friedmann (1982), Srinivasan and Fabunmi (1984), Imregun and Ewins (1984), Bendiksen (1986), Kielb and Kaza (1985), Kielb and Ramsey (1989), Smith and Kadambi (1991), Klose (1992). Variations of this method were also studied by Lee (1986) and Williams, Cho & Dalton (1991). The shortcomings of the aeroelastic eigensolution method, as well as an alternative solution technique using aeroelastic frequency response functions, are discussed by Imregun (1994).

A further variant of the aeroelastic eigensolution method is to base the aerodynamic calculation on free vibration mode shapes, such as the panel method used by Cebeci et al. (1992). However, this approach is limited by the simplifications that the aerodynamic model must undergo in order to be compatible with the frequency-domain calculations and it may not be appropriate for turbomachinery applications.

State-Space Representation

This method was first introduced by Karpel (1982) and further investigated by Batina and Yang (1984), and Leishman and Nguyen (1990). The aeroelastic model consists of a set of structural modes and of airloads calculated using linearised unsteady aerodynamics (usually potential) theories. The generalised aerodynamic forces are approximated using interpolation in the complex s-plane, the process being very similar to that used in the indicial method. The N second-order structural differential equations are reduced to 2N first-order differential equations, a transformation that leads to a first-order state-space model. This last set of equations can then be solved by the convolution integral. The success of the method largely depends on the validity of linearising the unsteady aerodynamic equations and problems may be expected for transonic turbomachinery applications such as fans.

Energy Method

The energy method is based on calculating the sum of the work done by unsteady (linearised or non-linear) aerodynamic forces usually at a number of typical 2D sections, the motion of which is determined from a 3D free-vibration analysis. However, the approach is not restricted to 2D and there are many applications where 3D aerodynamic and structural codes are used by integrating the incremental work over the blade surface. In any case, it is inherently assumed that the flutter behaviour is linear, negative work indicating instability. The application of the energy method to

real cases requires a number of educated guesses and a large amount of engineering judgement as the results may well depend on the number of sections used. This method was first adopted by Carta (1967), and later extended by Snyder & Commerford (1974) and, Mikolajczak et al. (1975). Also, Takahara et al. (1980) used an Euler code to investigate stall flutter in cascades.

This approach and its many variants represent more or less the state-of-the-art in turbomachinery flutter analysis in aerospace industry because of both their simplicity in formulation and their compatibility with section-by-section design procedures. However, the fluid and structure domains are still treated as two separate media without any attempt to model the coupling between them. 3D methods along these lines have also been used, e.g. Hall and Lorence (1992) and He (1993).

2.4.2 Integrated Aeroelasticity Methods

Integrated aeroelasticity methods are those that do not uncouple the fluid motion from that of the structure, but attempt to treat the problem of aeroelasticity in one continuous medium. The need for such an approach arises from the non-linear response of fluid flow to the motion of solid boundaries, especially at transonic flow speeds for which flutter often occurs, and the existence of non-linear structural effects such as friction damping in the blade roots and shroud interfaces. The non-linearity in transonic flutter has been shown for wings e.g. Edwards et al. (1983), and is thought to be potentially important for turbomachinery. It has yet to be conclusively demonstrated when linear methods can be applied, and when not and good experimental evidence is currently lacking (possibly due to commercial sensitivity). Nevertheless, some discussions on the non-linearity of turbomachinery aeroelasticity is given in Chi & Srinivasan (1985), and in the stall flutter chapter of the AGARD Manual (1985). Thus the mathematical formulation needs to be devised in such a way that the fluid is allowed to modify the structural motion, and vice-versa, as the phenomenon occurs in nature. It then becomes possible to include non-linear effects for both the fluid and the structure and take into account various interactions that can take place between them. The most striking difference between the classical methods and integrated ones is that the former can only predict the onset of flutter as a sudden change from a stable to an unstable region while the latter are capable of predicting limit cycle behaviour. The engineering value of such methods is evident since there is enough experimental evidence to suggest that flutter occurs in pockets of limit cycle with varying amplitude levels. This observation has a crucial implication on flutter analyses: the prediction of the flutter onset may not be as important as predicting the actual vibration amplitude since limit cycles can be tolerated if the amplitude is small.

Indeed, it is quite possible that many existing designs experience a number of very small amplitude limit cycles that are not detected by monitoring equipment.

As with classical flutter analysis methods, different formulations are possible for the integrated methods.

2.4.2.1 Partially-Integrated Methods

The partially-integrated method involves the solution of the fluid and structural equations separately but information is exchanged at each time step so that the solution from one domain is used as boundary condition for the other domain. In other words, a new blade position is calculated at each time step using the fluid forces of the previous time step and this new position is used as the new fluid/structure boundary for the next time step when the aerodynamic forces are computed first. Within this general framework, there are a number of possible approaches that will be described below. Some of these have been used extensively, especially for wing flutter; whereas others are relatively untried.

Reduced Modal Equations

The reduced modes method was developed in the late 1970s for transonic wing flutter - Ballhaus & Goorjian, (1978). The aerodynamic model is usually based on (but not restricted to) transonic small disturbances while the structural model comes from a finite element analysis of the free-free structure. The structural model can be determined by experimental modal analysis (system identification), Rayleigh-Ritz methods, or by the finite element method. Only the modes of interest (usually the first five or so) are retained in the problem, the higher modes being considered to be beyond the frequency range at which flutter is expected to occur. Thus, the response of the structure is calculated as the superposition of these orthogonal modes, the so-called modal summation technique. It is more common to expand the structural data onto the aerodynamic mesh rather than to reduce the aerodynamic mesh to the size of the structural one. The solution to the aeroelastic equations of motion is sought in the time domain with constant diagonal mass, stiffness, and damping matrices which are expressed in principal co-ordinates so that the structural part can be dealt with in the most efficient manner. The dependent variables in the aeroelastic equations of motion then become the modal variables, rather than the spatial variables. The mapping takes place at the start of the computation, and not at each time step, a feature which reduces the computational effort further. Since there is exchange of information between the structure and the fluid, the model can be used to predict limit-cycles and divergence, the computing power required being dictated by the CFD technique employed.

A number of different ways have been proposed for integrating the aeroelastic equations of motion in modal or principal co-ordinates. Ballhaus and Goorjian (1978) put forward a simple first-order-accurate time integration technique for their 2DOF model which was also used by Wu (1987). Rizzetta (1979) used the Adams-Moulton predictor-corrector technique while Borland and Rizzetta (1982), and Sisto et al. (1991) tried a central-differencing type solution. However, these methods are now superseded by at least two recent developments. The first one, which is a member of the Newmark-β family of integrators, uses a linear variation of the acceleration to determine the velocities and accelerations at the end of each time step. (Guruswamy and Yang (1981), Yang and Batina (1983), Guruswamy and Goorjian (1987, 1988), Guruswamy (1989, 1990), Bakhle et al. (1992)). The second one, proposed by Edwards (1983), uses linear system convolution integrals to solve the state equations resulting from the aeroelastic equations of motion rewritten in a linearised form. Variations of this latter approach have subsequently been used by Berry and Batina (1986), Gallman et al. (1988), Cunningham et al. (1988), Batina (1989), Rausch et al. (1990), Robinson et al. (1991), Bendiksen and Kousen (1987), Kousen and Bendiksen (1988, 1989), Yang and Zhao (1988), and Vahdati and Imregun (1994).

Periodic Mode Updating Method

This method, recently proposed by Gerolymos (1992b), is a hybrid between classical and partially-integrated aeroelasticity methods. It is similar to the aeroelastic eigensolution method but it uses non-linear time-marching, albeit with a prescribed blade motion. A free vibration problem is solved in the frequency domain and the mode shape of interest is used to describe the blade motion for one period using a 3D time-marching non-linear CFD code. The mode shape is then updated using aerodynamic coefficients which were calculated in the previous period, via a frequency-domain structural calculation based on modal projection. This cycle of time-domain aerodynamics, followed by frequency-domain structural dynamics is repeated until the mode calculated in the frequency domain converges. The likelihood of flutter is determined via an energy calculation based on the work of the aerodynamic forces. The method is probably better suited to full 3D analyses to avoid excessive interpolations but it cannot predict a limit cycle behaviour as the blade motion is prescribed and not computed independently. However, the technique has an advantage in that it is computationally much less expensive than other 3D fluid/structure time-marching methods.

Structural Reduction Methods

A reduced set of mass and stiffness matrices (Guyan 1965) are used to obtain a time-accurate solution for the structural motion, the main idea being the condensation of the structural model for efficient numerical treatment when it is not desirable to use principal co-ordinates. Certain nodes in the structural model are thus identified as masters, the rest becoming slaves. Although the nodes common to both structural and aerodynamic meshes would constitute the most convenient masters, they would not necessarily the best ones to choose from a reduction algorithm viewpoint. Once a selection is made, the equations are re-arranged so as to solve for the motion of the master nodes only and hence the size of the system can be reduced dramatically, with the added benefit of relaxing the time step. In this way, the structural motion can, in principle, be non-linear but the task is not straightforward since the connectivity information is lost with almost all reduction techniques.

Using this method, a number of hybrid schemes can be devised where more fluid time steps are shorter than the structural ones, depending on the individual discretisations of the two domains. Also, the interpolation effort can be reduced by using as many co-incident nodes as possible.

Full Time-Marching Method

As the name implies, such a method involves using time-marching for both structural and fluid calculations and the structural model can be used in its entirety, without a principal co-ordinate representation or a reduction in size. In this way, it is possible to include all type of structural non-linearities (friction damping, non-standard material properties, etc.), including geometric ones that arise under the centrifugal loads. The solution is advanced in time by calculating the structural motion resulting from the fluid pressures calculated at the previous time step, and then the fluid calculation is updated based on that new position of the structure. Thus, this method can utilise any combination of fluid/structure code, as long as both codes employ time-marching and are compatible in the number of variables used. The structural model can be assembled at the global or the local level, whichever is more convenient for the integration technique employed. The main drawback is the computational cost, not only due to time-marching but also to the interpolation of data between the two domains at each time step. However, if the method is used for static aeroelasticity calculations, it is not imperative to retain the time-accuracy as only the final equilibrium position/shape is of importance, unless of course instabilities are likely to be encountered along the way.

Cases studies in static aeroelasticity have been discussed by Tatum and Giles (1988), Srivastava et al. (1991), and Yamamoto (1992). Gea et al. (1992) have applied a similar approach to helicopter rotors using linearised-potential aerodynamics.

2.4.2.2 Fully-Integrated Methods

Fully-integrated methods differ from their partially-integrated counterparts in the discretisation and subsequent numerical treatment of the governing equations. However, both techniques should approach the same solution as the time step approaches zero.

Fully-integrated methods are based on formulating the structural and fluid dynamic together so that they can be solved at each time step using the same integrator. This is done by discretising the two domains into one arbitrary Lagrangian-Eulerian space: the consequence of this is that the motion of the grid becomes an integral part of the equations of motion and does not have to be handled separately. At least two distinct methods can be found from the published literature.

Direct Method

The direct method is due to Bendiksen (1991) who applied it to both wing and turbomachinery blade flutter. It uses an explicit temporal discretisation which is integrated using a five-stage Runge-Kutta scheme and upwind differencing is used for the spatial discretisation of the arbitrary Lagrangian-Eulerian formulation of the aeroelasticity equations. The structural equations are formulated on a local nodal level which enables them to be discretised using the same five-stage Runge-Kutta integrator. Thus the integrator can handle both sets of equations simultaneously at the same time step without distinguishing between the fluid and the structure. This model is claimed to calculate the energy transfer between the structure and the fluid more accurately then similar partially-integrated schemes since there is no possibility of a time-lag between the structure and the fluid.

Iterative Method (ICED-ALE)

The implicit continuous-fluid Eulerian (ICE) arbitrary Lagrangian-Eulerian (ALE) method can be considered to be an extension of the finite element technique for studying fluid-structure interactions, especially those in the nuclear industry (Hirt et al. 1974 and Donea et al. 1982). In spite of being pressure-driven, it is applicable to all flow speeds but problems can be anticipated for transonic regimes. The basic method uses a semi-implicit time-marching algorithm, with a semi-staggered spatial discretisation model that defines fluid velocities at cell vertices, and pressures at cell

centres. The solution is advanced in three stages: explicit Lagrangian, implicit pressure calculation and convective flux convection. The pressure calculation is performed iteratively, hence the name of the method. The structural dynamic solver is brought in to the explicit Lagrangian stage, and can use any spatial or modal description of the structure. More recently these methods have been used in commercial software, using the techniques of Hughes et al. (1981) or Farhat et al. (1995).

2.4.3 Methods for Forced Response Prediction

Although substantial progress has been made, both in the definition of flow defects (such as wakes), and in unsteady flow models to predict the unsteady forces resulting from disturbances, further experimental work is needed for the validation of the existing models, and perhaps for the development of empirical models. The paper by Chiang and Kielb (1992), which presents an industrial design prediction system for forced response, also reviews much of the research in this area.

Classical forced response models for cascades of flat plates are based on wake coefficients which are usually scaled to some arbitrary constant so that representative response levels are obtained (Whitehead (1970), Whitehead & Nagashima (1977)) Such models are also capable of handling potential disturbances. Linearised models (e.g. Hall & Clark (1991) and Holmes & Chuang (1991)) have also been used to predict forced response. These methods solve the linearised field equations (potential or Euler) to obtain the unsteady pressures acting on the blade due to the incoming disturbances. The state-of-the-art is to solve the fully non-linear Euler or Navier-Stokes equations for the blade row of interest, and to simulate the disturbance (wake or potential) moving past at blade passing velocity. Hodson (1984) and Giles (1988) used the inviscid Euler equations to predict wake-rotor interaction. Similar work is also reported by Fransson & Pandolfi (1986) and Gerolymos (1988). A full stator-rotor interaction model using Navier-Stokes equations was developed in 2D by Giles (1990), and in 3D by Rai (1987). Results from some of the models above are compared to experimental data in the paper by Manwaring & Wisler (1992).

2.5 EXPERIMENTAL DATA

The lack of reliable and well-documented experimental data for the evaluation of turbomachinery aeroelasticity methods continues to be a major problem. The ideal measurement system would need to be completely non-intrusive to be able to measure the coupled fluid/structure response to the required degree of accuracy, including perhaps a limit cycle amplitude. However in practice this is almost unattainable

considering the compact nature of turbomachinery flows: contacting measurement devices, such as strain gauges, seem to be the only way to get a description of the mode shapes but this type of instrumentation tends to change both the flow and the structure and invariably affects the aeroelastic response. Non-contacting measurement techniques, such as blade tip-timing, are probably better suited to obtain time histories at a specific near the blade tip but the interpretation of the laser probe signal is not always straightforward. Also, the current technology does not allow for obtaining measurements at various position along the blade height. Although tests are routinely conducted by engine manufacturers, even when the flutter boundaries are known with good accuracy, the information about the flow characteristics and the modes of vibration tends to be patchy.

A large body of published data exists for steady turbomachinery flows, though it is not altogether certain whether such flows can ever be truly steady. The experimental results for the NASA Rotor 67 are documented in Pierzga & Wood (1985). In these particular cases, the instrumentation is almost non-intrusive through the use of laser inferrometry and holography techniques. A great deal of work is currently being done to validate 3D Navier-Stokes codes with data such as these, with emphasis on the turbulence modelling (e.g. Dawes (1987), Turner & Jennions (1992)).

The picture is not so promising in the case of unsteady flows, especially those with oscillating blades. There is a reasonable body of data for isolated rigid aerofoils that are driven by some external device but there is no relationship between the structural modes and the excitation frequency (Visbal & Shang (1989), He and Denton (1991b)). The data are thus more suitable to validate simplified unsteady aerodynamics codes than aeroelasticity methods. Self excited oscillations have been investigated by Yamamoto and Tanida (1990), and the effects of aerofoil flexibility have been studied by Greenhalgh et al. (1984).

Unsteady flow measurements in cascades are much more difficult because of the added complication of interacting aerofoils. 2D section data have been obtained on both linear and annular cascades, albeit with rigid, structurally unrepresentative blades that are driven externally. Published flow data, usually in the form of pressure distribution along chord, include the investigations by Kovats (1980), Davies and Bryanston-Cross (1985), Shaw et al. (1986), and Namba and Toshimitsu (1993). Useful benchmark data, which became a de facto standard for unsteady cascade flows, can be found in Bölcs and Fransson (1985) for the EPFL series of standard configurations. The geometrical and time-averaged flow conditions of nine two-

dimensional and quasi three-dimensional experimental turbomachinery-cascades are presented in detail. A number of aeroelasticity cases, consisting of sets incidence angles, Mach numbers, interblade phase angles, reduced frequencies, etc., are defined for each configuration. However, the blades are rigid and the unsteadiness is due to the cascade being driven externally at some arbitrary excitation frequency. Another important feature of the work are the detailed comparisons between 15 prediction methods and experimental data from the standard configurations.

Unsteady flow measurements in the form of unsteady pressure data, obtained from actual engine and/or rig tests have been reported by Halliwell et al. (1984), Srinivasan and Cutts (1985), and Crawley and Ducharme (1990). However, genuine aeroelasticity data obtained for 3D rotating geometries near or at a flutter regime are almost non-existent for a variety of reasons. First, it is very difficult to measure parameters of interest without modifying the characteristics of the system. Second, regulations would not allow a real engine to spend enough time at or near flutter regime, data can thus only be recorded before the onset of the instability. Third, the inlet and exit conditions can rarely be recorded to a desired degree of accuracy and hence a number of assumption need to be made when defining the input conditions to the theoretical model. Finally, the manufacturers would be more than reluctant to publish such useful data even if they were available.

2.6 CRITICAL REVIEW OF THE STATE-OF-THE-ART

(i) It is clear from the literature that a large number of approaches have been tried by different researchers in attempting to solve various turbomachinery aeroelasticity problems. Early attempts were dominated by the need for computational efficiency albeit at the expense of oversimplifying the physics of the fluid/structure interaction. It is now possible to obtain 3D unsteady viscous solutions for representative geometries but we are still not in a position to be able to ignore the computational costs as our expectations and demands increase even faster than routinely available CPU power.

(ii) The success in flutter prediction has not been commensurate with the advances in CFD or structural analysis methods, most aeroelasticity prediction tools suffering from an inappropriate combination of fluid and structural models. It is not unusual to couple a 2 degree-of-freedom rigid section aerofoil with a viscous time-domain representation of aerodynamics, or a very large finite element model with classical linearised aerodynamic theories. Furthermore, the aerodynamic and structural analyses are usually kept separate from each other with no aerodynamic feedback into the

structural motion and vice-versa, a route that does not allow an accurate modelling of the energy transfer between the two media.

(iii) Broadly speaking, the aeroelasticity analyses can be subdivided into two classes: classical and integrated. The former combine the fluid and structural equations in an uncoupled fashion while the latter attempt to solve the equations together by either exchanging information at each time step (partially-integrated) or by formulating the aeroelasticity problem in a single unified fluid/structure medium (fully-integrated).

(iv) The major advantage of partially-integrated methods is that they are independent of the CFD code used so that they can provide a basic framework onto which new developments can be added as they emerge. Some of the basic ideas have already been tried in the field of wing flutter with clear improvements over classical methods.

(v) Fully-integrated methods may prove to be the best tools in the long term, but they are relatively untried, and therefore they may require a great deal of development. This is due to the highly integrated finite-volume nature of the combined fluid and structural equations. Since most structural representations are based on a finite element formulation, an incompatibility exists between such fully-integrated models and current industrial practice. However, fully-integrated methods have the advantage of not requiring any interpolation and of not giving rise to time-lags between the structure and the fluid.

(vi) Aeroelasticity methods based on external flows tend to be more advanced than their turbomachinery counterparts since the latter have many extra complications due to interacting blade-rows. Integrated methods that use 3-D Euler or even Reynolds-averaged Navier-Stokes equations for sub-assembly configurations are beginning to emerge and calculations for whole vehicles are being reported. However, such approaches are still relatively uncommon in turbomachinery aeroelasticity where the norm is probably an uncoupled analysis based on 3-D linearised Euler equations.

(vii) The aeroelasticity methods seem to have reached a point where much depends on the available computational power. Theoretically, it is possible to predict the time-accurate flutter behaviour of multi-stage, whole annulus bladed-disk assemblies with non-linear structural models using a fully integrated method. However, it is not clear how the time step should be chosen to balance numerical stability with computational feasibility and how the results of such an analysis could be validated.

Figure 2.1 **Breakdown of Aeroelasticity Prediction Methodologies**

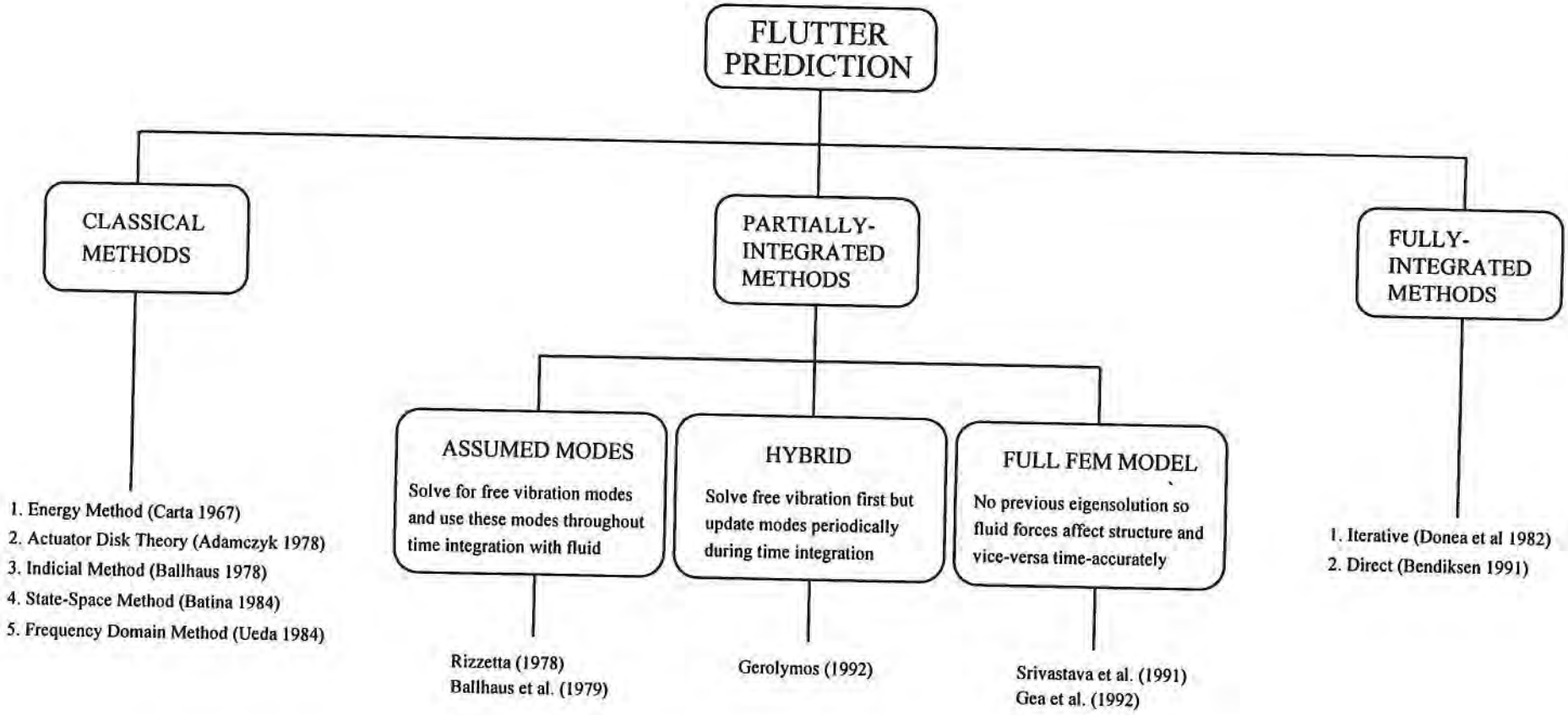

Chapter 3

Mathematical Formulation of Partially-Integrated Non-Linear Methods

3.0 About this Chapter

This chapter discusses the mathematical formulation of partially-integrated non-linear aeroelastic analyses. The partially-integrated method involves solving the governing equations of fluid and structural motion alternately, with information being passed as boundary conditions between the two domains. By solving fluid and structural equations together in a time accurate fashion, the fluid forces affect the motion of the blade and vice-versa, as occurs in reality, rather than assuming a forced harmonic motion. A number of different possibilities exist for the implementation of this method in terms of the numerical modelling, and it is also possible to use different models of the fluid- and structural-dynamics. This chapter outlines the mathematical formulation of a number of methods which were identified as being the most likely to be successful in application to turbomachinery problems.

3.1 INTRODUCTION

A survey of the published literature has been carried out, which outlines previous work that has been done on aeroelastic methods. Based on this, a number of perceived improvements over so-called traditional methods have been identified by adopting an integrated non-linear approach. Integrated methods attempt to take account of any non-linearities in the equations modelling the fluid and structure, and to solve them in a coupled fashion as occurs in reality, which can be achieved by solving the equations governing the fluid and structure together in the time domain. More specifically, partially-integrated methods solve the equations for the two domains alternately and the information about one domain at the end of each time-step is passed to the other domain as a boundary condition for the next calculation. It is also possible to formulate fully-integrated methods, where the equations for the two domains are solved together at each time-step by using the same numerical solver. Traditional methods have tended to treat the coupled problem separately, which may partly explain their relative lack of success.

The following section outlines possible methods for transient structural dynamics. Section 4 describes the fluid modelling, and Section 5 details the partially-integrated method of solution for the aeroelastic problem. Finally, certain aspects of the numerical implementation are discussed, along with the perceived advantages of the approach over other possible methods.

3.2 AEROELASTIC EQUATIONS OF MOTION FOR THE STRUCTURE

3.2.1 Arbitrary Geometry

The aeroelastic equations of motion can be written for an arbitrary geometry, by applying Lagrange's equations. The equations for rigid bodies using the lumped parameter approach can also be derived from Lagrange's equations, but it is easier to resolve the forces and moments for such a simple geometry.

A discrete system, can be fully defined by n independent co-ordinates, known as generalised co-ordinates. However, as most real systems are continuous, and cannot be described by a finite number of co-ordinates, hence some process of discretisation must be employed to reduce the description to a finite number of degrees-of-freedom. The finite element technique, which is a Rayleigh-Ritz method, can be used to discretise the domain. The structure is split into a number of elements (areas in 2D, or volumes in 3D) over which the variation of parameters (e.g. stress, strain) is described by a continuous function of known form (e.g. piecewise-linear, -quadratic) - this is

known as the shape function. Thus the problem has now been reduced to a finite number of variables, namely the values at the vertices of the elements, and the equations of motion can be written in discrete form.

The structure itself can be assumed to be linear, and, in an approximate fashion, any non-linear effects (such as friction damping) can be applied as a forcing term on the right hand side of the equations. For such a system with n generalised co-ordinates, $q_i(t)$, $(i = 1,2,...,n)$, as above, the system kinetic energy, E_k can be written:

$$E_k = \tfrac{1}{2}\sum_{i=1}^{n}\sum_{j=1}^{n}\dot{q}_i m_{ij}\dot{q}_j + E_0 \tag{3.1}$$

where m_{ij} are constant symmetric mass coefficients. The potential energy of the system, E_p, due to elastic and gravitational forces, will be a function of the generalised co-ordinates alone:

$$E_p = E_p(q_1, q_2, ..., q_n) \tag{3.2}$$

Now viscous damping forces, which always exist to some degree in real structures can be approximated as a Coulomb friction force. In such a viscous damper, the rate of energy dissipation is as follows:

$$E_d = \tfrac{1}{2}\sum_{i=1}^{n}\sum_{j=1}^{n}\dot{q}_i c_{ij}\dot{q}_j \tag{3.3}$$

where c_{ij} are constant (usually symmetric) damping coefficients. Remaining external generalised forces that do not fall into the above categories, P_i ,which may include non-linear forces as described above, are given by the following virtual work expression:

$$\delta W = \sum_{i=1}^{n}\int P_i \delta q_i \tag{3.4}$$

where δq_i are the generalised virtual displacements. The system Lagrangian, L, is defined as:

$$L = E_k - E_p \tag{3.5}$$

The equations of motion can then be described by Lagrange's equation:

$$\frac{d}{dt}\left(\frac{\partial L}{\partial \dot{q}_i}\right) - \frac{\partial L}{\partial q_i} + \frac{\partial E_d}{\partial \dot{q}_i} = P_i \tag{3.6}$$

However we are interested in motions about an equilibrium point. If E_p is the dynamic potential energy, the constant (trivial) solution can be ignored, and as the structure is linear and non-linearities only apply through forcing terms, the dynamic potential energy, E_p can be expressed as:

$$E_p(q_1, q_2, ..., q_n) = \tfrac{1}{2}\sum_{i=1}^{n}\sum_{j=1}^{n} q_i k_{ij} q_j \tag{3.7}$$

where k_{ij} are constant symmetric stiffness coefficients. Thus the explicit equations of motion are obtained from putting expressions for E_k, E_d, E_p, & L given in equations (3.1,3,5&8) above into Lagrange's equation (3.6):

$$\sum_{j=1}^{n}\left[m_{ij}\ddot{q}_j + c_{ij}\dot{q}_j + k_{ij}q_j\right] = P_i, \quad (i = 1,2,\ldots,n) \tag{3.8}$$

If we introduce a matrix notation such that:

$$\mathbf{q} = \left[q_i\right] \; \mathbf{M} = \left[m_{ij}\right] \; \mathbf{C} = \left[c_{ij}\right] \; \mathbf{K} = \left[k_{ij}\right] \; \& \; \mathbf{p}(t) = \left[P_i\right] \tag{3.9}$$

the equations become:

$$\mathbf{M}\ddot{\mathbf{q}} + \mathbf{C}\dot{\mathbf{q}} + \mathbf{K}\mathbf{q} = \mathbf{p}(t) \tag{3.10}$$

In the context of aeroelasticity the $\mathbf{p}(t)$ vector of external non-conservative, and possibly non-linear forces will be the vector of aerodynamic loads, calculated by integrating the pressure over the entire structure as it applies to each co-ordinate node. For viscous flows the effect of the viscous stresses acting on the surface of the structure must also be included in the aerodynamic forcing term. The fluid pressures and stresses are calculated using computational fluid dynamics to solve the governing equations of fluid flow - this will be covered in Section 3.

The full structural N DOF model could now be integrated in time, using the physical co-ordinates as the dependent variables in the EOM. The aerodynamic load vector at each timestep would be obtained by interpolating the fluid pressure onto the structural grid, and the force on each surface element will be this pressure multiplied by the area over which it acts. New positions and velocities of each node could be interpolated back onto the fluid grid, to obtain its new position and velocity for the next timestep. This would be the ultimate PI model, however it would be computationally very expensive to implement. However the equations of motion have properties which give the possibility of reducing the computational effort.

3.2.2 Properties of the Equations of Motion

The structural equations of motion have a number of useful properties: one of the most important is orthogonality. If we first solve the undamped free vibration problem:

$$\mathbf{M}\ddot{\mathbf{q}} + \mathbf{K}\mathbf{q} = \mathbf{0} \tag{3.11}$$

Equation (3.11) is solved by assuming harmonic vibration:

$$\mathbf{q} = \hat{\mathbf{q}}e^{i\omega t} \tag{3.12}$$

This leads to an eigenvalue problem:

$$\left[\mathbf{K} - \omega^2\mathbf{M}\right]\hat{\mathbf{q}} = \mathbf{0} \tag{3.13}$$

$$\lambda_r \mathbf{M}\psi_r = \mathbf{K}\psi_r \qquad (r = 1,2,\ldots,n)$$

where: λ_r, eigenvalues, $= \omega_r^2$, square of natural frequencies (3.14)

ψ_r, eigenvectors (modeshapes)

If: $\Lambda = [\mathrm{diag}(\lambda_r)]$ matrix of eigenvalues

$\Psi = [\psi_1, \psi_2, \ldots, \psi_r]$ matrix of eigenvectors (3.15)

The eigenvectors are orthogonal with respect to the mass and stiffness matrices:

$\Psi^T \mathbf{M} \Psi = [\mathrm{diag}(m_r)]$ where m_r is the modal mass

$\Psi^T \mathbf{K} \Psi = [\mathrm{diag}(k_r)]$ where k_r is the modal stiffness (3.16)

If the (arbitrary) eigenvectors are also normalised with respect to the mass matrix, then:

$$\phi_r = \frac{1}{\sqrt{m_r}} \psi_r \qquad (3.17)$$

Now we can define a mass-normalised modeshape matrix $\Phi = [\{\phi_1\}, \{\phi_2\}, \ldots, \{\phi_N\}]$, such that:

$$\Phi^T \mathbf{M} \Phi = \mathbf{I}$$

$$\Phi^T \mathbf{K} \Phi = \Lambda \qquad (3.18)$$

Thus the system response can be expressed as a linear combination of the eigenvectors, ϕ_r (mode shapes), by a new set of co-ordinates, η_r, which are known as principal co-ordinates:

$$\mathbf{q}(t) = \sum_{r=1}^{n} \eta_r(t)[\phi_r] = \Phi\eta \qquad (3.19)$$

However these properties of the equation of motion do lead to alternative ways of formulating the equations for continuous systems (other than the finite element method). The Rayleigh-Ritz method, and the closely-related assumed modes method (which will be described below) represent the motion of the structure at any time by a finite number of selected modes. This is an approximation, but has the advantage of limiting the number of degrees of freedom of the system; this obviously requires prior knowledge of the system as to which modes are important to a particular problem. Thus the *modal* model can be obtained from a finite element formulation, or from a modal test of the structure. Whichever method is employed to formulate the equations, they will still retain the same form as those derived above (3.11).

Thus the aeroelastic equation of motion can be formulated for any real system, although assumptions must be made in the case of a continuous structure. In all cases the equations have the same form - N second order linear differential equations, which in general will be coupled, both through the structure, and through the aerodynamic forcing term. The numerical solution of these equations will be discussed in section 4.

3.2.3 Formulation for 3D Engineering Structures

As described above, models for representative structures with complex features (e.g. blade cores, cooling holes, root fixings) can have many thousands of degrees-of-freedom. This causes two potential problems: the memory required to store all the data; and the CPU time required to solve the equations given the small time-step limits in structures (due to the high wave speed in solids). Thus methods that can reduce the computational effort on the structural side are highly desirable. They are possible because the structural behaviour (totally unlike the fluid behaviour) can be reasonably accurately described by a small number of modes provided interest is confined to the frequency range of the chosen modes. Also the assumption is made that the fluid loading does not change these structural modes - this is justified by the relatively high mass ratios that are typical of turbomachinery aeroelasticity. Two possible methods for reducing the structural computation are outlined.

Assumed Modes Method

This method relies directly on the use of the modal description of the structural dynamics as described above. The assumed modes method, in general, is an extension of the Rayleigh-Ritz formulation, which states that solution of the EOM can be expressed as a series of linearly independent trial functions. In the assumed modes method the trial functions used are the modal vectors themselves, so the deflections at a set of discrete points (which can be the aerodynamic grid points) are expressed as linear combinations of the modes included in the analysis.

Once the eigen solution of Eq. 3.10 is obtained, new co-ordinates, known as principal co-ordinates, can be defined so that the system matrices are diagonalised:

$$\{\eta\} = [\Phi]^T \{q\} \qquad \text{or: } \{q\} = [\Phi]\{\eta\} \tag{3.20}$$

Putting these into the full EOM, and premultiplying by $[\Phi]^T$:

$$[\Phi]^T[\mathbf{M}][\Phi]\{\ddot{\eta}\} + [\Phi]^T[\mathbf{C}][\Phi]\{\dot{\eta}\} + [\Phi]^T[\mathbf{K}][\Phi]\{\eta\} = [\Phi]^T\{\mathbf{p}(t)\} \tag{3.21}$$

So, assuming proportional damping (if damping is a linear combination of mass and stiffness, then the equations remain uncoupled):

$$\{\ddot{\eta}\} + [diag(2\zeta_i\omega_i)]\{\dot{\eta}\} + [diag(\omega_i^2)]\{\eta\} = [\Phi]^T\{\mathbf{p}(t)\} = \Pi(t) \tag{3.22}$$

Now the structural EOM may be reduced to a smaller number of degrees of freedom, m, from the full number of co-ordinates (DOFs) in the FE model, N, by removing high frequency modes, and modes which are not of interest in the aeroelasticity problem. This is possible as the equations have been uncoupled by the modal matrix, and so are independent. The justification for this is that, for aeroelasticity, only the lower modes are of interest. This will reduce the computational expense for the structural

calculation, and also, high frequency modes either cause timestep limitations or are damped out in the structural time integration.

$$[\mathbf{M}]_{N\times N}\{\ddot{\eta}\}_N + [\mathbf{C}]_{N\times N}\{\dot{\eta}\}_N + [\mathbf{K}]_{N\times N}\{\eta\}_N = \{\mathbf{p}(t)\}_N \quad (3.23)$$

Now: $\{\eta\}_N \rightarrow \{\eta\}_m = [\Phi]^T_{N\times m}\{\mathbf{q}\}_N$

$$\{\ddot{\eta}\}_m + \left[diag(2\zeta_i\omega_i)\right]_{m\times m}\{\dot{\eta}\}_m + \left[diag(\omega_i^2)\right]_{m\times m}\{\eta\}_m = [\Phi]^T{}_{N\times m}\{\mathbf{p}(t)\}_N \quad (3.24)$$

This is now an uncoupled *m* DOF equation of motion, with the reduced modal matrix giving the relationship between the physical co-ordinates and the co-ordinates in the equations. The EOM can then be solved by a partially-integrated method as described in Section 5.

Guyan Reduction Method

An approach which does not assume the modeshapes to be constant (i.e. not affected by the fluid loading) is ultimately desirable, where the full effect of the structural motion can affect the fluid flow, and vice-versa.

As described above, the calculation of the structural motion using the full number of co-ordinates in the EOM would be computationally very expensive, and a formulation which reduces the number of DOF of the structural EOM is desirable. One possible method would be to use a very coarse mesh in the FE model, but this would probably lead to very poor resolution of the structure, and the natural frequencies of the model might be far from those of the real structure.

One possible dynamic reduction method is due to Craig & Bampton (1968). Another possible method of reducing the system matrices to a smaller number of DOFs is due to Guyan (1965). This involves selecting a number of co-ordinate nodes in the FE model which are to be 'master nodes' (M), the rest becoming slaves (S). Thus the system matrices can be partitioned as follows (if we can assume damping to be negligible):

$$\left[\begin{array}{c|c}[\mathbf{M}_{MM}] & [\mathbf{M}_{MS}]\\ \hline [\mathbf{M}_{SM}] & [\mathbf{M}_{SS}]\end{array}\right]\left\{\begin{array}{c}\{\ddot{\mathbf{q}}_M\}\\ \hline \{\ddot{\mathbf{q}}_S\}\end{array}\right\} + \left[\begin{array}{c|c}[\mathbf{K}_{MM}] & [\mathbf{K}_{MS}]\\ \hline [\mathbf{K}_{SM}] & [\mathbf{K}_{SS}]\end{array}\right]\left\{\begin{array}{c}\{\mathbf{q}_M\}\\ \hline \{\mathbf{q}_S\}\end{array}\right\} = \left\{\begin{array}{c}\{\mathbf{p}(t)_M\}\\ \hline \{\mathbf{0}\}\end{array}\right\}$$

the only assumption being that $\{\mathbf{p}(t)_S\} = \{\mathbf{0}\}$ (3.25)

If this requirement cannot be met an assumption must be made otherwise there will be an extra unknown - it can be accomplished by choosing slave co-ordinates at which forces do not act, or by interpolating the forces onto master co-ordinates only. Now, if sinusoidal motions are assumed then:

$$\left[\begin{array}{c|c}[\mathbf{K}_{MM}]-\omega^2[\mathbf{M}_{MM}] & [\mathbf{K}_{MS}]-\omega^2[\mathbf{M}_{MS}]\\ \hline [\mathbf{K}_{SM}]-\omega^2[\mathbf{M}_{SM}] & [\mathbf{K}_{SS}]-\omega^2[\mathbf{M}_{SS}]\end{array}\right]\left\{\begin{array}{c}\{\mathbf{q}_M\}\\ \hline \{\mathbf{q}_S\}\end{array}\right\} = \left\{\begin{array}{c}\{\mathbf{p}(t)_M\}\\ \hline \{\mathbf{0}\}\end{array}\right\} \quad (3.26)$$

$$\text{or:} \quad \left[\begin{array}{c|c} [\mathbf{D}_{MM}] & [\mathbf{D}_{MS}] \\ \hline [\mathbf{D}_{SM}] & [\mathbf{D}_{SS}] \end{array}\right]\left\{\begin{array}{c} \{\mathbf{q}_M\} \\ \hline \{\mathbf{q}_S\} \end{array}\right\} = \left\{\begin{array}{c} \{\mathbf{p}(t)_M\} \\ \hline \{\mathbf{0}\} \end{array}\right\} \qquad \text{where: } [\mathbf{D}] = [\mathbf{K}] - \omega^2[\mathbf{M}] \quad (3.27)$$

Now, as we have two sets of equations $\mathbf{q}_S$ can be eliminated, as follows:

$$[\mathbf{D}_{MM}]\{\mathbf{q}_M\} + [\mathbf{D}_{MS}]\{\mathbf{q}_S\} = \{\mathbf{p}(t)_M\}$$
$$[\mathbf{D}_{SM}]\{\mathbf{q}_M\} + [\mathbf{D}_{SS}]\{\mathbf{q}_S\} = \{\mathbf{0}\} \quad (3.28)$$

Eliminating $\{\mathbf{q}_S\}$ gives:

$$\left[[\mathbf{D}_{MM}] - [\mathbf{D}_{MS}][\mathbf{D}_{SS}]^{-1}[\mathbf{D}_{SM}]\right]\{\mathbf{q}_M\} = \{\mathbf{p}(t)_M\} \quad (3.29)$$

If the term $[\mathbf{D}_{SS}]^{-1}$ is expanded:

$$[\mathbf{D}_{SS}]^{-1} = \left[[\mathbf{K}_{SS}] - \omega^2[\mathbf{M}_{SS}]\right]^{-1} = [\mathbf{K}_{SS}]^{-1} + \omega^2[\mathbf{K}_{SS}]^{-1}\left[[\mathbf{M}_{SS}][\mathbf{K}_{SS}]^{-1}\right]^1 + \ldots\ldots + (\omega^2)^n[\mathbf{K}_{SS}]^{-1}\left[[\mathbf{M}_{SS}][\mathbf{K}_{SS}]^{-1}\right]^n \quad (3.30)$$

This can now be reinserted into equation (3.29), dropping all terms containing ω to higher than quadratic powers, to give:

$$\left[[\mathbf{K}^R] - \omega^2[\mathbf{M}^R]\right]\{\mathbf{q}_M\} = \{\mathbf{p}(t)_M\} \quad \text{in the frequency domain}$$
$$\text{or:} \quad [\mathbf{M}^R]\{\ddot{\mathbf{q}}_M\} + [\mathbf{K}^R]\{\mathbf{q}_M\} = \{\mathbf{p}(t)_M\} \quad \text{in the time domain} \quad (3.31)$$

where:

$$[\mathbf{M}^R] = [\mathbf{M}_{MM}] - [\mathbf{K}_{MS}][\mathbf{K}_{SS}]^{-1}[\mathbf{M}_{SM}] - [\mathbf{M}_{MS}][\mathbf{K}_{SS}]^{-1}[\mathbf{K}_{SM}] + [\mathbf{K}_{MS}][\mathbf{K}_{SS}]^{-1}[\mathbf{M}_{SS}][\mathbf{K}_{SS}]^{-1}[\mathbf{K}_{SM}]$$
$$[\mathbf{K}^R] = [\mathbf{K}_{MM}] - [\mathbf{K}_{MS}][\mathbf{K}_{SS}]^{-1}[\mathbf{K}_{SM}]$$

The new EOM will now have M DOFs instead of the original $M+S=N$. This method was originally intended as a quicker method of solving the eigenvalue problem for large problems. However, the method should be acceptable for time marching if the reduced equations contain all the modeshapes of interest to a desired level of accuracy. This can be achieved by careful selection of the master co-ordinates, however, this technique requires that the master nodes be chosen as those with the largest mass terms. So some extra interpolation may be required as the fluid forces act on the surface nodes, which may not be the co-ordinates with largest inertia.

3.2.4 Formulation for 2D Sections

Rigid Section

Two dimensional formulations are useful for code validation against experimental data, and they can also provide useful test cases as less computation is involved, and most of the available experimental data is in 2D. The most widely used model is the rigid section, where the structural dynamics is described by translations and rotations

of a rigid ('typical') section of the blade or wing. The most obvious problem with this approach is the difficulty of relating what is happening on different sections, which in this approach occur entirely separately, whereas in the real structure are fixed by compatibility relations. This may not be a problem if only one section is analysed, which is thought to be representative of the whole problem, or if the geometry is inherently 2D anyway. Also, many valuable experimental data sets are for 2D rigid aerofoils driven at fixed frequency. Thus the approach continues to be used, and the formulation for the wing 'standard section' is given in more detail in chapter 4, and a possible formulation for turbomachinery blades is given in the appendix.

Flexible Section

Rigid section formulations for turbomachinery bladerows are capable of modelling many important effects, however there is one further effect that would be useful to include. This is the effect of camberline bending - i.e. a non-rigid section that is free to respond to differential pressure forces along its length, as well as gross translations and rotations. This has been found to be of importance by Bendiksen (1991) both for aerofoil and turbomachinery aeroelasticity.

In order to formulate the equations for a flexible section aeroelastic model, it is first necessary to undertake a vibration analysis of the complete 3D structure. Once the natural frequencies and modeshapes have been obtained, the in-plane modes at the section to be modelled must be identified (i.e. modes which have no effect on the motion of the 2D section are ignored) and the out of plane co-ordinate components must be removed. Then these sectional modeshape vectors can be used in the EOM as described above for the 3D formulation (assuming unit length in the third direction).

3.3 UNSTEADY AERODYNAMIC ANALYSIS

3.3.1 Navier-Stokes Equations

The Navier-Stokes (N-S) equations govern the flow of air at all speeds in the bladerows of turbomachines. The equations are derived by applying the principles of conservation of mass, momentum, and energy to the fluid flow (strictly the N-S equations are the momentum equations alone, but it is accepted practice to refer to the full set of equations as the N-S equations). The principles may either be applied to an infinitesimal control volume, which leads to differential forms of the equations of motion, or to a finite control volume which gives integral forms of the equation. These different forms are mathematically identical, and indeed one form can be obtained

directly by manipulation of the other form, but there are connotations when it comes to the discretisation of the equations.

Most fluid dynamic applications use fixed control volumes on which the equations are discretised in space, as the fluid flows through - this is known as an Eulerian description. In structural dynamic applications the equations are written for control volumes that move with the domain - known as a Lagrangian description. But, for aeroelasticity applications, the equations must be written for control volumes that can move in space, as control volumes of fluid which are near to moving structures must themselves move, to avoid the computational mesh becoming distorted. Thus an arbitrary Lagrangian-Eulerian description is required for the combined fluid/structure domain for aeroelastic applications. This change of reference frame affects the calculation of fluxes of variables across the boundaries of control volumes: the relative velocity of fluid flow across the boundary must be used in the flux terms.

The equations of motion are derived by applying conservation laws to control volumes, as stated above. The continuity equation, obtained by applying conservation of mass, in differential conservation form is as follows:

$$\frac{\partial \rho}{\partial t} + \nabla \bullet (\rho \mathbf{v}) = 0 \qquad (3.32)$$

where ρ is fluid density and $\mathbf{v}$ is fluid velocity vector

The conservation form is obtained by applying the lāw to a control volume fixed in space; the non-conservation form is obtained by using a control volume that convects with the fluid particles. In 3-D Cartesian co-ordinates, the above equation can be written:

$$\frac{\partial \rho}{\partial t} + \frac{\partial}{\partial x}(\rho v_x) + \frac{\partial}{\partial y}(\rho v_y) + \frac{\partial}{\partial z}(\rho v_z) = 0 \qquad (3.33)$$

where v_x, v_y, & v_z represent the x, y, & z components of $\mathbf{v}$

However, as mentioned above, the equations have to be modified for control volumes that are moving, as will be the case for aeroelastic calculations. Terms in the equations which refer to fluxes through the control volume must use the relative velocity of the fluid flow. Thus if the control volume (which will be the grid cell in the numerical calculation) moves with the velocity vector $\mathbf{v}_g = (v_{gx}, v_{gy}, v_{gz})$ then the x-component of the flux of mass out of the control volume becomes $\rho\ (v_x - v_{xg})$ instead of ρv_x. Thus this equation in differential form is unchanged, but in integral form it becomes:

$$\frac{\partial}{\partial t}\iiint \rho dx dy dz + \oint \rho(v_x - v_{xg}) dy dz + \rho(v_y - v_{yg}) dx dz + \rho(v_z - v_{zg}) dx dy = 0 \qquad (3.34)$$

The momentum (or Navier-Stokes) equations can be obtained by applying Newton's second law to the control volume. In differential conservation law form in vector notation they are written as follows:

$$\frac{\partial}{\partial t}(\rho \mathbf{v}) + \nabla \bullet \rho \mathbf{v}\mathbf{v} = \rho \mathbf{f} + \nabla \bullet \Xi_{ij}$$

where: $\mathbf{f}$ is body force vector per unit volume, (3.35)

Ξ_{ij} is surface force per unit volume due to external stresses

$$\Xi_{ij} = -p\delta_{ij} + \mu\left\{\frac{\partial v_i}{\partial x_j} + \frac{\partial v_j}{\partial x_i}\right\} - \frac{2}{3}\mu\delta_{ij}\frac{\partial v_k}{\partial x_k} \quad (i,j,k = 1,2,3)$$

where: p is the fluid pressure

μ is the fluid viscosity (3.36)

$v_1 = v_x,\ v_2 = v_y,\ v_3 = v_z,\ \&\ x_1 = x,\ x_2 = y,\ x_3 = z$

δ_{ij} is the Kronecker delta function ($\delta_{ij} = 1$ if $i = j$; $\delta_{ij} = 0$ if $i \neq j$)

The three momentum equations in differential form become:

$$\begin{aligned}
&\frac{\partial \rho v_x}{\partial t} + \frac{\partial}{\partial x}(\rho v_x^2 + p - \tau_{xx}) + \frac{\partial}{\partial y}(\rho v_x v_y - \tau_{xy}) + \frac{\partial}{\partial z}(\rho v_x v_z - \tau_{xz}) = \rho f_x \\
&\frac{\partial \rho v_y}{\partial t} + \frac{\partial}{\partial x}(\rho v_y v_x - \tau_{yx}) + \frac{\partial}{\partial y}(\rho v_y^2 + p - \tau_{yy}) + \frac{\partial}{\partial z}(\rho v_y v_z - \tau_{yz}) = \rho f_y \\
&\frac{\partial \rho v_z}{\partial t} + \frac{\partial}{\partial x}(\rho v_z v_x - \tau_{zx}) + \frac{\partial}{\partial y}(\rho v_z v_y - \tau_{zy}) + \frac{\partial}{\partial z}(\rho v_z^2 + p - \tau_{zz}) = \rho f_z
\end{aligned} \tag{3.37}$$

Where: $\tau_{xx} = 2\mu\frac{\partial v_x}{\partial x} - \frac{2}{3}\mu\left\{\frac{\partial v_x}{\partial x} + \frac{\partial v_y}{\partial y} + \frac{\partial v_z}{\partial z}\right\},\ \tau_{xy} = \tau_{yx} = \mu\left\{\frac{\partial v_x}{\partial y} + \frac{\partial v_y}{\partial x}\right\},$

$$\begin{aligned}
&\tau_{yy} = 2\mu\frac{\partial v_y}{\partial y} - \frac{2}{3}\mu\left\{\frac{\partial v_x}{\partial x} + \frac{\partial v_y}{\partial y} + \frac{\partial v_z}{\partial z}\right\},\ \tau_{xz} = \tau_{zx} = \mu\left\{\frac{\partial v_x}{\partial z} + \frac{\partial v_z}{\partial x}\right\}, \\
&\tau_{zz} = 2\mu\frac{\partial v_z}{\partial z} - \frac{2}{3}\mu\left\{\frac{\partial v_x}{\partial x} + \frac{\partial v_y}{\partial y} + \frac{\partial v_z}{\partial z}\right\},\ \tau_{yz} = \tau_{zy} = \mu\left\{\frac{\partial v_y}{\partial z} + \frac{\partial v_z}{\partial y}\right\}.
\end{aligned} \tag{3.38}$$

The energy equation for fluid flow is obtained by applying the first law of thermodynamics (conservation of energy) to the same control volume. Written in differential conservation form, in vector notation, it is as follows:

$$\frac{\partial \rho E}{\partial t} + \nabla \bullet \rho E\mathbf{v} = \frac{\partial Q}{\partial t} + \nabla \bullet \mathbf{q} + \rho \mathbf{f} \bullet \mathbf{v} + \nabla \bullet (\Xi_{ij} \bullet \mathbf{v}) \tag{3.39}$$

where: E is the fluid total energy per unit volume $= I + \frac{1}{2}\mathbf{v} \bullet \mathbf{v}$

I is the fluid internal energy per unit volume

Q is the heat added per unit volume

$\mathbf{q}$ is the heat conduction from the volume $= -k\nabla T$

Therefore the energy equation in differential form becomes:

$$\begin{aligned}\frac{\partial \rho E}{\partial t}-\frac{\partial Q}{\partial t}-\rho(v_x f_x+v_y f_y+v_z f_z)\\ +\frac{\partial}{\partial x}(\rho v_x E+pv_x-\tau_{xx}v_x-\tau_{xy}v_y-\tau_{xz}v_z+q_x)\\ +\frac{\partial}{\partial y}(\rho v_y E+pv_y-\tau_{yx}v_x-\tau_{yy}v_y-\tau_{yz}v_z+q_y)\\ +\frac{\partial}{\partial z}(\rho v_z E+pv_z-\tau_{zx}v_x-\tau_{zy}v_y-\tau_{zz}v_z+q_z)=0\end{aligned} \tag{3.40}$$

We now have five equations, and six unknowns (ρ, v_x, v_y, v_z, E, & p) assuming we know the grid velocities, so we require a final equation in order to be able to solve the equations. This must be an equation of state for the fluid: for a perfect gas, which is the fluid we are usually dealing with, this is as follows:

$$\begin{aligned}&p=\rho RT\\ &\text{where } R \text{ is the gas constant}\\ &\text{if } \gamma \text{ is the ratio of specific heats, } \frac{c_p}{c_v}, \text{ then } I=\frac{RT}{(\gamma-1)}=c_v T\end{aligned} \tag{3.41}$$

Also the viscosity and thermal conductivity vary with the state of the fluid; from kinetic theory it is found that these quantities depend on temperature as follows:

$$\begin{aligned}&\mu=\frac{C_1 T^{\frac{3}{2}}}{T+C_2};\ \text{Prandtl number, } Pr=\frac{c_p\mu}{k}\\ &\text{where } C_1,\ C_2,\ \&\ Pr \text{ are constant for the fluid}\end{aligned} \tag{3.42}$$

Now we have five equations in five unknowns which govern the fluid motion. The equations in integral form can be expressed in the following vector notation:

$$\begin{aligned}\frac{\partial}{\partial t}\iiint \mathbf{U}dxdydz+\oint(\mathbf{F}dydz+\mathbf{G}dxdz+\mathbf{H}dxdy)\\ =\oint(\mathbf{F}_v dydz+\mathbf{G}_v dxdz+\mathbf{H}_v dxdy)+\iiint \mathbf{S}dxdydz\end{aligned} \tag{3.43}$$

Where state vector $\mathbf{U}$, flux vectors $\mathbf{F}$, $\mathbf{G}$, & $\mathbf{H}$ viscous terms $\mathbf{F}_v$, $\mathbf{G}_v$, & $\mathbf{H}_v$, and source term $\mathbf{S}$ are given by:

$$\mathbf{U}=\begin{bmatrix}\rho\\ \rho v_x\\ \rho v_y\\ \rho v_z\\ \rho E\end{bmatrix},\quad \mathbf{F}=\begin{bmatrix}\rho(v_x-v_{gx})\\ \rho v_x(v_x-v_{gx})+p\\ \rho v_y(v_x-v_{gx})\\ \rho v_z(v_x-v_{gx})\\ \rho E(v_x-v_{gx})+pv_x\end{bmatrix},\quad \mathbf{G}=\begin{bmatrix}\rho(v_y-v_{gy})\\ \rho v_x(v_y-v_{gy})\\ \rho v_y(v_y-v_{gy})+p\\ \rho v_z(v_y-v_{gy})\\ \rho E(v_y-v_{gy})+pv_y\end{bmatrix},\quad \mathbf{H}=\begin{bmatrix}\rho(v_z-v_{gz})\\ \rho v_x(v_z-v_{gz})\\ \rho v_y(v_z-v_{gz})\\ \rho v_z(v_z-v_{gz})\\ \rho E(v_z-v_{gz})+pv_z\end{bmatrix},$$

$$\mathbf{S}=\begin{bmatrix}0\\ \rho f_x\\ \rho f_y\\ \rho f_z\\ \rho(v_x f_x+v_y f_y+v_z f_z+\dot{Q})\end{bmatrix},\quad \mathbf{F}_v=\begin{bmatrix}0\\ \tau_{xx}\\ \tau_{xy}\\ \tau_{xz}\\ v_x\tau_{xx}+v_y\tau_{xy}+v_z\tau_{xz}-q_x\end{bmatrix},$$

$$\mathbf{G}_v=\begin{bmatrix}0\\ \tau_{yx}\\ \tau_{yy}\\ \tau_{yz}\\ v_x\tau_{yx}+v_y\tau_{yy}+v_z\tau_{yz}-q_y\end{bmatrix},\quad \mathbf{H}_v=\begin{bmatrix}0\\ \tau_{zx}\\ \tau_{zy}\\ \tau_{zz}\\ v_x\tau_{zx}+v_y\tau_{zy}+v_z\tau_{zz}-q_z\end{bmatrix}, \tag{3.44}$$

The above equations are written with the viscous terms separated; if these terms are assumed to be negligible, then the equations reduce to the inviscid Euler equations. With the additional assumptions that the flow is adiabatic (Q=0), and that there body forces are negligible (**f**=0), the equations simplify further. Also it is usual to non-dimensionalise the equations as follows:

$$\rho'=\frac{\rho}{\rho_{ref}},\quad x'=\frac{x}{L},\ \text{etc.},\quad v'=\frac{v}{U_{ref}},\ \text{etc.},\quad \mu'=\frac{\mu}{\mu_{ref}},\quad p'=\frac{p}{\rho_{ref}U_{ref}^2} \tag{3.45}$$

where: ρ_{ref}, L, U_{ref}, and μ_{ref} are reference values

With these non-dimensional variables, the equations remain the same, apart from the viscous stresses, and heat flux terms. These terms are divided by the Reynolds number, Re, where:

$$Re=\frac{\rho_{ref}U_{ref}L}{\mu_{ref}} \tag{3.46}$$

Thus the non-dimensional Navier-Stokes equations become:

$$\frac{\partial}{\partial t}\iiint \mathbf{U}dxdydz+\oint(\mathbf{F}dydz+\mathbf{G}dxdz+\mathbf{H}dxdy)$$
$$=\tfrac{1}{Re}\oint(\mathbf{F}_v dydz+\mathbf{G}_v dxdz+\mathbf{H}_v dxdy)+\iiint \mathbf{S}dxdydz \tag{3.47}$$

All the terms in (3.47) are non-dimensional, but with the primes now dropped. The Euler equations are hyperbolic in time, so they may be advanced in steps of time from an initial condition of **U** - this process is known as time marching. So for a steady flow, the solution may be advanced from an initial guess for **U** by driving the time dependent terms, $\partial\mathbf{U}/\partial t$ towards zero. The full Navier-Stokes equations are parabolic, but the time marching strategy is still valid for the high speed flows that will be encountered. For unsteady flow the solution may be advanced from the initial solution (e.g. steady flow solution); the solution will be time accurate if the time dependent term is discretised to a suitable level of accuracy (e.g. second order accurate).

Cartesian co-ordinates are normally chosen for two-dimensional applications; the equations may also be modified to allow a variation of streamtube height - then the equations become quasi-three-dimensional. However for 3-D turbomachinery applications in rotor stages, the frame of reference is rotating. In this situation extra rotational terms come into the equations (due to centripetal and coriolis accelerations acting on fluid particles); here it becomes easier for the geometry being considered to write the equations in cylindrical polar co-ordinates (r, θ, z) with the z axis along the shaft of the rotor - see Chapter 6.

The Navier-Stokes equations are valid for both laminar and turbulent flow regimes. However, to obtain a solution for a turbulent flowfield it would be necessary to model the turbulent eddies down to the smallest scales of turbulence. This would require an extremely small mesh, which would result in a mesh refinement of several orders of magnitude (depending on the Reynolds number of the problem) - an approach that is impractical for unsteady flows with todays computers. To solve this problem the equations are Reynolds-averaged: this involves replacing the flow variables which change randomly in time by mean values and perturbations. The equations then retain the same form as above, but the viscosity and conductivity of the fluid are increased over and above the laminar values, to account for the effect of the turbulence:

$$\mu = \mu_l + \mu_t \quad \text{and:} \quad k = k_l + k_t, \quad k_t = \frac{c_p \mu_t}{Pr_t} \tag{3.48}$$

where subscript l is the laminar value as above, and subscript t is the extra turbulent value, and Pr_t is the Prandtl-Schmidt number. This approximation of a turbulent viscosity must then be modelled throughout the flowfield. There is a hierarchy of available turbulence models: the simplest are algebraic models known as mixing length models (e.g. Baldwin-Lomax (1978), Cebeci-Smith (1974)). These use representative length scales derived from the mean flow to determine the turbulent shear stresses. The next level, known as the one equation models or κ-l model uses a transport equation for the turbulent kinetic energy, κ, but still prescribes the length scale. Two equation, usually κ-ε, models use a second transport equation for the turbulent dissipation rate, ε; this is becoming the most popular model. It is also possible to use Reynolds stress equation models (6 equations in 2-D and 9 in 3-D). However, these have not proved to offer any particular advantage over the κ-ε model, while being more computationally expensive, so they are rarely used. These turbulence models, although semi-empirical, are now fairly well established and may be found in the literature. However, models are not so well justified for unsteady and separated flows which is an important aeroelastic effect that requires modelling. So

turbulence modelling remains an area of active research, and will have an important effect on the success of aeroelastic models.

3.3.2 Methods of Solution

The solution of the time-dependent Navier-Stokes (or Euler) equations is achieved by advancing the numerical solution forward in time from an initial guessed solution - known as time-marching. Time-marching is valid for unsteady solutions as long as the time-dependent terms are discretised in a time-accurate fashion. The use of the differential form of the governing equations, discretised by 'finite-difference' methods, has become widespread in the field of external aerodynamics. The method involves transforming the physical grid on which the calculation is to be performed to a rectangular computational domain with equal grid spacings in each direction, on which the equations can be discretised. For common structures such as wings the required transformations and the associated grids are well known, so the extra complication of transforming the computational space is not too much of a problem. Solutions have been obtained using both explicit time-marching e.g. MacCormack (1976), and Lax-Wendroff schemes, or implicit schemes e.g. Beam & Warming (1978).

The finite-volume method uses the integral form of the equations which are discretised as fluxes through finite control-volumes of known shape but arbitrary size. Thus no transformation is required, and the calculation takes place in the physical domain. The method was first developed in explicit form by Jameson et al. (1981) and in turbomachine applications by Denton (1975 & 1983), but has also been formulated more recently in implicit form e.g. by using ADI or LU decomposition to solve the resulting block tri-diagonal matrix equation. As the method does not require a grid transformation, it has proved to be more popular than finite-difference methods for turbomachinery applications, where geometries are often more complicated and highly three-dimensional. Some recent research has been done into unstructured adaptive gridding techniques which are ideal for such geometries, and are applicable to finite-volume codes. Both finite-volume and finite-difference methods can be accelerated to convergence using, for example, multigrid, or local time-stepping techniques, which will be further discussed in the section on numerical issues.

Based on the basic ideas outlined above, a large number of different CFD methods have been developed over the last two decades. A summary of the differences between various methods is listed as follows:

- the governing equations used (potential, Euler, or Navier-Stokes)
- the discretisation of the equations (finite difference, finite volume; cell centred, cell vertex, staggered)
- the integration schemes for solving the numerical equations (explicit - central differencing, predictor-corrector, Runge-Kutta; implicit - ADI or LU decomposition)
- the turbulence models (algebraic, one equation - k-l, or two-equation - k-ε)
- the gridding strategies (structured - O, C, or H, unstructured, adaptative, dynamic grids)
- implementation of the boundary conditions (farfield - non-reflecting, periodic, moving boundaries).

It is possible to use many combinations of the above as viable alternatives for the unsteady fluid dynamic calculation required for the aeroelasticity calculations. As mentioned above, finite volume methods are better suited to applications where the geometries may be complex, such as turbomachinery cases. These methods require the governing equations to be written in integral form (as the control volumes on which the discretisation occurs are of finite size, as the name implies) which can be written:

$$\frac{\partial}{\partial t}\iiint \mathbf{U}dV + \oint(\mathbf{F}n_x + \mathbf{G}n_y + \mathbf{H}n_z)dS = \tfrac{1}{Re}\oint(\mathbf{F}_v n_x + \mathbf{G}_v n_x + \mathbf{H}_v n_x)dS + \iiint \mathbf{S}dV \tag{3.49}$$

where: n_x, n_y, & n_z are components of vector normal to control surface area (S)

The equations can be discretised in a typical cell-centred scheme (flow variables are stored at the centre of grid cells) as follows. The integrals are approximated on each cell, so the volume (surface in 2-D) integral of **U** becomes cell volume times the cell value:

$$\frac{\partial}{\partial t}\iiint \mathbf{U}dxdydz \Rightarrow \frac{\partial}{\partial t}(V_{ijk}\mathbf{U}_{ijk}) \quad \text{where } V_{ijk} \text{ is cell volume} \tag{3.50}$$

The flux terms **F**, **G**, & **H** are discretised as the average of neighbouring cells:

$$\oint(\mathbf{F}n_x + \mathbf{G}n_y + \mathbf{H}n_z)dS \Rightarrow (\overline{\mathbf{F}}n_x + \overline{\mathbf{G}}n_y + \overline{\mathbf{H}}n_z)\Delta S \tag{3.51}$$

The viscous terms $\mathbf{E}_v$, $\mathbf{F}_v$, & $\mathbf{G}_v$ are approximated on the cell faces by using a control volume for each face of the cell which spans that face. Source terms become cell volume times the cell value. Finally the contribution of all the cell faces to the flux, viscous, and source terms are added up to obtain the cell residual, $\mathbf{R}_{ij}$:

$$\mathbf{R}_{ijk} = \sum_{\text{faces}}((\overline{\mathbf{F}} - \tfrac{1}{Re}\mathbf{F}_v)n_x + (\overline{\mathbf{G}} - \tfrac{1}{Re}\mathbf{G}_v)n_y + (\overline{\mathbf{H}} - \tfrac{1}{Re}\mathbf{H}_v)n_z)\Delta S - \mathbf{S}_{ijk}V_{ijk} \tag{3.52}$$

Thus the semi-discrete equations become:

$$\frac{\partial}{\partial t}\left(V_{ijk}\mathbf{U}_{ijk}\right) = -\mathbf{R}_{ijk} \tag{3.53}$$

The equations can now be time-marched in an explicit fashion, by discretising the time dependent term in (3.53) above. A number of stable schemes are possible, including the predictor-corrector two-stage scheme, and the four-stage Runge-Kutta scheme proposed by Jameson (1981); they are as follows:

Predictor - corrector	4 - stage Runge - Kutta
$V_{ijk}^{(p)}\mathbf{U}_{ijk}^{(p)} = V_{ijk}^{n}\mathbf{U}_{ijk}^{n} - \Delta t\mathbf{R}_{ijk}^{n}$	$V_{ijk}^{(1)}\mathbf{U}_{ijk}^{(1)} = V_{ijk}^{n}\mathbf{U}_{ijk}^{n} - \frac{1}{4}\Delta t\mathbf{R}_{ijk}^{n}$
$V_{ijk}^{n+1}\mathbf{U}_{ijk}^{n+1} = V_{ijk}^{n}\mathbf{U}_{ijk}^{n} - \Delta t\mathbf{R}_{ijk}^{(p)}$	$V_{ijk}^{(2)}\mathbf{U}_{ijk}^{(2)} = V_{ijk}^{n}\mathbf{U}_{ijk}^{n} - \frac{1}{3}\Delta t\mathbf{R}_{ijk}^{(1)}$
	$V_{ijk}^{(3)}\mathbf{U}_{ijk}^{(3)} = V_{ijk}^{n}\mathbf{U}_{ijk}^{n} - \frac{1}{2}\Delta t\mathbf{R}_{ijk}^{(2)}$
	$V_{ijk}^{n+1}\mathbf{U}_{ijk}^{n+1} = V_{ijk}^{n}\mathbf{U}_{ijk}^{n} - \Delta t\mathbf{R}_{ijk}^{(3)}$

(3.54)

The time-step limit for stability, is given by the Courant-Freidrichs-Lewy (CFL) condition, equivalent to not allowing numerical information to spread through the computational domain faster than physical information flows:

$$\Delta t \le \frac{\Delta x}{U_{ref} + c} \tag{3.55}$$

where: Δx is the smallest grid size in the flowfield

c is the local speed of sound $= \sqrt{\gamma RT}$

This is the limit that applies to the predictor-corrector scheme, however the four stage Runge-Kutta scheme has a limit $2\sqrt{2}$ times as large. This is an effective improvement of $\sqrt{2}$ times (as twice as many calculations are done). Also, if the Navier-Stokes equations are to be solved with all the viscous terms, it is found that the time-step limitation for explicit calculations becomes even more restrictive due to the small grid sizes required to model viscous layers. In such cases it is found preferable to use an implicit formulation.

Implicit numerical formulations allow the discrete information to travel much further through the computational domain at each time-step, thus they are not restricted to such small time-steps. This is achieved by changing the time discretisation of the equations so that values **U** at the new time level are coupled together through the values at the old time level. This produces a set of N simultaneous equations (where N is the number of grid points) which must be solved by matrix techniques, but the scheme is unconditionally stable and the time-step size is limited by desired accuracy only.

Even in 2D, the block penta-diagonal matrix equations that result would be prohibitively expensive to solve in their initial form. Thus, an additional assumption is

made - the matrices are factorised in an approximate fashion. Two techniques are commonly used: the first is known as alternating direction implicit (ADI) where the matrices are split into separate horizontal and vertical pieces. The second is lower-upper (LU) decomposition where the matrices are split into upper and lower diagonal pieces.

The final requirement for a finite volume flow solver is numerical smoothing. This is because the numerical equations are unstable to certain types of disturbances in the flowfield, such as a sawtooth waveform, which is an allowable solution to the steady flow equations. This problem can be removed by adding a combination of second- and fourth-order smoothing terms to the numerical equations.

3.3.3 Boundary Conditions

Section 3.2 outlined how the equations of motion for a fluid (specifically the high speed flow of air) could be solved by numerical techniques. The solution cannot be obtained until known conditions (in time and space) have been specified on the boundaries of the computational domain. These are known as the boundary conditions and there are three types that need considering for unsteady flow in turbomachinery problems.

The first type is the condition on the surface of the blade, which in this case will be moving. For inviscid flow the physical condition must be that the relative velocity between the blade and the fluid is tangential to the surface of the blade at each point (i.e. no mass flux through the wall). For viscous flow the relative velocity must be zero (the no-slip condition). For aeroelasticity applications the surface of the blade is where the information is transferred from the fluid domain to the structural domain. The new position and velocity of the blade, which are obtained from the structural calculation, are used to update the fluid calculation to the next time-level. Then the resulting pressure distribution around the blade is used to update the structure again to this new time-level. Thus the specific way in which the blade boundary conditions are implemented are particularly important in aeroelasticity applications, and will require further investigation.

Periodic boundaries are necessary because it is desirable to calculate the fluid flow through one blade passage only. The simplest way (for steady or unsteady flows) to achieve the periodic condition would be to calculate the flow in the whole annulus and simply equate the state at one end of the computational domain to the state at the other (which in reality is the same point in the flow). But calculating all blade passages is

extremely expensive computationally as will be seen in Chapter 8. So using one blade passage only, the condition for steady flow is that the flow variables at the upper periodic boundary are equated to those at the lower, which is simple to apply. But for unsteady flow the situation becomes more complicated. For flows of a periodic nature (where the period is known in advance) the method due to Erdos et al. (1977) can be used. This method stores all the flow variables on the upper and lower periodic boundaries during each period of calculation. Then the state on the upper boundary is related to the state at the same point on the lower boundary at a previous time (given by the blade passing frequency), and vice-versa. However, for a fully-transient flutter analysis it may not be possible to implement this technique in a very physical way, as strictly the period is not known beforehand, and it may become necessary to calculate the whole annulus.

The last type of boundary conditions are those upstream and downstream of the blade row - known as the farfield boundary conditions. These are applied in an arbitrary position given by how far the computational grid extends - but this is normally chosen to be far enough away from the blades so as to not affect the calculation. These are complex for two reasons: first, how they are applied depends on the flow speed as different conditions are required for subsonic and supersonic flows. Second, for unsteady flow, any disturbances emanating from the flow inside the computational domain must pass through the boundaries as if they were not there. Waves must not be reflected back into the flow, which would lead to an incorrect solution. For example, for 2D subsonic flow, four pieces of information are required for the four equations. Examination of the characteristic waves shows that three waves run in the flow direction, and one upstream. Thus, at inflow three quantities must be specified, and one extrapolated from an interior cell. At outflow one quantity must be specified, and three extrapolated from an interior cell. The extrapolations must be achieved in such a way so as not to reflect outgoing waves back into the flow.

Aerodynamic Load Vector

Section 3.3 has given an outline of the solution of the fluid-dynamic equations of motion. The finite-volume methods described do not solve for pressure as one of the dependent variables (although some CFD methods do). In any case, the pressure at any point in the flow can easily be obtained as:

$$p = (\gamma - 1)\left(\rho E - \tfrac{1}{2}\rho(v_x^{\,2} + v_y^{\,2} + v_z^{\,2})\right) \tag{3.56}$$

Once the pressure is obtained at each point on the blade surface in the fluid grid the values can be integrated over the surface to provide forces acting on each element of the structural grid. The same method can be used to find forces acting on the structure

due to viscous stresses, if they are present. Thus the aerodynamic load vector in modal co-ordinates can be found at each time-step for solution of the aeroelastic equation of motion as follows:

$$\Pi(t) = [\Phi]^T \mathbf{p}(t) = \left\{ \sum_{\text{aero nodes}} p_i(\phi_{i,r} \bullet \mathbf{n}_i) \right\}_{r=1,N} \tag{3.57}$$

where ϕ is the modeshape vector as defined above, and $\mathbf{n}$ is the area normal vector.

3.4 NUMERICAL SOLUTIONS FOR AEROELASTICITY

3.4.1 Time-Marching Solution of Global Equations

The aeroelastic equations of motion can be formulated for discrete systems, or continuous systems, usually using an assumed modes method obtained from a finite element description as was seen in section 2. The global equations of motion will then have the following form in generalised co-ordinates:

$$\mathbf{M}\ddot{\mathbf{q}} + \mathbf{C}\dot{\mathbf{q}} + \mathbf{K}\mathbf{q} = \mathbf{p}(t) \tag{3.10}$$

A transformation into principal co-ordinates yields:

$$\{\ddot{\eta}\} + [diag(2\zeta_i\omega_i)]\{\dot{\eta}\} + [diag(\omega_i^2)]\{\eta\} = [\Phi]^T\{\mathbf{p}(t)\} = \Pi(t) \tag{3.22}$$

In the former case this is a set of N coupled second order differential equations, and in the latter it is N uncoupled equations. Furthermore, unless further assumptions are made, the aerodynamic load vector $\mathbf{p}$ can only be obtained at each time level, as a function of the structural displacement and velocity. As we are expecting this loading to be non-linear, we cannot make any assumptions about this term being harmonic, which would allow us to express it explicitly in time as the sum of Fourier components. This approach would also allow the possibility of frequency domain solutions, but these possibilities are ruled out for integrated non-linear solutions. A number of different time-integration schemes have been identified, which are detailed section 3.4.3.

3.4.2 Local Assembly Time-Marching Solution

Bendiksen (1991) has proposed an alternative formulation of the equations of motion which is based on a local (element) level. Thus the large global matrices do not need to be assembled which may be a benefit when the number of degrees of freedom becomes large (e.g. for 3D problems). Direct integration of the equations of motion, as in section 3.4.1, causes no problems with the computational cost if the equations are formulated by the assumed modes method where the number of degrees-of-freedom is low (this is the main reason for using the method). However, if the equations are formulated for a 3D geometry by the finite element method, then the number of DOFs

is several orders of magnitude larger. An efficient route for the direct time marching of the structural equations, especially as time steps will have to be kept small due to limitations from the fluid dynamic calculations, is subject to contemplation. The local assembly method was proposed by Bendiksen, as the equations when formulated in this way (via state-space representation) have a similar form to the fluid equations. Thus the same numerical integrator can be used simultaneously on both computational domains (fluid and structure) - hence a fully integrated aeroelasticity method. Bendiksen used a four-stage Runge-Kutta integrator, as this is in common usage for the fluid-dynamic part of the code. The structural equations formulated in this way could also be used in a partially-integrated approach, however, this approach is less commonly used in structural dynamics, so there would be litte reason to adopt it. The local assembly method is not adopted here as it is thought that it would be too restrictive on the structural model used, particularly in the case of complex turbomachinery blading, and would need too much computational time.

3.4.3 Time Integration Methods of Solution

Irrespective of its formulation, the basic approach of a partially integrated solution method is as follows:

1. A computational fluid dynamics method is used to obtain the state of the flow at each time level, based on the current position and velocity of the grid (which is fitted to, and moves with, the structure)
2. The unsteady aerodynamic forces are obtained by integrating the instantaneous pressure acting on the surface of the structure. These forces must then be converted into components of the aerodynamic force vector - how this is done depends on the model being used.
3. Displacements and velocities of the structure are calculated from the aeroelastic equations of motion at each time level, using the last/current aerodynamic load vector. The time-integration of the structural equation of motion is done by a time-marching method of which there are a number of possibilities.
4. New displacements and velocities of aerodynamic grid nodes on the surface of the structure are interpolated from the displacements and velocities in the equation of motion; this information is used to update the position and velocity of the aerodynamic grid.

Steps 1-4 are repeated in steps of time for a fully transient aeroelastic analysis. This can be represented by the following flow chart:

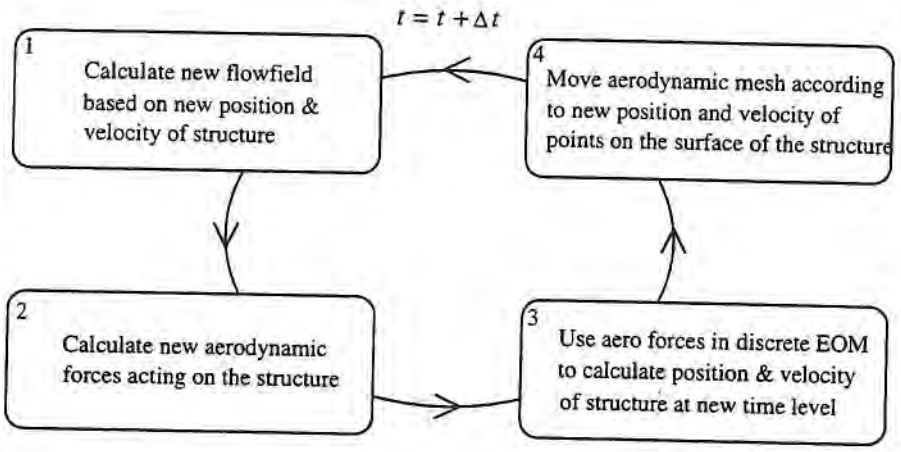

Using this method, it is possible to use separate fluid- and structural-dynamic codes, and the grids do not have to be related in any specific fashion (as long as the mapping relationship is known). The most important feature of the method is how the structural equations of motion are advanced in time - this affects how the energy is transferred between the two domains: structure and fluid, which is the essential feature of aeroelasticity that requires careful modelling. There are a number of possible methods, some of which are outlined below.

Newmark-β Family of Methods

A general aeroelastic equation of motion can be written as follows Eq. 3.10. Discretisations for the Newmark method are proposed as follows:

$$\{\dot{\mathbf{q}}\}_{t+\Delta t} = \{\dot{\mathbf{q}}\}_t + (1-\gamma)(\Delta t)\{\ddot{\mathbf{q}}\}_t + \gamma(\Delta t)\{\ddot{\mathbf{q}}\}_{t+\Delta t}$$

$$\{\mathbf{q}\}_{t+\Delta t} = \{\mathbf{q}\}_t + (\Delta t)\{\dot{\mathbf{q}}\}_t + (\tfrac{1}{2}-\beta)(\Delta t)^2\{\ddot{\mathbf{q}}\}_t + \beta(\Delta t)^2\{\ddot{\mathbf{q}}\}_{t+\Delta t}$$

where: $\{\mathbf{q}\}_t$ is the displacement vector at time t (3.58)

Δt is the fixed time step

$\beta \& \gamma$ are constants

Putting these expressions into the equation of motion, evaluated at time $(t+\Delta t)$ gives:

$$\{\ddot{\mathbf{q}}\}_{t+\Delta t} = [\mathbf{A}]\left\{\begin{array}{l}\{\mathbf{p}(t)\}_{t+\Delta t} - [\mathbf{C}]\left\{\{\dot{\mathbf{q}}\}_t + (1-\gamma)(\Delta t)\{\ddot{\mathbf{q}}\}_t\right\} \\ \qquad -[\mathbf{K}]\left\{\{\mathbf{q}\}_t + (\Delta t)\{\dot{\mathbf{q}}\}_t + (\tfrac{1}{2}-\beta)(\Delta t)^2\{\ddot{\mathbf{q}}\}_t\right\}\end{array}\right\} \quad (3.59)$$

where: $[\mathbf{A}] = \left[[\mathbf{M}] + \gamma(\Delta t)[\mathbf{C}] + \beta(\Delta t)^2[\mathbf{K}]\right]^{-1}$

Note that this method is considering equilibrium of the equation of motion at time $(t+\Delta t)$, so the value of the aerodynamic load vector at this time is required. This is unknown (unless the function $\mathbf{p}(t)$ is known explicitly for simple cases), so an assumption must be made. The simplest possibility is to consider $\mathbf{p}(t)$ to be constant over this time interval as the timestep is small. Other methods would be to extrapolate

the value forward in time from the known values at previous times (t), $(t-\Delta t)$, etc. using an order of accuracy compatible with the CFD discretisation, e.g.:

$$\begin{aligned} &2^{nd}\text{ Order Accurate:} \quad \mathbf{p}(t+\Delta t)_{extrap} = 2\mathbf{p}(t) - \mathbf{p}(t-\Delta t) \\ &3^{rd}\text{ Order Accurate:} \quad \mathbf{p}(t+\Delta t)_{extrap} = 3\mathbf{p}(t) - 3\mathbf{p}(t-\Delta t) + \mathbf{p}(t-2\Delta t) \end{aligned} \tag{3.60}$$

The Newmark method is self-starting, second-order accurate, and is unconditionally stable if $\gamma \geq \frac{1}{2}$, $\beta \geq \frac{1}{4}(\gamma+\frac{1}{2})^2$. The method reduces to other methods, such as linear acceleration method, depending on the choice of the parameters.

State Vector Integration Method

If: $\mathbf{x} = \begin{Bmatrix} \mathbf{q} \\ \dot{\mathbf{q}} \end{Bmatrix}$, the state vector, then the equations can be rewritten:

$$\begin{Bmatrix} \dot{\mathbf{q}} \\ \ddot{\mathbf{q}} \end{Bmatrix} = \begin{bmatrix} \mathbf{0} & \mathbf{I} \\ \mathbf{M}^{-1}\mathbf{K} & \mathbf{M}^{-1}\mathbf{C} \end{bmatrix} \begin{Bmatrix} \mathbf{q} \\ \dot{\mathbf{q}} \end{Bmatrix} + \begin{Bmatrix} \mathbf{0} \\ \mathbf{M}^{-1}\mathbf{p} \end{Bmatrix}, \text{ or } \quad \dot{\mathbf{x}} = \mathbf{A}\mathbf{x} + \mathbf{b}(t) \tag{3.61}$$

Matrix A is not diagonal so these are $2N$ coupled 1st order equations. These can be solved using a convolution integral method (which involves a linearising assumption):

$$\begin{aligned} &\mathbf{x}(t) = \phi(t)\mathbf{x}(t) + \int_0^t \exp[\mathbf{A}(t-\tau)]\mathbf{b}(\tau)\mathrm{d}\tau \\ &\text{where:} \quad \phi(t) \equiv \exp[\mathbf{A}t] \end{aligned} \tag{3.62}$$

For discrete time solution, assuming $\mathbf{b}$ to be constant over Δt:

$$\mathbf{x}(t+\Delta t) = \phi(\Delta t)\mathbf{x}(t) + \mathbf{b}(t)\int_0^{\Delta t} \exp[\mathbf{A}(\Delta t-\tau)]\mathrm{d}\tau \tag{3.63}$$

Alternatively for a linear variation of $\mathbf{b}$ (similar to extrapolations above):

$$\mathbf{b}(t) \Rightarrow \left[\frac{3}{2}\mathbf{b}(t) - \frac{1}{2}\mathbf{b}(t-\Delta t)\right] \tag{3.64}$$

This method has been proposed by Edwards et al. (1983) but it is not favoured as a number of linearising assumptions have been made, and this may no longer be appropriate if a non-linear structural model is required (which is possible with the other approaches mentioned here).

Runge-Kutta Methods

Alternatively, if the $2N$ equations (eq. 3.61) can be uncoupled using the modal matrix, Φ, then:

$$\begin{aligned} &\mathbf{x} = \mathbf{U}\mathbf{y}, \text{ then} \quad \dot{\mathbf{y}} = \mathbf{U}^{\mathrm{T}}\mathbf{A}\mathbf{U}\mathbf{y} + \mathbf{U}^{\mathrm{T}}\mathbf{b}(t) \\ &\text{thus 2n equations of the form: } \dot{y}_i = a'_{ii}y_i + b'_i(t) \end{aligned} \tag{3.65}$$

Otherwise, independent equations can be obtained by lumping off-diagonal terms of the system matrix $\mathbf{A}$ into the force vector $\mathbf{b}$. These equations can be integrated by a multi-stage Runge-Kutta method as follows:

N-stage Runge-Kutta, to solve: $\dot{y} = f(y,t)$, with y_n known at time t_n, timestep Δt

$$
\begin{aligned}
y^{(1)} &= y_n - \alpha_1 \Delta t\, \mathrm{f}(y_n, t_n) \\
y^{(2)} &= y_n - \alpha_2 \Delta t\, \mathrm{f}(y^{(1)}, t^{(1)}) \\
y^{(3)} &= y_n - \alpha_3 \Delta t\, \mathrm{f}(y^{(2)}, t^{(2)}) \\
&\cdots \\
y_{n+1} &= y_n - \alpha_N \Delta t\, \mathrm{f}(y^{(N-1)}, t^{(N-1)})
\end{aligned}
\tag{3.66}
$$

The constant coefficient, α_n, can be as follows:

Predictor - Corrector: $\alpha_1 = 1,\ \alpha_2 = 1;$

2 - stage RK: $\alpha_1 = \frac{1}{2},\ \alpha_2 = 1;$

3 - stage RK: $\alpha_1 = 0.21,\ \alpha_2 = \frac{1}{2},\ \alpha_3 = 1;$

4 - stage RK: $\alpha_1 = \frac{1}{4},\ \alpha_2 = \frac{1}{3},\ \alpha_3 = \frac{1}{2},\ \alpha_4 = 1;$

5 - stage RK: $\alpha_1 = \frac{1}{4},\ \alpha_2 = \frac{1}{6},\ \alpha_3 = \frac{3}{8},\ \alpha_4 = \frac{1}{2},\ \alpha_5 = 1.$

This is an explicit method so it has a time-step limitation, i.e. it is not unconditionally stable. The limit is governed by the Courant criterion, such that numerical information does not cross the domain faster than physical information (speed of sound in the medium). Also values of aerodynamic forces for vector **b** are required at times later than (t) which are unknown - thus these values must be estimated by extrapolation from values at previous times.

Central Difference Method

Discretisations are as follows:

$$
\begin{aligned}
\{\ddot{\mathbf{q}}\}_t &= (\Delta t)^{-2}\left\{\{\mathbf{q}\}_{t+\Delta t} - 2\{\mathbf{q}\}_t + \{\mathbf{q}\}_{t-\Delta t}\right\} \\
\{\dot{\mathbf{q}}\}_t &= (2\Delta t)^{-1}\left\{\{\mathbf{q}\}_{t+\Delta t} - \{\mathbf{q}\}_{t-\Delta t}\right\}
\end{aligned}
\tag{3.67}
$$

The scheme is conditionally stable with $\Delta t < \Delta t_{cr}$, given by a fraction of the period of the highest mode being modelled in the system (Courant number). Also the method is not self-starting i.e. values of the structural variables are required before t=0 to start the calculation; these are obtained by extrapolation.

Putting these expressions into the EOM evaluated at time t gives:

$$
\begin{aligned}
\{\mathbf{q}\}_{t+\Delta t} &= [\mathbf{A}]\left\{\begin{array}{r} \{\mathbf{p}(t)\}_t + (\Delta t)^{-2}[\mathbf{M}]\{2\{\mathbf{q}\}_t - \{\mathbf{q}\}_{t-\Delta t}\} \\ + (2\Delta t)^{-1}[\mathbf{C}]\{\mathbf{q}\}_{t-\Delta t} - [\mathbf{K}]\{\mathbf{q}\}_t \end{array}\right\} \\
\text{where: } [\mathbf{A}] &= \left[(\Delta t)^{-2}[\mathbf{M}] + (2\Delta t)^{-1}[\mathbf{C}]\right]^{-1}
\end{aligned}
\tag{3.68}
$$

For this method no extrapolation of the aerodynamic load vector is required. However the method is not self-starting, and there is a timestep limitation for stability.

Wilson-θ Methods

This method assumes that acceleration is linear over time $\theta\Delta t$ (for $\theta>1$)

$$\{\ddot{\mathbf{q}}\}_{t+\tau} = \{\ddot{\mathbf{q}}\}_t + \frac{\theta}{\tau}\left\{\{\ddot{\mathbf{q}}\}_{t+\theta\Delta t} - \{\ddot{\mathbf{q}}\}_t\right\} \qquad 0 \le \tau \le \theta \tag{3.69}$$

Integrating expressions and evaluating at $\tau = \theta$

$$\begin{aligned}\{\dot{\mathbf{q}}\}_{t+\theta\Delta t} &= \{\dot{\mathbf{q}}\}_t + \tfrac{1}{2}(\theta\Delta t)\left\{\{\ddot{\mathbf{q}}\}_{t+\theta\Delta t} + \{\ddot{\mathbf{q}}\}_t\right\} \\ \{\mathbf{q}\}_{t+\theta\Delta t} &= \{\mathbf{q}\}_t + (\theta\Delta t)\{\dot{\mathbf{q}}\}_t + \tfrac{1}{6}(\theta\Delta t)^2\left\{\{\ddot{\mathbf{q}}\}_{t+\theta\Delta t} + 2\{\ddot{\mathbf{q}}\}_t\right\}\end{aligned} \tag{3.70}$$

Rearrange to give:

$$\begin{aligned}\{\ddot{\mathbf{q}}\}_{t+\theta\Delta t} &= 6(\theta\Delta t)^{-2}\left\{\{\mathbf{q}\}_{t+\theta\Delta t} - \{\mathbf{q}\}_t\right\} - 6(\theta\Delta t)^{-1}\{\dot{\mathbf{q}}\}_t - 2\{\ddot{\mathbf{q}}\}_t \\ \{\dot{\mathbf{q}}\}_{t+\theta\Delta t} &= 3(\theta\Delta t)^{-1}\left\{\{\mathbf{q}\}_{t+\theta\Delta t} - \{\mathbf{q}\}_t\right\} - 2\{\dot{\mathbf{q}}\}_t - \tfrac{1}{2}(\theta\Delta t)\{\ddot{\mathbf{q}}\}_t\end{aligned} \tag{3.71}$$

The method is unconditionally stable for $\theta \ge 1.37$ (1.4 is usually used).

The EOM evaluated at $t = t + \theta\Delta t$ gives:

$$[\mathbf{M}]\{\ddot{\mathbf{q}}\}_{t+\theta\Delta t} + [\mathbf{C}]\{\dot{\mathbf{q}}\}_{t+\theta\Delta t} + [\mathbf{K}]\{\mathbf{q}\}_{t+\theta\Delta t} = \{\mathbf{p}\}_t + \theta\left\{\{\mathbf{p}\}_{t+\theta\Delta t} - \{\mathbf{p}\}_t\right\} \tag{3.72}$$

Substituting in the above expressions gives:

$$\{\mathbf{q}\}_{t+\theta\Delta t} = [\mathbf{A}]\left\{\begin{array}{l}\theta\{\mathbf{p}(t)\}_{t+\theta\Delta t} - (\theta-1)\{\mathbf{p}(t)\}_t \\ \quad + [\mathbf{M}]\left\{6(\theta\Delta t)^{-2}\{\mathbf{q}\}_t + 6(\theta\Delta t)^{-1}\{\dot{\mathbf{q}}\}_t + 2\{\ddot{\mathbf{q}}\}_t\right\} \\ \quad + [\mathbf{C}]\left\{3(\theta\Delta t)^{-1}\{\mathbf{q}\}_t + 2\{\dot{\mathbf{q}}\}_t + \tfrac{1}{2}(\theta\Delta t)\{\ddot{\mathbf{q}}\}_t\right\}\end{array}\right\} \tag{3.73}$$

where $[\mathbf{A}] = \left[6(\theta\Delta t)^{-2}[\mathbf{M}] + 3(\theta\Delta t)^{-1}[\mathbf{C}] + [\mathbf{K}]\right]^{-1}$

This method is unconditionally stable for $\theta > 1.37$ and a value of 1.4 is most often used. The method is self-starting, but extrapolation of **p** is required.

Gladwell and Thomas Methods

Thomas & Gladwell (1988) propose general two, three, and four stage methods. The methods have different characteristics depending on the selection of the parameters. The three-stage method is as follows:

$$\begin{aligned}\{\tilde{\mathbf{q}}\}_{t+\Delta t} &= \{\mathbf{q}\}_t + \psi_1(\Delta t)\{\dot{\mathbf{q}}\}_t + \psi_2(\Delta t)^2\{\ddot{\mathbf{q}}\}_t \\ \{\tilde{\dot{\mathbf{q}}}\}_{t+\Delta t} &= \{\dot{\mathbf{q}}\}_t + \psi_3(\Delta t)\{\ddot{\mathbf{q}}\}_t \\ \{\tilde{\ddot{\mathbf{q}}}\}_{t+\Delta t} &= \{\ddot{\mathbf{q}}\}_t\end{aligned} \tag{3.74}$$

$$\left[\psi_4\mathbf{M} + \psi_5(\Delta t)\mathbf{C} + \psi_6(\Delta t)^2\mathbf{K}\right](\Delta t)\beta_n = \{\mathbf{p}(t)\}_{t+\psi_1\Delta t} - [\mathbf{M}]\{\tilde{\ddot{\mathbf{q}}}\}_{t+\Delta t} - [\mathbf{C}]\{\tilde{\dot{\mathbf{q}}}\}_{t+\Delta t} - [\mathbf{K}]\{\tilde{\mathbf{q}}\}_{t+\Delta t} \tag{3.75}$$

$$\{\mathbf{q}\}_{t+\Delta t} = \{\mathbf{q}\}_t + (\Delta t)\{\dot{\mathbf{q}}\}_t + \tfrac{1}{2}(\Delta t)^2\{\ddot{\mathbf{q}}\}_t + \tfrac{1}{6}(\Delta t)^3\beta_n$$

$$\{\dot{\mathbf{q}}\}_{t+\Delta t} = \{\dot{\mathbf{q}}\}_t + (\Delta t)\{\ddot{\mathbf{q}}\}_t + \tfrac{1}{2}(\Delta t)^2\beta_n \qquad (3.76)$$

$$\{\ddot{\mathbf{q}}\}_{t+\Delta t} = \{\ddot{\mathbf{q}}\}_t + (\Delta t)\beta_n$$

where: $\psi_{1\text{-}6}$ are fixed constants

The method is unconditionally stable, for a properly chosen set of parameters; it is self-starting, but extrapolation is required. The method will reduce to various other methods if the parameters are chosen appropriately.

For the purpose of aeroelastic calculations, the integration method should be: self-starting, second-order accurate, unconditionally stable, and capable of controlling the damping of higher modes where necessary, so Newmark or Gladwell & Thomas methods are suitable. But for the studies with a simple assumed modes structural model, any of the above integration routines are acceptable without timestep restrictions (unless very high frequencies are being studied). This is due to the much more restrictive timestep limitations on the fluid calculation for the low frequency motions that are of interest. However the choice of structural integration routines becomes much more important when more detailed or full structural models are considered using physical co-ordinates.

3.5 NUMERICAL ISSUES AND IMPLEMENTATION

This chapter has outlined the possibilities for numerical implementation of a partially-integrated aeroelasticity method. However, a number of possibilities were put forward for the formulation and numerical solution of both the structural and fluid equations respectively and the best single approach has not yet been defined. Some of the specific possibilities, which were identified in Chapter 2, are as follows:

(i) Multiple degree of freedom (e.g. 2/3 DOF total) rigid section' (blade with rigid section free to move on springs) with 2D aerodynamics, obtaining lumped parameters of the section from modal identification, e.g.: Ballhaus & Goorjian (1978), Rizzetta (1979), Guruswamy & Yang (1981) and Edwards et al. (1983).

(ii) Multiple degree-of-freedom (MDOF) flexible section: 2D aerodynamics with assumed modes structural model reduced to the 2D section of interest, e.g. Bendiksen (1991).

(iii) Same approach as in (ii), but 3-D aerodynamics along with 3-D assumed modes description of the blade obtained previous FE calculation; the modal

co-ordinates become the dependent variables in the aeroelastic EOM. e.g.: Guruswamy (1989, 1990, & 1992).

(iv) 3-D as in (iii) but with full M, K, & C structural description from an FE model, with physical nodal co-ordinates as dependent variables in aeroelastic EOM, with possible use of Guyan reduction to reduce the computational effort for the structure. This requires interpolation of data on the fluid / structure interface at each timestep, e.g.: Srivastava et al. (1991), Yamamoto & August (1992), and Gea et al. (1992).

(v) 3-D time domain aerodynamics with uncoupled structural motion during the unsteady fluid calculation, but periodic updating of the structural modes using frequency domain mode modification technique to obtain the effect of the fluid on the structural motion, e.g. Gerolymos (1992).

Any of the above five methods could be implemented, using the procedures described above. In each case listed above, it is possible to use:

- different aerodynamic codes (subject to 2-D restrictions in (i) & (ii))
- different structural codes (subject to time-marching restriction in (iv))
- different methods of integrating the aeroelastic equation of motion (in (i) - (iv))

Within this framework the adopted model can be used to research many of the unknown numerical issues such as:

- Different numerical integration techniques for the aeroelastic equation of motion (implicit/explicit)
- Meshes: structured/unstructured; grid motion; size dependency; adaptivity
- Implementation of boundary conditions
- Interfacing & Interpolation
- Stability of numerical schemes: time-step limitations; numerical flutter?
- Starting Strategies: disturb blade (by how much?) or force blade for a few periods before freeing.

It is not clear what effect some of these numerical issues will have on the prediction of flutter, and the only way to test some of these out will be to try to implement them in the model, and compare the results with available aeroelastic benchmarks.

The best 3-D approach is more open to debate and could involve any of approaches (iii) - (v). Initially the assumed modes method of (iii) is more likely to be of use, as

time integrating a full FE model would be computationally very expensive. The work with 2-D case studies, which is presented in Chapter 4, was used to help finalise the 3-D model which is described in the remainder of this work. The partially-integrated approach has the advantage of being fairly independent of which aerodynamic code is used, so the factors which dictate which one will be used are: availability, time for implementation, and the type of equations solved. It is felt that a non-linear Euler code would suit the requirements best, as linear codes are used to best advantage in the traditional aeroelastic approaches. However some viscous capability would be desirable, as this is thought to be an important factor in the onset of flutter.

Stability and Solution Acceleration

There is one further issue relating to the stability of the partially integrated scheme that is proposed, and that is the possibility of 'numerical flutter'. This might occur even if the fluid and structural solvers were both operating in a stable manner (i.e. below their time-step limit), but that the coupling itself caused an artificial instability to occur. Thus a diverging response could be produced even though it was unwarranted by the fluid forces. This problem has been investigated by Giles (1994) using a simple 1-D model of a solid wall with cross flow undergoing oscillations normal to the flow direction. A stability analysis was done of different types of coupling, and it was concluded that there should be no problems of this type with the partially integrated scheme, assuming the individual parts are operating in a stable fashion.

Finally, there is one area of interest that is not directly related to the aeroelastic model and its accuracy over traditional methods. That is obtaining the maximum performance from the aeroelasticity code, with the available computing power. This can be achieved by acceleration schemes to the numerical model, and by optimising how the code runs on the computing platform.

For the CFD part of the code, possible acceleration techniques include: residual smoothing, local time-stepping, multi-grid, and implicit methods. The first method introduces a degree of implicitness into the model by smoothing the resulting residuals. This can be used in unsteady methods if correctly implemented. The second method is purely for steady flows, as the solution is accelerated by allowing each mesh cell to take a timestep up to its limit - i.e. time accuracy is not maintained throughout the domain. The multigrid method, originally developed for steady flows, but now also implemented in a time accurate fashion (He (1993)), uses two or more grids of varying degrees of coarseness. Thus larger timesteps can be taken on the

coarse grid, while allowing the residuals to converge on the fine grid, and so the solution on the fine grid is obtained faster. Fully implicit time-stepping methods can also be used in order to take much larger timesteps than given by the CFL criterion, however care must be taken to ensure accuracy is maintained.

For the structural dynamic part of the code techniques are also available to speed up the solution. Implicit time integrators tend to be the norm for the structure, due to the much more restrictive time-step limits in solids. Most of the methods described above are implicit (apart from the central difference and Runge-Kutta methods). Other methods that can be used to help speed up the structural part of the code would be to use intelligent time-step selection and/or different timesteps for two domains. Thus the structural part of the code could use a timestep up to is stability limit (or accuracy limit in the case of implicit methods), while the CFD code (having a smaller timestep limit) took a number of timesteps in the same time.

The last possibilities involve computational issues such as optimisation, vectorisation, and parallelisation of the code. Even for well written code it is important to take full advantage of these techniques, so that the code runs as fast as possible on the hardware available.

Conclusions

It is clear from the literature that a large number of differing approaches have been tried by different researchers attempting to solve the difficult problem of aeroelasticity. Early attempts were dominated by the need for efficiency in the amount of calculation required by the method and, indeed even with the advent of supercomputers, the computational cost is still a major limiting factor.

Methods in the related field of wing flutter tend to be more advanced than those currently adopted in turbomachinery because of the extra complication in the latter case of having many interacting blade-rows. Integrated time-marching methods were first investigated fifteen years ago for transonic wing flutter, and the state-of-the-art is to use the 3-D Reynolds-averaged Navier-Stokes equations coupled with a 3-D modal description of the wing Guruswamy (1992). On the other hand, the most advanced methods for turbomachinery use 3-D Euler equations with a traditional uncoupled aeroelastic model Gerolymos (1992a).

Fully-integrated methods may prove to be the best in the long term, but they are relatively untried in the field of turbomachinery, and therefore may require a great deal

of development. The highly integrated nature of the equations, mean that it is difficult to incorporate existing methods (which would speed up the development time). It is easier to write a fully-integrated code from scratch, although the result is that extensive validation of the new code will be required.

As there are a number of possible approaches suggested for partially-integrated methods alone it is thought that there is a good chance of one or more of these methods being successful in improving flutter prediction techniques, once implemented, using 3-D aero- and structural- dynamics. Also, as it is far from clear which method offers the best tool for aeroelasticity analysis, it is thought that there is plenty of scope for research in the area of partially-integrated (PI) methods. Another advantage of PI aeroelasticity methods is that they are fairly independent of the CFD code used, so existing work can easily be incorporated into new methods when they emerge. For these reasons, it is thought appropriate to conduct a course of research into PI methods for turbomachinery aeroelasticity analysis.

The choice of which of the above are used will partly depend on availability, but the minimum requirements to model the problem correctly must be recognised, and decisions made accordingly.

Chapter 4

Aeroelastic Analysis of 2D Aerofoils

4.0 About this Chapter

This chapter outlines the aeroelasticity analysis of 2D rigid section aerofoils using the proposed partially-integrated method. The case study is focused on the NACA 64A006 aerofoil, as the results may be compared with those obtained from the published literature. Two different structural models, a 2DOF standard section and a flexible MDOF section are described, but only the former is used in this study. The unsteady time-marching CFD program used is an inviscid code using a totally unstructured triangular mesh (UV2D). The test case is used to illustrate issues such as non-linear aeroelastic phenomena (limit cycles), the effect of starting conditions, and the accuracy of the partially-integrated model.

This chapter has been published in the paper '*A Partially-Integrated Time-Domain Flutter Prediction System*', which was presented at the XII International Symposium on Air Breathing Engines, in Melbourne, September 1995.

4.1 INTRODUCTION

One of the first aeroelasticity problems that caused significant problems, and yet could not be accurately predicted by classical methods, was the so-called transonic dip in the wing flutter boundary. It was found that the linearised, uncoupled methods of the 70's, e.g. Ballhaus & Goorjian (1977), could adequately predict the flutter boundary up to a Mach number of about 0.8, but at higher values, where the flow has significant supersonic regions (*transonic* flow), flutter was known to occur at lower wing stiffnesses than was expected. This presented an important problem as the range M = 0.85 - 0.87 is around the cruising speed of most subsonic commercial aircraft for reasons of optimum drag against speed performance for minimum fuel consumption over a particular flight.

The first attempts to solve this problem involved trying to incorporate non-linearities into the classical formulations (e.g. Ueda & Dowell (1984)). But it was soon realised that direct simulation of the equations of motion were the best way to avoid too many simplifying assumptions in the analysis, while at the same time revealing a greater insight into phenomena that were occurring. This period coincided with the beginning of the rapid improvement in the performance of digital computers, so it became possible to solve the large numerical problems involved.

The need for more combined fluid/structure time-marching approaches arises from the non-linear response of transonic flow to the motion of solid boundaries. As explained in chapter 3, the partially-integrated method involves solving the governing equations of fluid and structural motion alternately, with information being passed as a boundary condition between the two domains at each timestep. By solving fluid and structural equations together in a time-accurate fashion, the fluid forces affect the motion of the blade and vice-versa, as occurs in reality, rather than assuming a forced harmonic motion.

The NACA006 aerofoil has been selected as a test case for aeroelasticity studies in 2D. It is chosen because a large body of published information exists on this case using classical, partially- and fully-integrated analysis methods. More interestingly, this case exhibits non-linear behaviour of the fluid in the transonic flow regime, and may give rise to limit cycle behaviour which cannot be predicted by the classical methods.

The structural model used is the 2DOF typical section - these cases can be compared with Kousen & Bendiksen (1988, 1989), and others. The unsteady time-marching

CFD code used is an inviscid solver with a totally unstructured moving triangular mesh (UV2D - Peraire et al. 1991). In Chapter 5, a 3D model to allow for non rigid-body motion of the section using the assumed modes method has been used, which will then be compared to the 2D model here.

4.2 FORMULATION

4.2.1 Structural Models

2-DOF 'Standard Section'

The two-dimensional, two degree-of-freedom 'standard section' has been used as an aeroelastic model for wing flutter (e.g. Ballhaus & Goorjian (1978), Rizzetta (1979), Guruswamy & Yang (1981) and Edwards et al. (1983). Let us consider an isolated aerofoil, with semichord $b=c/2$, pitching and plunging about the elastic axis, positioned $a_h b$ behind mid-chord:

Figure 4.1 2D 2-DOF Standard Aerofoil Section

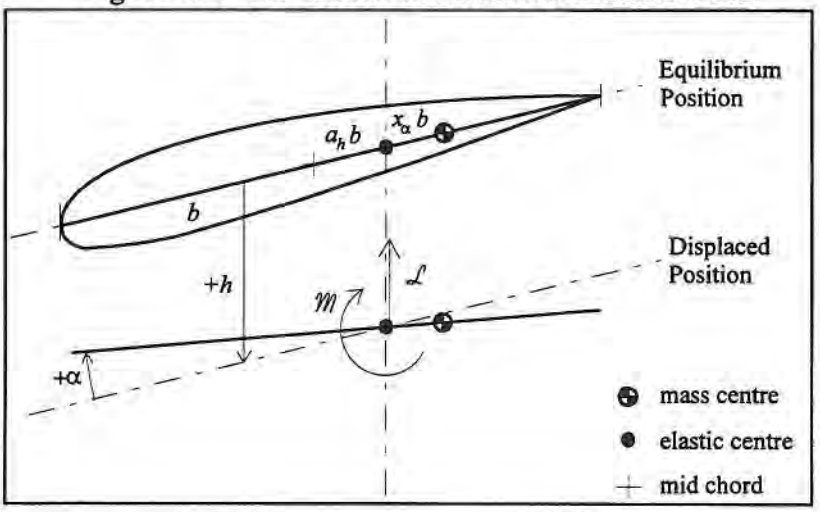

The co-ordinate system used in this model is consistent with conventional notation for aerofoils, though it may be non-standard with respect to other notations.

Torsional and translational (y-dir.) springs and dampers are connected from ground to the elastic axis, thus the section has the following structural parameters:

$\overline{m} = \int \rho_s dx$, section mass per unit span (ρ_s is the material density)

$S_\alpha = \int \rho_s x dx = \overline{m} x_\alpha b$, section static moment about the elastic axis

$I_\alpha = \int \rho_s x^2 dx = \overline{m} r_\alpha{}^2 b^2$, section moment of inertia about the elastic axis

k_h = translational stiffness of section; c_h = translational damping

k_α = torsional stiffness of section; c_α = torsional damping. (4.1)

Applying Newton's Laws of motion to derive the equations of motion (EOM):

$$m\ddot{h} + S_\alpha \ddot{\alpha} + C_h \dot{h} + K_h h = -L$$

$$S_\alpha \ddot{h} + I_\alpha \ddot{\alpha} + C_\alpha \dot{\alpha} + K_\alpha \alpha = M \tag{4.2}$$

Non-dimensionalising the equations, by differentiating with respect to non-dimensional time $\omega_\alpha t$ (where ω_α is the pitch alone natural frequency), and dividing the plunge displacement by the semi-chord, b:

$$\xi'' + x_\alpha \alpha'' + \left(\frac{\omega_h}{\omega_\alpha}\right)^2 \zeta_h \xi' + \left(\frac{\omega_h}{\omega_\alpha}\right)^2 \xi = \frac{-L}{\overline{m} b \omega_\alpha^2}$$

$$x_\alpha \xi'' + r_\alpha^{\,2} \alpha'' + \zeta_\alpha \alpha' + r_\alpha^{\,2} \alpha = \frac{M}{\overline{m} b^2 \omega_\alpha^2} \tag{4.3}$$

$$\xi = \frac{h}{b},\ x_\alpha = \frac{S_\alpha}{\overline{m} b},\ r_\alpha = \sqrt{\frac{I_\alpha}{\overline{m} b^2}},\ \omega_h = \sqrt{\frac{k_h}{\overline{m}}},\ \omega_\alpha = \sqrt{\frac{k_\alpha}{I_\alpha}},\ \zeta_h = \frac{c_h}{\overline{m}\omega_h},\ \zeta_\alpha = \frac{c_\alpha}{\overline{m} b^2 \omega_\alpha}$$

Writing the equations in matrix form:

$$\begin{bmatrix} 1 & x_\alpha \\ x_\alpha & r_\alpha^{\,2} \end{bmatrix} \begin{Bmatrix} \xi'' \\ \alpha'' \end{Bmatrix} + \begin{bmatrix} \overline{\omega}\zeta_h & 0 \\ 0 & \zeta_\alpha \end{bmatrix} \begin{Bmatrix} \xi' \\ \alpha' \end{Bmatrix} + \begin{bmatrix} \overline{\omega}^2 & 0 \\ 0 & r_\alpha^{\,2} \end{bmatrix} \begin{Bmatrix} \xi \\ \alpha \end{Bmatrix} = \left(\frac{\overline{U}^2}{\pi \mu}\right) \begin{Bmatrix} -C_L \\ 2C_M \end{Bmatrix} \tag{4.4}$$

where: reduced speed, $\overline{U} = \dfrac{U_\infty}{b\omega_\alpha}$, frequency ratio, $\overline{\omega} = \dfrac{\omega_h}{\omega_\alpha}$, mass ratio, $\mu = \dfrac{\overline{m}}{\pi \rho_\infty b^2}$;

dynamic lift and moment coefficients, $C_L = \dfrac{L}{\frac{1}{2}\rho_\infty U_\infty^{\,2} c}$, & $C_M = \dfrac{M}{\frac{1}{2}\rho_\infty U_\infty^{\,2} c^2}$;

ρ_∞ & U_∞ are reference fluid density and velocity respectively.

The reduced frequency, κ_c, is defined as $\kappa_c = \dfrac{\omega c}{U_\infty}$. So for uncoupled calculations where the aerofoil is driven in a prescribed motion and ω is known, and fixed throughout the calculation, κ_c can be defined (e.g. in terms of $\overline{U}$ & $\overline{\omega}$). However, for integrated aeroelasticity calculations, ω is not known and is a *result* of the calculation.

Letting:

$$\{\mathbf{q}\} = \begin{Bmatrix} \xi \\ \alpha \end{Bmatrix},\ \{\mathbf{p}\} = \left(\frac{\overline{U}^2}{\pi \mu}\right) \begin{Bmatrix} -C_L \\ 2C_M \end{Bmatrix}, \text{ the aerodynamic load vector}$$

$$[\mathbf{M}] = \begin{bmatrix} 1 & x_\alpha \\ x_\alpha & r_\alpha^{\,2} \end{bmatrix},\ [\mathbf{C}] = \begin{bmatrix} \overline{\omega}\zeta_h & 0 \\ 0 & \zeta_\alpha \end{bmatrix},\ [\mathbf{K}] = \begin{bmatrix} \overline{\omega}^2 & 0 \\ 0 & r_\alpha^{\,2} \end{bmatrix} \tag{4.5}$$

Then the EOM can be written in the standard form.

$$[\mathbf{M}]\{\mathbf{q}''\} + [\mathbf{C}]\{\mathbf{q}'\} + [\mathbf{K}]\{\mathbf{q}\} = \{\mathbf{p}(t)\} \tag{4.6}$$

where dashes represent differentiation with respect to non-dimensional time, $\omega_\alpha t$.

For single degree-of-freedom cases (i.e. plunging or pitching alone) the same 2DOF method can be used with x_α set to zero, and the appropriate initial conditions. The structural parameters in the EOM can be derived from vibration analysis of a real 3D

structure, providing that two such rigid modes are a reasonable estimate of the dynamic behaviour of the section of the wing in question.

1-DOF Pitch

If plunging motions are not considered the equation of motion is:

$$I_\alpha \ddot{\alpha} + C_\alpha \dot{\alpha} + K_\alpha \alpha = M \tag{4.7}$$

Then, non-dimensionalising using the same notation as above:

$$r_\alpha{}^2 \alpha'' + \zeta_\alpha \alpha' + r_\alpha{}^2 \alpha = \frac{M}{\overline{m} b^2 \omega_\alpha^2} = \frac{2\overline{U}^2}{\pi\mu} C_M \tag{4.8}$$

where all terms are as defined above.

If: $\mu^* = \frac{I_\alpha}{\pi \rho_\infty b^4} = r_\alpha^2 \mu$ and: $\zeta_\alpha{}^* = \frac{c_a}{I_a \omega_a} = \frac{\zeta_\alpha}{r_\alpha^2}$:

then the EOM becomes:

$$\alpha'' + \zeta_\alpha^* \alpha' + \alpha = \frac{2\overline{U}^2}{\pi\mu^*} C_M \tag{4.9}$$

1-DOF Plunge

If pitching motions are not considered, the equation of motion is:

$$m\ddot{h} + C_h \dot{h} + K_h h = -L \tag{4.10}$$

The equation is non-dimensionalised by differentiating with respect to $\omega_h t$ (where ω_h is the plunge alone natural frequency), and by dividing displacements by semichord:

$$\xi'' + \zeta_h \xi' + \xi = \frac{L}{\overline{m} b \omega_h^2} = -\frac{\overline{U}^2}{\pi\mu} C_L \tag{4.11}$$

where for plunging, $\overline{U} = \frac{U_\infty}{b\omega_h}$ and other terms are as above.

Thus for single degree-of-freedom cases, the same 2DOF method can be used with x_α set to zero, and appropriate starting conditions.

Calculation of Aerodynamic Forces

The aerodynamic forces acting on the structure (lift and moment about the elastic axis) can be calculated from the instantaneous pressure forces acting on the surface. The grid for the fluid-dynamic calculation will contain nodes on the surface of the structure. The pressure, p, at these nodes can be calculated from the fluid primitive variables at that node (ρ, ρv_x, ρv_y, ρE) by:

$$p = (\gamma - 1)\left(\rho E - \tfrac{1}{2}\rho(v_x{}^2 + v_y{}^2)\right) \tag{4.12}$$

The aerodynamic load vector for the 2 DOF system can then be calculated:

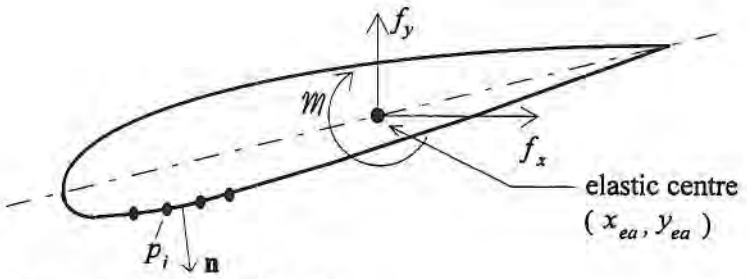

Unsteady force per unit span: $\mathbf{f} = \int p\mathbf{n}ds$

Unsteady moment per unit span: $M = \int p_i \mathbf{r} \times \mathbf{n}ds$

where: p is the fluid pressure, and $\mathbf{n}$ is the surface normal vector and $\mathbf{r}$ is the position vector relative to the elastic axis (i counter running clockwise).

Thus in discrete form:

$$f_x = \tfrac{1}{2}\sum_{i=1}^{n-1}(p_{i+1}+p_i)(y_{i+1}-y_i), \quad f_y = -\tfrac{1}{2}\sum_{i=1}^{n-1}(p_{i+1}+p_i)(x_{i+1}-x_i) \tag{4.13}$$

$$M = \tfrac{1}{2}\sum_{i=1}^{n-1}(p_{i+1}+p_i)\left\{\begin{array}{l}(x_{i+1}-x_i)(\tfrac{1}{2}(x_{i+1}+x_i)-x_{ea}) \\ \quad +(y_{i+1}-y_i)(\tfrac{1}{2}(y_{i+1}+y_i)-y_{ea})\end{array}\right\} \tag{4.14}$$

For perturbation values, where the motion of the blade is calculated from the steady flow equilibrium position, the steady lift and moment, L_0 and M_0 are subtracted from these values.

2D Flexible Section

The above formulation for 2DOF standard sections is capable of modeling many important effects. However, there is one further effect that would be useful to include. This is the effect of camberline bending - i.e. a non-rigid section that is free to respond to differential pressure forces along its length, by bending as well as executing gross translations and rotations. This has been found to be of importance by Bendiksen (1991) both for aerofoil and turbomachinery aeroelasticity. Also, the formulation is similar to that necessary for three-dimensional applications, whilst remaining computationally less expensive.

In order to formulate the equations for the flexible section aeroelastic model it is first necessary to undertake a vibration analysis of the complete 3D structure. Once the natural frequencies and modeshapes have been obtained, the in-plane modes at the section to be modeled must be identified (i.e. modes which have no effect on the motion of the section in the 2D plane of interest are usually ignored) and the out of plane co-ordinate direction must be removed.

Thus, the full EOM with N DOF, which can come from a finite element model of the 3D structure, is as in Eq. 3.23. Now the structural EOM may be reduced to a smaller number of degrees of freedom, m, from the full number of DOFs in the FE model, N, by removing high frequency modes, and modes which are not in the plane of interest (Eq. 3.24). The justification for this is that, for aeroelasticity, only the lower modes are of interest. This will reduce the computational expense for the structural calculation, and also, high frequency modes either cause timestep limitations (explicit time-integration) or are damped out (implicit time-integration).

$$\{\ddot{\eta}\}_m + \left[diag(2\zeta_r\omega_r)\right]_{m\times m}\{\dot{\eta}\}_m + \left[diag(\omega_r^2)\right]_{m\times m}\{\eta\}_m = [\Phi]^T_{N\times m}\{\mathbf{p}(t)\}_N \tag{3.24}$$

This is now an uncoupled m DOF equation of motion, with the reduced modal matrix giving the relationship between the physical co-ordinates and the co-ordinates in the equations. The EOM can then be solved by a partially-integrated method, similar to that adopted by Guruswamy (1989), as described below.

Structural Integration

Time integration of the structural dynamic equation of motion has been achieved using the Newmark-β method, as described in chapter 3. In this case β=1/6, and γ=0.5, with second order accurate extrapolation are used, unless otherwise stated.

4.2.2 Fluid Model

Euler Equations

The Euler equations in integral form, in 2D Cartesian co-ordinates with a moving co-ordinate system, can be written in the following vector notation:

$$\frac{\partial}{\partial t}\iint \mathbf{U}dxdy = -\oint(\mathbf{F}n_x + \mathbf{G}n_y)ds + \iint \mathbf{S}dV \tag{4.15}$$

Where state vector **U**, and flux vectors **F** and **G** are given by:

$$\mathbf{U} = \begin{bmatrix} \rho \\ \rho u \\ \rho v \\ \rho E \end{bmatrix},\quad \mathbf{F} = \begin{bmatrix} \rho(v_x - v_{xg}) \\ \rho v_x(v_x - v_{xg}) + p \\ \rho v_y(v_x - v_{xg}) \\ \rho E(v_x - v_{xg}) + pv_x \end{bmatrix},\quad \mathbf{G} = \begin{bmatrix} \rho(v_y - v_{yg}) \\ \rho v_x(v_y - v_{yg}) \\ \rho v_y(v_y - v_{yg}) + p \\ \rho E(v_y - v_{yg}) + pv_y \end{bmatrix} \tag{4.16}$$

The equations are written with non-dimensionalised variables as described above. It is usual to make the additional assumptions that the flow is adiabatic ($q_x = q_y = 0$), and that the body forces are negligible (**f**=0), so the source term (**S**) is zero for this case. The equations are closed using the perfect gas law $p = \rho RT$. Thus pressure can be eliminated from the above equations using Eq. 4.12.

Discretisation & Method of Solution

For the UV2D code the fluid domain is discretised in space by splitting it into a large number of triangular control volumes by applying an unstructured mesh to fit the domain boundaries. In this way the domain can be efficiently gridded, using a minimum number of points as small cells are used near the blade, and where there are likely to be rapid changes in fluid variables (e.g. near shocks), and large cells at the farfield. The position of the far-field boundary is arbitrary but should be placed as far from the blade as possible (and three chord lengths were used in this case). The CFD program used was developed by Dr.M.Vahdati (Peraire, Vahdati et al. (1991)), and the unstructured grids have been generated using an advancing front mesh generator.

Finite volume / element methods require the governing equations to be written in integral form, the control volumes on which the discretisation occurs being of finite size, as the name implies, which can be written:

$$\frac{\partial}{\partial t}\iint \mathbf{U}dxdy = -\oint(\mathbf{F}n_x + \mathbf{G}n_y)ds \tag{4.17}$$

Space discretisations for the UV2D code have been based on a central difference scheme - higher-order accuracy is preserved by using flux corrected transport to limit the amount of added artificial dissipation. The data structure is edge based, which is particularly good for aeroelastic problems where how the information is transferred at the blade surface is of great importance. Thus once the flux terms have been spatially discretised to give the residual term, **R**, the semi-discrete equations become:

$$\frac{\partial}{\partial t}\left(A_{ij}\mathbf{U}_{ij}\right) = -\mathbf{R}_{ij} \tag{4.18}$$

None of the above schemes are stable for non-physical oscillations, as the discrete equations are underdamped. To correct this, second and fourth order smoothing terms are added to the spatial discretisation, which are similar in form to viscous terms.

Then the equations can be time-marched in an explicit fashion, by discretising the time-dependent term (left hand side of the equation). This is accomplished using the four-stage Runge-Kutta scheme which can maintain time-accuracy for unsteady flows:

$$\begin{aligned}
A_{ij}^{(1)}\mathbf{U}_{ij}^{(1)} &= A_{ij}^{n}\mathbf{U}_{ij}^{n} - \frac{\Delta t}{4}\mathbf{R}_{ij}^{n} \\
A_{ij}^{(2)}\mathbf{U}_{ij}^{(2)} &= A_{ij}^{n}\mathbf{U}_{ij}^{n} - \frac{\Delta t}{3}\mathbf{R}_{ij}^{(1)} \\
A_{ij}^{(3)}\mathbf{U}_{ij}^{(3)} &= A_{ij}^{n}\mathbf{U}_{ij}^{n} - \frac{\Delta t}{2}\mathbf{R}_{ij}^{(2)} \\
A_{ij}^{n+1}\mathbf{U}_{ij}^{n+1} &= A_{ij}^{n}\mathbf{U}_{ij}^{n} - \Delta t\mathbf{R}_{ij}^{(3)}
\end{aligned} \tag{4.19}$$

The timestep limit for stability for this explicit method is governed by the Courant-Freidrichs-Lewy (CFL) condition. This is equivalent to not allowing numerical information to spread through the computational domain faster than physical information, which flows at the characteristic wave speed. This timestep restriction is of utmost importance in aeroelastic analyses, for both fluid and structural calculations. It is expected for these 2D cases that the fluid condition will be more restrictive.

Boundary Conditions

The equations of motion for the fluid cannot be solved without boundary conditions being specified. These are the flow conditions in space at the edge of the fluid domain (blade surface & farfield), and for unsteady calculations, the conditions in time. CFD program UV2D is suited to this study as the boundary conditions are designed for use with external flows such as those encountered in isolated aerofoil calculations. For inviscid flow, the condition on the blade surface is no mass flow through the blade surface (in the relative frame if the blade is moving). Thus this is a condition which implies zero velocity normal to the wall - a slip condition. At the farfield non-reflecting boundary conditions may be applied to allow waves to cross the edge of the flow domain as if it were not there (the real boundary condition should be at infinity). The unstructured mesh moving algorithm allows the mesh to move to fit the aerofoil surface position at all times - even up to large deformations.

In order to ensure that the fluid and structural-dynamic parts of the code are dimensionally consistent (as both parts are non-dimensionalised in different ways), the following non-dimensionalisations are performed in the fluid program:

Table 4.1 Non-dimensional Variables (*)

Variable	Fluid	Structure	Conversion
time	$t_f^* = \frac{tU_\infty}{c}$	$t_s^* = \omega_\alpha t$	$t_f^* = \frac{\overline{U} t_s^*}{2}$
displacement	$h_f^* = \frac{h}{c}$	$h_s^* = \xi = \frac{h}{b}$	$h_f^* = \frac{h_s^*}{2}$
velocity	$\dot{h}_f^* = \frac{\dot{h}}{U_\infty}$	$\dot{h}_s^* = \xi' = \frac{\dot{h}}{\omega_\alpha b}$	$\dot{h}_f^* = \frac{\dot{h}_s^*}{\overline{U}}$
pressure	$p_f^* = \frac{p}{\rho_\infty U_\infty^2}$	$p_s^* = \frac{p}{\frac{1}{2}\rho_\infty U_\infty^2}$	$p_f^* = \frac{p_s^*}{2}$

Thus, appropriate conversions were performed when transferring variables from this program to a structural-dynamic code or vice-versa.

4.2.3 The Partially-Integrated Aeroelastic Method

The equations of motion were solved using the partially integrated method as described in chapter 3.

Timestep

The timestep used is the same for both fluid and structural calculations. For these preliminary studies, with restricted numbers of degrees of freedom, timestep size is not a problem for the structural part of the code. This is because the fluid code has a much more restrictive timestep limit, which becomes the timestep criterion for the whole problem.

Starting Conditions

Combinations of velocities and displacements of the specified degrees of freedom can be selected as initial conditions for structural equations. The starting conditions for flow variables is from a steady flow calculation, or by continuing a forced unsteady calculation, with the structure now free to move according to the integrated aeroelastic equation of motion.

Thus the initial conditions for the complete aeroelastic calculation can be considered to be various forms of perturbations from the steady flow equilibrium condition. In the case of a purely linear system, the response exhibited should not depend on the starting conditions (within the accuracy of the method). However, the fluid part of the coupled calculations here are non-linear - thus this may no longer be the case. How the final response is reached may well differ somewhat for different initial conditions as the calculation will show a complete time history of the motion - not just predict the final behaviour (stable/unstable). In some cases the final response may also differ - e.g. a small initial impulse could lead to a weak divergence, whereas a large one could lead to a limit cycle behaviour.

4.3 CASE STUDY: NACA006 AEROFOIL

The aeroelastic stability of the NACA 64A006 aerofoil has been analysed using the above methods at a range of flow speeds. The following structural parameters for the rigid section model have been used:

$a_h = -0.2, \quad x_\alpha = 0.2, \quad r_\alpha = 0.5385,$

$\overline{\omega} = 0.3434, \; \zeta_h = 0.0, \quad \zeta_\alpha = 0.0,$

$\mu = 10.0, \quad \overline{U} =$ varying from 1.5 - 2.5

Thus the reduced frequency for this problem is around 1.0 (as $\kappa_{c(\omega_\alpha)} = \frac{2}{U}$ for pitching), or around 0.3 for plunging.

4.3.1 Steady Flow

Steady flows for this aerofoil have been produced at free stream Mach numbers of: 0.6, 0.8, 0.85, 0.87, and 0.92 using UV2D. This 2D flow is inviscid, using a mesh with 4346 elements (2237 points) with the farfield boundary 3 chord lengths away from the aerofoil, as can be seen in **Fig. 4.2**. The steady flow surface pressure distributions are shown in **Fig. 4.3** - above M=0.8 the flow is transonic, with a strong shock on the blade surface, which moves downstream as the Mach number increases. The Mach number contours for the M=0.87 case show that the normal shock is well resolved (see **Fig. 4.4**).

4.3.2 Fluid Mesh Kinematics

For aeroelastic analyses it is necessary to calculate the flow in the fluid as the structure moves. As the fluid equations are Eulerian in nature, and are non-linear, this requires that the fluid mesh deforms to follow the surface of the aerofoil as it moves. The UV2D code has this capability for unsteady flows, using an algorithm which considers the mesh as a network of springs so the displacements become zero some distance from the blade. This then takes full account of the unsteady fluxes which arise due to the changes in cell volumes at each timestep. Some examples of the moving mesh for both rigid and non-rigid body aerofoil motions can be seen in **Fig. 4.5**.

4.3.3 Uncoupled Unsteady Calculations

In order to test the unsteady response of the fluid due to motion of the structure, a number of 'uncoupled' unsteady calculations were performed - where the aerofoil is driven in a prescribed motion. In this case the rigid section was sinusoidally plunged and pitched with the amplitude and frequency fixed. This method is traditionally used for aeroelastic calculations, but it allows one-way interaction only - the structural motion affects the fluid, but the fluid forces do not affect the motion of the structure.

The following cases at Mach number 0.87 were examined:

Table 4.2 Uncoupled Unsteady Calculations

Pitching cases	Reduced Freq. (κ_c)	Amplitude (rad)	C_L magn.	C_L phase (deg)	C_M magn.	C_M phase (deg)
1	1.0	0.01	0.040	+5°	0.010	+95°
2	0.1	0.01	0.130	-10°	0.005	+55°
3	1.0	0.07	0.300	+5°	0.060	+92°
Plunging case	Reduced Freq. (κ_c)	Amplitude (h/b)	C_L magn.	C_L phase (deg)	C_M magn.	C_M phase (deg)
4	1.0	0.01	0.019	+100°	0.002	+175°

The time-history results are shown in **Figs. 4.6**. The lift and moment coefficients are plotted against non-dimensional time (2π radians = 1 period) - five periods of oscillation are calculated to ensure convergence, using a CFL number of 5.0 in each case. This gives 420 iterations per period for the unstructured UV2D grid for the calculations at a reduced frequency of 1.0, and 4000 for the lower reduced frequency (0.1).

These calculations give an indication of the unsteady behaviour of this aerofoil in the absence of any coupling between the two modes. The phase plane plots are shown in **Fig.4.7** - these show the relationship between the non-dimensional forces (or moments) with the motion in that co-ordinate, for the final period of motion. The area inside the loop gives the work done by the fluid on the aerofoil, and in a classical calculation this could be used to determine the stability of the aerofoil at these conditions. The reason that the coupling is so important is that the pitching motion gives rise to both a lift and a moment, however the effect of this resulting lift on the plunge co-ordinate is ignored, and vice-versa.

A typical Mach number contour plot during pitching at M=0.87 is shown in **Fig. 4.8**. It can clearly be seen that the large unsteady forces arise due to the motion of shocks on the upper and lower surface of the blade.

4.3.4 Aeroelastic Calculations

In order to assess the aeroelastic stability of the NACA64A006 aerofoil in rigid body motion, calculations have been performed using the partially-integrated method described above. These calculations take as their starting point a steady flow calculation, whereupon the blade is given a small disturbance, or continued from a previous unsteady calculation described above. The solution is then advanced in time until one of the following situations occurs:

- oscillations die away (stable),
- oscillations remain at a constant amplitude (neutrally stable),
- oscillations grow but then level off at a new constant amplitude (unstable - limit cycle),
- oscillations grow until their magnitude cannot be handled by the program (unstable or explosive flutter).

Traditional aeroelastic analyses cannot predict limit cycles (which are observed in practice) as the analysis is linear and involves small perturbations about an equilibrium point. The last category is somewhat unphysical, as the limit of aerofoil motion set by the program has no physical basis. In reality, the blade might reach a large limit cycle, break, or even recover when the flow separates.

To compute the flutter stability of the 2D standard section, the solution was started from the steady flow, and the blade was given a small velocity to initiate its motion. The subsequent time history was computed until the nature of the response was identified in each case. For each flow condition the reduced speed was modified to determine the flutter boundary. When a limit cycle behaviour was encountered, its amplitude was described by the amplitude of the pitch motion.

The following cases were calculated using UV2D:

Table 4.3 Aeroelastic Calculations

Case	Mach No., M	Reduced Speed, U*	Result
1	0.60	1.65	Unstable
2	0.60	1.70	Stable
3	0.80	1.55	Stable
4	0.80	1.60	Neutrally Stable
5	0.80	1.65	Limit Cycle (0.12 rad)
6	0.80	1.70	Unstable (Limit Cycle ?)
7	0.80	1.80	Explosive Flutter
8	0.87	1.80	Stable
9	0.87	1.90	Neutrally Stable
10	0.87	1.925	Limit Cycle (0.11 rad)
11	0.87	1.95	Limit Cycle (0.15 rad)
12	0.87	1.975	Limit Cycle (0.17 rad)
13	0.87	2.00	Limit Cycle (0.19 rad)
14	0.87	2.10	Unstable (Limit Cycle ?)
15	0.87	2.25	Explosive Flutter
16	0.92	2.00	Neutrally Stable
17	0.92	2.05	Limit Cycle (0.11 rad)
18	0.92	2.10	Limit Cycle (0.12 rad)
19	0.92	2.15	Limit Cycle (0.13 rad)
20	0.92	2.20	Limit Cycle (0.14 rad)

Fig. 4.9a shows results for M=0.87; it can be seen that as the reduced speed varies (corresponding to different flight conditions) the aeroelastic response varies. The neutrally stable value of U* gives the flutter boundary. Above this value of reduced speed, a family of limit cycles are produced. It is caused by the fact that once the aerofoil has reached a certain amplitude of motion, the shock reaches the trailing edge when the motion is at its greatest extent. At this point the lift cannot increase further, even for larger amplitudes of motion - thus the oscillations remain at a constant magnitude. In practice the flow may separate before this point, which would also limit the motion. This also explains why at lower Mach numbers, the limit cycle amplitudes are larger, because a larger motion is required before the shock motion reaches its greatest extent - i.e. the trailing edge.

The energy plot for the U^*=2.0 case at M=0.87 (case 13) is shown in **Fig.4.9b**. This figure shows the energy in the structure (E_{tot}), the work done by the fluid on the structure (WD), and the difference between the two (E_0). It can be seen that the E_{tot} and WD curve follow each other closely an they increase rapidly as the aerofoil flutters, and then reaches a limit cycle. Despite this large rate of transfer of energy, the

partially-integrated approach has modeled the interaction accurately, which is confirmed by the E_0 curve which remain constant at the initial energy in the structure.

As the reduced speed increases further, the size of the limit cycle increases, and the time taken to reach a limit cycle reduces. Also, the amplitude of oscillations can overshoot, before settling to a constant level - see **Fig. 4.10**. Below the transonic Mach number range (M<0.8) limit cycles are not produced, as no shocks are present, causing non-linear behaviour.

It is clear from the nature of the motion (**see Fig. 4.10**), that the flutter mechanism is due to the coupling between the plunge and pitch modes. The motion in the two modes can be see to lock into one coupled aeroelastic mode with one frequency, and with a phase of about 180°. Thus the presence of the fluid has been enough to shift the response frequency from the natural values to a value in between the two. If the non-dimensional natural frequency of pitching is `1.0`, giving the plunge frequency as `0.343` in non-dimensional units, then the aeroelastic response frequency for the flutter cases is around `0.628` units. This represents a shift of around the same order of magnitude as the original frequency, and it is due to the low mass ratios encountered in these wing problems. Thus it is clear that in these problems why the classical methods produce such poor results owing to the fact that they do not allow for any frequency shift. Also, the assumption that the modeshape remains fixed (in this case the 'modeshapes' are the rigid body motions) during the aeroelastic calculation may be invalid if the frequency shifts are as large as these.

Further Parametric Studies

Case 13 in **Table 4.5** was further investigated. This was originally run with Newmark-β = 1/6, timestep (fluid) = 0.015, 2nd order extrapolation of aerodynamic forces, with an initial pitch rate of 0.01 rad/s from the steady flow field. The following other calculations were performed with parameters as above unless otherwise stated.

Table 4.4 Parameter Variation Cases

Case	Parameters	Result
13A	Newmark-β = $^1/_4$	same as case 13
13B	Constant extrapolation	almost same as case 13
13C	Parabolic extrapolation	same as case 13
13D	Initial plunge rate = 0.01 (pitch rate = 0.0)	same L.C. as case 13
13E	Initial flow file from pitching (case 1)	same L.C. as case 13
13F	Finer mesh with timestep = 0.004	larger L.C. than 13

The first parameter that was changed was the Newmark-β factor. The cases were originally run as a linear acceleration scheme (β=1/6). Case 13A was run the same as case 13 but with a constant acceleration scheme (β=1/4), and no difference in the results was observed. This is mainly due to the large number of timesteps per cycle that are required, due to the time-step limit from the CFL condition in the fluid explicit scheme.

The calculations were also performed with different orders of accuracy in the extrapolation of the aerodynamic forces (cases 13B & C). It is found that there is virtually no difference between the 2nd and 3rd order extrapolation cases, and that the 1st order case is only slightly different. It should be adequate to use the linear extrapolation in most cases.

The effect of starting conditions was assessed, by varying how the coupled solution was begun (cases 13D & E), shown in **Fig. 4.11**. This figure shows that the same limit cycle is reached as before, independent of the starting conditions, even though the transient response is different. Finally the same case was run with a finer aerodynamic mesh (3672 points), which had a lower timestep limit (0.004). This was found to give a slightly different limit cycle amplitude but still within 5% of that of the coarser mesh.

The limit cycle behaviour of this aerofoil can be displayed in a bifurcation diagram - see **Fig. 4.12**. This plots the limit cycle pitching amplitude against the reduced speed. Small differences between the two can be accounted for by the different fluid models, and the level of numerical damping in each. The results obtained in the present work have been compared with those of Kousen & Bendiksen (1990) and a reasonable agreement is obtained. The flutter boundary is plotted in **Fig. 4.13** - the agreement with the reference work is good. This shows the expected 'transonic dip' in the flutter boundary which would not be predicted by traditional linear methods (Borland & Rizzetta, 1982) - although non-linear small perturbation transonic codes have been used with success (Edwards et al., 1983).

4.4 CONCLUSIONS

(i) Two methods for the aeroelasticity analysis of isolated aerofoils in transonic flow using the partially-integrated technique have been presented, using a rigid body model of the structure.

(ii) The fluid model has been used in an uncoupled fashion to determine the unsteady forces arising from the aerofoil motion in pitching and plunging. If this

method is used to determine the stability at transonic speeds then the flutter speed is significantly overestimated. This is due to the coupling between the modes which is ignored in the classical method.

(iii) The inviscid aeroelasticity analysis of the NACA006 aerofoil has been shown to agree well with published results which use a similar method (within 3%). Limit cycle flutter has been simulated using the partially-integrated method, and the transonic dip in the flutter boundary has been noted, which cannot be predicted by traditional methods.

(iv) The flutter mechanism for this aerofoil involves the pitching and plunging modes coalescing into one combined flutter mode, at a frequency between the two natural frequencies. This coupled mode involves plunging and pitching about 180° out of phase from each other, and the frequency shift is 50-80% of the natural value.

(v) The aerofoil exhibits a limit cycle behaviour at transonic speeds, which is a non-linear phenomenon that cannot be predicted by classical approaches. The physical reson for the limit cycle is that the unsteady shocks moving along the aerofoil surfaces reach the trailing edge once the aerofoil motion has reached a large enough amplitude, which is the limit of lift that can be produced.

(vi) The partially-integrated method has been shown to model the energy transfer between the fluid and the structure with sufficient accuracy to be able to model these aeroelastic phenomena, where the energy transfer rate is much higher that that likely to be seen in the turbomachinery environment (where mass ratios are much higher).

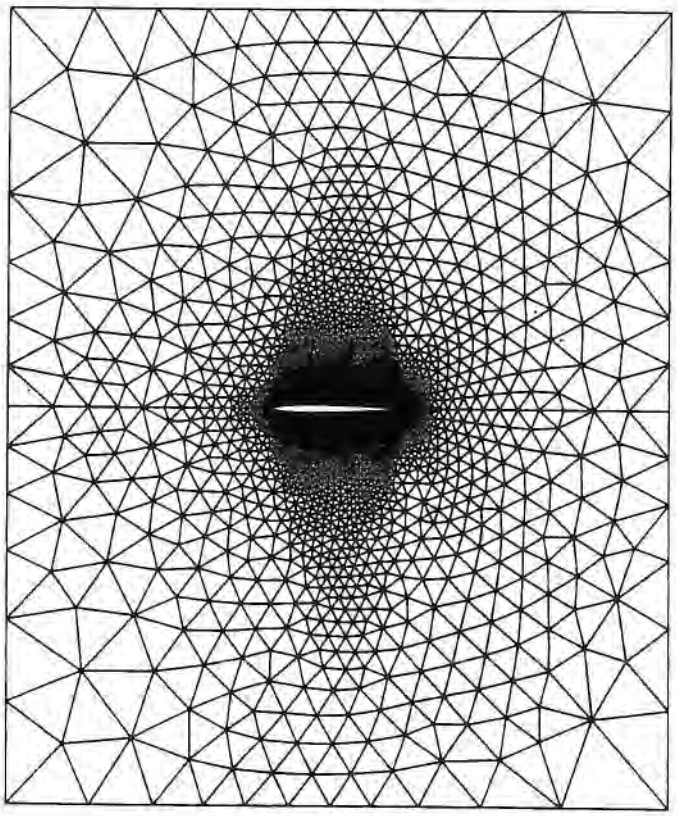

Fig. 4.2 Aerodynamic Mesh

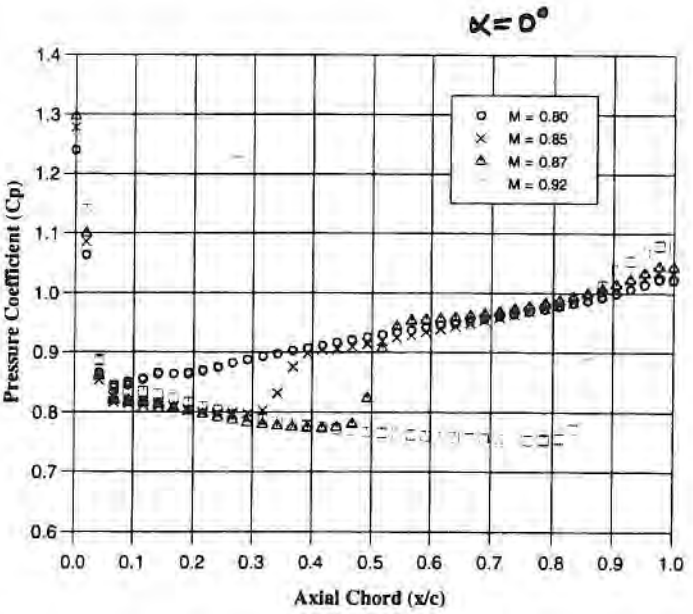

Fig. 4.3 Surface Static Pressures

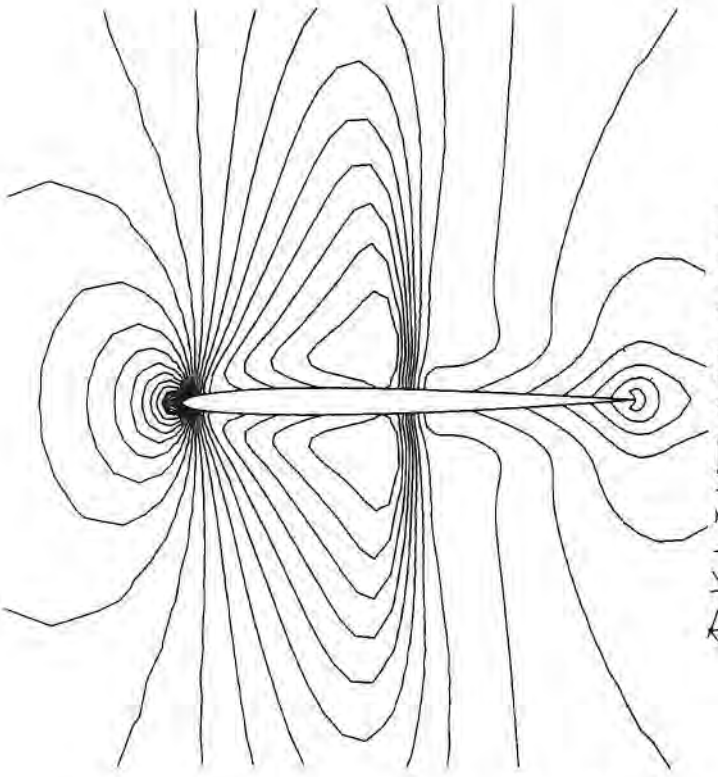

Fig. 4.4 Mach Number Contours (M=0.87)

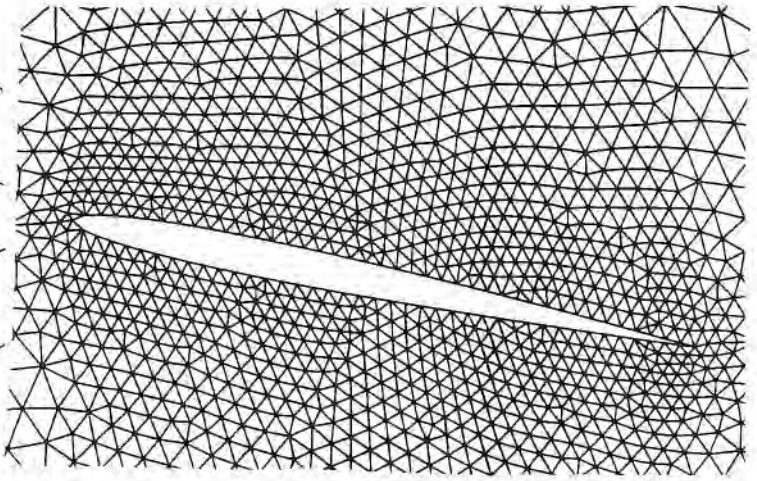

Fig. 4.5 Mesh Motion Detail

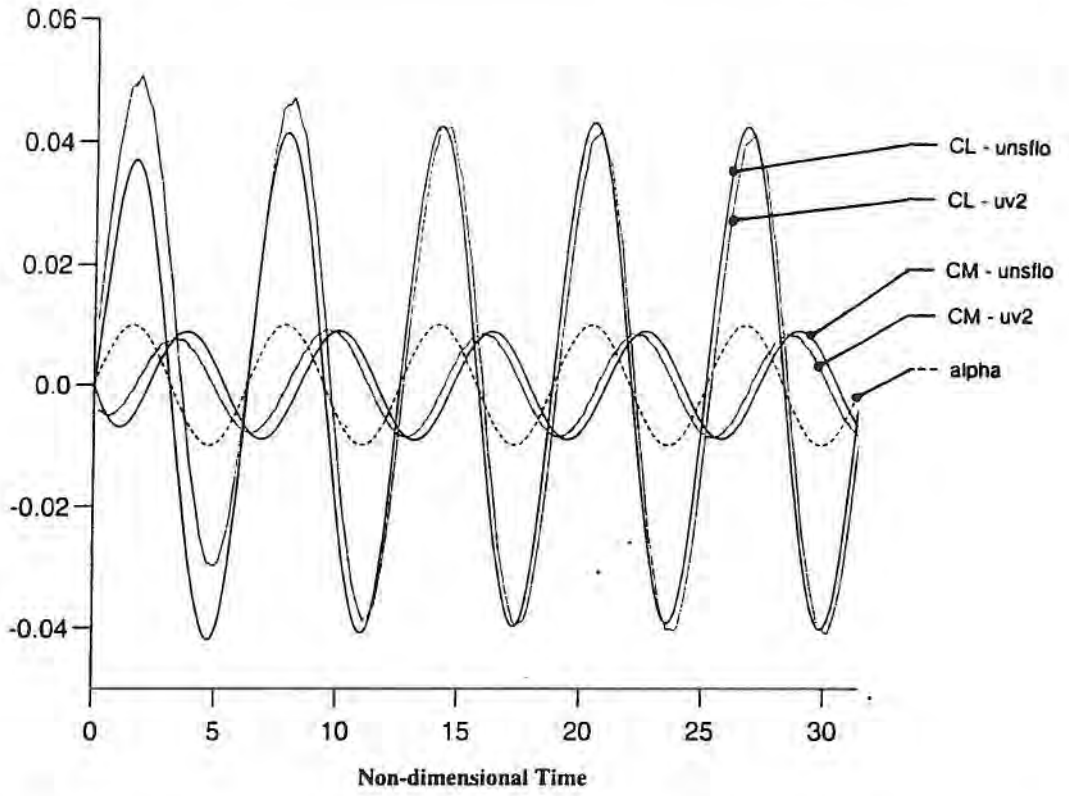

Fig. 4.6a Uncoupled Pitch Time History (M=0.87, Kc=1.0, Amp=0.07)

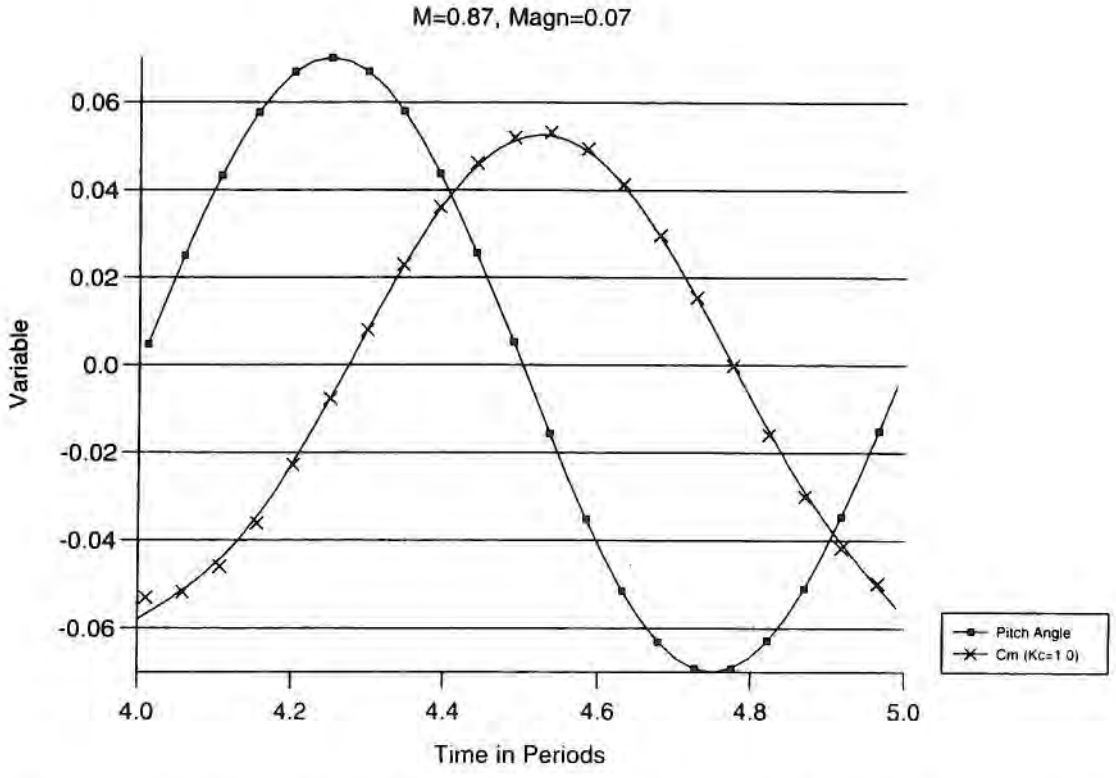

Fig. 4.6b Uncoupled Pitch Time History Detail (M=0.87, Kc=1.0, Amp=0.07)

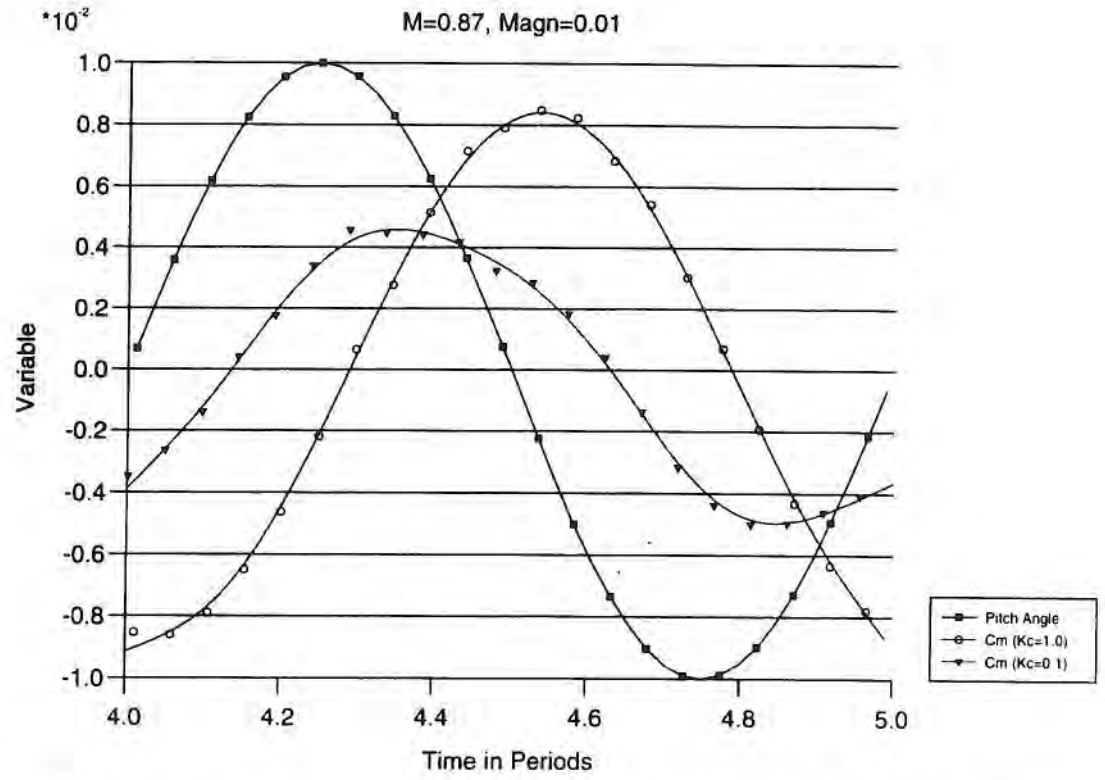

Fig. 4.6c Uncoupled Pitch Time History Detail (M=0.87, Kc=1.0 & 0.1)

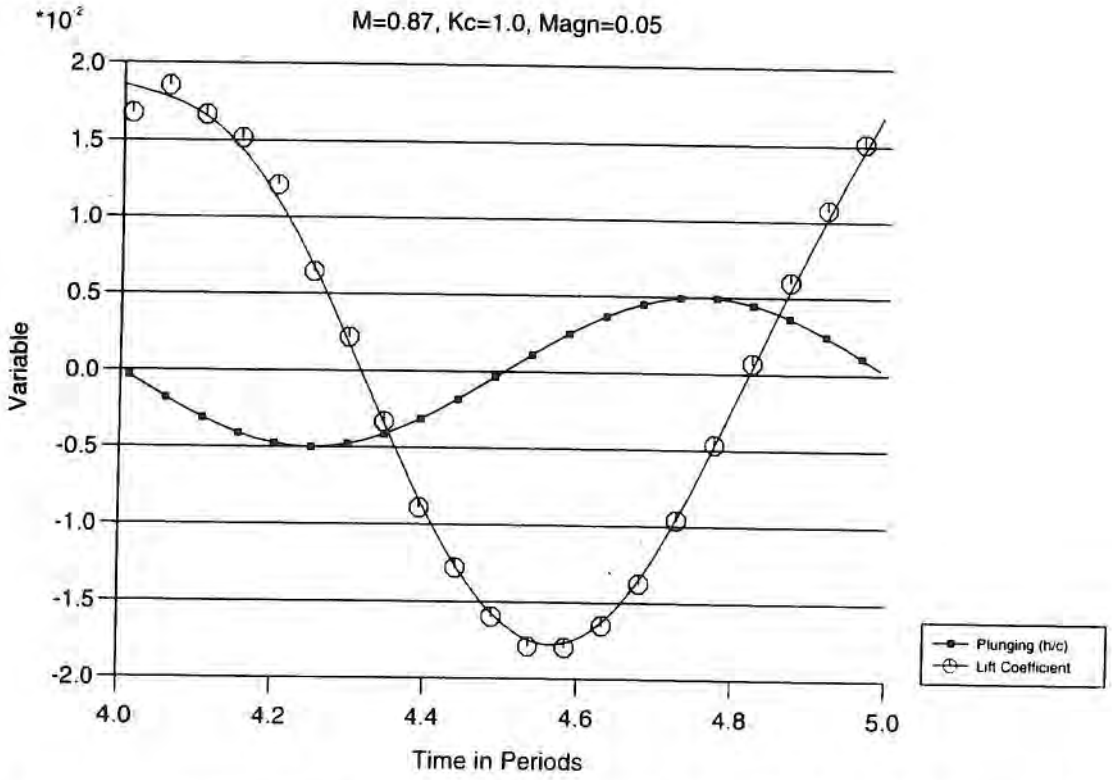

Fig. 4.6d Uncoupled Plunge Time History Detail (M=0.87, Kc=1.0, Amp=0.05)

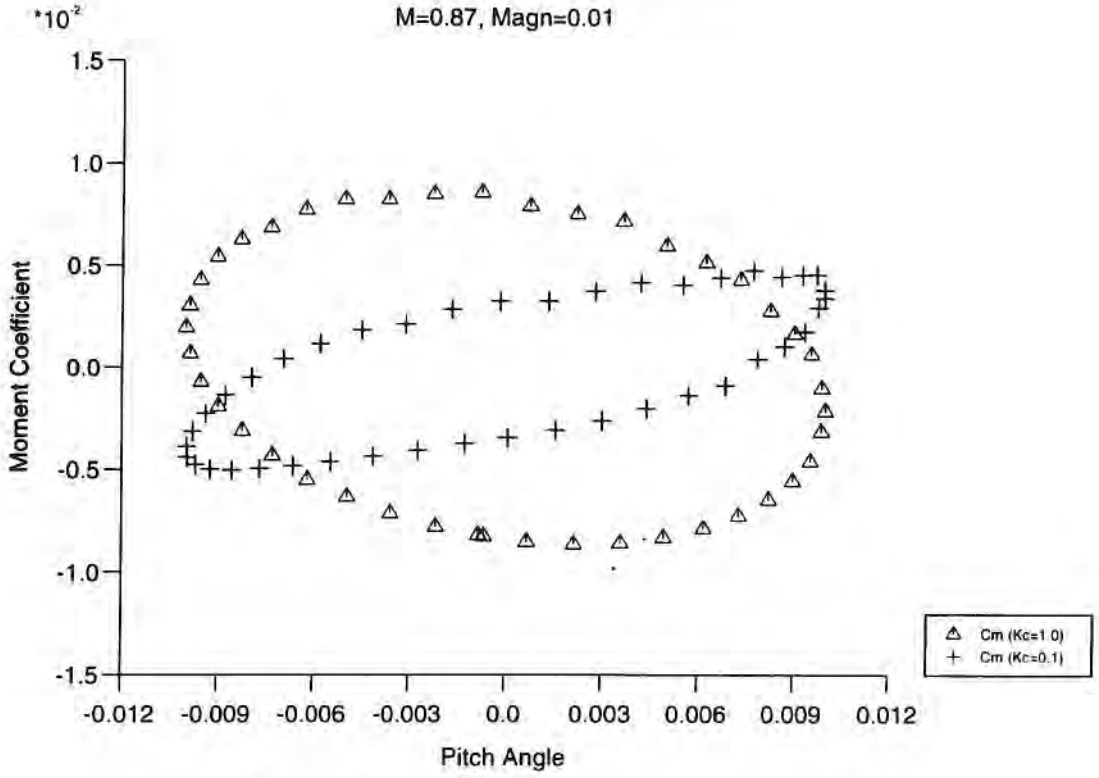

Fig. 4.7a Uncoupled Pitch Phase Plane (M=0.87)

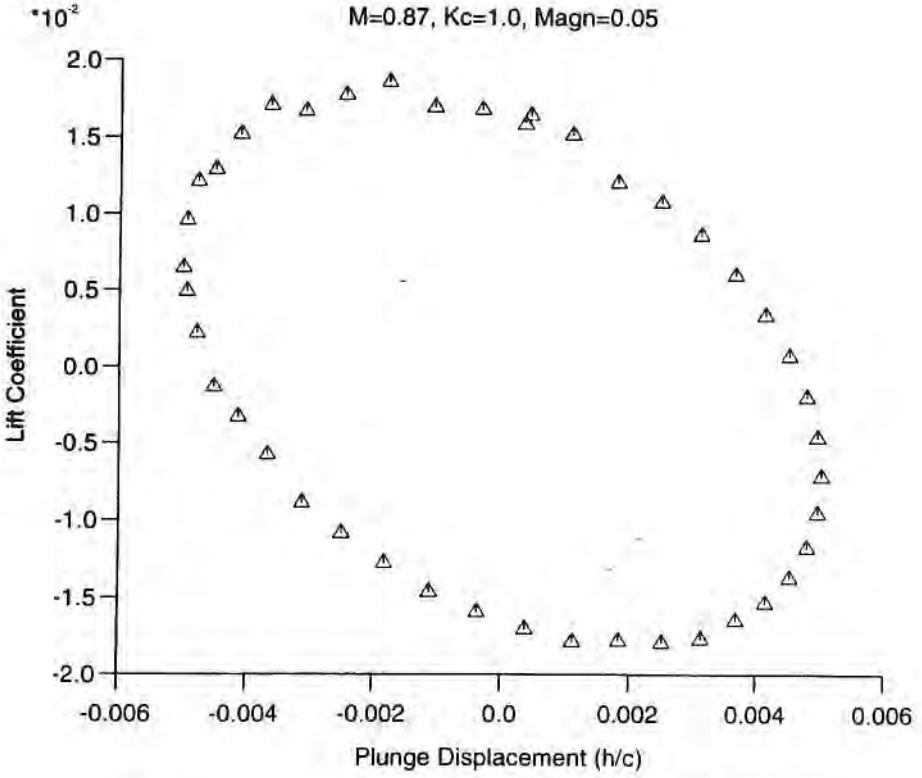

Fig. 4.7b Uncoupled Plunge Phase Plane (M=0.87)

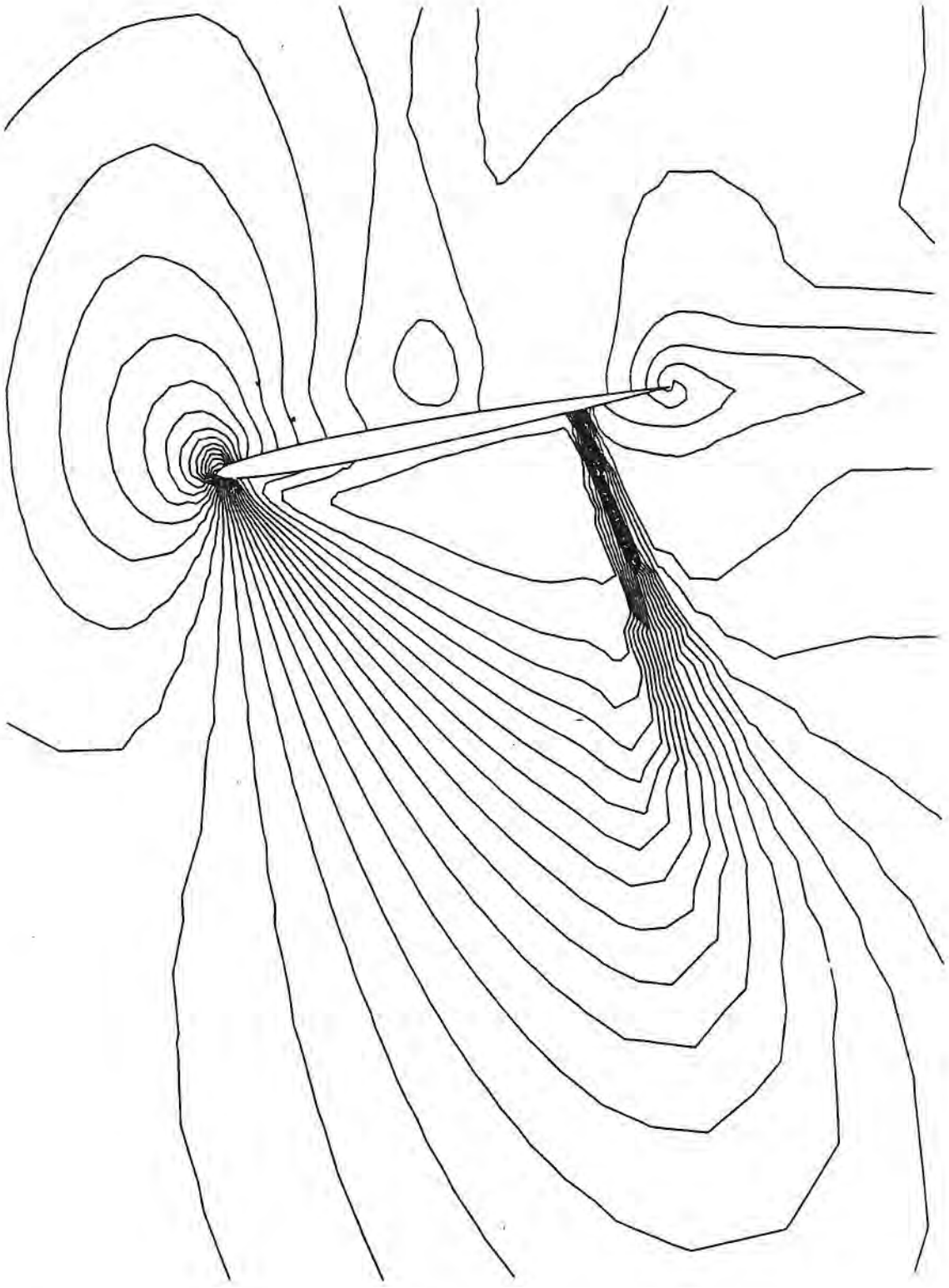

Fig. 4.8 Snapshot Mach Number Contours during Pitching (M=0.87)

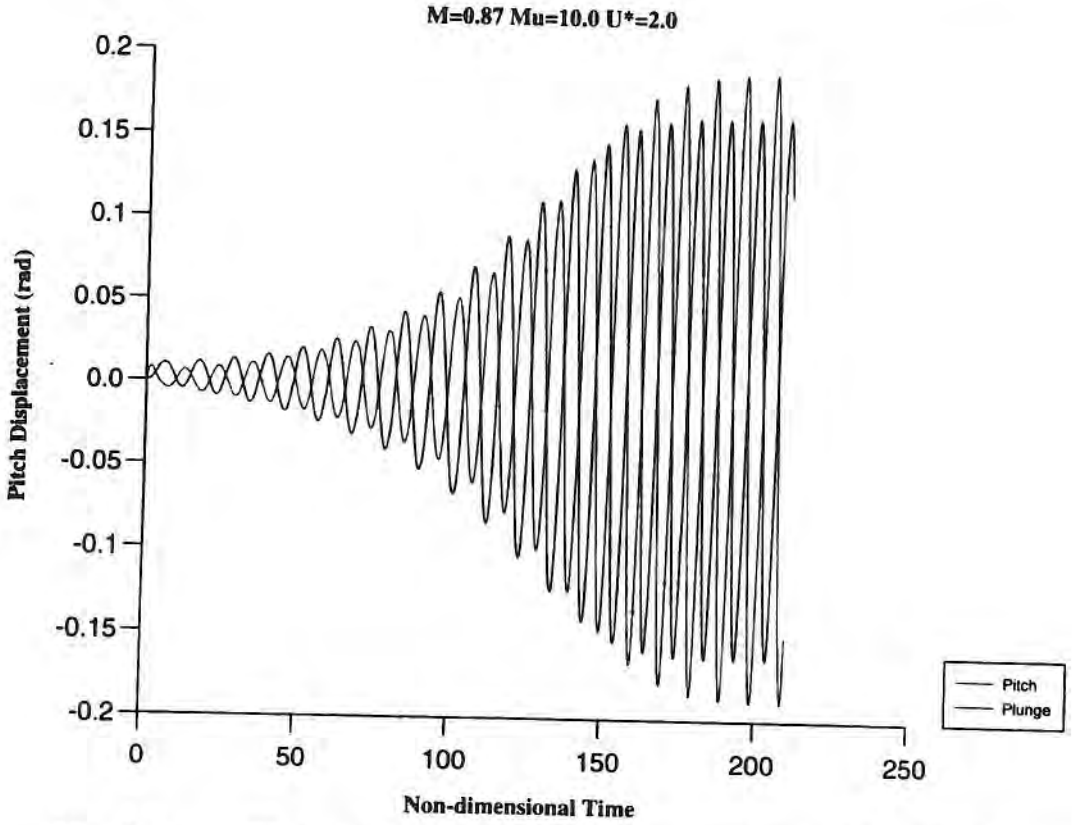

Fig. 4.9a Flutter Time History - Displacements (M=0.87, U*=2.0)

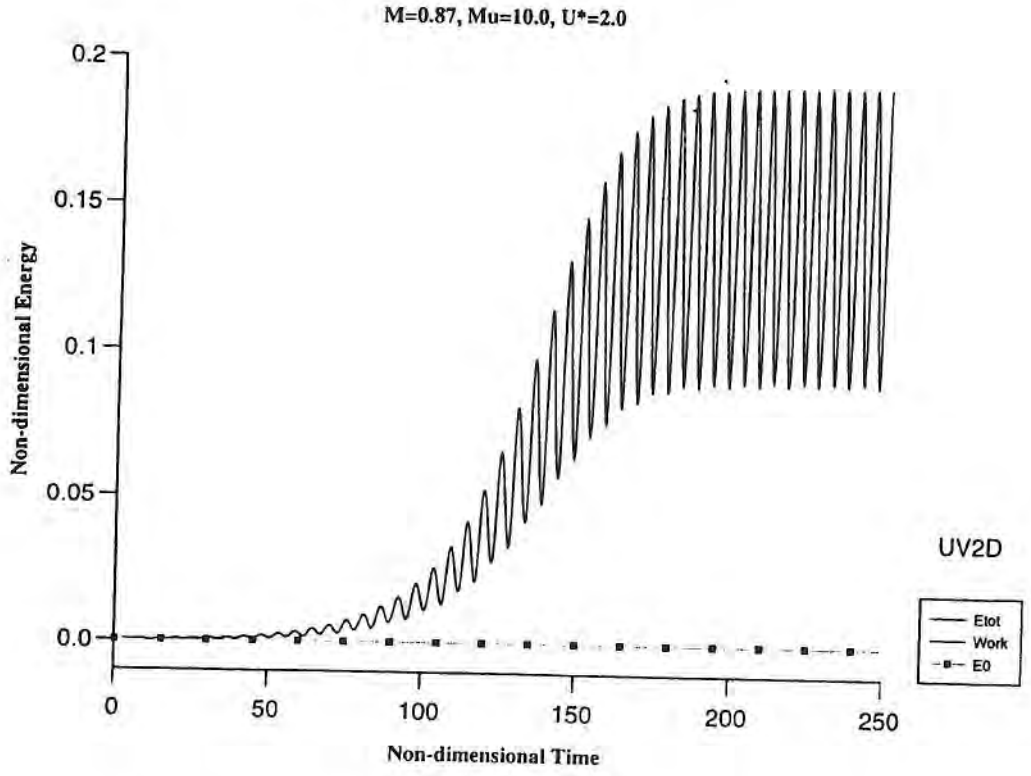

Fig. 4.9b Flutter Time History - Energy (M=0.87, U*=2.0)

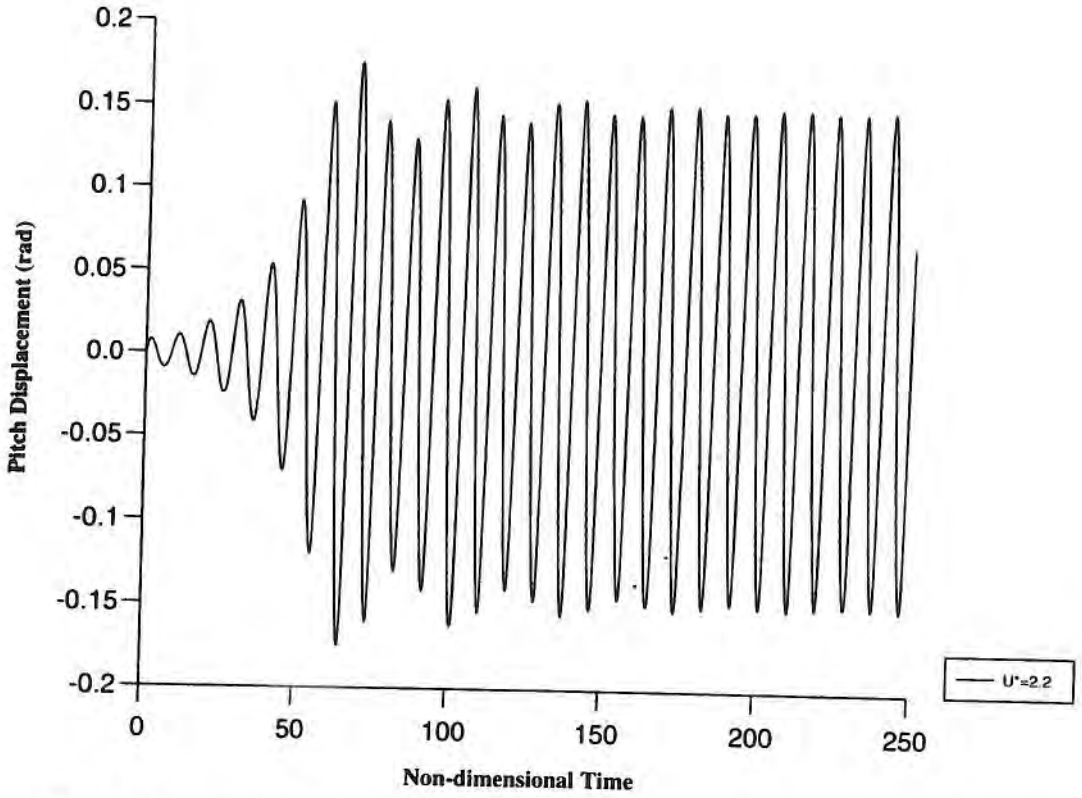

Fig. 4.10 **Flutter Time History - Displacements (M=0.92, U*=2.2)**

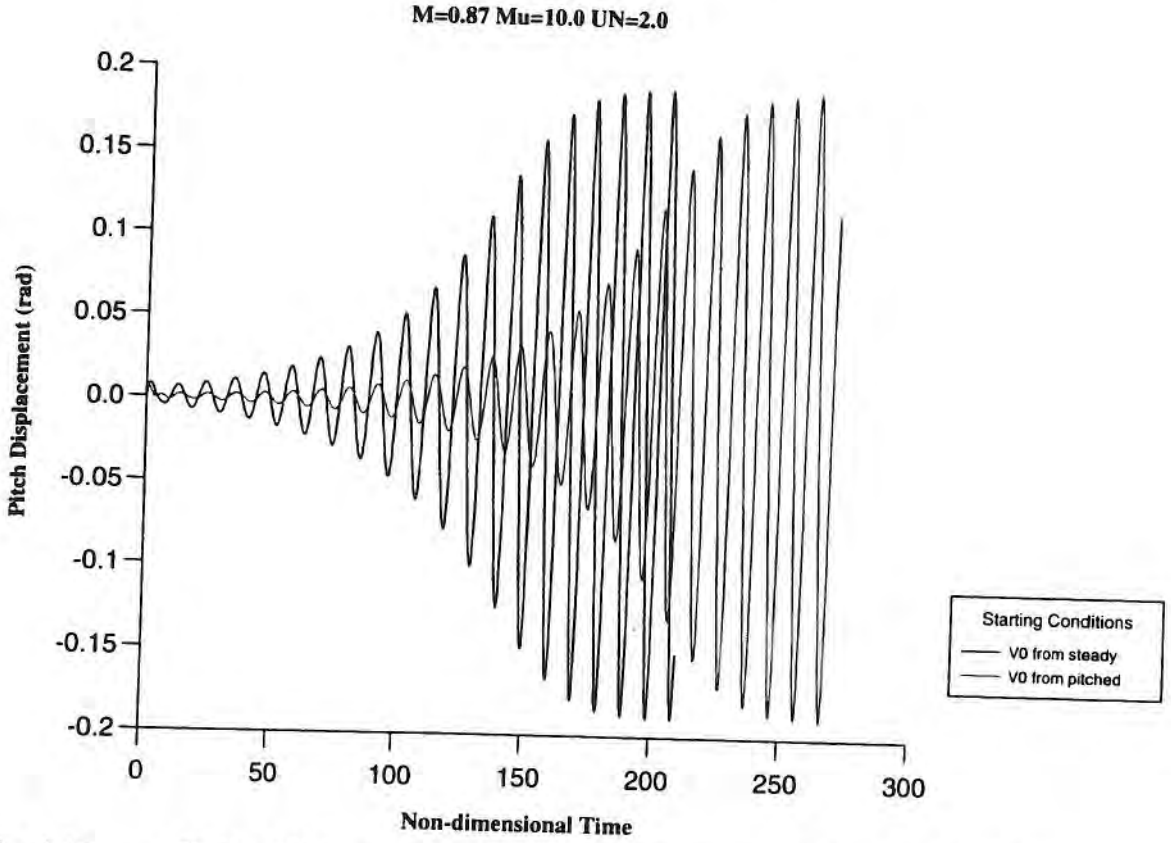

Fig. 4.11 **Flutter History - Effect of Starting Conditions (M=0.87, U*=2.0)**

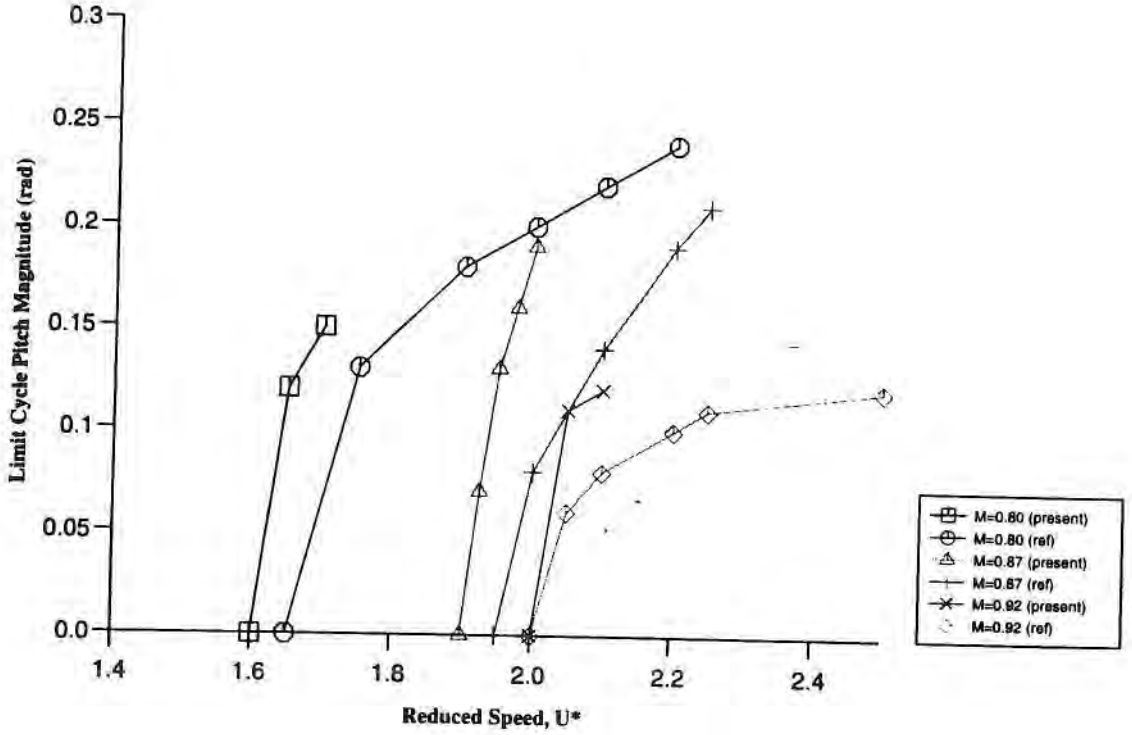

Fig. 4.12 Bifurcation Diagram

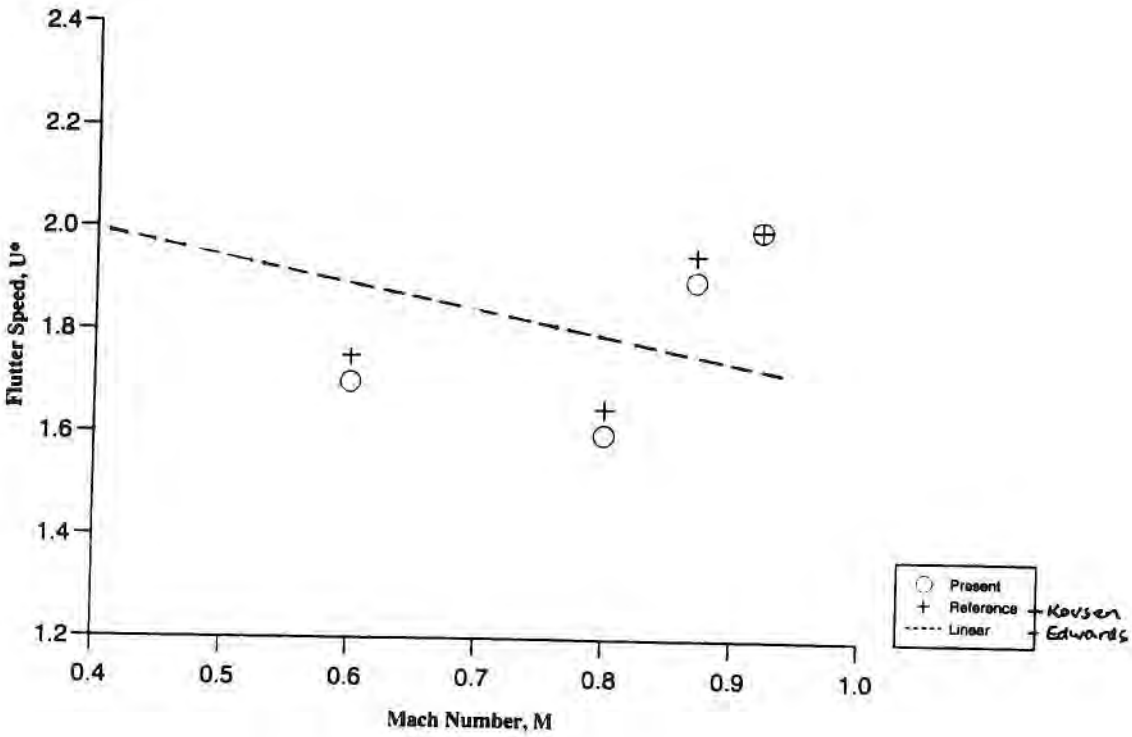

Fig. 4.13 Flutter Boundary

Chapter 5

Aeroelasticity Analysis of 3D Wings

5.0 About this Chapter

The partially integrated method presented in Chapter 3 is now developed for use with 3-D geometries. This chapter presents the well known case study of a wing of NACA64A006 section in transonic flow. The model employed here consists of an inviscid 3D solver with a structured H-type mesh and of a linear structural representation of a hollow wing. For this structure, the first 3 flexible modes, obtained from a prior FE analysis, were used in the solution. The results are compared with the 2D analysis of the previous chapter, and with published work. Particular emphasis is placed on the accuracy of integration, and on the importance of structural flexibility on the flutter boundary.

This chapter has been published in the paper '*A Partially-Integrated Time-Domain Flutter Prediction System*', which was presented at the XII International Symposium on Air Breathing Engines, in Melbourne, September 1995.

5.1 INTRODUCTION

Wing aeroelasticity in the transonic flow regime is an important problem, for reasons outlined at length in Chapter 4. The 2D method described previously is useful for looking at the trends and mechanisms of this kind of flutter, however it misses out the important three-dimensionality of real geometries. This is particularly the case for aeroelasticity phenomena, as the problem is strongly coupled, so if a 2-D or quasi 3-D approach is adopted, then it is difficult to relate the phasing of the separate sections to satisfy basic compatibility relations in the structure. Thus a 3-D approach is desirable, if not essential.

Recently, other methods have been proposed which involve solving for the structural motion simultaneously with advancing the fluid solution fully in three dimensions. Guruswamy (1989) modelled a B1 wing. Batina et al. (1991) have used such an approach to predict aeroelastic effects in a complete fighter aircraft configuration using unstructured meshes.

The 3-D method described herein uses the same partially-integrated approach as described in previous chapters. This method accurately models the energy interchange between the fluid and structure, and thus is applicable to a variety of aeroelastic phenomena for external flow geometries. However, the results presented here are for a NACA006 wing geometry, so that they may be compared with the results of the previous chapter. Also, the effect of aerofoil flexibility is examined, mainly in the form of camberline bending, as the section is free to respond to differential pressure forces along its length, by bending as well as executing gross translations and rotations. This has been found to be of importance by Bendiksen (1991) both for aerofoil and turbomachinery aeroelasticity.

5.2 FORMULATION

5.2.1 Structural Model

In order to formulate the equations for the flexible wing aeroelastic model it is first necessary to undertake a vibration analysis of the 3D structure. Once the natural frequencies and modeshapes have been obtained, the modeshapes can be interpolated onto the aerodynamic grid points. This feature is necessary as it is usually necessary to have a much finer mesh in the axial (flow) direction for the CFD code, than is required for the FE analysis. Thus, the full EOM with N DOFs, which can come from a finite element model of the 3D structure can be written as Eq. 3.23.

Now the structural EOM may be reduced to a smaller number of degrees of freedom, m, from the full number of DOF in the FE model, N, by removing high frequency modes, and modes which are known not to be of interest in the aeroelastic calculation. This is possible as the equations have been uncoupled by the modal matrix, and so are independent. This is done in order to substantially reduce the computational expense for the structural calculation; the reduced EOM with m degrees-of-freedom (from N) can be written as in Eq. 3.24:

$$\{\ddot{\eta}\}_m + \left[diag(2\zeta_r\omega_r)\right]_{m\times m}\{\dot{\eta}\}_m + \left[diag(\omega_r^2)\right]_{m\times m}\{\eta\}_m = [\Phi]^T_{N\times m}\{\mathbf{p}(t)\}_N \quad (3.24)$$

The modal force vector (r.h.s. of above equation) can be calculated at each time step by integrating ($p\bullet\mathbf{n}\times\phi$) over the blade surface for each mode. This is possible as the modeshapes have already been interpolated onto the aerodynamic mesh, and remain constant throughout the calculation. The EOM can then be solved by a partially-integrated method, similar to that adopted by Guruswamy (1989) , as described below. Time integration of the structural dynamic equation of motion is achieved using a structural integration routine such as the Newmark-β method which is described above. In the present study $\beta = \frac{1}{6}$ and $\gamma = \frac{1}{2}$ are used unless otherwise stated.

5.2.2 Inviscid Fluid Modelling

Euler Equations

The integral form of the 3-D Euler equations with a moving Cartesian co-ordinate system, can be extended from the 2-D equations described in Chapter 4:

$$\frac{\partial}{\partial t}\iiint \mathbf{U}dV + \oint\left\{(\mathbf{F}-\mathbf{U}v_{xg})n_x + (\mathbf{G}-\mathbf{U}v_{yg})n_y + (\mathbf{H}-\mathbf{U}v_{zg})n_z\right\}dA = 0 \quad (5.1)$$

where (v_{xg}, v_{yg}, v_{zg}) are the components of the grid velocities including the rotation velocity. Thus state vector **U**, and flux vectors **F**, **G**, & **H** are given by:

$$\mathbf{U} = \begin{bmatrix} \rho \\ \rho v_x \\ \rho v_y \\ \rho v_z \\ \rho E \end{bmatrix},\ \mathbf{F} = \begin{bmatrix} \rho v_x \\ \rho v_x^2 + p \\ \rho v_x v_y \\ \rho v_x v_z \\ (\rho E + p)v_x \end{bmatrix},\ \mathbf{G} = \begin{bmatrix} \rho v_y \\ \rho v_y v_x \\ \rho v_y^2 \\ \rho v_y v_z \\ (\rho E + p)v_y \end{bmatrix},\ \mathbf{H} = \begin{bmatrix} \rho v_z \\ \rho v_z v_x \\ \rho v_z v_y \\ \rho v_z^2 + p \\ (\rho E + p)v_z \end{bmatrix} \quad (5.2)$$

The equations are closed by use of the perfect gas equation for the sixth unknown variable, p, such that: $p = (\gamma - 1)\left(\rho E - \frac{1}{2}\rho(v_x^2 + v_y^2 + v_z^2)\right)$

Fluid Discretisation & Time Integration

The Euler equations are hyperbolic in time, so they may be integrated in time from an initial condition of **U**. For unsteady flow the solution may be advanced from the initial solution (i.e. steady flow solution), as long as the integration is performed in a time-

accurate fashion. The model described herein has been developed by He (1993). The fluid domain is spatially discretised using a cell-vertex finite volume scheme. Thus the semi-discrete equations become:

$$\frac{\partial}{\partial t}\left(A_{ij}\mathbf{U}_{ij}\right) = -\mathbf{R}_{ij}$$

where: $$\mathbf{R}_i = \sum\left\{(\mathbf{F}-\mathbf{U}v_{xg})\Delta A_x + (\mathbf{G}-\mathbf{U}v_{yg})\Delta A_y + (\mathbf{H}-\mathbf{U}v_{zg})\Delta A_z\right\} \qquad (5.3)$$

Then the equations are time-marched in an explicit fashion, by discretising the time-dependent term (left hand side of the equation) using the four-stage Runge-Kutta scheme originally proposed by Jameson et al. (1981) as described above (Eq. 4.19). The numerical damping term, D, is formed using a second and fourth order adaptive smoothing in the axial direction, and a simple second order smoothing in the pitchwise and radial directions.

The explicit timestep limit for stability, governed by the Courant-Freidrichs-Lewy (CFL) condition is relaxed by the use of a time-accurate two-grid integration process. In this procedure the mesh is split into the existing mesh (fine) and a second coarser mesh where a number of the smallest cells (usually in the boundary layers) are placed into one coarse mesh block. In this way all the cells in the coarse mesh are of comparable size, which is good for time-accurate unsteady solutions which have a timestep fixed throughout the domain. The solution is then advanced in two steps, one based on the residuals on the coarse mesh, the second on the fine mesh on which the flow variables are stored, and the fluxes evaluated. Thus the solution is accelerated, as the allowable timestep is increased - the ratio of speed up being given by the ratio of sizes of grids. This procedure is explained in greater detail in He (1993b).

Fluid Boundary Conditions

The equations of motion for the fluid cannot be solved without boundary conditions being specified. These are the flow conditions in space at the edge of the fluid domain (blade surface & farfield), and for unsteady calculations, the conditions in time. On solid surfaces a slip condition is used, i.e. normal velocities are set to zero. The wall shear stress for turbulent flow is determined by the log law approximation.

At the inlet and outlet boundaries, the 1D non-reflecting boundary conditions are adopted to prevent the unwanted effect of artificial reflections passing back into the domain, as in Giles (1990b).

The mesh movement for moving blade calculations was achieved using a spring analogy. The motion of the blade surface was obtained from the structural part of the code, then the motion of grid points in the blade passage were calculated by linear interpolation, reaching zero far from the blade.

5.2.3 Partially-Integrated Method of Solution

The fluid and structural equations are solved together in partially-integrated manner as described above. The timestep used is the same for both fluid and structural calculations. Combinations of velocities and displacements of specified degrees of freedom can be selected as initial conditions for the structural equations. Steady flow is the starting condition for the flow variables; i.e. the initial conditions for the aeroelastic problem are perturbations from this equilibrium condition. Alternatively, the motion of the structure can be prescribed for a number of periods (e.g. pitching at a fixed amplitude) and then the coupled calculation can be continued from this. The solution is then advanced in time and the aeroelastic response is observed.

Energy Analysis of Flutter

Due to the complex nature of the results of time-accurate integrated non-linear aeroelasticity analysis, and the added uncertainty owing to arbitrary starting conditions, energy analysis may help in interpreting the results. Also this will demonstrate the accuracy of the partially-integrated approach, compared to the so called fully-integrated approach, where fluid and structural equations are formulated and solved together in time.

The governing structural equations can also be written in terms of energy, from Lagrange's equation (3.6). The kinetic energy in the structure is,

$$E_k = \tfrac{1}{2}\sum_{i=1}^{n}\sum_{j=1}^{n}\dot{q}_i m_{ij}\dot{q}_j = \tfrac{1}{2}\dot{\mathbf{q}}^T\mathbf{M}\dot{\mathbf{q}} = \tfrac{1}{2}\dot{\eta}^T\dot{\eta} \tag{5.6}$$

and elastic potential energy is,

$$E_p = \tfrac{1}{2}\sum_{i=1}^{n}\sum_{j=1}^{n} q_i k_{ij} q_j = \tfrac{1}{2}\mathbf{q}^T\mathbf{K}\mathbf{q} = \tfrac{1}{2}\eta^T\left[(diag\omega_n^2)\right]\eta \tag{5.7}$$

and viscous damping energy dissipation is,

$$E_d = \tfrac{1}{2}\sum_{i=1}^{n}\sum_{j=1}^{n}\dot{q}_i c_{ij}\dot{q}_j = \tfrac{1}{2}\dot{\mathbf{q}}^T\mathbf{C}\dot{\mathbf{q}} = \tfrac{1}{2}\dot{\eta}^T\left[diag(2\zeta_n\omega_n)\right]\dot{\eta} \tag{5.8}$$

and the work done by the fluid is,

$$\delta W_F = \sum_{i=1}^{n}{}_S\int (F_F)_i dq_i = \int \{\mathbf{p}(t)\}_i \bullet \mathbf{dq} = \int \Phi^T\mathbf{p}(t)d\eta \tag{5.9}$$

In this particular study, Lagrange's equation can be simplified as E_p is a function of co-ordinate only (not velocities), and E_k is a function only of velocity:

$$\frac{d}{dt}\left(\frac{\partial E_k}{\partial \dot{q}_i}\right)+\frac{\partial E_d}{\partial \dot{q}_i}+\frac{\partial E_p}{\partial q_i}=\frac{\partial W_F}{\partial q_i} \tag{5.10}$$

Thus, defining ΔE_{tot} to be the change in total energy in the structure:

$$\Delta E_{tot}=\Delta E_k+\int E_d dt+\Delta E_p=\Delta W_F \tag{5.11}$$

Thus by calculating the structural energy and the work done by the fluid on the structure, a measure of the accuracy of the method can be produced: in the absence of any damping of the structure, their difference should remain constant at the initial energy of the structure (E_o)

5.3 CASE STUDY: NACA006 WING

The NACA64A006 aerofoil has been selected as a test case for the aeroelasticity studies, since a large body of published information exists on this case. Ballhaus & Goorjian (1978) used various classical approaches to predict the flutter stability, and compared them with a time-marching approach. Guruswamy & Yang (1981) presented an integrated approach, and Kousen & Bendiksen (1989) presented an exhaustive study of this case in 2D, against which the present analyses can be compared. This case exhibits non-linear behaviour of the fluid in the transonic flow regime, and thus the classical methods have failed to predict the flutter point accurately.

Flexible Wing Model

The parameters used in the rigid section analysis were as follows:

$a_h = -0.2, \quad x_\alpha = 0.2, \quad r_\alpha = 0.5385,$

$\overline{\omega} = 0.3434, \ \zeta_h = 0.0, \quad \zeta_\alpha = 0.0,$

$\mu = 10.0, \quad \overline{U} =$ varying from 1.5 - 2.5 (n.b. $\kappa_{c(\omega_\alpha)} = \frac{2}{\overline{U}}$)

The model described herein is an attempt to improve the structural formulation of the 2-D rigid model of Chapter 4 by moving to a 3D wing, using the CFD code AV3D - this compares with the work of Bendiksen (1991) and Guruswamy (1989, 90).

The structural parameters for the flexible wing have been calculated using an FE vibration analysis (ANSYS) of a straight untapered NACA006 wing of length 3 chords, clamped at one end. The chord length was taken as 1m. The section was modelled using 3mm thick shell elements on the aerofoil skin, with extra bar elements at 30% & 70% chord to increase the through section rigidity. The material density (ρ_s = 1310 kg/m^3) was chosen to give a total mass of 23.9kg (mass per unit length = 7.967 kg/m). This gives a mass ratio, μ, of about 10, as for the rigid section. The Young's modulus was taken as that of Aluminium (E = 1690 MN/m^2). The resulting 10 lowest modes are as follows:

Table 5.1 Finite Element Modes

Mode	Freq. (Hz)	Description
1	9.19	1st flap
2	33.66	1st combined
3	40.16	1st torsion
4	50.91	2nd flap
5	66.61	3rd flap
6	70.14	2nd combined
7	84.00	4th flap
8	91.50	2nd torsion
9	100.55	5th flap
10	107.48	3rd combined

The FE mesh and the calculated modeshapes can be seen in **Fig.5.1** (scaling is given by mass-normalisation). The mode shapes have been directly interpolated onto the fluid surface mesh points for non-rigid body motion calculations. The first three modes were used in the flutter analysis.

Steady Flow Results

The steady flow has also been calculated in 3D using the AV3D code. The mesh used was 51 x 71 x 11 grid points, giving 880 points on the two wing surfaces, as shown in **Fig. 5.2**. The inlet and outlet boundaries were placed 2 chords upstream and downstream, and the farfield boundary was placed 3 chords away from the wing surface, in order to minimise any boundary effects, including reflections. Nevertheless the code uses non-reflecting boundary conditions for unsteady flow. For this grid, the timestep limit from the CFL number gave around 2000 timesteps per cycle of the lowest frequency mode. Thus, even for higher modes there were enough timesteps to ensure an accurate solution of the structural motion.

The steady flow for this configuration was computed at Mach numbers of 0.80, 0.85, 0.87, & 0.92. The wing pressure coefficient, C_p is plotted against axial distance in **Fig. 5.3**. These can be compared with **Fig. 4.4** from the 2D code. The Mach number contours at M=0.87 can be seen in **Fig. 5.4.** It can be seen that the shocks in the transonic cases are predicted to be in the same position in both cases. However the 3D code predicts a distinct suction peak immediately behind the leading edge, a feature which is not so clear in the 2D code - which may be due to mesh resolution.

Fluid Mesh Kinematics

For aeroelastic analyses it is necessary to calculate the flow in the fluid as the structure moves. This requires that the fluid mesh deforms to follow the surface of the aerofoil as it moves. The AV3D code has this capability for unsteady flows, using a simple spring analogy where the mesh points move with a simple linear distribution so that displacements are zero far from the solid surface. The code takes full account of the unsteady fluxes which arise due to the changes in cell volumes at each timestep. Some examples of the moving mesh for non-rigid body aerofoil motions on the structured grid can be seen in **Fig. 5.5**.

Flexible Wing Aeroelasticity Calculations

As explained above, the modeshapes which are obtained from an FE free vibration calculation are interpolated onto the fluid mesh to be used. The surface of the aerofoil then moves according to a summation of the current modal displacements. For the original frequencies, the reduced speeds based on the torsional frequency (mode 3, f_α = 40.16 Hz) for the Mach numbers of interest, are shown in **Table 5.2**, as follows:

Table 5.2 Reduced Speeds

Mach No., M	**Flow Speed, U_∞ (m/s)**	**Reduced Speed, U^***
0.80	272.1	2.16
0.87	296.0	2.35
0.92	313.0	2.48

These values of reduced speed are relatively high, so the wing is liable to diverge or flutter violently. For this case, as a real geometry is being used for both the fluid and the structural domains, it was necessary to artificially modify the frequencies of the modes to achieve the desired parametric study of reduced speeds. Otherwise the geometry would have to be changed, which would mean a recalculation of the free vibration modeshapes for each case.

Thus, to achieve lower reduced speeds, the torsional frequency was increased to give the required value, and the other modes were scaled by the same amount (this is equivalent to changing the material Young's modulus to stiffen the wing). To compute the flutter boundary for this wing, the torsion frequency was raised to a maximum value of 53 Hz (a maximum change of about 30%). The plunge (1st flap) frequencies have also been adjusted to give have the desired frequency ratio of 0.3434 (max. change about 90%).

Table 5.3 Change in Reduced Speed for New Frequencies

Mode 1 (1st bending) Freq., f_h (Hz)	Mode 3 (1st torsion) Freq., f_α (Hz)	Reduced speed, U^* (M=0.80)	Reduced speed, U^* (M=0.87)	Reduced speed, U^* (M=0.92)
17.97	52.34	not used	1.80	1.90
17.10	49.81	not used	1.89	2.00
16.18	47.10	1.84	2.00	2.12
15.20	44.28	1.96	2.13	2.25
14.37	41.87	2.07	2.25	not used
13.79	40.16	2.16	2.35	not used

The flutter stability of this wing was then investigated around transonic flow speeds. The time-accurate solution was started from steady flow by giving the structure a small velocity in mode 3 (equivalent to hitting the structure with an impulsive force). From the resulting time history the flutter stability was determined, as shown in **Table 4.** Note that these cases can be broadly compared with the 2-D results from Chapter 4, however the reduced frequencies used are non identical in all cases.

Table 5.4 Aeroelastic Calculations

Case	**Mach No. M**	**educed peed,. U^***	**Result (LC in m & deg)**
A	0.80	1.84	Stable
B	0.80	1.96	Neutrally Stable
C	0.80	2.07	L.C. (0.3m, 20°)
D	0.80	2.16	L.C. (0.6m, 30°)
E	0.87	1.80	Stable
F	0.87	1.89	Stable (diverges)
G	0.87	2.00	Neutrally Stable
H	0.87	2.13	L.C. (0.25m, 8°)
J	0.87	2.25	L.C. (0.4m, 12°)
K	0.87	2.35	L.C. (0.5m, 20°)
L	0.92	1.90	Stable
M	0.92	2.00	Divergence / L.C.
N	0.92	2.12	L.C. (0.1m, 2.5°)
P	0.92	2.25	L.C. (0.25m, 5°)

It can be seen that the transonic flutter stability for this wing is broadly similar to the results for the 2D standard section. The reduced speeds used in this case do not exactly correspond to the 2D case, as flutter occurs in at a slightly different value for each Mach number. Furthermore, this 3D model also models the energy exchange between the fluid and structure as well as for the 2D case. This can be seen in **Figs. 5.6a-c** for which the energy is plotted along with the modal and real displacements.

Here, a limit cycle of large amplitude is produced, however the difference between the total energy in the structure and the work done by the fluid remains equal to the initial energy of the structure.

The aeroelastic behaviour at 0.87 Mach number can be seen in **Fig. 5.7**, from stable behaviour, through neutrally stable to limit cycle flutter. Note that the stable case does not return to the initial position - this is because there are equilibrium points either side of the central position where the lift balances the elastic forces in the wing. At M=0.92, the same coupled flexure/torsion flutter mode is evident as in the 2D case - see **Fig. 5.8.**

As the reduced speed increases further, the size of the limit cycle increases, and the time taken to reach a limit cycle reduces, as is the case with the 2D rigid section. It is clear from the nature of the motion (**see Fig. 5.6b**), that the flutter mechanism is still coupling between the plunge and pitch modes, but with a phase of about 120° in this case. This change from the 180° phase in the rigid case is due to the camberline bending effects.

A number of other interesting effects can be see from this case study. Firstly the non-linearity of the flow at transonic speeds makes the response non-linear. The M=0.80 case is shown in **Fig. 5.9**. This shows that for different sizes of initial impulse, the response of the wing is quite different - all cases are stable at U^*=1.96, however for small initial motion the wing returns to a symmetrical position (with a very small motion that does not show up on the scale shown), but for a larger initial motion, the wing executes some large oscillations, before finally settling to a pitched up position.

Secondly the effect of section flexibility can be seen from the behaviour at M=0.87 in **Fig. 5.7**. Here the wing, at a reduced speed, U^*, of 2.25 exhibits a limit cycle similar to the 2D case with one important difference - the motion is not symmetrical about the initial position. This shows the effect of the flexibility which is not possible with the rigid section. Note that the motion could equally well be started in the opposite direction which gives a mirror image motion about the time axis.

Finally the Bifurcation diagram for this wing is shown in **Fig. 5.10** - the pattern is broadly similar to the 2D case, however it is not possible to directly compare them as the parameters μ, U^* and R, are identical but r_α, and x_α are not exactly the same for this wing as for the standard section. Also there are the effects of the camberline bending, and the 3-dimensional motion of the wing, that introduce differences

between the two models. The main difference has come about for the M=0.80 case - the point at which the transonic dip is most noticeable in the rigid case. Obviously the flutter mechanism is most sensitive to parameter variation at this Mach number.

5.4 CONCLUSIONS

(i) A 3-D partially-integrated methodology for the aeroelastic analysis of wings in transonic flow has been presented. The main features include an inviscid Euler analysis of the fluid flow, and an assumed modes model of the structure.

(ii) The aeroelastic analysis of the NACA006 wing has been shown to agree qualitatively with published results for rigid aerofoils: limit cycle behaviour is observed in most cases, a feature which cannot be predicted by linear and decoupled analyses. The flutter mechanism is found to be the coupling of translational and torsional modes with slight differences due to slightly different parameters to the rigid case.

(iii) The 3D flexible wing analysis shows the importance of non-linearities, and the effects of flexibility on the aeroelastic behaviour of the wing. This is highlighted by the asymmetrical behaviour of the response, and the existence of different responses to different initial conditions.

(v) The energy interchange between the fluid and the structure is shown to be modelled accurately for the partially-integrated method. This applies even up to large amplitudes of motion at which the validity of the model becomes questionable.



Fig. 5.1a FE Mesh

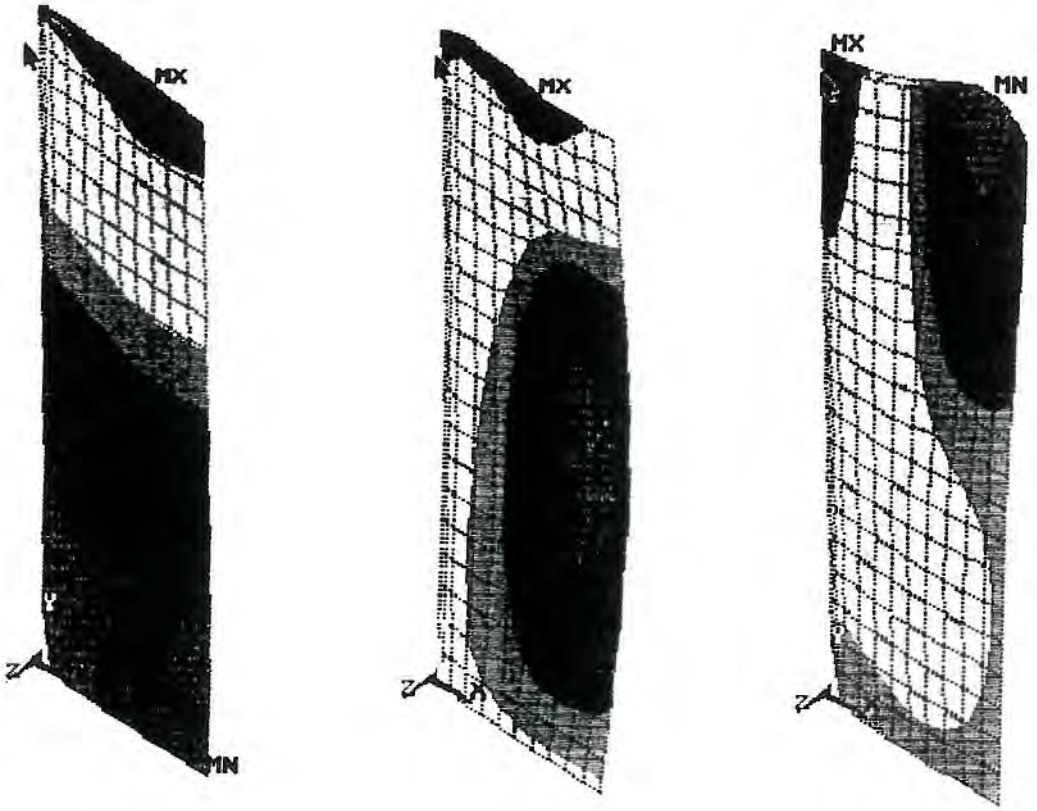

b) Mode 1 c) Mode 2 d) Mode 3

Fig. 5.1 FE Vibration Modeshapes

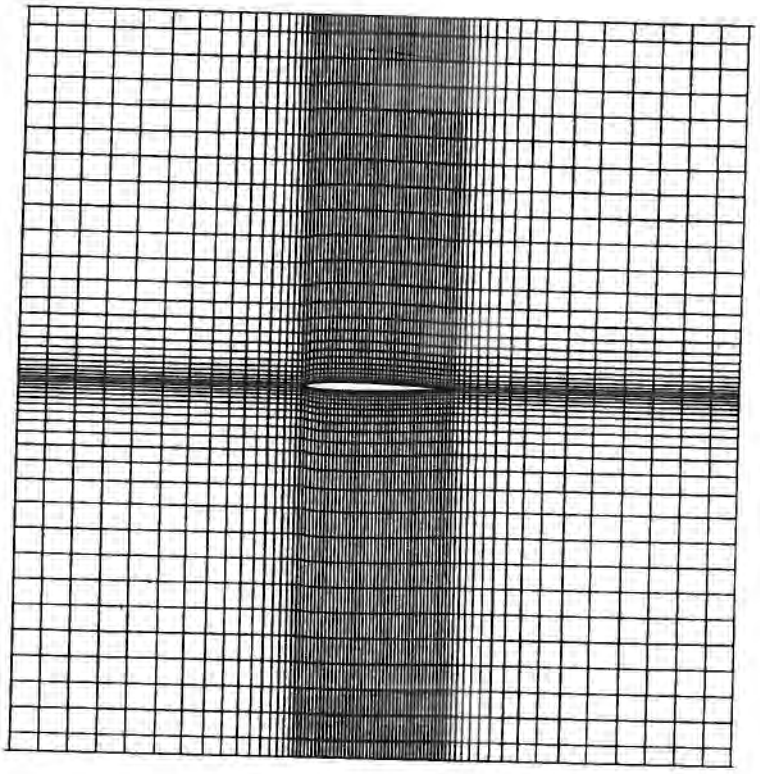

Fig. 5.2 Aerodynamic Mesh

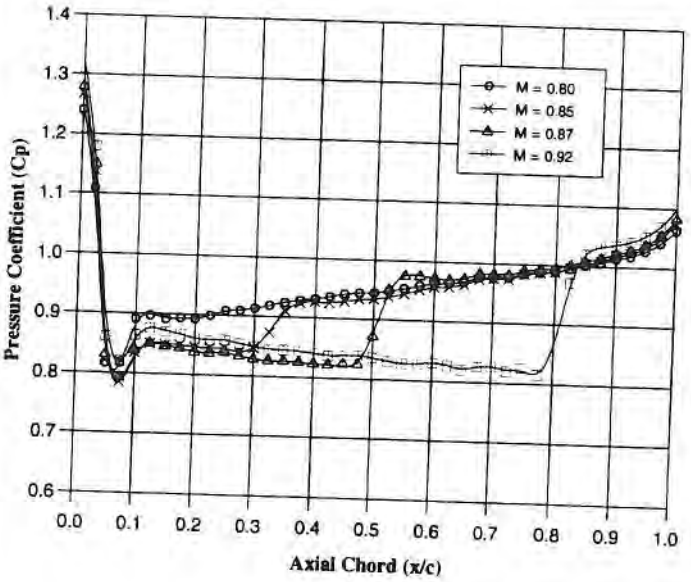

Fig. 5.3 Surface Static Pressures

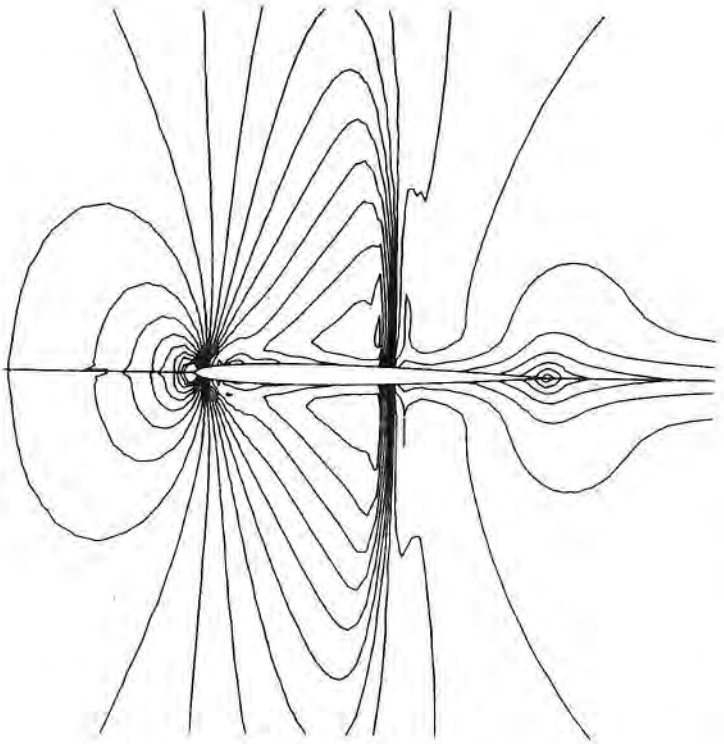

Fig. 5.4 Mach Number Contours (M=0.87)

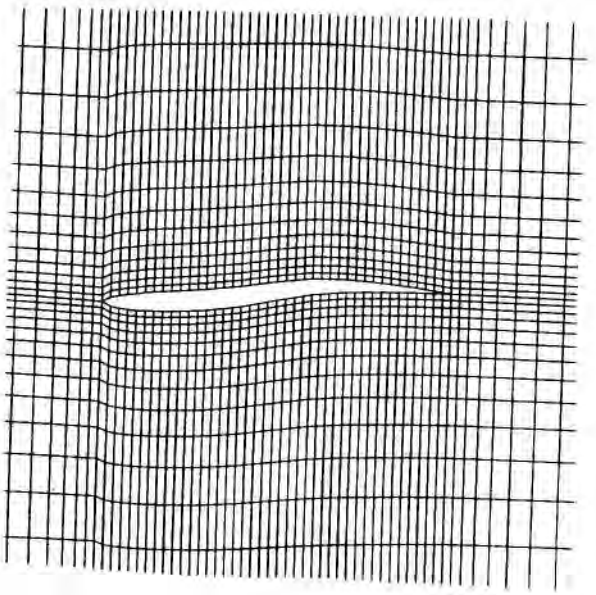

Fig. 5.5 Mesh Motion Detail

a) Tip Displacement

b) Modal Displacement

c) Energy

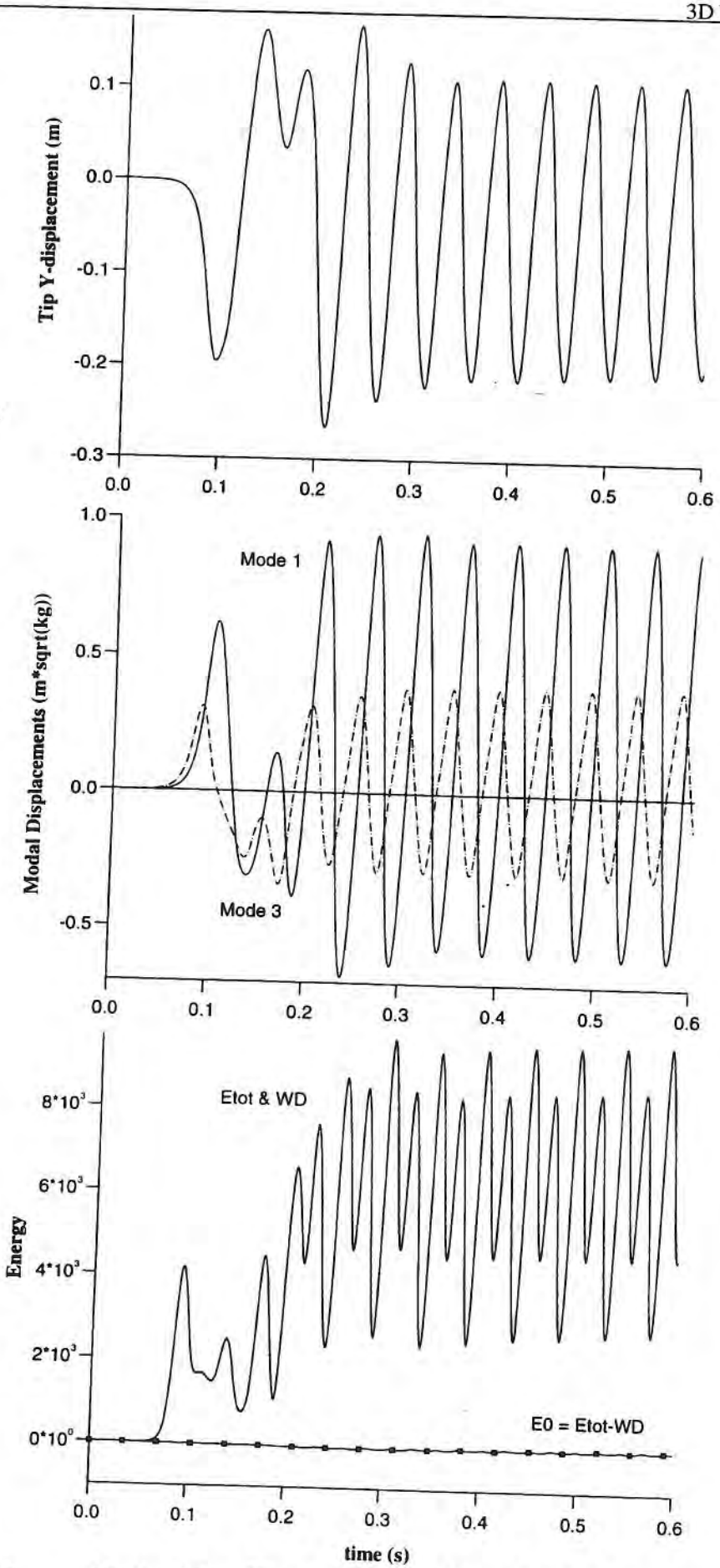

Fig. 5.6 Flutter Time History (M=0.80, Mu=10, U*=2.07)

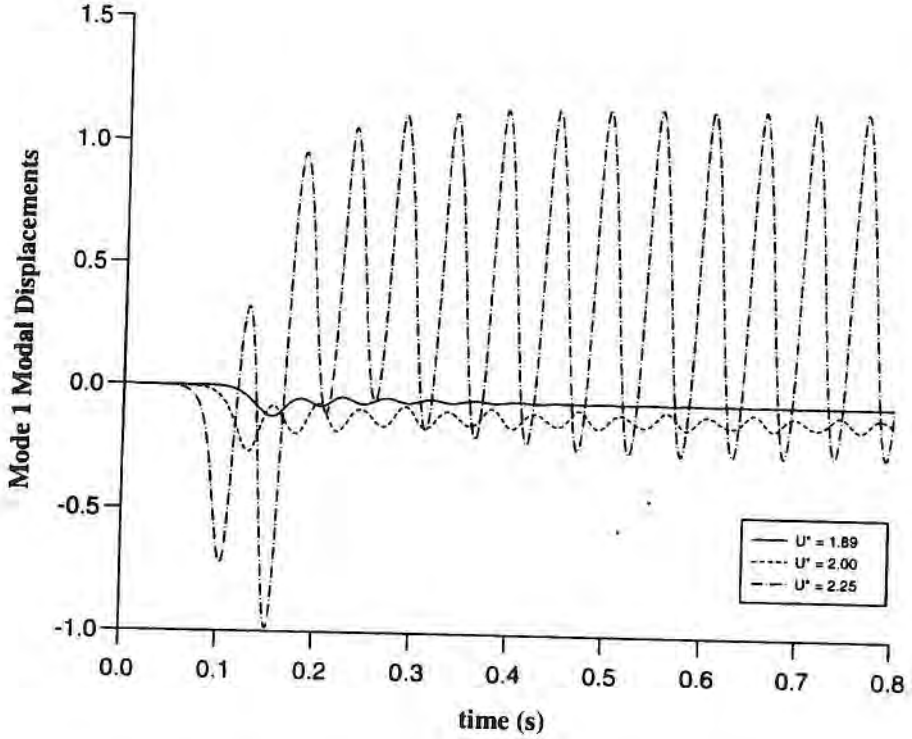

Fig. 5.7 **Flutter Time History (M=0.87, Mu=10, U*=1.89, 2.00 & 2.25)**

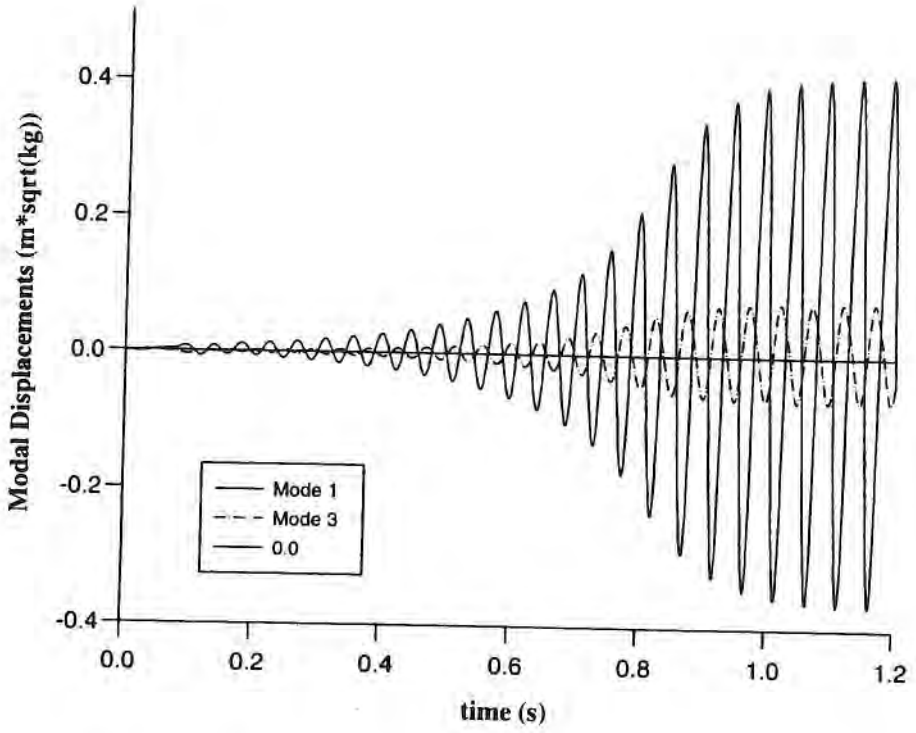

Fig. 5.8 **Flutter Time History (M=0.92, Mu=10, U*=2.12)**

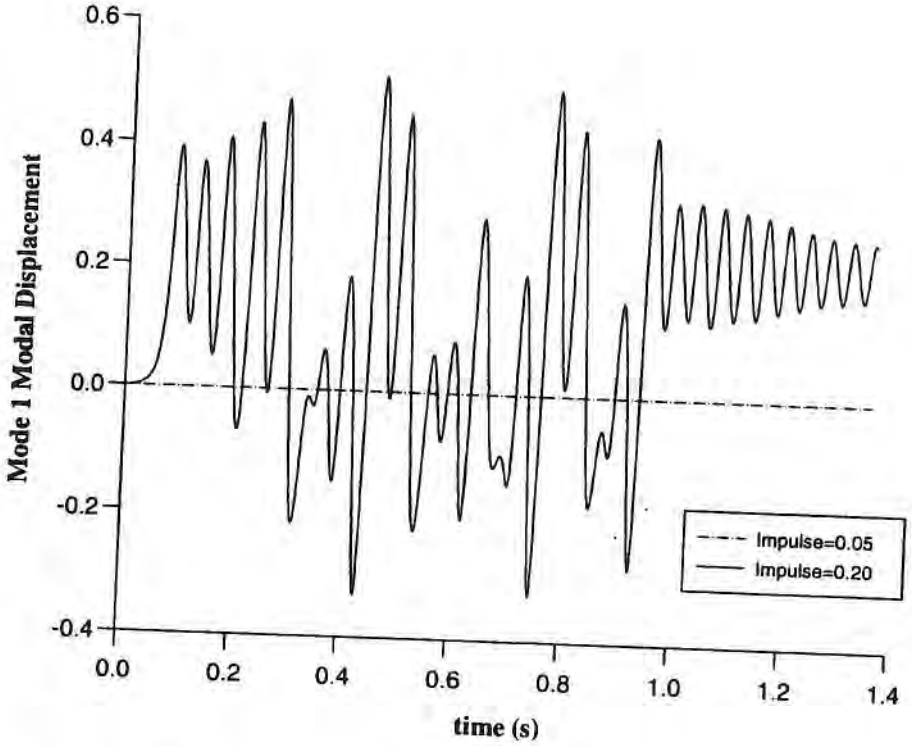

Fig. 5.9 **Effect of Starting Conditions (M=0.80, Mu=10, U*=1.96)**

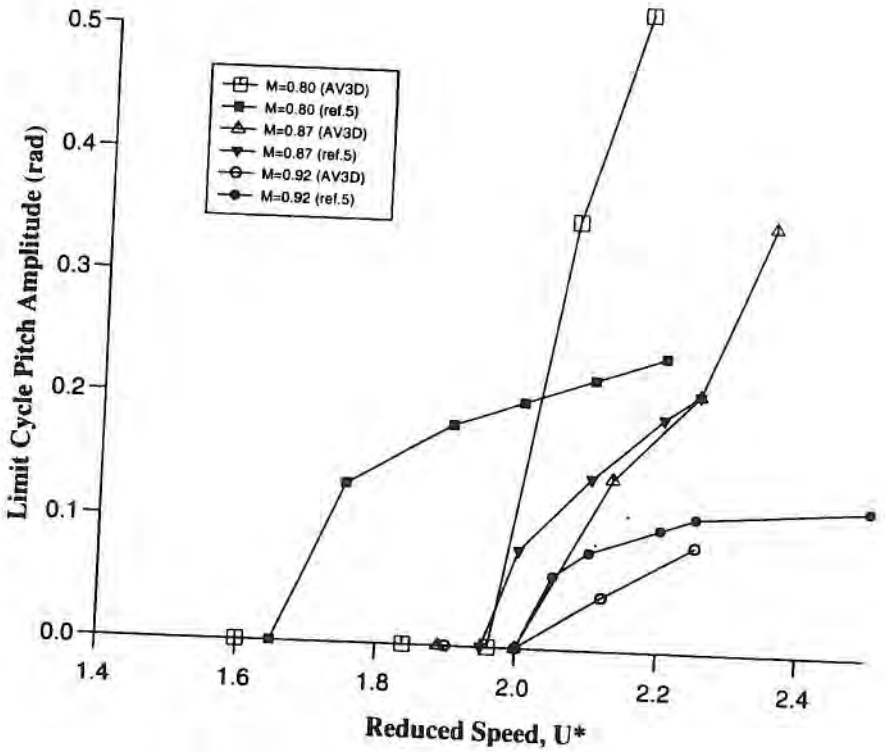

Fig. 5.10 **Bifurcation Diagram**

Chapter 6

An Example of Static Aeroelasticity: 3D Blade Untwist

6.0 About this Chapter

As described in previous chapters, the calculation of the blade running shape is an important first step towards a subsequent full aeroelastic analysis, as well as performance analysis. The integrated aeroelasticity method of Chapter 3, has been applied to the case of a three-dimensional front stage compressor rotor, typical of contemporary design. This research fan blade operates over a wide range of speeds and pressure ratios, and its performance is crucial to the overall performance of the whole aeroengine. Furthermore, the blades are of cantilever design, with a low hub/tip ratio, and the flow is transonic with a high stage loading, so the tip deflections due to rotation and gas loads are likely to be high.

The integrated time-marching approach is used to calculate the gas deflections at running speed, with the centrifugal force corrected vibration modeshapes coming from a FE calculation. This approach has a number of advantages compared to the classical static aeroelasticity analysis, to which it will be compared. The static analysis includes the full effect of geometrical non-linearity due to rotation, whereas in the current integrated model, the centrifugal forces are assumed to be constant as the blade moves due to the gas loads.

6.1 INTRODUCTION

The accurate prediction of the static blade deflection under running conditions has been a long standing problem in the turbomachinery industry. The blades deform elastically from their original manufactured shape under the combined effect of centrifugal loads and gas pressure, a phenomenon colloquially known as *blade untwist*. Although the blade untwist is sometimes considered to be a rigid body rotation of the various blade sections, the actual profile of these sections may also change.

In turbomachinery, the problem is in effect an inverse one: a shape for the blade is designed to give optimum aerodynamic efficiency at some working condition; but this is not the shape that must be manufactured. The manufactured or 'cold' blade shape must be calculated by taking off the effect of centrifugal and pressure loads - this is known as 'blade unrunning'. If the calculation of the manufactured shape is incorrect, the shape at running speed will not be that desired, and the efficiency of the machine will suffer. For calculations at off-design conditions (e.g. a flutter analysis) the shape at that state must first be calculated from the cold shape, otherwise the steady state aerodynamic calculation will refer to a wrong blade position.

There are two possible approaches for static aeroelasticity using a partially-integrated method.

6.1.1 Iterative Approach

The iterative method is similar to that currently employed by the aerospace industry. The method aims at avoiding the use of time accurate CFD codes to save computational effort. However, in order to do this, the aerodynamic solution must be fully converged to each new position before then moving the structure, else errors may occur if time accuracy were not preserved. This method is similar to that proposed by Srivastava et al. (1991), and Yamamoto et al. (1992), for use with propfans. The normal starting point for calculations during the design of a blade is the running condition (i.e. the fully deflected position of the blade). Thus the gas loads can be calculated without iteration, then the blade is 'unrun' (i.e. loads under running conditions are removed), to calculate the blade shape to manufacture. The run-up calculation is being performed here in order to provide a direct comparison with the integrated approach, which cannot perform unrunning calculations.

In general, the method involves using pressure distributions calculated by a 3D steady flow aerodynamic code which are then interpolated onto the mesh used in the

structural (FE) model. Thus the deflection of the blade can be calculated by balancing the aerodynamic, elastic and centrifugal forces acting on the structure. This process should be repeated, by recalculating the steady flow in the deflected position of the blade and iterating until convergence is reached (i.e. all forces balance and the blade does not move significantly if a further iteration is performed). This iteration, however, is often not performed, as 'unrunning' calculations are more usual, where no iteration is required. However, it may become important to iterate this calculation, particularly at off-design conditions, as the effect of the change in blade shape on the steady flow pressure distribution cannot be ignored.

A schematic of the solution procedure, and some advantages and disadvantages of the method are shown below.

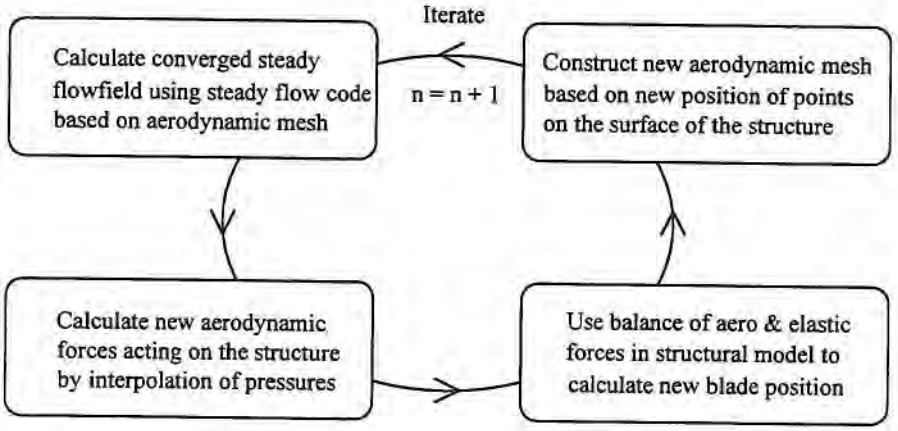

Advantages:

- existing programs can be used
- user has control at all stages of the analysis before proceeding
- possibly faster runtime
- can be accelerated by standard techniques

Disadvantages:

- user input is required at each stage
- convergence is not guaranteed
- repeated interpolation may be required

The problem with this type of method is the spliting of the calculation into separate parts for each of the two domains. So no matter how good the individual aerodynamic and structural calculations, the untwist may be incorrect as the coupling effects have been neglected, if the iteration is not fully completed or diverges. In summary, this

method is slow to produce results as much user input is required, and inefficient as the boundary conditions from one domain are only imposed on the other periodically.

6.1.2 Direct Approach

Instead of adopting an iterative steady-flow based approach, the solution can be marched in time from an appropriate starting point (e.g. steady flow of the blade in its cold position). The main advantage of this approach is that the data exchange between the two domains (fluid and structure) occurs automatically at each time-step, and the aerodynamic mesh moves to fit the blade motion - so the user does not have to regenerate the mesh each time. However, to do this, a fully time-accurate unsteady CFD code must be employed. This approach is similar to those proposed by Tatum et al. (1988), and Guruswamy (1989), used in the context of static aeroelasticity. A schematic of the method has already been described in Chapter 3, section 3.4.3, and the advantages and disadvantages are shown below.

Advantages:

- Only one job to set up and submit for running, so less elapsed time
- Method is basically the same as for dynamic aeroelasticity (flutter)
- More control on numerical convergence (use structural damping - see below)

Disadvantages:

- No user control or viewing of intermediate stages - only final result
- Little experience with the numerical behaviour of this method

It has been stated that the need for a more integrated approach arises from the non-linear response of fluid flow to the motion of solid boundaries, especially at transonic flow speeds, and the existence of non-linear structural effects such as non-linear material properties and large displacements. It is necessary to solve the fluid and structural equations together for static as well as dynamic aeroelasticity. However it is possible that for static aeroelasticity calculations accuracy in time may not need to be maintained throughout the two domains (fluid & structure) during the solution. This is obviously not the case for flutter calculations, but here we are only interested in the final position, not necessarily the history of how that equilibrium point came about. So a possible method of accelerating these calculations for production use would be to use local time stepping (where each grid cell uses a timestep up to its local limit, rather than a fixed global timestep based on the smallest cell). Finally, the solution may be accelerated, and more control placed on the convergence, by adding damping

to the structure. This will not affect the final converged position, but it will damp out the initial motions more rapidly, and thus save CPU time.

6.2 FORMULATION

The formulation for the integrated approach adopted is as described in chapter 3. Features that differ from that described above, especially for the static problem, are detailed below.

6.2.1 Structural Model

The structural part of the computation for untwist cases is conducted in two parts. First a finite element calculation is made of the blade alone, including centifugal (CF) effects, but without the fluid flow effects. Then these modeshapes are used in the coupled (PI) solution method, having been interpolated onto the aerodynamic mesh points. The solution is marched in time from an appropriate starting point: in this case the steady flow around the blade geometry at the appropriate speed in vacuo. The data exchange between the fluid and structure domains occurs automatically at each time-step, without futher interpolation, and the aerodynamic mesh moves according to the blade motion.

The unsteady structural motion was computed via modal summation over the modes kept in the analysis - in this case up to 20 modes were retained, and the effect of higher modes was found to be minimal. The equations were advanced in time using the Newmark-β method, which is unconditionally stable, with data exchange occurring alternately. In any case, accuracy was ensured by using a time step 50 times smaller than the period of the highest mode considered. However, in most cases, the time step was chosen according to restrictions imposed by the fluid solver which is much more restrictive (especially for viscous calculations). For these calculations the same time-step was used throughout the fluid-structure domain, but for a production tool, it may be possible to use acceleration schemes where each part of the domain takes different time-steps up to its stability limit in order to reach the equilibrium position more rapidly.

6.2.2 Aerodynamic Model

The fluid model is the same 3D model as used in Chapter 5, as devolped by He (1993b). However, for turbomachinery geometries cylindrical polar coordinates in the absolute frame of reference are used, and the viscous terms are switched on. Thus the details of the model are as follows:

Navier-Stokes Equations

The integral form of the Navier-Stokes equations with a cylindrical polar co-ordinate system in the absolute frame of reference, can be written in the following notation:

$$\frac{\partial}{\partial t}\iiint_{\Delta V}\mathbf{U}dV+\oiint_{dA}\begin{Bmatrix}(\mathbf{F}-\mathbf{U}v_{xg})\mathbf{n}_x+(\mathbf{G}-\mathbf{U}v_{\theta g})\mathbf{n}_\theta\\+(\mathbf{H}-\mathbf{U}v_{rg})\mathbf{n}_r\end{Bmatrix}dA=\iiint_{\Delta V}\{\mathbf{S}_i+\mathbf{S}_v\}dV \quad (6.1)$$

where $(v_{xg},v_{\theta g},v_{rg})$ are the components of the grid velocities including the rotation velocity. Thus state vector **U**, flux vectors **F**, **G**, & **H**, inviscid source term $\mathbf{S}_i$ are given by:

$$\mathbf{U}=\begin{bmatrix}\rho\\ \rho v_x\\ \rho v_\theta r\\ \rho v_r\\ \rho E\end{bmatrix},\ \mathbf{F}=\begin{bmatrix}\rho v_x\\ \rho v_x v_x+p\\ \rho v_x v_\theta r\\ \rho v_x v_r\\ (\rho E+p)v_x\end{bmatrix},\ \mathbf{G}=\begin{bmatrix}\rho v_\theta\\ \rho v_\theta v_x\\ (\rho v_\theta v_\theta+p)r\\ \rho v_\theta v_r\\ (\rho E+p)v_\theta\end{bmatrix},\ \mathbf{H}=\begin{bmatrix}\rho v_r\\ \rho v_r v_x\\ \rho v_r v_\theta r\\ \rho v_r v_r+p\\ (\rho E+p)v_r\end{bmatrix},\ \mathbf{S}_i=\begin{bmatrix}0\\ 0\\ 0\\ \rho v_\theta{}^2/r\\ 0\end{bmatrix} \quad (6.2)$$

In this model, the viscous source term $\mathbf{S}_v$ is obtained using a number of approximations in order to reduce the computational effort. A simplified form of the thin-layer Navier-Stokes equations are adopted (Denton, 1983). The viscous terms in the energy equation are neglected, the justification for this being that at Prandtl numbers near unity (which is typical of the type of flows in turbomachines) the viscous shear forces are roughly cancelled by the heat conduction terms. So only the viscous shear terms in the three momentum equations remain, which are further simplified by only allowing shear tangential to solid surfaces. For laminar flows, the shear stress, τ, from a solid surface at normal distance n, is as follows:

$$\tau=\mu\frac{\partial v}{\partial n} \quad (6.3)$$

Thus the viscous source terms in a body force form can be approximated as follows:

$$\iiint_{\Delta V}\mathbf{S}_v dV=\oiint_{A}\mathbf{T}_v dA \quad (6.4)$$

where: $\mathbf{T}_v=\begin{bmatrix}0\\ \tau\cos\alpha_x\\ \tau\cos\alpha_\theta\\ \tau\cos\alpha_r\\ 0\end{bmatrix}$

α_x, α_θ, & α_r are the angles between the flow velocity and the 3 co-ordinate directions respectively. For turbulent flows the shear stress is modelled by an eddy viscosity:

$$\tau=\rho\varepsilon_m\frac{\partial v}{\partial n} \quad (6.5)$$

The eddy viscosity is obtained using a mixing length model, and is set to zero far from solid surfaces:

$$\varepsilon_m = (0.41n)^2 \left| \frac{\partial v}{\partial n} \right| \tag{6.6}$$

We now have five equations, and six unknowns (ρ, v_x, v_θ, v_r, E, and p), assuming we know the grid velocities, so we require a final equation in order to be able to solve the equations. This must be an equation of state for the fluid: for a perfect gas, which is the fluid we are usually dealing with, this is as follows:

$$p = \rho RT \tag{6.7}$$

thus: $p = (\gamma - 1)\left(\rho E - \frac{1}{2}\rho(v_x^2 + v_\theta^2 + v_r^2)\right)$

Fluid Discretization & Time Integration

The above equations can be integrated in time in order to solve both steady, and unsteady flows (as long as the scheme is time-accurate). The model described herein has been developed by He (1993b). The fluid domain is spatially discretized using a cell-vertex finite volume scheme on a simple H type mesh. Thus the semi-discrete equations become:

$$\frac{\partial}{\partial t}\left(A_{ij}\mathbf{U}_{ij}\right) = -\mathbf{R}_{ij} \tag{6.8}$$

Then the equations are time-marched in an explicit fashion, by discretizing the time-dependent term (left hand side of the equation) using the four-stage Runge-Kutta scheme as described in Chapter 3. The residual terms are formed thus:

$$\begin{aligned} \mathbf{R}_i &= \sum \left\{ (\mathbf{F} - \mathbf{U}v_{xg})\Delta A_x + (\mathbf{G} - \mathbf{U}v_{\theta g})\Delta A_\theta + (\mathbf{H} - \mathbf{U}v_{rg})\Delta A_r \right\} + \mathbf{S}_i \Delta V \\ \mathbf{R}_v &= \sum \mathbf{T}_v \Delta A \end{aligned} \tag{6.9}$$

The numerical damping term is formed using a second and fourth order adaptive smoothing in the axial direction as originally used by Jameson et al. (1983), and a simple second order smoothing in the pitchwise and radial directions.

The explicit timestep limit for stability, governed by the Courant-Freidrichs-Lewy (CFL) condition is relaxed by the use of a time-accurate two-grid integration process. In this procedure the mesh is split into the existing mesh (fine) and a second coarser mesh where a number of the smallest cells (usually in the boundary layers) are placed into one coarse mesh block. In this way all the cells in the coarse mesh are of comparable size, which is good for time-accurate unsteady solutions which have a timestep fixed throughout the domain. The solution is then advanced in two steps, one based on the residuals on the coarse mesh, the second on the fine mesh on which the flow variables are stored, and the fluxes evaluated. Thus the solution is accelerated, as the allowable timestep is increased. This procedure is explained in greater detail in He (1993a).

Fluid Boundary Conditions

The equations of motion for the fluid cannot be solved without boundary conditions being specified. These are the flow conditions in space at the edge of the fluid domain (blade surface & farfield), and for unsteady calculations, the conditions in time. On solid surfaces a slip condition is used, i.e. normal velocities are set to zero. The wall shear stress is determined by the log law approximation.

At the inlet and outlet boundaries, the 1D non-reflecting boundary conditions are adopted to prevent the unwanted effect of artificial reflections passing back into the domain, as in Giles (1990b).

For steady flow, at the periodic boundaries, the fluid state variables are averaged and the values on the upper and lower boundaries are then set equal to this mean value. This ensures the spatial periodicity of the flow. For unsteady flows with zero inter-blade phase angle (IBPA), as is the case for untwist problems, this condition still holds for unsteady flow.

The mesh movement for moving blade calculations was achieved using a spring analogy. The motion of the blade surface was obtained from the structural part of the code, then the motion of grid points in the blade passage were calculated by linear interpolation, reaching zero far from the blade. This fluid code is able to handle a simple model of tip-leakage, but this was not used in this study.

6.3 CASE STUDY: TRANSONIC FAN UNTWIST

The case study used is that of a contemporary design of front stage compressor rotor. This research fan blade operates over a wide range of speeds and pressure ratios, and its performance is crucial to the overall performance of the whole aeroengine. Furthermore the blades are of cantilever design, with a low hub/tip ratio, and the flow is transonic with a high stage loading, so the tip deflections due to rotation and gas loads are likely to be high.

Two different operating conditions are used to demonstrate the integrated method as applied to static aeroelasticity. The first case is at the design point, at high speed, at sea level conditions; here the gas loads are likely to be largest, and the results from the direct (unsteady) approach using the new integrated aeroelasticity method are compared to the results from the iterative (steady) method, and experiment, both of which are available from the industrial sponsor for this case. The second is a low

speed characteristic of this compressor, at sea level conditions (i.e. a range of operating conditions from choke, through peak efficiency to stall, at fixed speed).

In both cases a great deal of attention is paid to the aerodynamic side of the calculation, as the 3D viscous flow in a transonic compressor rotor is a particularly difficult problem (and a subject of active research in its own right). The meshes used were 33×99×33 and 25×81×25 grid points respectively. The second, coarser, mesher is used for the low speed case, as this case is used for a flutter analysis described in Chapter 8, and the finer mesh (with about twice as many points) would require too much CPU time for the flutter analysis. These mesh resolutions enabled the surface viscous boundary-layers (both blade surfaces and end-walls) to be adequately captured, with the wall-functions used in the code. The first layer for the blade surface was set at a y+ value of about 100 (1mm from wall) which is well within the log-law region.

6.3.1 Static Non-Linear Predictions - Sea Level Design Point (High Speed)

Untwist calculations for this blade were performed by the industrial sponsor using their in-house 3D steady flow viscous code to predict the blade pressure distribution. This CFD code is similar to AV3D in its structured grid methodology, however it is a cell-centred code, with full Navier-Stokes viscous terms, and using a k-l one equation turbulence model. The structural analysis used is the static 'iterative' method describe above, incorporating the geometrical non-linearity of the centrifugal forces. In these calculations, the pressure distributions over the blade surfaces were already available for the final position (i.e. the answer) as this is the desired 'design' geometry, thus no iteration was required. This is somewhat of a retrospective prediction so as to test the new method against the most accurate existing method. Normally the static method is only used to unrun the blade, as described above. To avoid this 'cheat' the aerodynamic calculation would have to be iterated, especially for points on the characteristic away from the design point, where the final geometry is unknown.

The value of the tip untwist was calculated as 3.56° using the static non-linear method. This may be compared with a value of 3.17° that was measured on the experimental rig test. The accuracy of the rig test measurements is thought to be about $\pm 0.3^{\circ}$, and there may also have been blade to blade variations in the untwist (the quoted value being the mean).

6.3.2 FE Solution

The FE mesh used for the structural analysis is made of 210 20-node brick elements with a total of 3926 nodes to form the aerofoil, excluding the root - the model is shown in **Fig. 6.1**.

The finite element analysis was performed at Low and High speeds. The CF-corrected mode shapes are input to the aeroelasticity code, as described above, to avoid direct integration of the mass matrix at each time step. Thus the static deflection due to the centrifugal loads alone are first added to the cold blade shape before the untwist due to the gas loads are calculated - the contours of displacement due to the CF loads are shown in **Fig. 6.2**. One consequence of this assumption is that the change in centrifugal loads when the blade moves due to the fluid loads is ignored. To overcome this the non-linear structural calculation would have to be integrated with the non-linear fluid calculation (which would be very CPU intensive). However for the cases examined, this effect was found not to be large as the gas loads are smaller than the centrifugal loads, so it should only be a second order effect.

The natural frequencies for Low & High speed are listed in **Table 6.1** for the first 8 modes (20 modes were calculated). The corresponding modal masses are also given. The material properties at the running temperature (80°C) were as follows: Young's modulus, $E = 1.106\times10^{11}$ N/m^2 ; material density, $\rho = 4428.8$ kg/m^3 ; Poisson's ratio, $\nu = 0.32$. The FE code was run in its preferred units (mm & Mg) and the mode shape data were converted to SI units after interpolation.

Table 6.1 FE Calculated Natural Frequencies (Low & High speed)

Mode	Description	Low Speed Frequency (Hz)	High Speed Frequency (Hz)	High Speed Modal mass (kg)
1	1st flap (1F)	186.0	216.1	1.520
2	1st edgewise (1E)	390.9	449.8	0.160
3	1st torsion (1T)	704.4	706.6	0.026
4	2F	811.7	888.5	0.034
5	2T	1171.7	1174.8	0.003
6	Combined	1399.5	1453.6	0.002
7	3F	1500.9	1525.7	0.005
8	3T	1864.2	1903.5	0.002

The resultant displacement contours of modes 1 and 3 for High speed are shown in **Fig. 6.3&4** respectively, for later comparison with the interpolated modeshapes. Thus it can been seen from the High speed modal masses that the higher modes are likely to have much less influence on the final deflected position. After some deliberation it

was decided to use 8 modes initially in the calculations as it was found that the displacement of the higher modes was small. However, the effect of the number of modes kept in the analysis is investigated further in **Section 6.3.6**.

6.3.3 Interpolation onto the Aerodynamic Mesh

An interpolation program was used to transfer the data, including the interpolation of both static deflections (untwist due to centrifugal loads alone), and the mass-normalised mode shapes, which are required for the untwist calculation.

The initial aerodynamic meshes were obtained from the blade definition for the cold geometry and the aerodynamic boundary conditions. H-type structured meshes with about 50,000 nodes (25×81×25) and 100,000 nodes (33×99×33), were generated for this static geometry - see **Fig 6.5**. These grids give 2,050 points and 3,300 points on the blade surfaces respectively. However, as the mode shape data were defined in terms of the FE mesh, the displacements were interpolated from the finite element mesh (210 20-node brick elements, giving 3926 nodes) onto the aerodynamic mesh. First the static displacements were interpolated to give the new blade geometry at speed in vacuo. Results are shown in **Fig. 6.6** (compare with **6.2**). Then the modal displacements were then interpolated onto this new (CF untwisted) aerodynamic mesh for each mass-normalised mode in turn.

The validity of the interpolation was checked by displaying the aeroelastic mesh along with displacements in the same format as the structural model. The interpolated results (modes 1& 3) are shown in **Fig. 6.7&8** (compare with **6.3&4**). These figures show a good agreement as care was taken to make sure the aerodynamic grid points line up with the FE mesh. To do this, as the blade is shroudless, the tip leading edge point was used as the reference point for these interpolations. This was found to give a better mapping than if the hub point was used, as this point is not explicitly defined on the FE mesh (it is given by the interface between the blade and the hub surface liner in reality).

6.3.4 Steady Flow Results

The steady flow was first obtained for the blade in the CF-alone untwist position (i.e. as if rotating in a vacuum). Then the coupled fluid/structure calculation was started, with the fluid forces providing the initial condition to start the structural motion. Once the blade was observed to reach a new equilibrium position under the gas load, the calculation was stopped. A new steady flow was therefore obtained for the blade in its final untwisted position due to both CF and gas loads.

High Speed Design Condition

This section aims at comparing the accuracy of the aerodynamic calculation at steady flow on different meshes densities. For these untwist calculations the 33×99×33 grids was used - this is the same size and type of spacing that was used for the sponsor's calculations, although that grid was for the 'correct' blade geometry (i.e. the running geometry as designed). Untwist results are shown for the final equilibrium position (after gas untwist) in order to compare them with the sponsor's steady solution. It should be noted, therefore, that the solutions is for slightly different blade positions (since the amount of untwist calculated is slightly different). These solutions are shown in **Figs. 6.9 - 6.12**.

The boundary conditions used for all calculations are identical. These plots show a good level of agreement between the AV3D calculations and the sponsor's calculations, especially when the same grid is used. The AV3D calculation does not predict the shock in exactly the same position as for the 'correct' geometry. Obtaining the right shock position is critical for the accurate calculation of both untwist and performance. For these cases the smoothing was modified in order to correct this: the results shown are for the optimum value of smoothing. However the flow still exhibits a slight overshoot at the shock, were it is strongest near the tip (see 90% height pressure distributions). It is thought that to prevent this, especially where the grid is highly skewed due to the blade stagger, the smoothing model could be improved in AV3D.

Also, to compare the AV3D and sponsor's results, mass-averaged radial distributions of various quantities have been calculated using a post-processing program. This code assumes that the streamlines are as from the throughflow calculation (not recalculated based on the 3D flow field). This may be a simplification but the same code was used to process all the data, so it is valid to compare them. The plots are shown in **Fig. 6.13**.

These plots are more revealing than the above contour and surface plots. They show that the two codes agree closely in overall integrated quantities, but their spatial distribution with radial height varies. This is illustrated by the pressure and temperature ratio plots, where it can be seen that the AV3D results are resonably close to the experimental results. The correct prediction of the radial profile is crucial to the successful prediction of the fan's performance.

Low Speed Sea Level Characteristic

The blade untwist results were also calculated for part speed conditions along the whole characteristic using the 25×81×25 grid. To obtain the different operating conditions the value of exit static pressure at the tip was specified (raised/lowered from the nominal value) and the radial distribution was obtained by radial equilibrium (an option in AV3D). These calculations were performed as the first step toward a flutter analysis, which will be described in **Chapter 8**. The results are shown for after the blade untwist, normalised to the value at peak efficiency. Three particular points on the characteristic will be examined in detail, namely: maximum flow or choke (MF), peak efficiency (PE), and near stall (NS). The resulting flow fields are shown here, and the untwist results will be examined in more detail in **Section 6.3.5**.

Table 6.2 Performance after Untwist along Low Speed Characteristic

Case	Tip Static Pressure (+/- %)	Total Pressure Ratio	Inlet Mass Flow	Inlet Meridional Velocity	Total Untwist (deg)
0 (stalls)	+7.2	-	-	-	-
1- NS	+6.1	1.0085	0.8551	0.810	3.07
2	+5.0	1.0106	0.8945	0.859	3.00
3	+4.2	1.0106	0.9196	0.891	2.95
4	+2.9	1.0085	0.9514	0.932	2.85
5	+1.7	1.0049	0.9762	0.966	2.74
7 - PE	0.0	1.0000	1.0000	1.000	2.55
10	-3.3	0.9803	1.0191	1.027	2.36
12	-5.0	0.9690	1.0240	1.034	2.31
15	-6.7	0.9577	1.0279	1.039	2.27
20 - MF	-10.1	0.9316	1.0345	1.048	2.20

Note that the reference back pressure is that used in case 7 (PE), and the rest are obtained by making a percentage increase or reduction from that value at the tip, with the radial profile obtained from radial equilibrium. Although a steady flow was obtained about the CF only geometry for case 0, once the untwist calculation was started, the blade *numerically stalled*. The term numerical stall is used as at this high incidence value, the simplified viscous model predicts a boundary layer completely separated by the shock, and once the blockage due to this effect increases sufficiently, the flow can no longer be supported and reverses. Although this phenomenon is of physical origin, this type of flow is beyond the limits of the 'thin-layer' assumption in the fluid model, so it cannot be termed a true stall.

The steady flow profiles are shown in **Figs. 6.14-17**. These exhibit shock positions after untwist near the tip from right at the back of the passage (near choke) to the front

(near stall). The effect of the shock position can be seen more clearly in the plot of blade loading for cases 1, 7, & 20 (**Fig 6.17**) - it can be seen that the centre of pressure varies from 15% chord near stall, through 45% chord at peak efficiency, to 65% chord at max flow. The variation in untwist is around 1° from choke to stall and this is accounted for by the shock position which mainly affects the size and sign (+ve or -ve) of the contribution from mode 3 (torsion).

The performance characteristics for these set of results is shown in **Fig 6.13**. Qualitatively the results look reasonable, however quantitatively the predicted pressure rise is too low, due to limitations in the viscous modelling in the current version of AV3D. This study is intended as a demonstration of the use of the aeroelasticity code in the prediction of blade performance along a characteristic where flow and structure change simultaneously.

The overall performance map is shown in **Fig. 6.14** along with the characteristics plotted from the tested performance map. It can be seen that the mass-flows (normalised to the PE value) as calculated by AV3D are quite close to the desired values at the points near stall. Also, the AV3D characteristics are somewhat low on the predicted pressure ratio; again this is down to the viscous modelling. However, it is important that the position on the operating characteristic can be established, in order to understand the flutter results.

Max Flow

At the maximum flow condition, also known as choke, the shock is strong and at the trailing edge of the suction surface. Thus further reductions in back pressure cannot move the shock any further downstream, and so the flow does not change. As the flow is choked - i.e. sonic at the throat (minimum area location) no more mass flow can be passed, so the flow is termed choked.

The fluid loading in this case thus produces roughly the same amount of 'lift' as the other cases, and the moment loading is anti-clockwise (looking in the negative radial direction). Thus the motion of mode 3 (torsion) counteracts the small clockwise twist in mode 1 (flap), and the overall gas untwist is almost zero. This is shown by the untwist data in setion 6.3.5.

Peak Efficiency

At the peak efficiency condition, the shock is in an intermediate position - i.e. about midway along the suction surface. Here the shock has a characteristic *lambda* shape,

which helps not to thicken the boundary-layer in the shock boundary-layer interaction. Thus the losses are lower near this condition, and efficiency is a maximum.

As the shock is halfway along the suction surface, the untwist gas loading is intermediate between the two extreme cases (NS & MF). Therefore there is some untwisting, but not as much as for the near stall case.

Near Stall

Near stall the flow exhibits a shock which stands outside the blade passage, as at these off- design conditions there is a large flow incidence. This shock tends to separate the boundary layer, especially lower down the blade, and for the lower rotational speed case. **Fig. 6.15** shows that on untwist the shock moves further upstream, as the blade twist increases the incidence. So, for these cases the flow is close to stalling, which the untwist exacerbates. This effect means that it could be difficult to obtain solutions at these conditions - if the back pressure is raised too much then numerical stall could occur, whereupon the blade returns to the CF only position as the gas loading becomes small.

From these steady solutions mass-averaged radial profiles were produced of quantities that can be compared with test data - shown in **Fig. 6.18**. These plots show the variation over the span of predicted and measured rotor pressure ratio and temperature rise ratio. There can be seen to be substantial discrepancies in the prediced data. It is thought that this is because AV3D (which solves for the thin-layer Navier-Stokes equations with a simple boundary layer model) over predicts the boundary layer separation. This increases the blade loading, which increases the untwist, which in turn increases the incidence, and thus higher loading. So the untwist predicted here may be slightly higher than expected, and the stall margin may be less than as tested.

6.3.5 Untwist Results

High Speed on Sea Level Design Point

The untwist time history is shown in **Fig. 6.19**. The contribution of the individual modes is shown in **Fig. 6.19a** in terms of the modal displacements. It can be seen that the overall displacement is dominated by mode 1, with small contributions from modes 2 and 3. Also **Fig. 6.19b** shows the time history of the modal forces; these hardly change as the blade moves - again because the main motion is in the flap direction which does not greatly alter the blade loading. For untwist calculations 12 modes were retained in the analysis. The time-histories, in terms of the tip-stagger angle, for both cases are shown in **Fig. 6.23**.

For these calculations the structure was heavily damped (90% critical damping). This is also a way of accelerating the computation, because the fluid on its own provides only a small amount of damping (and off design the blades could even be unstable). So with this assumption, the blade will reach its equilibrium position with a minimum number of over/undershoots but all indications of instability will also be damped out. This assumption was checked by running the code with very little structural damping. It was observed that the same equilibrium position would be reached, but in a much longer time interval. The calculation was therefore stopped when it became clear that the oscillations were about the expected equilibrium position.

Once a new equilibrium position was indicated by the time histories predicted at various locations on the blade, the untwisted blade geometry was defined using the tip section. It should be stressed that this method calculates deflections at all points over the 3D blade, not just rigid body rotation angles, however the tip stagger angle is the most convenient way of expressing the overall deflection. The calculation of a 2D twist angle has a built-in approximation of a rigid chord, but, as the displacement values are small, the calculation of the tip untwist angle is very sensitive to small changes.

The maximum blade displacement under both the gas and CF loads was predicted to be about 4.0 mm at the leading edge. This displacement is partly due to the CF load which accounts for about 3.0 mm. However, as shown in **Fig. 6.21a**, the CF load causes a displacement mainly in the torsional direction while the gas load results in a displacement in a bending direction. Since the displacement under the gas load only is of primary interest here, the CF effect has been removed before plotting the displacement contours of **Fig. 6.21b**. In this case, the predicted value for maximum blade resultant displacement under the gas load only is about 3.0 mm - see **Tab. 6.3**.

Table 6.3 Tip Untwist Displacements & Angles for High Speed Design Point

Parameter	dX_{LE} (mm)	dY_{LE} (mm)	dX_{TE} (mm)	dY_{TE} (mm)	Total Untwist (deg)
CF-only	-2.59	-0.95	+4.28	-3.92	3.29
CF+Gas	-3.87	+1.71	+3.32	-1.49	3.47
Gas-only	-1.29	+2.66	-0.96	+2.43	0.18

These results compare well with the computed and tested results. The untwist prediction is 3.47°, compared to 3.56° for the classical method, while the measured value from the rig test is 3.17°. It should be noted that the tip untwist angle depends heavily on the shock position; more specifically, the bulk of the untwist at the tip is

built up from mode 3 (1st torsion) and mode 1 (1st bending), which has a small torsional component in the opposite direction to a positive displacement in mode 3. The contribution from mode 1 is affected by the blade 'lift', so it does not change much with shock position; whereas mode 3 is affected by the gas moment, so changes markedly with shock position. Thus the balancing of the two effects determines the overall gas untwist.

Low Speed Sea Level Characteristic

The untwist time history of the tip stagger angle is shown in **Fig. 6.23** along with the High speed case. It can be seen how the loading in the torsional direction changes along the Low speed characteristic, leading to as much as 1° change in untwist angle from choke to stall.

The contribution of the individual modes for the Low speed case is shown in **Fig. 6.25a** in terms of the modal displacements. It can be seen that the overall displacement is dominated by mode 1, with small contributions from modes 2 and 3. Also **Fig. 6.25b** shows the time history of the modal forces (Low speed, NS); in contrast to the High speed design case, it can be seen that in mode 3 (torsion) the modal force increases as the blade twists, thus twisting it more. This creates a larger gas untwist contribution than for the design case.

Furthermore for these off-design conditions near the stall / flutter boundary, the blade as it untwists, increases the flow incidence onto the blade. This proved to be a problem as it was found that for a fixed back pressure distribution (the given one) the flow around the blade numerically stalled before equilibrium could be reached. To prevent this from happening the pressure at the tip was specified, and the back pressures determined by radial equilibrium. For the unsteady (untwist) calculation non-reflecting boundary conditions were used to allow perturbations to pass out of the domain.

The maximum blade displacement under both the gas and CF loads was predicted to be about 4.0 mm at the leading edge. This displacement is partly due to the CF load which accounts for about 3.0 mm. However, as shown in **Fig. 6.24** (for the NS case), the CF load causes a displacement mainly in the torsional direction while the gas load results in a displacement in a bending direction. In these cases, the predicted value for maximum blade resultant displacement under the gas load only varies between 1.6 - 3.9 mm - see **Table 6.5**. The results are also expressed in the form of a tip twist angle - see **Table 6.4**

Table 6.4 Tip Untwist Displacements & Angles for Low Speed Characteristic
(MF = Max Flow, PE = Peak Efficiency, NS = Near Stall)

Parameter	dX_{LE} (mm)	dY_{LE} (mm)	dX_{TE} (mm)	dY_{TE} (mm)	Tot. Unt. (deg)	Gas Unt. (deg)
CF-only	-1.23	-1.20	3.23	-3.09	2.05	-
CF+Gas MF	-1.90	0.31	2.69	-1.69	2.20	0.07
CF+Gas PE	-2.72	1.22	2.56	-1.13	2.55	0.42
CF +Gas NS	-3.67	1.81	2.69	-1.04	3.07	0.94

For these near-stall cases the tip untwist angle is particularly sensitive to shock position; here the mode 3 (1st torsion) component is larger than in the working line cases. The contribution from mode 1 (bending) does not change much with shock position; whereas the mode 3 contribution determines the incidence, which in turn effects the shock position, and thus the moment on the blade. So at off-design conditions the integrated method, which updates both structure and fluid domains together stands the best chance of correctly predicting blade untwist (and thus performance and flutter as well) unless iteration is performed in the uncoupled case. For these three cases the gas untwist increases slightly with speed, but the total untwist increases more markedly with speed due to the CF loads.

Table 6.5 Tip Gas Untwist Displacements for Low Speed Characteristic

Parameter	dX_{LE} (mm)	dY_{LE} (mm)	Magn. LE (mm)	dX_{TE} (mm)	dY_{TE} (mm)	Magn. TE (mm)
MF Gas	-0.67	1.51	1.65	-0.54	1.40	1.50
PE Gas	-1.50	2.42	2.85	-0.67	1.96	2.07
NS Gas	-2.45	3.01	3.88	-0.54	2.05	2.12

Table 6.5 shows the LE and TE displacements due to the gas loads alone, where dX and dY are X and Y displacements respectively. The displaced blade positions as calculated here have been used as the starting point for flutter predictions on this blade. The time-histories, in terms of the tip-stagger angle, for both cases are shown in **Fig. 6.23**. This shows how the untwist varies with operating point on the characteristic. Also, due to increase in the torsional component near stall, the amount of gas untwist near stall is greater than that at the design point. This is important for flutter prediction, as small errors in the prediction of untwist will not affect the performance much at the design point, but the same errors would have a large effect on the predicted position of the flutter boundary.

6.3.6 Effect of the Number of Structural Modes

Initially 12 modes from the FE analysis were retained in the assumed modes untwist calculation. Although this seems a small number, it was found that the modal displacements reduce rapidly with higher mode number - although the overall modal force of these modes can be as high as the lower modes. This is due to the fact that the modal mass of the modes reduces dramatically with increasing mode number. Thus the contribution of the higher modes to the blade displacement is probably beyond the numerical accuracy of the method.

As a further check, 2 other runs were performed, retaining 5 and 8 modes in the calculation respectively. As expected, results remained almost identical to those from the first calculation. The number of modes does not significantly affect the CPU time, as the structural equations are reduced to the principal co-ordinates and hence the computational effort is minimal compared to the fluid part of the calculation. However the required memory does increase rapidly with the number of modes, as the mode shape at each aerodynamic surface point has to be stored. The fine mesh of 33×99×33 was used when investigating the effect of the number of modes on blade untwist for the High speed case. Results are listed in **Table 6.6** below.

Table 6.6 Blade Untwist - Effect of Number of Modes

Parameter	Total Untwist °	Gas Untwist °
5 modes	3.437	0.145
8 modes	3.445	0.153
12 modes	3.467	0.175

This investigation shows that the total untwist angle could still be computed within 1% error if 5 modes only were retained in the analysis. Errors due to other sources, such as the viscous approximations in the code, are probably much larger than this. This result is partly masked by the small amount of gas untwist compared to the CF untwist, however the maximum error is still around 10% of the gas untwist in isolation. This sounds large but the absolute magnitude is only $0.03°$, which is considerably less than the error in the tested result. The contribution of each individual mode in the case of 12 modes to the final blade displacement is shown in **Table 6.7**.

Table 6.7 Contribution of Each Mode to Blade Untwist

Mode	Modal Mass (kg)	Modal force at equilibrium ($N/kg^{1/2}$)	Modal Displacement ($m\ kg^{1/2}$)	Approx. Contribution to Tip Disp. (mm)
1	1.520	-1464.5	-7.945×10^{-4}	-2.973
2	0.160	-548.7	-6.870×10^{-5}	-0.382
3	0.026	807.2	4.095×10^{-5}	0.353
4	0.034	-764.7	-2.454×10^{-5}	-0.143
5	0.003	76.4	1.402×10^{-6}	0.022
6	0.002	-838.8	-1.006×10^{-5}	-0.157
7	0.004	-343.8	-3.741×10^{-6}	-0.033
8	0.002	531.5	3.716×10^{-6}	0.039
9	0.001	-6.5	-3.998×10^{-8}	-0.001
10	0.001	-225.9	-1.098×10^{-6}	-0.005
11	0.002	-368.1	-1.524×10^{-6}	-0.031
12	0.001	176.6	6.562×10^{-7}	0.007

Table 6.7 shows the contribution of each mode to the final displacement, based on the final modal displacement at equilibrium. It can be seen that the contribution from the higher modes drops off sharply to fractions of millimetres, due to the increasing stiffness (shown by the reducing modal mass), even though the modal forces for these modes are almost as large as for the first mode. Thus it can be concluded that for this case, 8-12 modes is an acceptable number for untwist calculations.

6.4 CONCLUSIONS

Untwist calculations have been performed for a transonic fan blade using the integrated aeroelastic method. The steady flow results compare reasonably well for the High speed sea level condition with both the sponsor's numerical results and test data. The following conclusions have been drawn:

i) The untwist results for the High speed sea level case agree very well with the sponsor's predictions, at around $3.5°$ and reasonably well with the rig measured value. A measurement accuracy of $\pm0.3°$ may bring this into line with the calculated values.

ii) Steady flow evaluations have been made of AV3D with the Industrial CFD code - the agreement is reasonably good, especially when the same grid is used. However the viscous modeling and the smoothing could be improved.

iii) For the Low speed cases, untwist results have been produced along the characteristic. It is clear that at off design conditions use of the integrated method has a greater advantage over the uncoupled methods than at the design condition. This is because the flow changes significantly as the blade untwists, which is not

the case near the working line. So if the traditional method is used, many iterations would be necessary to calculate the untwist (assuming that the method converges). There are no measured untwist data available for these cases.

iv) The steady flow results for these cases are also presented, and are compared with some measured performance data. Here the agreement is not that good, especially for the blade efficiency, which is predicted much worse than measured. It is thought that near stall AV3D overpredicts the boundary layer growth, as these cases may near the limits of the thin-layer Navier-Stokes assumption that the code uses.

v) The use of 12 modes in the model was found to be adequate for predicting the untwist of this blade. However, even with as few as 5 modes, the errors were not large, and probably within the accuracy of other parts of the calculation.

vi) The assumed modes structural model is linear, and takes no account of the change in CF loading as the blade moves due to the gas loads. However, the method still compares well with the static non-linear calculation (including the correct CF loads). This is partly due to the fact that the gas loads are somewhat smaller than the CF loads in this case, but also that the accurate modelling of the complex fluid flow is probably the most important issue in these calculations. Here the integrated approach has a significant advantage over the classical approach in that it updates the fluid flow automatically as the blade moves.

vii) The method presented here was not particularly optimised for computational efficiency in this application. Many standard techniques could be used to speed up the calculation as time accuracy is not necessary for untwist calculations. Nevertheless the run times were acceptable, being about 2-3 times those required for a steady flow calculation without untwist on the same grid.

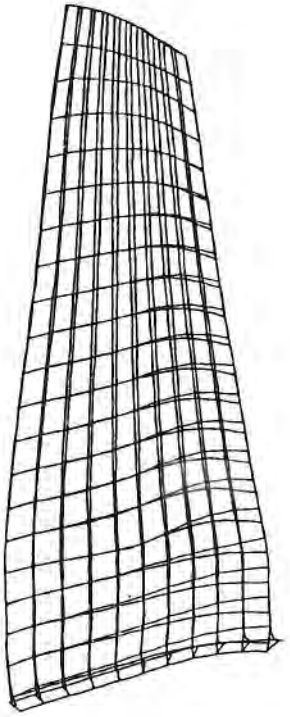

Fig. 6.1 FE Mesh

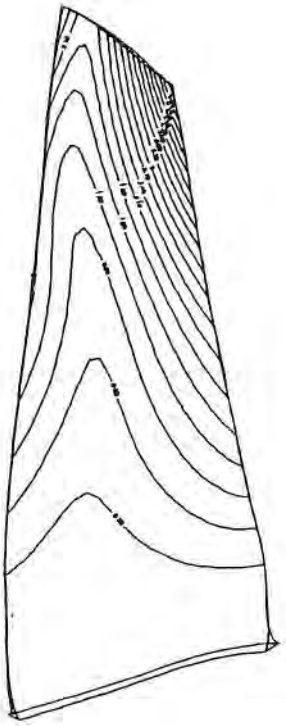

Fig. 6.2 CF Displacements

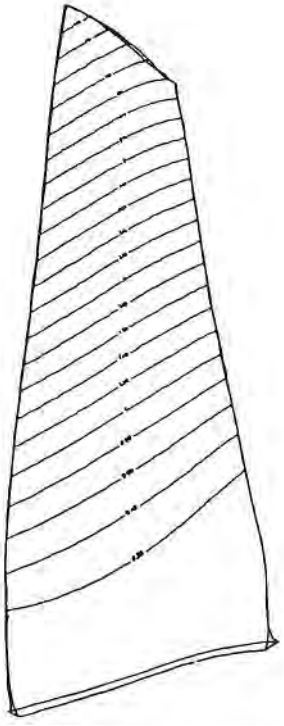

Fig. 6.3 Mode 1

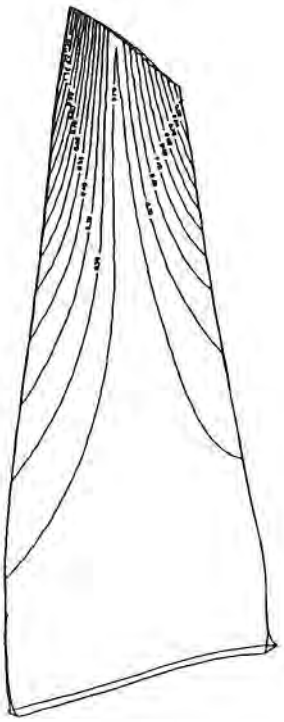

Fig. 6.4 Mode 3

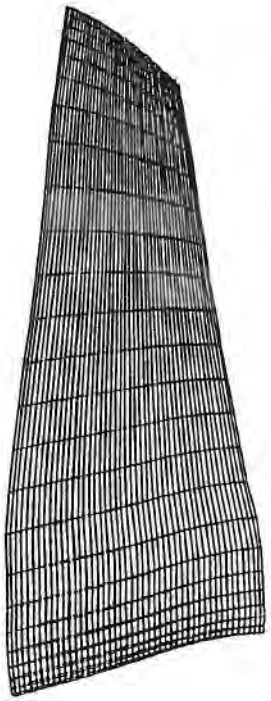

Fig. 6.5 AV3D Mesh

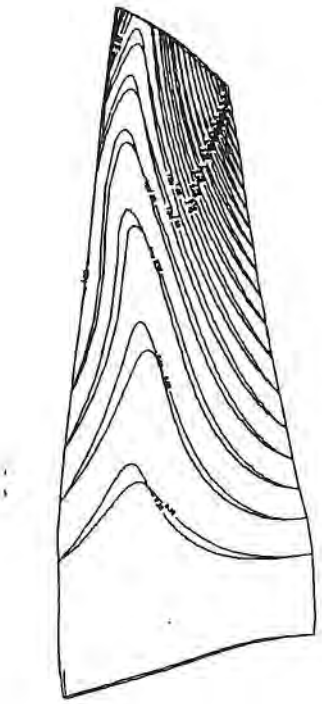

Fig. 6.6 Interpolated CF Displacements

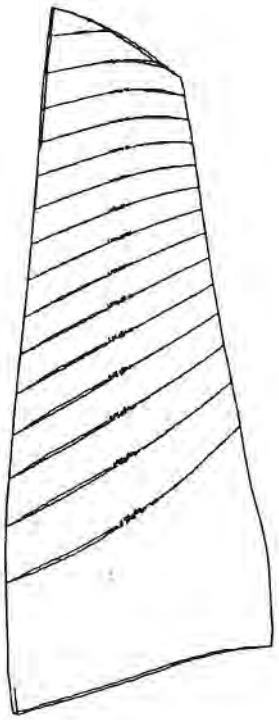

Fig. 6.7 Interpolated Mode 1

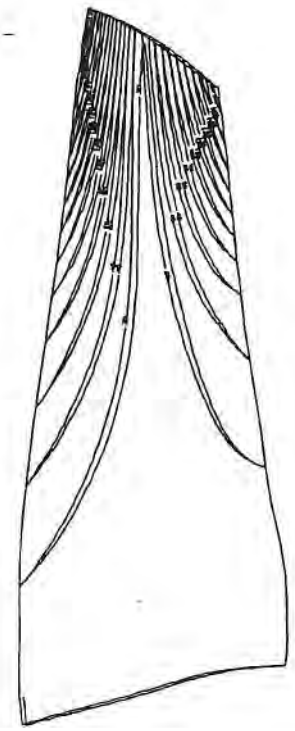

Fig. 6.8 Interpolated Mode 3

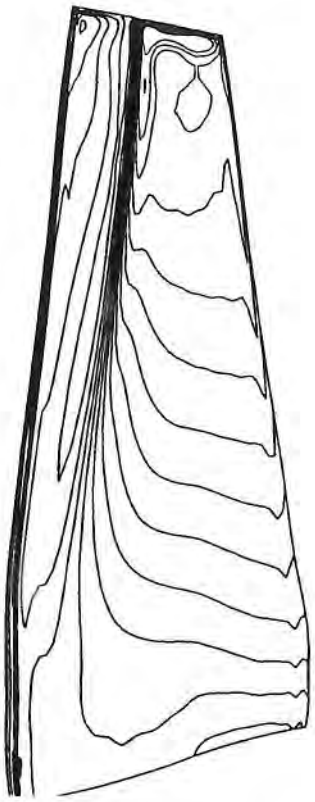

Fig. 6.9a AV3D PS Pressure Contours

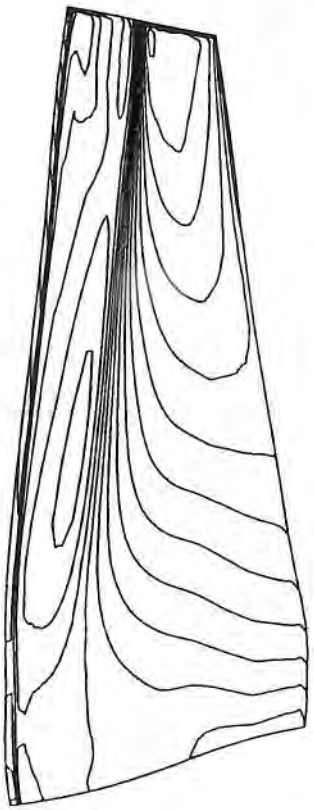

Fig. 6.9b Sponsor PS Pressure Contours

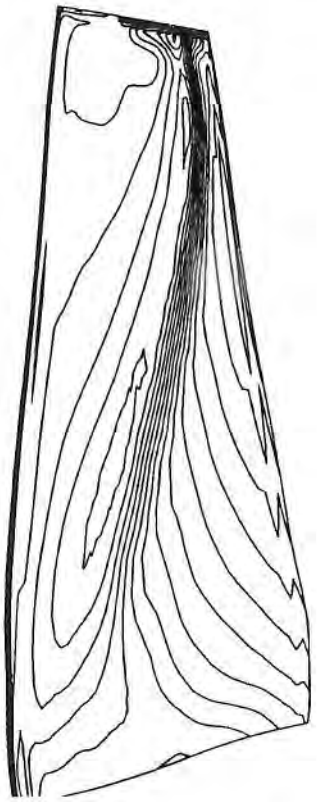

Fig. 6.10a AV3D SS Pressure Contours

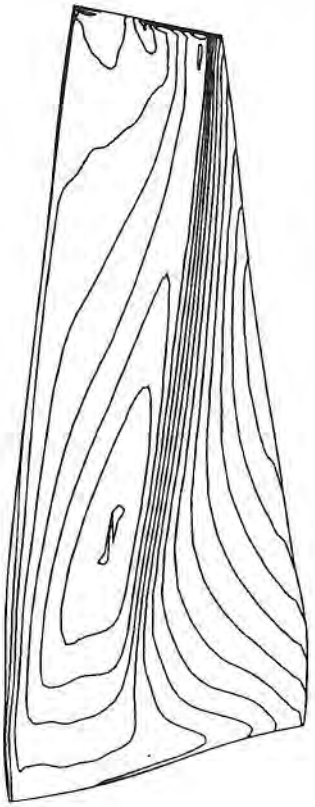

Fig. 6.10b Sponsor SS Pressure Contours

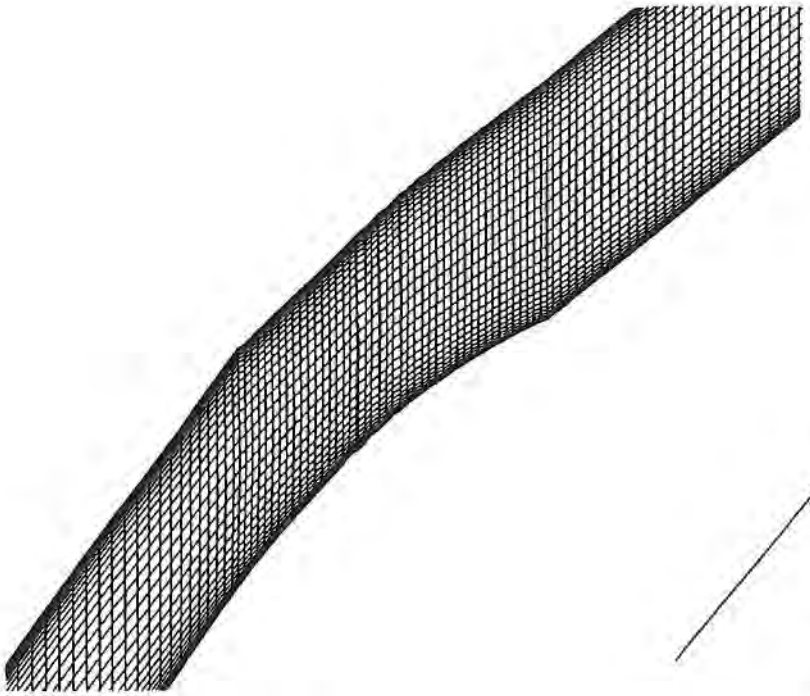

Fig. 6.11a Aero Mesh (50% Ht)

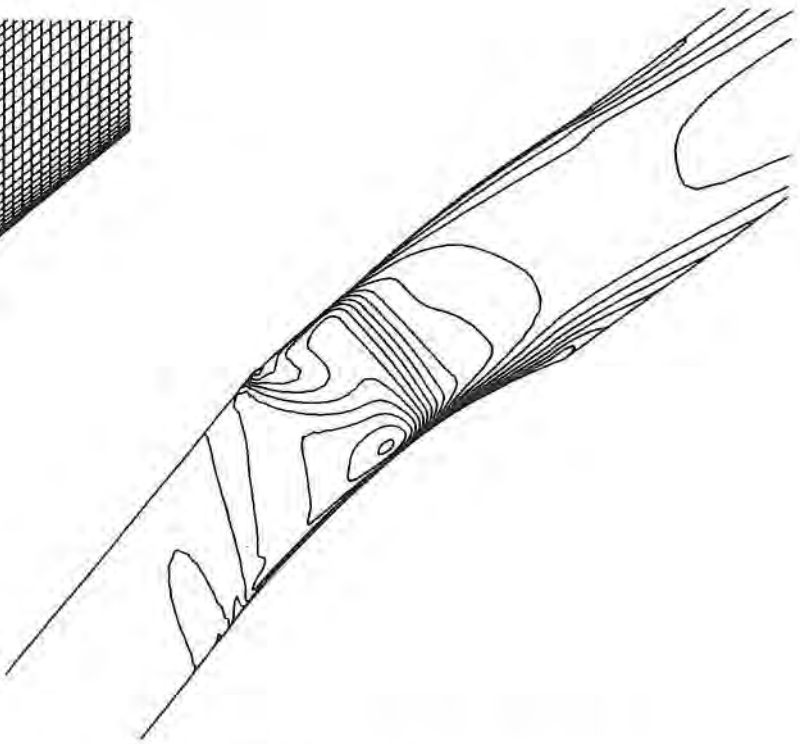

Fig. 6.11b AV3D Mach No. (50% Ht)

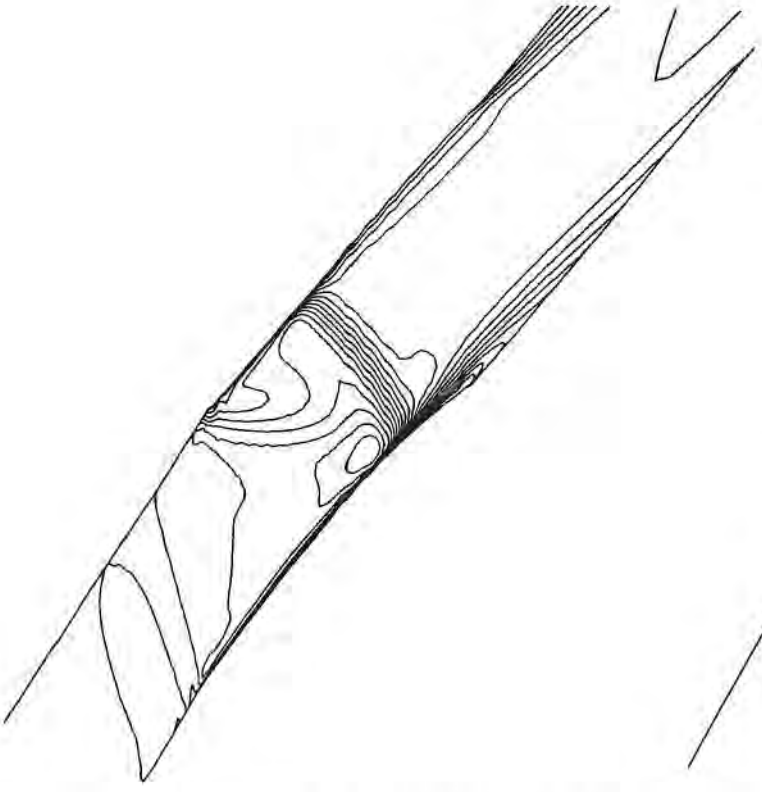

Fig. 6.11c AV3D Mach No. (70% Ht)

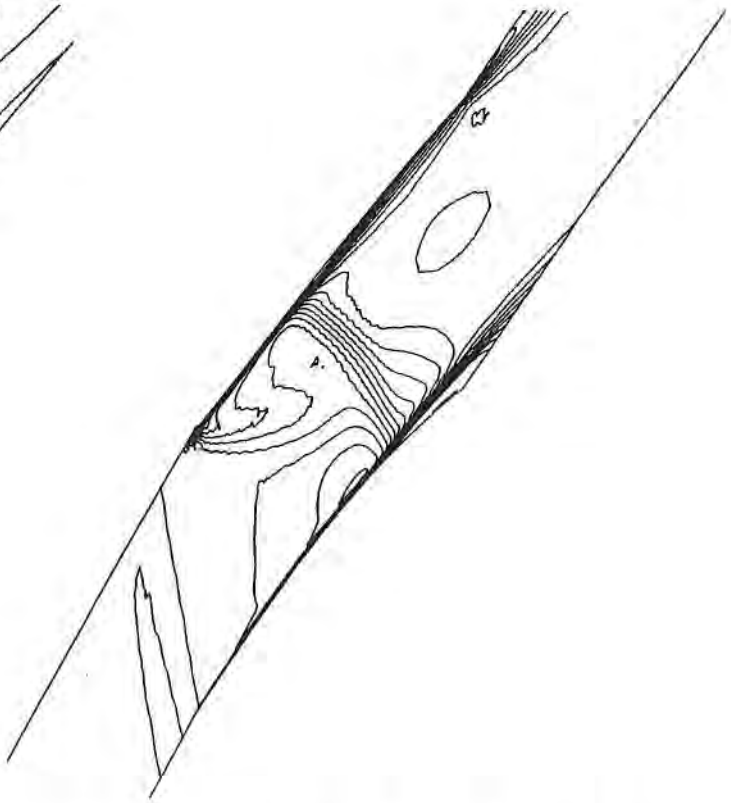

Fig. 6.11d Sponsor Mach No. (70% Ht)

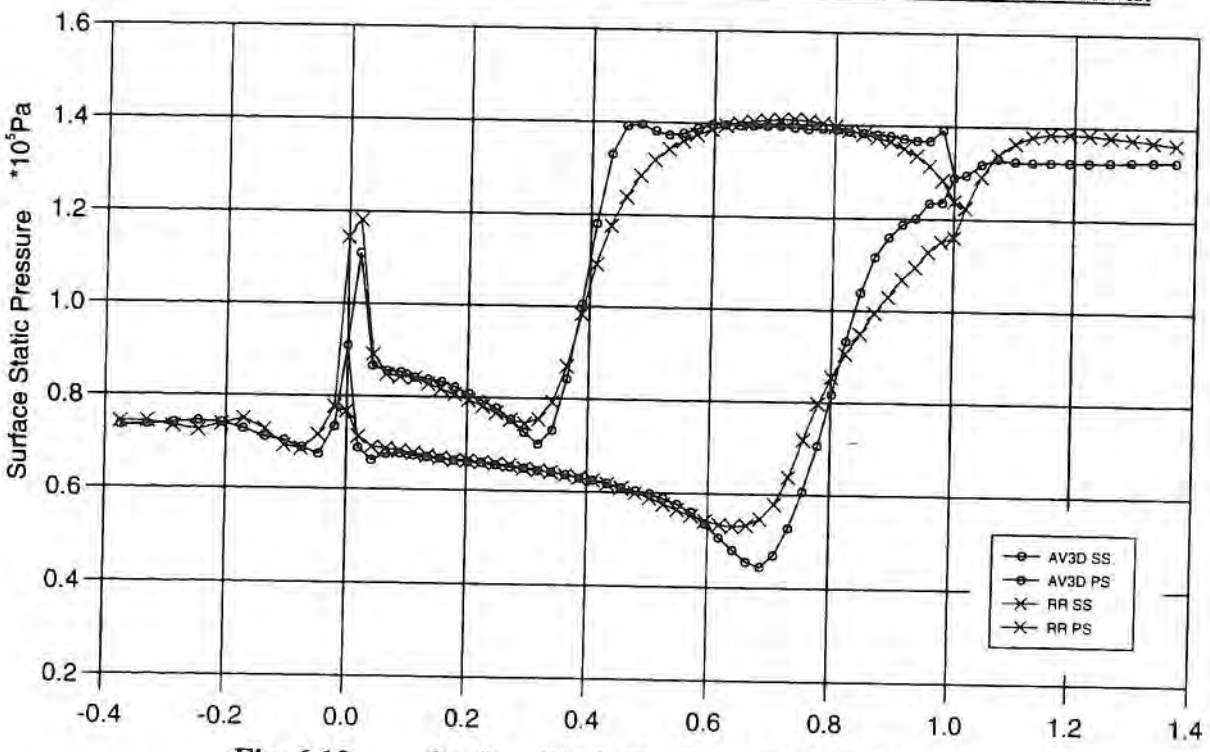

Fig. 6.12 Surface Static Pressure (70% Height)

a) Pressure Ratio

b) Temperature Ratio

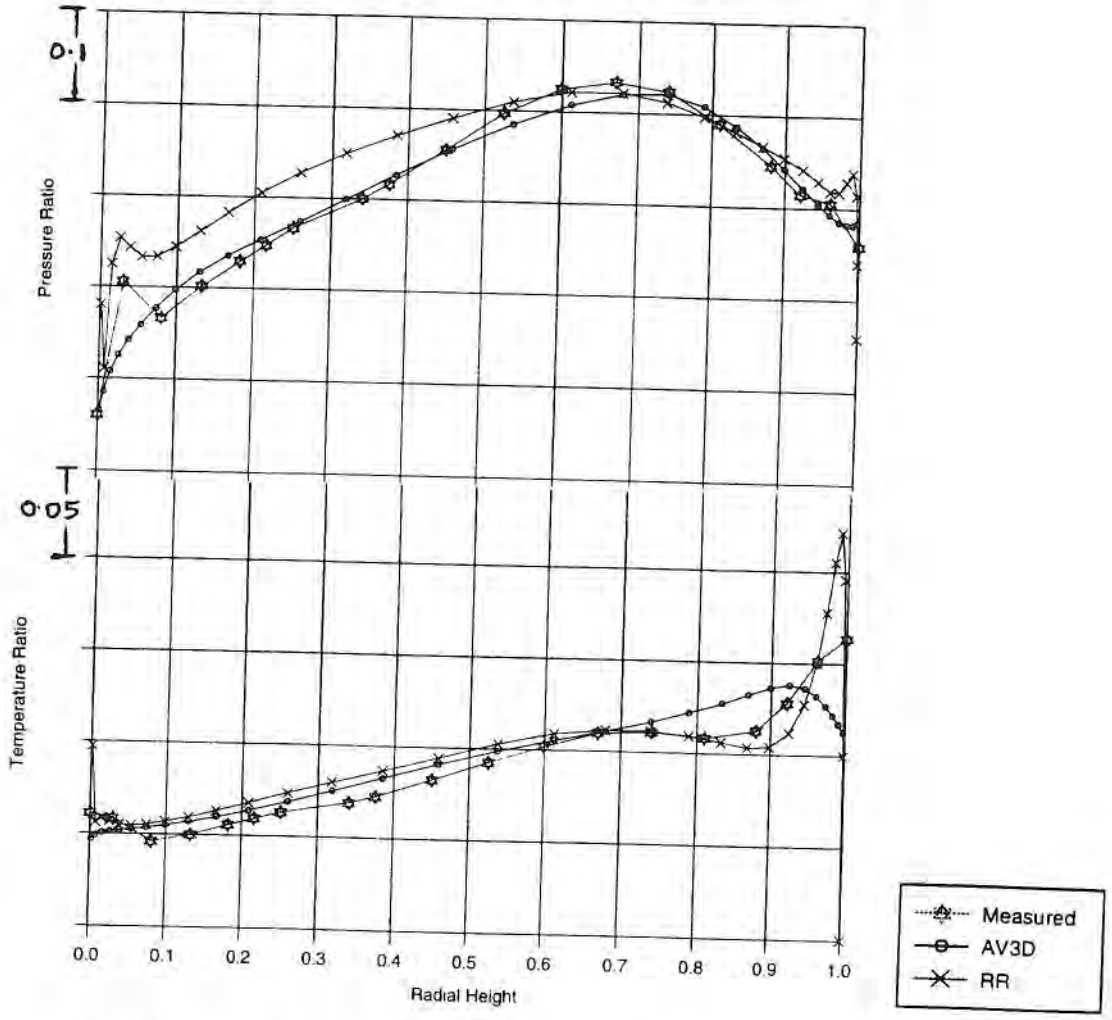

Fig. 6.13 Mass-averaged Radial Profiles

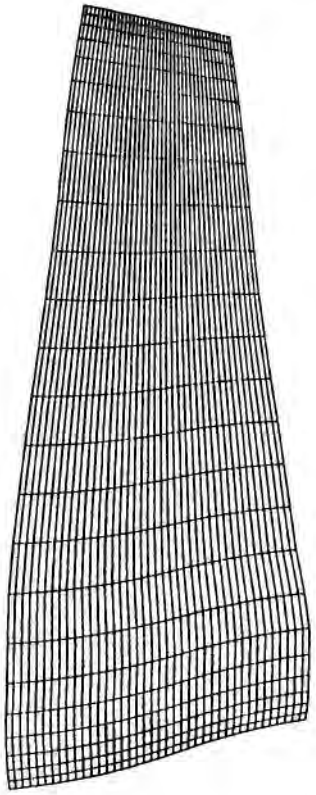

Fig. 6.14a Meridional Mesh

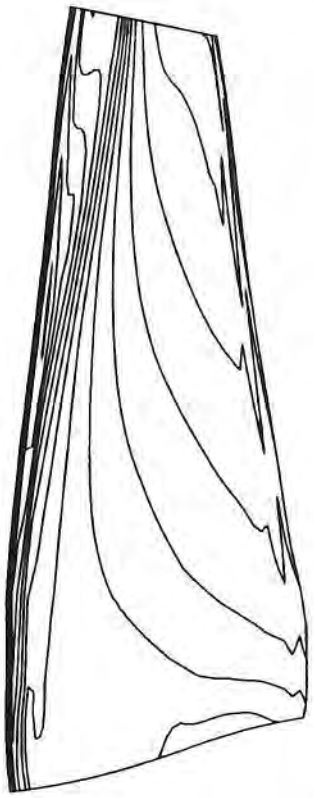

Fig. 6.14b SS Pressure Contours (NS)

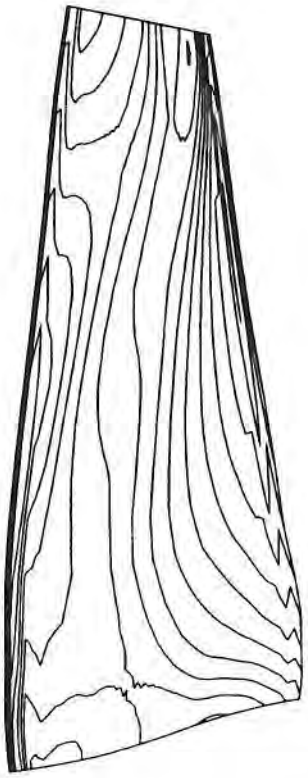

Fig. 6.14c SS Pressure Contours (PE)

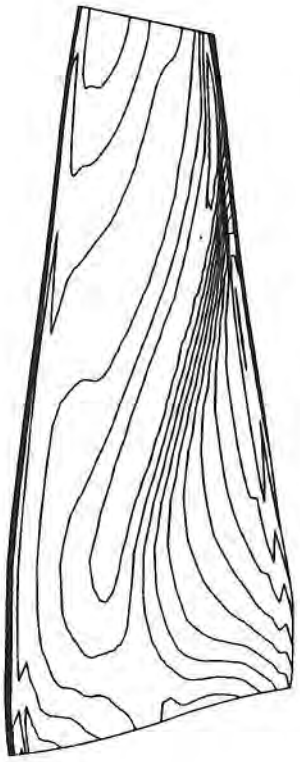

Fig. 6.14d SS Pressure Contours (MF)

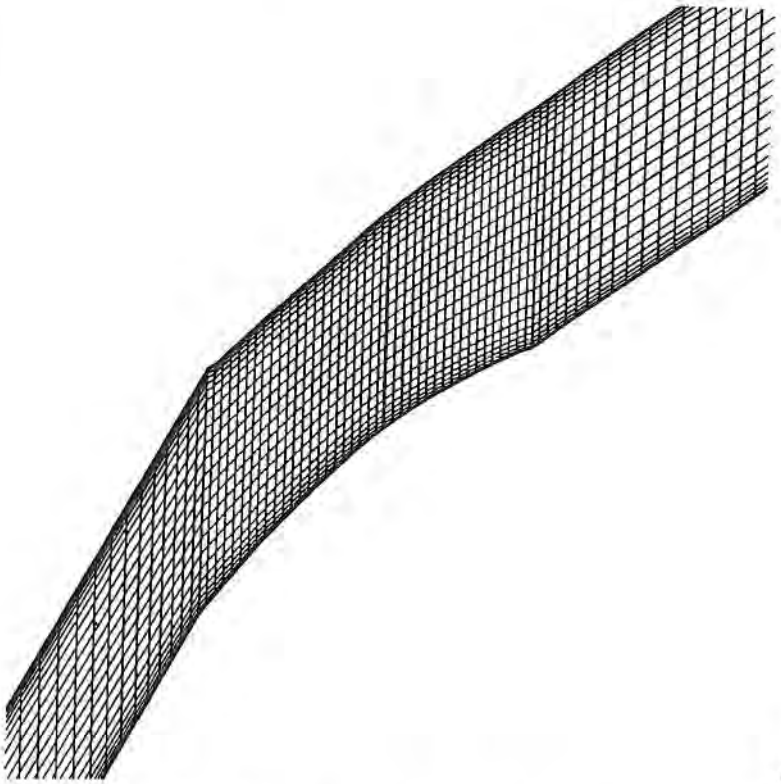

Fig. 6.15a Blade-to-blade Mesh

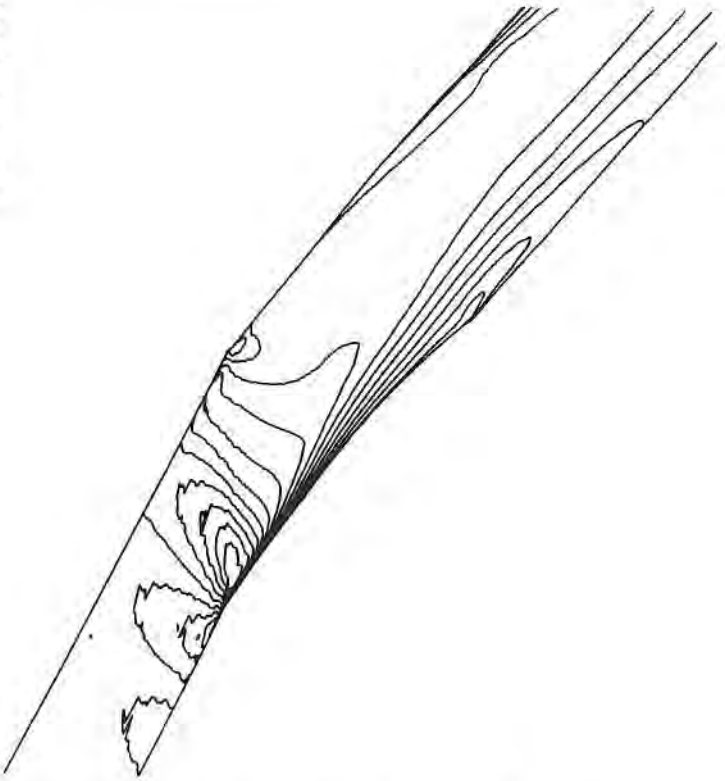

Fig. 6.15b Mach No. Contours 70% Ht. (NS)

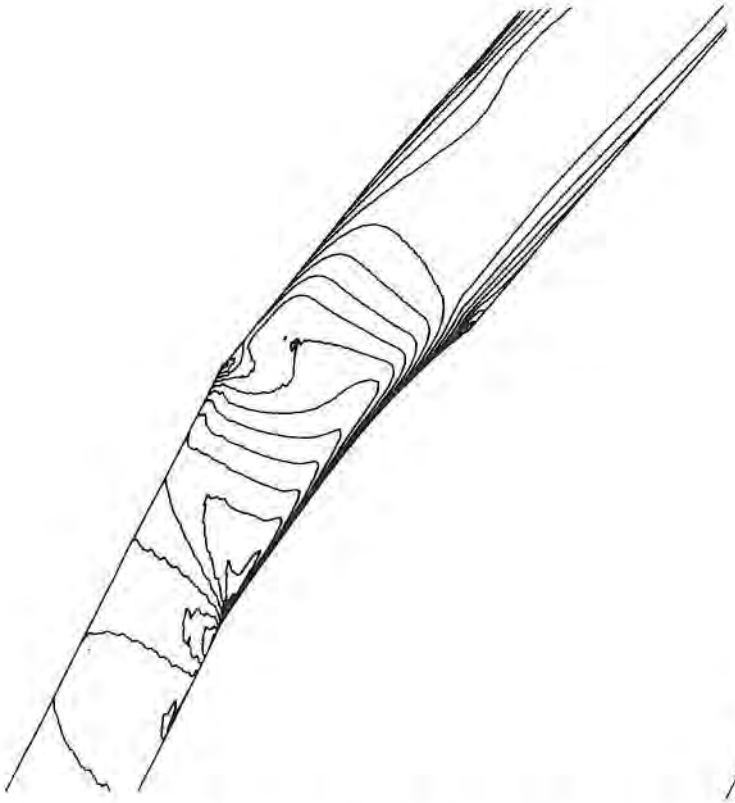

Fig. 6.15c Mach No. Cont. 70% Ht. (PE)

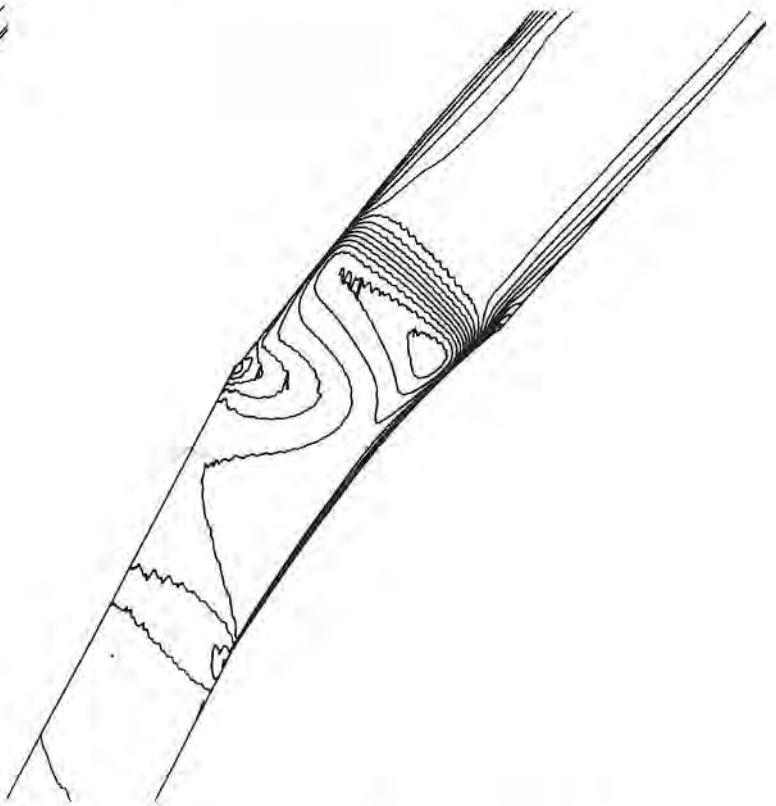

Fig. 6.15d Mach No. Cont. 70% Ht. (MF)

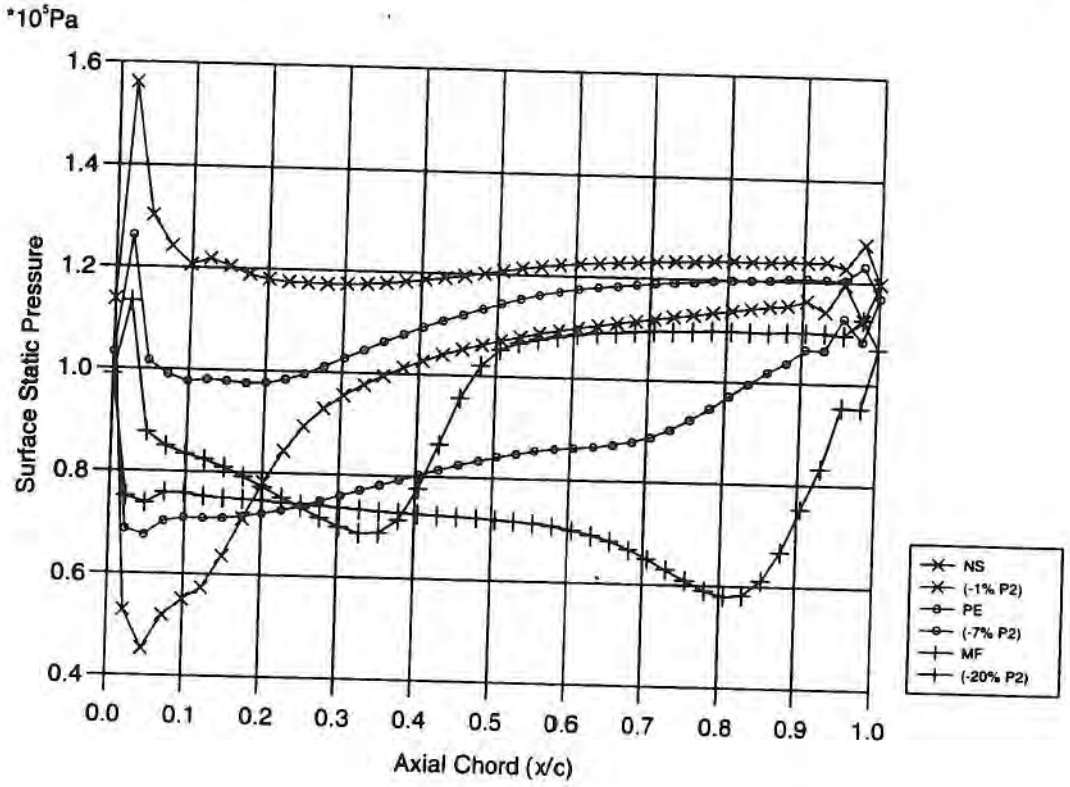

Fig. 6.16 **Surface Static Pressure 70% Height (NS, PE, MF)**

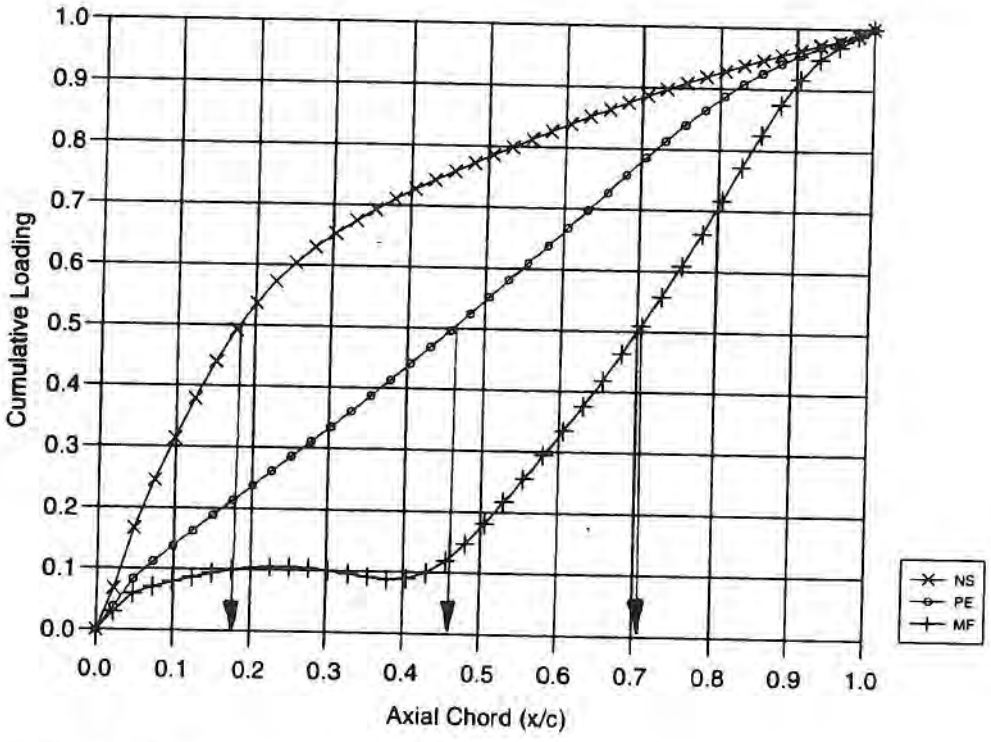

Fig. 6.17 **Cumulative Loading 70% Height (NS, PE, MF)**

a) Rotor Pressure Ratio

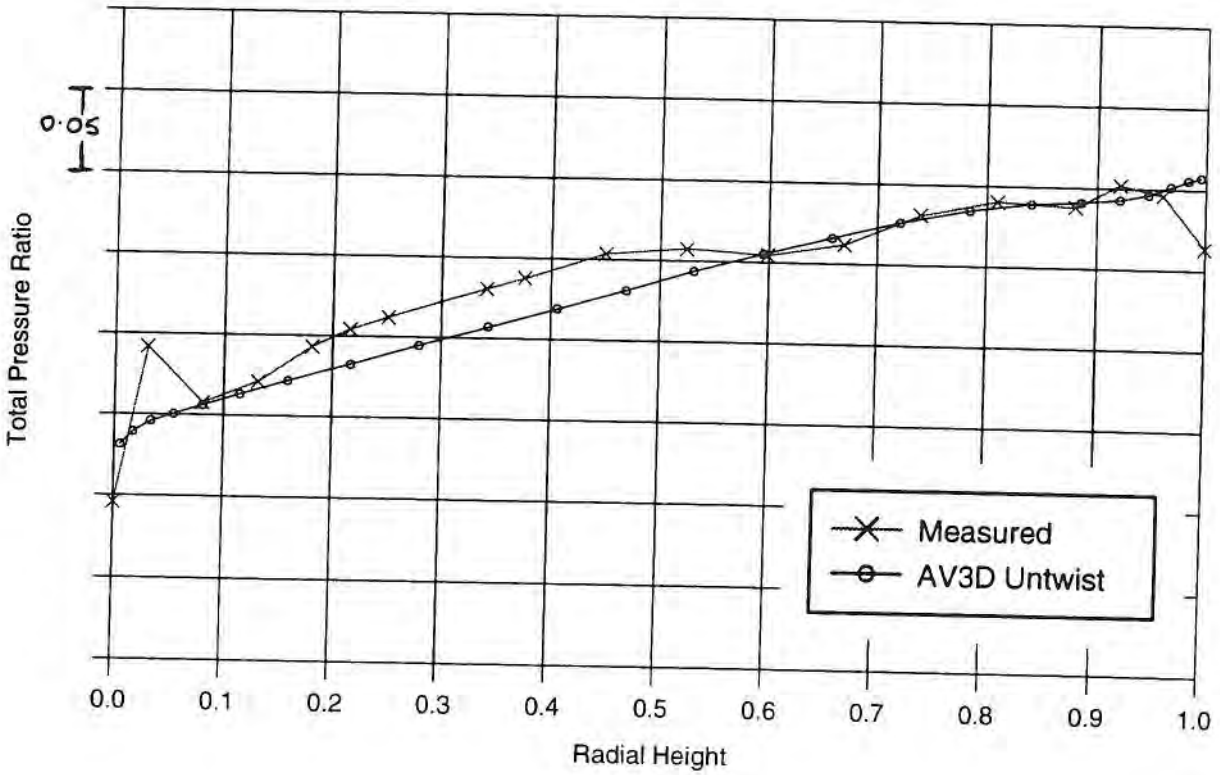

b) Temp. Ratio

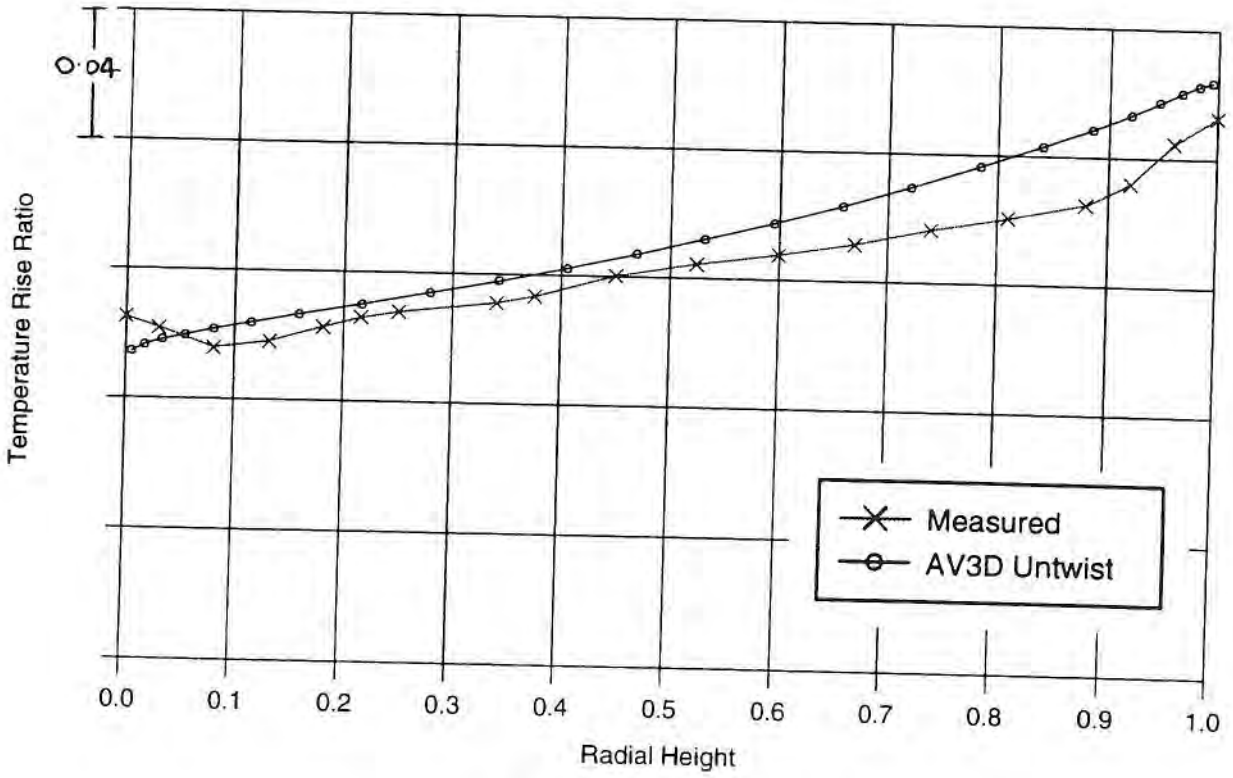

Fig. 6.18 Mass-averaged Radial Profiles (Low Speed NS)

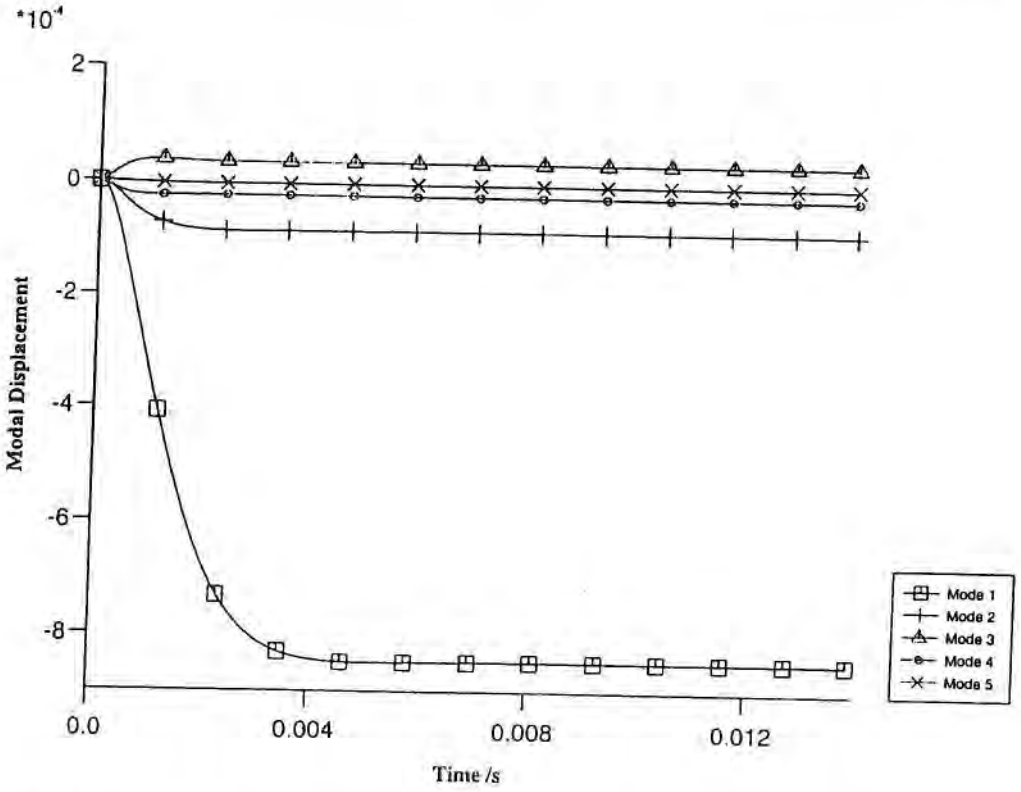

Fig. 6.19a Untwist Time History - Modal Displacements (High Speed)

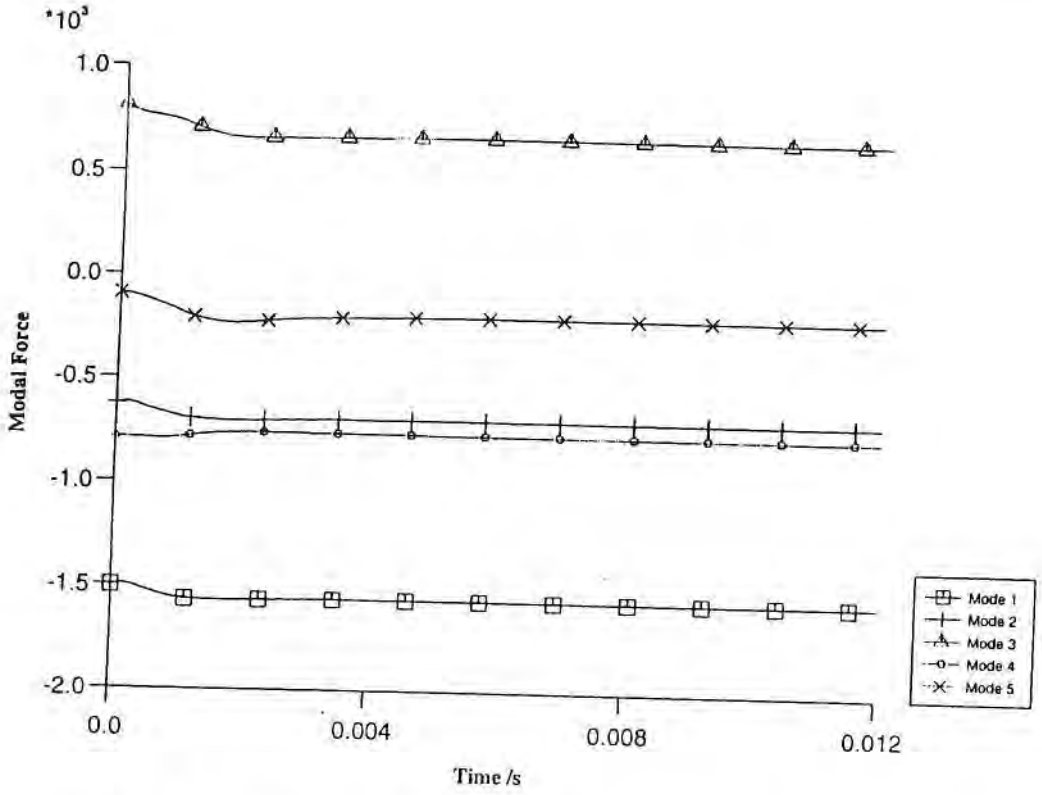

Fig. 6.19b Untwist Time History - Modal Forces (High Speed)

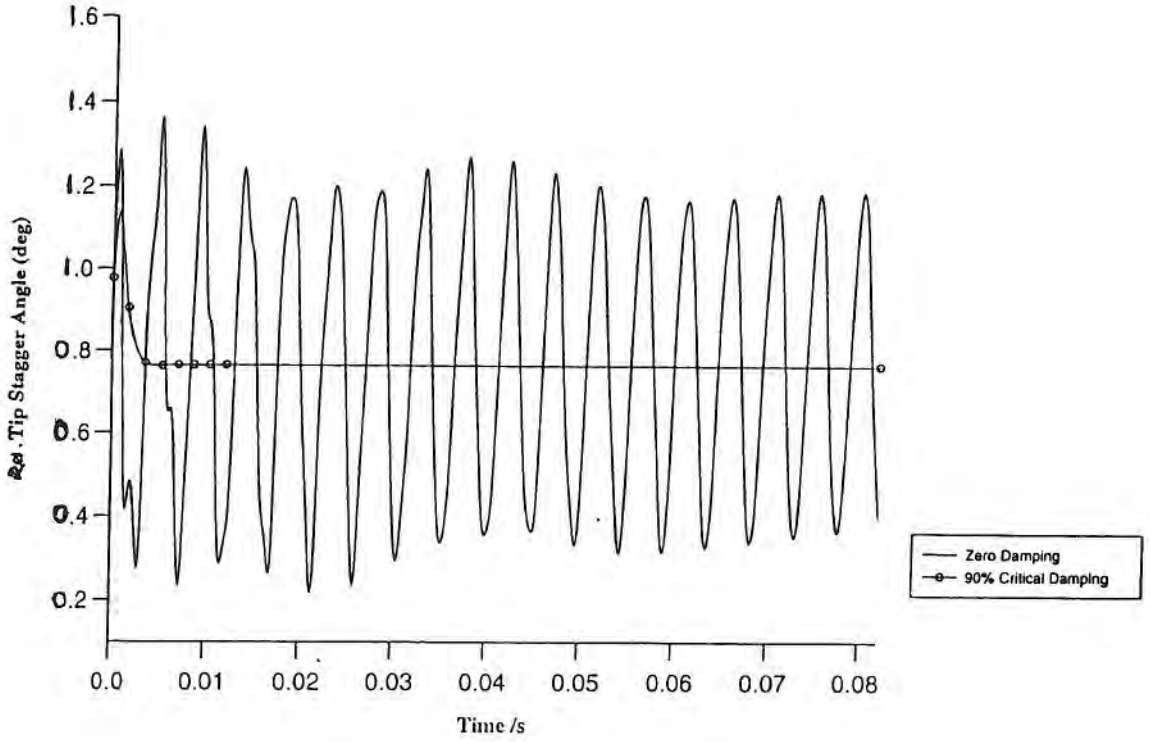

Fig. 6.20a Untwist Time History (Tip Stagger)- Effect of Damping

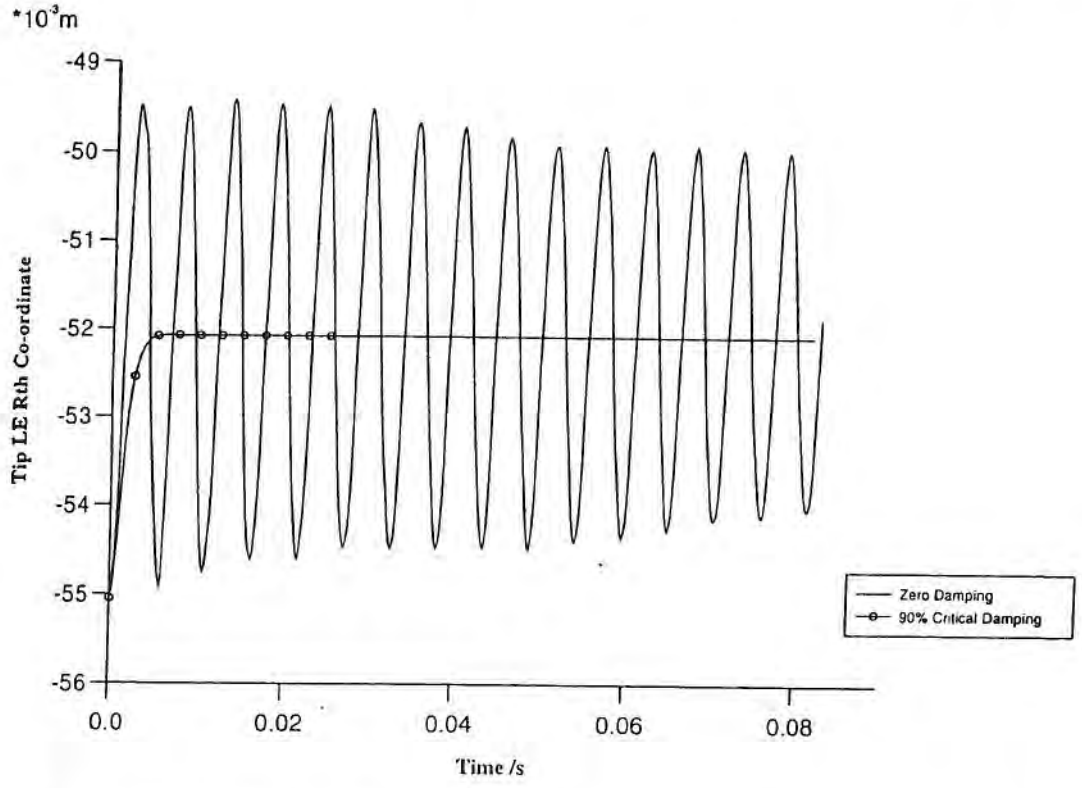

Fig. 6.20b Untwist Time History (Tip LE Co-ord)- Effect of Damping

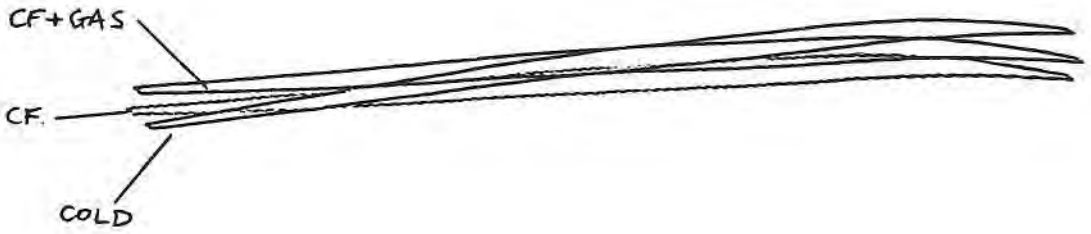

Fig. 6.21 Blade Tip Shape before/after Untwist (High Speed)

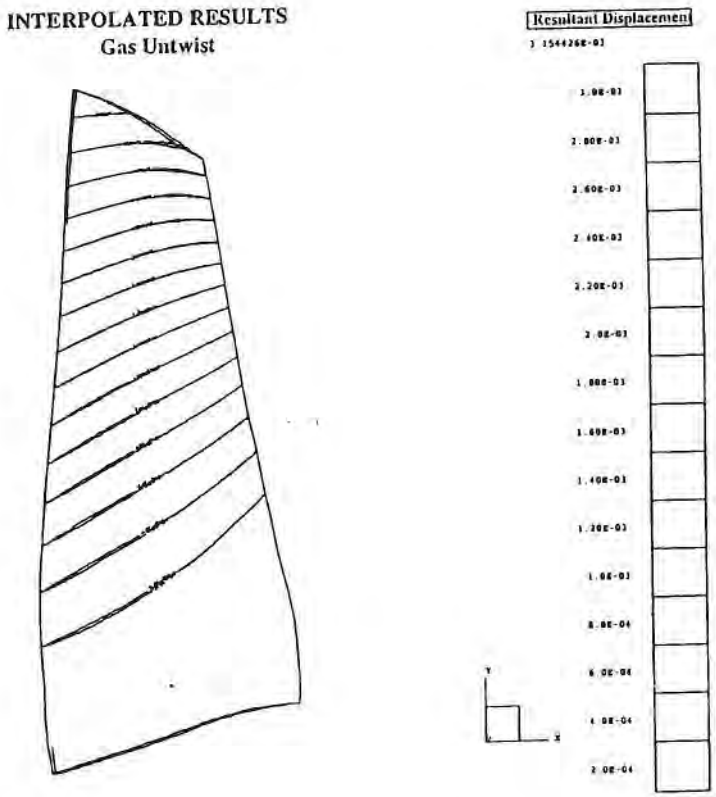

Fig. 6.22 Gas Untwist Displacement Contours (High Speed)

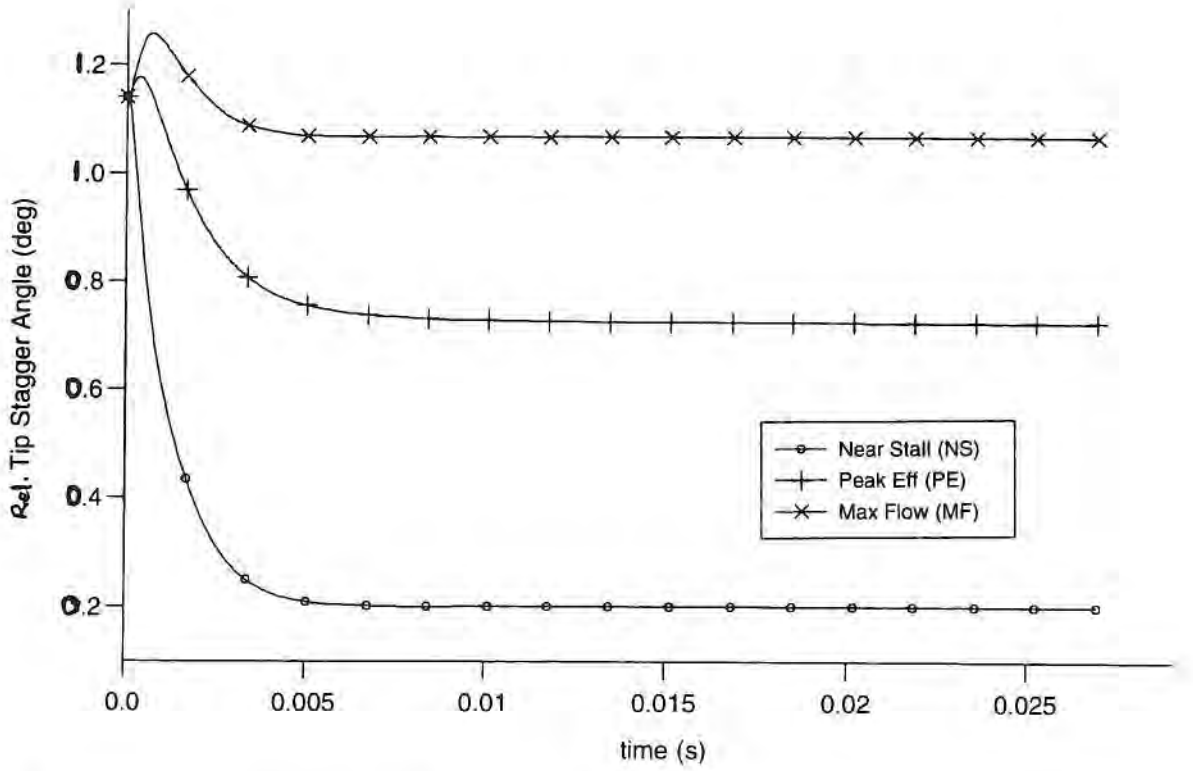

Fig. 6.23 Untwist Time History (Tip Stagger) Low Speed along Characteristic

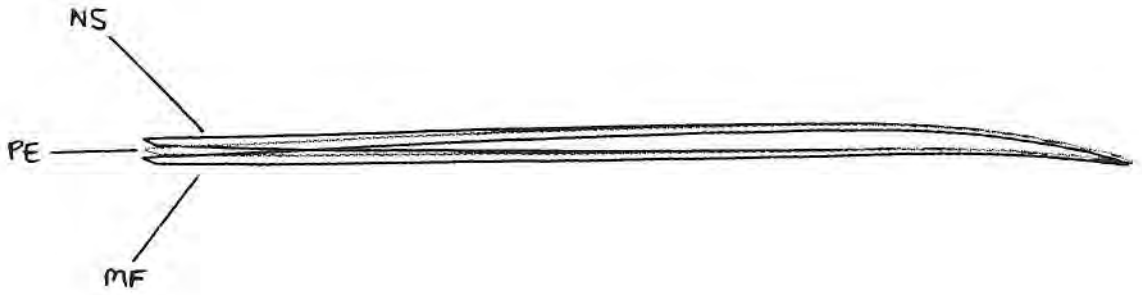

Fig. 6.24 Blade Shape - Low Speed (NS, PE, MF)

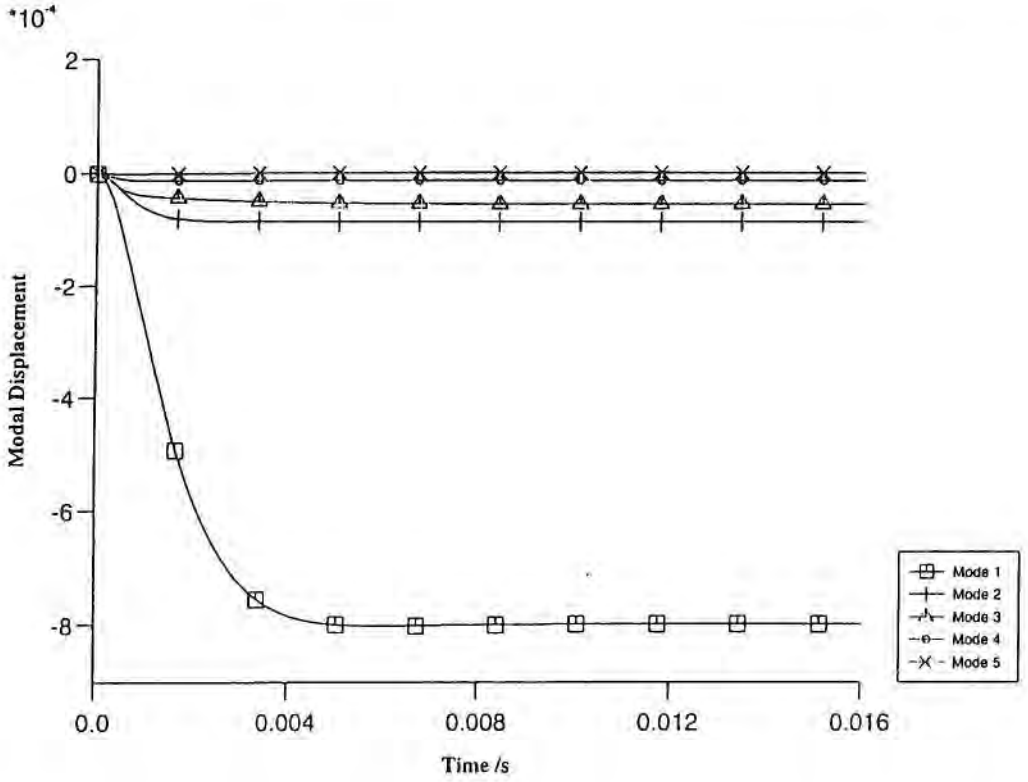

Fig. 6.25a Untwist Time History - Modal Displacements (Low Speed NS)

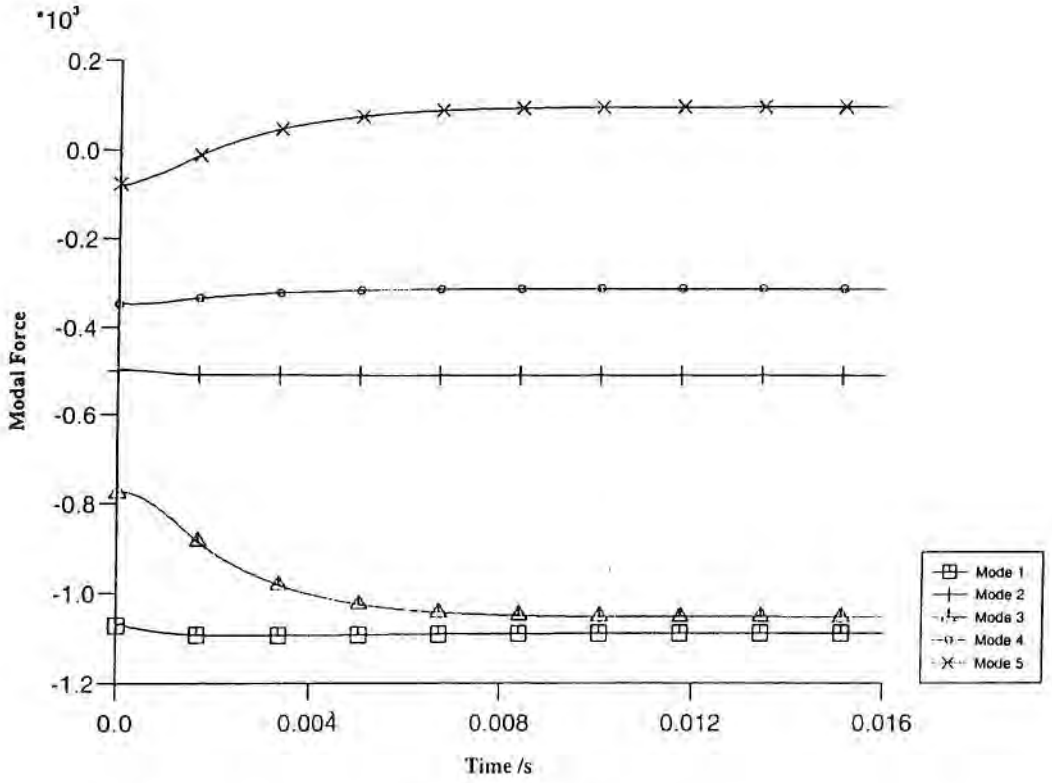

Fig. 6.25b Untwist Time History - Modal Forces (Low Speed NS)

a) Rotor Pressure Ratio

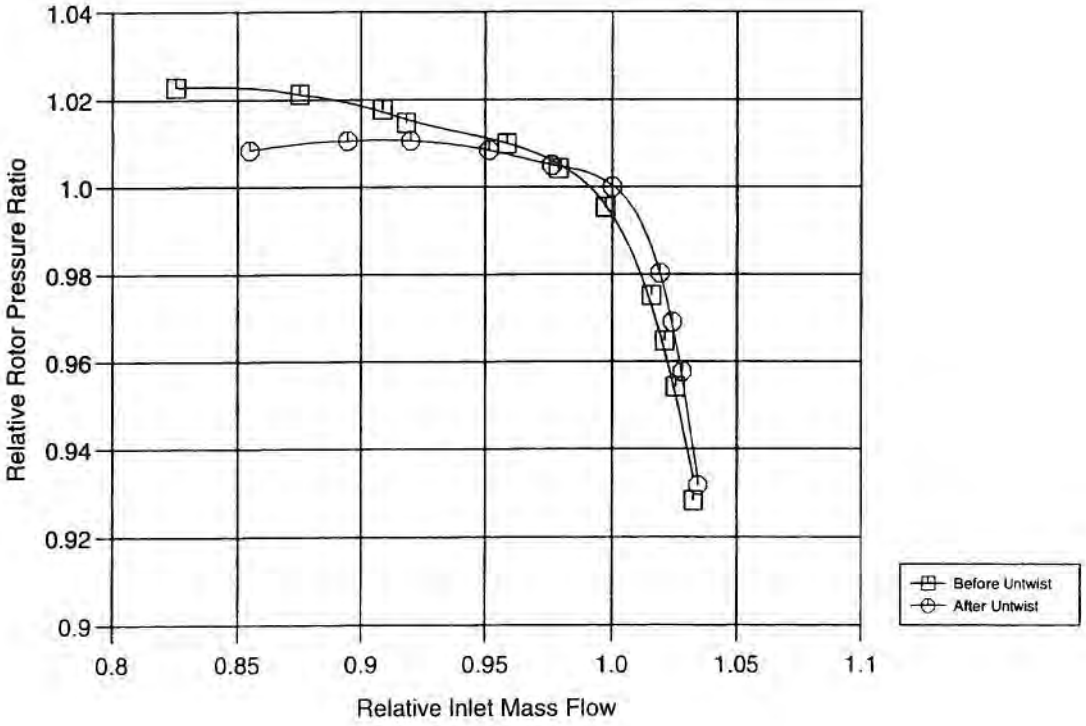

b) Tip Untwist

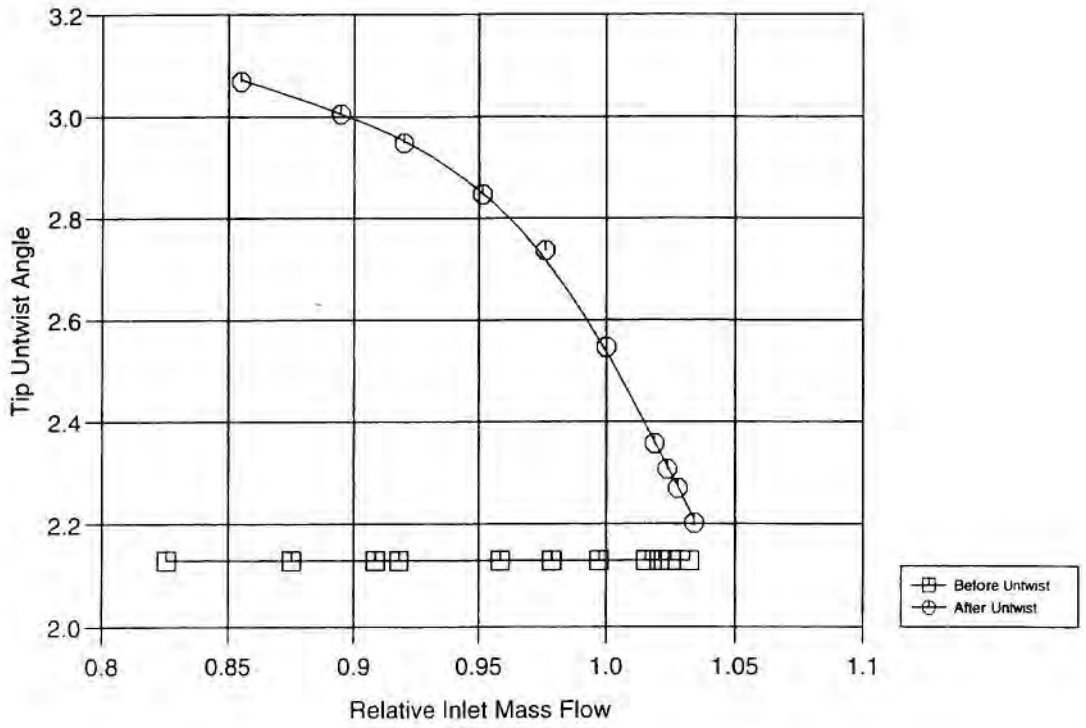

Fig. 6.26 Fan Performance Characteristics (Low Speed)

Chapter 7

3D Blade Flutter

7.0 About this Chapter

The aeroelasticity code that has been developed is now applied to the case of a three-dimensional transonic fanblade known as NASA Rotor 67. The blade geometry is typical of modern turbomachinery design, for which traditional flutter analyses are known to be less than effective in predicting the flutter boundaries accurately. Also, the steady flow aerodynamics of this blade have been extensively investigated both experimentally and numerically, and the results are in the public domain.

Steady flow results are presented first, and compared with experimental data. Both static (untwist) and dynamic aeroelasticity (flutter) results are also shown, though there are no experimental data with which to compare these results. The flutter analysis has been done with 3 different methods - (i) uncoupled, single passage, (ii) uncoupled, multiple passage, and (iii) coupled, with multiple blade-passages, to achieve the desired IBPAs. The relative advantages and shortcomings of these various approaches are discussed in detail.

Parts of this chapter have been published in the paper '*A 3D Time-Domain Flutter Prediction Method for Turbomachinery Blades*', which was presented at the CEAS International Forum on Aeroelasticity and Structural Dynamics, Manchester, June 1995. Other sections have been accepted to be presented as '*An Analysis of the Aeroelastic Behaviour of a Typical Fanblade with Emphasis on the Flutter Mechanism*', at the ASME Turbo Expo, Birmingham, June 1996.

7.1 INTRODUCTION

As intimated in previous chapters, the prediction of aeroelastic phenomena in compressor rotors is a particularly difficult problem. This is because modern axial flow compressors are capable of operating over a wide range of conditions, and aeroelastic instabilities may exist virtually anywhere within the possible operating range. Thus to be successful, a flutter prediction tool must be able to calculate the stability of the rotor anywhere on the compressor map, with a minimum number of assumptions. A full analysis of even one geometry is likely to be a time-consuming exercise because of many possible aerodynamic conditions, and to do comparisons between different designs even more so.

Fortunately, it may be sufficient for the operability of the machine to show that flutter does not occur over a number of prescribed operating conditions. To put this another way, it may be acceptable if the component flutters, as long as it is far enough from the working line that transient destabilising effects (such as a cross-wind, or a sudden change in shaft speed) do not move the compressor's operation into the flutter zone.

The importance of taking into account the blade untwist, and to have a good representation of the 3D flow have been described at length in Chapter 6. So in this study, a geometry was chosen for which there is good data available for the steady flow field, and the computed steady flow, including untwist, is compared to these data.

For the flutter investigation, two particular operating points have been picked out, and the stability over a range of IBPAs has been computed. In order to determine what is important for a successful flutter prediction method three different approaches are compared, using the same fluid model, on the same grid. A number of post-processing techniques, including the energy approach described in Chapter 5 have been used to evaluate the different methods.

7.2 FORMULATION

The structural and fluid models used as well as the partially-integrated coupling are the same as previously described.

Timestep

The timestep used is the same for both fluid and structural calculations, and is fixed throughout the time integration. For this flutter study, which is interested in the lower modes of vibration yielding low reduced frequencies, timestep size is not a problem

for the structural part of the code as the equations are advanced in time using the Newmark-β method, which is unconditionally stable. The fluid code has a much more restrictive timestep limit, this becomes the timestep criterion for the whole problem. In general, it is ensured that at least of 50 timesteps per period were used for all structural modes, to ensure accuracy of the Newmark method, which begins to deteriorate at 30 timesteps per period. In practice however, usually more than 50 timesteps per highest frequency period are used (with typically 3-5000 timesteps in the lowest frequency mode).

Starting Conditions

Combinations of velocities and displacements of the specified degrees of freedom can be selected as initial conditions for structural equations. In this case, as only one structural mode (at one IBPA) was investigated at a time, an impulse was given to that mode to start its motion. The only arbitrary variable therefore was how large to make the initial motion. This was usually made to be around the same order of magnitude as the untwist displacement. In the general case, with many possible modes, the issue of starting condition for non-linear problems becomes more of a problem.

The starting conditions for fluid flow variables is from a steady flow calculation. However, the fluid calculation can also be restarted from an unsteady condition, if required.

7.2.1 Energy Analysis of Flutter

Due to the complex nature of the results of time-accurate integrated non-linear aeroelasticity analyses, and the added uncertainty of the effects of starting conditions in general, a global parameter that describes the problem is highly desirable. To this end, the use of energy analysis of the results has been proposed by Bendiksen (1991). He also questioned the validity of the partially-integrated approach, compared to the so called fully-integrated approach, where fluid and structural equations are formulated and solved together in time. So the energy analysis serves two useful purposes:

i) To better understand the results, in terms of a few simple variables
ii) To show that the interaction is being accurately modelled, by monitoring the energy exchange between the fluid and the structure.

The equations for the energy in the structure, and the work done by the fluid are given in Chapter 5 (**Eqs. 5.6 - 5.11**). The only difference here is that there can be more than

one blade passage, which needs to be taken account of, but the principle is the same: the accuracy of the energy transfer can be assessed by monitoring the difference between the total energy in the structure, and the work done by the fluid (in the absence of any damping in the structure).

7.2.2 Inter-blade Phase Angle Considerations

Lane's assumption of constant inter-blade phase angle between vibrating blades (Lane, 1956) has been fully exploited by linear aeroelasticity methods. Even the implementation of such a simplification is not straightforward for unsteady flows because of the moving boundaries. Erdos et al. (1977) presented the so-called 'direct store' technique that can account for all allowable values of the inter-blade phase angle (IBPA) for non-linear unsteady flows. However, the formulation is limited to a single vibration mode, an assumption that is not necessarily true since flutter may involve the coupling of several structural modes, as suggested by experimental evidence. He (1992) proposed a method based on shape correction in order to deal with multiple perturbations. However, in such cases, the flutter mode shape may or may not be similar to in-vacuo structural mode shapes. In any case, all these techniques are approximate implementations of Lane's assumption, the applicability of which is debatable when dealing with transonic flows, shocks, etc., since the system is, evidently, no longer linear. In other words, the flutter mode shape is part of the solution rather than being a known input quantity to the analysis. Also, the direct store method requires a large amount space for storing the data on the periodic boundaries.

Most current flutter analyses are based on considering (what is judged to be) critical values of the IBPA using a single-passage solution via direct store and to determine the least stable mode. Three major shortcomings are associated with this approach. First, linearity of the aeroelastic system is inherently assumed since the time delay for the chosen IBPA is calculated from the natural frequency of the structural mode, which may or may not change under the effect of the flow. Second, the structure must be forced to adopt the suspected flutter mode with the given amplitude for a number of periods (say 10-15) to establish the time delay across the periodic boundaries in the fluid domain, an approach that requires significant CPU effort. Third, as mentioned before, only one structural mode at a time can be dealt with and hence any interaction between the structural modes is ignored.

The alternative to the above method, is to use multiple blade passages to achieve the desired IBPA. Thus if a the calculation is to be done with a phase angle of 180°, then

two blade passages can be employed. This has the advantage of not relying on the storage technique to update the fluid boundary conditions, so no 'time-delay' is used, and therefore any number of blade modeshapes can be used simultaneously to calculated the structural motion. The number of passages required for a 24 bladed-disc, for example, are shown in **Fig. 7.1**, below:

Table 7.1 Relationship between Nodal Diameters, IBPAs and Passages

Nodal Diameters		IBPA (deg)		No. Passages (min. required)
Plus	Minus	Forward	Backward	
0	0 (24)	0	360 (0)	1
1	23 (-1)	15	345 (-15)	24
2	22 (-2)	30	330 (-30)	12
3	21 (-3)	45	315 (-45)	8
4	20 (-4)	60	300 (-60)	6
5	19 (-5)	75	285 (-70)	24
6	18 (-6)	90	270 (-90)	4
7	17 (-7)	105	255 (-105)	24
8	16 (-8)	120	240 (-120)	3
9	15 (-9)	135	225 (-135)	24
10	14 (-10)	150	210 (-150)	24
11	13 (-11)	165	195 (-165)	24
12	12 (-12)	180	180 (-180)	2

Note that each nodal diameter pattern has a pair of modes corresponding to the forward and backward travelling modes, except for the nodal diameters corresponding to 0 and 180° IBPA, which are single. In flutter analyses, one calculation for each possible IBPA must be carried out, unless the whole annulus of blades is to be modelled, where (by definition) all modes can be accounted for.

The method of testing each IBPA in turn will be examined in this study, using both coupled and uncoupled approaches. In practice this may not be the most efficient means of flutter analysis, as overall more computation may be required than for one calculation of the whole annulus, involving all the modes. However, the current state-of-the art is to calculate separate IBPAs, so to compare the new method to the existing methods it is necessary to use this approach. This will allow the effects of each mode to be isolated (which may not be how the fluid-structure interaction works in reality), but the results are easier to interpret. The whole annulus approach, using all the nodal diameter modes is used in Chapter 8.

7.3 CASE STUDY - NASA Rotor 67 Fanblade

As a case study, the NASA Rotor 67 fan blade has been taken as it is typical of contemporary low aspect ratio transonic compressor blades design. The first step towards the full aeroelastic analysis is to obtain the structural dynamic behaviour of the blade. This is done in a finite element calculation using the ANSYS® package. The first 20 vibration modes of the structure were calculated, including the centrifugal stiffening effect at the given rotational speed (Ω=16,043 rpm). The material properties were taken as those for titanium. The results of this calculation are shown in **Table 7.2** for the first 8 modes:

Table 7.2 FE Modeshapes

Mode	Frequency (Hz)	Description
1	561.5	1st Flap
2	1686.0	2nd Flap
3	1911.7	1st Torsion
4	3516.3	1st Edgewise
5	4314.8	1st Combined
6	5257.7	1st Camberline
7	5407.5	2nd Combined
8	6718.2	3rd Combined

The FE mesh and modeshapes of modes 1 & 3 are shown in **Fig. 7.1**. The modeshapes from this FE calculation were then interpolated onto the fluid surface grid points. The reduced frequencies for this problem based on inlet relative velocity and axial chord at mid height are from 0.54 (mode 1) to 1.83 (mode 3).

7.3.1 Steady Flow

The second step in the aeroelastic analysis of this blade is to obtain steady flow solutions at the desired running conditions. In this case one point near peak efficiency (i.e. on the working line), and a second point near stall are selected, both at a speed Ω = 16,043 rpm. These steady flow operating conditions have been exhaustively investigated experimentally (Stratizar et al., 1983) and compared with numerical methods (Pierzga & Wood, 1985, Arnone, 1992, and He, 1993b).

In this study, the mesh used was 25×73×25 grid points, giving about 2000 points on the two blade surfaces. This mesh resolution enables the surface viscous boundary-layers to be captured adequately, with the use of wall-functions. The Reynolds number based on axial chord at mid height and relative exit velocity, $Re = 1\times10^6$. The first layer was set at a y^+ value of about 100 (1mm from wall) which is within the log-law region. The meridional view of the mesh is shown in **Fig. 7.2a**, and the blade to blade view at 70% from the hub is shown in **Fig. 7.2b**.

The flow was calculated using a simple tip-leakage model, with a tip gap of 0.8% of the blade span. The wall function parameters were chosen assuming fully turbulent inlet flow. The boundary conditions are given by specifying the absolute stagnation pressure and temperature, and the measured flow angle at inlet, and the exit static pressure. For the condition near stall, the tip exit static pressure was raised from the value at PE, with the radial distribution being determined by radial equilibrium. Thus at this condition the exit static pressure distribution may not be exactly the same as that during the experiment.

The blade to blade contours of Mach number are shown in **Fig. 7.3** (near peak efficiency) and **Fig. 7.4** (near stall), for 70% of span from the hub, compared with the experimentally derived values (from laser anemometry). It can be seen that the overall agreement as regards the shock position is quite good. Near peak efficiency the characteristic *lambda* shape of the shock can be seen near the tip, whilst near stall the shock has moved upstream to stand in front of the next blade. The shock becomes rather smeared near the tip - this is partly due to the skewness of the grid on account of the high stagger of the blade. Also, for the latter condition the shock stands outside the blade passage where there are fewer grid points. However this must be tolerated due to the computational requirements for unsteady, multiple blade passage analysis.

The steady flow results are also analysed by plotting the radial distributions of circumferentially mass-averaged quantities, downstream of the rotor. These values, compared with the experimental results are shown in **Fig. 7.5** (near peak efficiency), and **Fig. 7.6** (near stall). The agreement is reasonable, although the total pressure rise is somewhat under-predicted, and the temperature rise is rather over-predicted. This may be due to the relatively simple viscous model used in this study. Quite good agreement with the absolute exit angle is obtained, especially near peak efficiency, however the value is nearly 10 degrees too high at the tip near stall. This may be because the boundary layer is grossly separated near the tip, as can be seen from the Mach number contours. Once separation has occurred, the thin-layer assumption used in the present study no longer holds, however the results obtained are acceptable, bearing in mind the relatively coarse mesh which has 45,625 points per blade passage.

In terms of the aeroelastic characteristics of the blade, it is important to take into account the viscous losses. If a purely inviscid calculation were used, the shocks would be predicted in the wrong positions, and this would have a correspondingly large effect on the untwist and flutter characteristics of the blade.

7.3.2 Static Aeroelasticity Calculations

As a first step towards flutter calculations, the untwist behaviour of the Rotor 67 blade has been calculated at the given two operating conditions. It is assumed that the centrifugal part of the untwist (i.e. the position the blade would adopt spinning at the required speed in a vacuum) has already been taken into account in this case. Otherwise, the method is exactly the same as that used in Chapter 6. The gas load component of untwist can affect the blade stagger by the order of 1° from choke to stall as was seen in Chapter 6, whereas 0.5° change may be worth as much as 2% on efficiency. So the designer must know how much untwist there is in order to manufacture the correct blade shape, so the desired shape is obtained under running conditions.

The first 8 modeshapes from the FE analysis are used here (these modes contain the effect of centrifugal stiffening as the FE calculation is done at the required rotational speed). The only other assumption is that a large amount of viscous damping (90% critical) is used in each mode. This is done to damp the transient behaviour, while reaching the untwist position using the minimum CPU time.

The time histories of the deflections are shown in **Fig. 7.7** (near peak efficiency) and **Fig. 7.8** (near stall). These are shown in the modal domain, as well as the real tip displacements. It can be seen that the structure reaches the deflected position within about 2 periods of the lowest frequency mode, however the calculations were run on for at least 5 periods of this mode to ensure convergence. The time history of the tip stagger angles for both cases is shown in **Fig. 7.9** - this shows that the final stagger angles are 63.28° near peak efficiency, and 63.14° as compared with 63.37° before untwist. The modal domain plots show that the largest motion is in mode 1 (flap), in both cases, however, the contribution in modes 2 and 3 are much larger in the near stall condition. The effect of higher modes is almost negligible, and results for modes higher than 5 are not shown. The increased gas untwist (from 0.09° near peak efficiency to 0.23° near stall) comes about mainly due to the shock position. The forward position of the shock near stall loads the blade mainly towards the leading part of the blade, which increases the contribution from the torsional mode (mode 3). This point is illustrated by **Fig. 7.10** which shows the static pressure distribution along the blade chord at 70% span from the hub, before and after untwist. It can be seen that the shock does not move much, however, the method calculates this new final flowfield without any interaction or user input. In this case the untwist (and therefore the shock motion) is small due to the high rotational speed, and thus the large centrifugal stiffening effect.

7.3.3 Dynamic Aeroelasticity Calculations

Once the untwist calculations were performed, the final grid and steady flow variables were written to file, from which the flutter calculations were started. The major aim of this Chapter is to compare various analysis routes which are described below. Flutter calculations were performed for the two flow conditions in the 1st flap mode (mode 1) of vibration at 0°, +90°, 180° and -90° IBPAs. Also the stability in the first torsion mode (mode 3) was analysed at 0° IBPA only. The structural damping was taken as zero, as it is expected to be low for this rotor, and in any case this will be a conservative assumption in determining the flutter margins. For non-zero IBPAs, the single blade modeshape was expanded using the cyclic symmetry of the rotor assembly. Detailed descriptions of the methods are given, with a comparison of results following.

Method 1: Uncoupled Analysis using Multiple Blade Passages

In order to decouple the structural and fluid domains, the right-hand side of equation (4) was set to zero throughout the time integration and the structure was moved sinusoidally in its first mode of vibration for 10-20 periods of motion, until convergence of the unsteady forces was obtained. Multiple blade passages were used to represent non-zero IBPAs. Thus, 0° was achieved using one blade passage only and 180° using 2 passages. Four blade passages were used for +/-90° IBPAs, the cyclic-symmetry co-ordinate expansion for this case giving the two possible modeshapes which are 90° apart spatially. In the latter case the single blade modeshape was expanded to the remaining passages using the general expression:

$$\phi_{i,N} = \phi_{i,1} \cos\left\{\frac{2\pi\,(N-1)}{N_P}\right\} \tag{7.1}$$

where N is the current passage number, and N_P is the total number of passages. So, to give the plus and minus phase conditions, the two modes were given a 90° temporal phase by judicious choice of the initial conditions: displacement in one and a corresponding velocity in the other, the direction of the velocity determining the lagging/leading mode.

Once the time-histories of the motion were computed, each IBPA case was examined using the last period of the motion (i.e. once the unsteady solution had become periodic). In such uncoupled analyses, the flutter stability can be determined by integrating the product of modal forces with modal velocity over the vibration period. The logarithmic decrement (logdec) is related to this value by the kinetic energy (E_k) in that mode (Carta, 1967), as follows:

$$\log dec = \frac{-1}{2E_k}\int_0^{2\pi/\omega} \Phi^T \mathbf{p}(t) \bullet \dot{\eta}\, dt = \frac{-W_F}{2E_k} \tag{7.2}$$

However, it should be remembered that the logdec is a linear analysis tool and it should be applied to non-linear situations with caution. The *predicted* frequency shift to linear order can be calculated via an integration of the product of modal force with modal displacement over the cycle. This will given an indication of how accurate was the initial assumption of fixed frequency. This term may be derived from Harmonic Balance analysis, as follows:

$$\frac{\delta\omega}{\omega} = \frac{-1}{2E_k}\int_0^{\tau/\omega} \Phi^T \mathbf{p}(t) \bullet \eta dt \qquad (7.3)$$

However it should be noted that an uncoupled analysis inherently assumes no frequency shift, so this is only a prediction of the aeroelastic response frequency, and it does not come directly from the calculation as in the case of the coupled analysis. The cumulative work done (*WD*) by the fluid over the period, given by the integral term only in **Eq. 7.2**, and in a plot of modal force against displacement is equivalent to the area under the curve indicating the work done per cycle. This plot provides insight into which parts of the vibration cycle contribute to the work put into (or taken out of) the structure by the fluid.

Method 2: Uncoupled Analysis with Shape Correction

The second method used is the single passage version of method 1 and the desired IBPA is achieved using the shape correction method of He. This approach is essentially a 'direct store' type technique whereby the flow data on the periodic boundaries are related to those at an earlier time via the vibration frequency and phase angle. In order to save storage space, the variables are stored as a series of Fourier coefficients. Thus, for any IBPA, only one blade passage is required for the unsteady calculation but more periods of forced motion may be required for the unsteady forces to converge.

The determination of the flutter stability (logdec) is still given by **Eq. 7.2**, the main difference being that the data on the upper and lower blade surfaces refer to different blades as these are moving with different phases. Thus all variables on one surface must be phase-shifted back for information consistency on both surfaces of the blade. It should be noted that Methods 1 and 2 are identical for 0° IBPA. The predicted frequency shift can also be calculated in a similar fashion using **Eq. 7.3**.

Method 3: Coupled Analysis

The third method used is the coupled analysis as described in Chapter 3. In a coupled analysis, one cannot use the shape correction approximation to represent non-zero IBPAs as the unsteady pressures on both surfaces of the blade are not available at any instant in time, the solution being valid once it has converged to a periodic situation.

The only alternative is to use multiple blade passages, as described for Method 1. In this approach the stability (logdec), and the change in response frequency from the natural frequency of the blade, may be determined directly from the time history of motion. The results can then be computed directly from the time-histories, and expressed as a frequency shift, for comparison with the predicted shifts from methods 1& 2.

7.3.4 Results

Coupled Analysis of Mode 3 (0 IBPA)

First, the stability of the first torsion mode (mode 3) was examined using the coupled method only (method 3). This is to eliminated the possibility of torsional flutter, which is possible at high rotational speed on the working line. The motion was started in mode 3 (torsion) with an impulse - this gives an initial velocity in that mode. The resulting motion of mode 3 in the modal domain can be seen in **Fig. 7.11a**. The response of mode 3 is also stable, both near peak efficiency, and near stall, with the latter actually being more stable (logdec = `0.022, 0.027` respectively). The response frequency was about `1860` Hz, compared to the natural frequency of `1910` Hz. The energy plot is also shown in **Fig. 7.11b** - the energy in the structure decays as governed by the work done by the fluid, and the interchange of energy is modelled accurately as can be seen from the initial energy (E_0) plot which is constant with time.

It can be concluded that torsional flutter is not a problem at either of the operating conditions. Also, the response frequency of mode 3 is too high to be able to couple with mode 1 (1st flap) to cause a flutter mechanism. Thus the aeroelastic behaviour of mode 1 will now be further investigated.

Results for Mode 1 (1st Flap)

The results for the aeroelastic analysis of mode 1 (1st flap) from all three methods for the near PE case are summarised in **Table 7.3** (and plotted in **Figs.7.19&21**), and for the near stall case in **Table 7.4** (and plotted in **Figs.7.20&22**).

Table 7.3 Results from the 3 analysis methods near PE

Method	IBPA (deg)	Logdec	Frequency Shift (Hz)
1/2	0.0	0.0164	-1.7
3	0.0	0.0165	-2.4
1	+90.0	0.1210	+5.7
2	+90.0	0.1054	-0.3
3	+90.0	0.1250	+4.8
1	180.0	0.2200	+10.5
2	180.0	0.1804	+2.5
3	180.0	0.2157	-3.2
1	-90.0	0.0934	+1.1
2	-90.0	0.1369	+1.2
3	-90.0	0.0910	0.0

Table 7.4 Results from the 3 analysis methods near stall

Method	IBPA (deg)	Logdec	Frequency Shift (Hz)
1/2	0.0	0.0044	-3.4
3	0.0	0.0036	-17.1
1	+90.0	0.0247	+11.0
2	+90.0	0.0340	-2.6
3	+90.0	0.0110	+11.4
1	180.0	0.4800	+2.9
2	180.0	0.2114	-2.4
3	180.0	0.6078	-20.1
1	-90.0	0.1287	-2.2
2	-90.0	0.1878	+0.4
3	-90.0	0.1388	+4.8

For the uncoupled analysis (method 2) the phase plane plots in the modal domain are shown in **Fig. 7.12** for the 0° and 180° IBPA cases, and in **Fig. 7.14** for the +/-90° cases. These plots show that the fluid response given by the modal force changes considerably both with operating conditions and IBPA. Note that the motion in the 180° IBPA case is 5 times smaller than the 0° case. However the amplitude of the unsteady force is larger in the 180° case especially in the near stall condition. The phase of the force also varies from the 0° case to the 180° case, and the size of the area swept out by the curve indicates the work done per cycle. This is more clearly shown in **Fig. 7.13 & 7.15** which show the cumulative work done by the fluid over the period for the same cases.

Thus the 180° IBPA case is considerably more stable than the 0° case. At 0° IBPA the near peak efficiency case is more stable, with the near stall case only marginally stable. However, perhaps surprisingly, this situation is reversed at 180° with the near stall case being the more stable of the two, albeit both being very stable. The +/- 90° cases are somewhere in-between the other two cases in terms of stability. In the PE case the stability of the two is about the same, whereas at NS condition, the +90° case is somewhat less stable. Also for these uncoupled cases the predicted frequency shift has been determined by integrating modal force times displacement over the period.

For the coupled analysis (method 3), the time histories can be seen in **Figs. 7.16 - 18**. In all cases the motion of the blade decays, which is expected at this high rotational speed. However the responses again are quite different with operating condition and (especially) with inter-blade phase angle. In these cases of this coupled motion the energy in the system is plotted against time. It can be seen that the structural energy reduces from the initial value as the cumulative work done by the fluid becomes negative. Here again, the energy interchange can be seen to be modelled accurately, as the E_0 plots show, which does not change with time. In this case the work done per cycle could be used to determine the blade stability, however this changes with time as the amplitude of the motion decays (this can best be seen by the 180° case where the decay rate is large). Thus, to get a measure of the blade response the logdec is calculated from the modal displacements by comparing the amplitude over successive cycles, as described above.

In the plots of stability (logdec) against IBPA (**Figs.7.19&20**) it can be seen that the coupled results compare quite closely with the uncoupled analysis - the trends being in agreement. The worst case is consistently the 180° IBPA case where the decay rate is largest.

For the frequency shifts (**Figs.7.21&22**), note that the near peak efficiency case shows hardly any change in response frequency due to the presence of the fluid (< 1% or 5Hz according to the coupled results), and that the smaller the shift, the more the logdec values agree closely with the uncoupled values. However, the predictions of frequency shift in the uncoupled cases do not have much agreement to the coupled values. However, for the near stall case the reduction in frequency due to the fluid is much more pronounced (up to 4% or 20Hz), and correspondingly the uncoupled results for logdec are not so close.

Thus, it can be concluded that if the fluid does not change the frequency of response significantly from the natural frequency (say <1%), then the uncoupled analysis may well be adequate. However, with a non-linear fluid solver as used in this study, it is not normally possible to determine this frequency shift accurately without using the coupled analysis. This can be seen from the plots of frequency shift (**Figs.7.21&22**) where there is little correlation between the different methods, and also not much clear trend with IBPA. So for complex situations where there is an interaction between modes, or the response has more significant non-linear effects the coupled analysis is better placed to correctly predict the aeroelastic phenomenon.

To summarise, the following can be observed from the results for Rotor 67:

(i) As expected, all three methods produce very similar stability results for 0° IBPA, which is to be expected (and particularly because this case was near neutral stability as well).

(ii) For the peak-efficiency case, the agreement is quite good between Methods 1 and 3, Method 2 producing somewhat different stability margins especially at 180° IBPA.

(iii) For the near-stall case, Methods 1 and 3 are no longer in such good agreement, suggesting that the fluid/structure interaction has an important role to play, especially when the flow exhibits strong non-linear characteristics.

(iv) Method 3 (coupled) predicts significant frequency shifts between the in-vacuo and aeroelastic natural frequencies, a feature that also suggests that the fluid/structure interaction may be significant.

(v) There is no clear trend in the frequency shift results for either case, and the different methods do not agree well on this.

(vi) The least stable region would seem to occur between 0° and 90° IBPA near stall, indicating a possible flutter regime at this condition. The blade did not flutter on test, but the present method did not model the structural damping, or mistuning, which would both exist in the real case, and both have a stabilising effect.

7.4 CONCLUSIONS

1) The 3-dimensional steady flow NASA Rotor 67 is calculated at two operating conditions using the thin-layer Navier-Stokes equations with a mixing length turbulence model. The results compare reasonably with the experimental results, and with other numerical results that have used a considerably finer grid and more complex turbulence models.

2) A finite-element model of the blade structure has been used to determine the vibration behaviour of this blade rotating at speed, neglecting the effects of the disk flexibility.
3) A coupled aeroelastic model has been used to calculate the static and dynamic aeroelastic response of this blade. The untwist due to the gas loads was found to be small near peak efficiency, and about 0.3° near stall. The successful prediction of the operating shape at speed is the first step towards the flutter analysis.
4) The flutter stability of the blade was examined using both coupled and uncoupled analysis methods. Although the blade was found to be stable for all cases studied, the flutter margin was observed to vary qualitatively as one would expect with a compressor rotor of this type. Although these results are encouraging, more work is required to give guidance as to the best prediction method to use in the general case.
5) Using the coupled analysis, the stability in the first 5 modes was calculated. All were found to be stable at both operating conditions, at zero IBPA.
6) The partially-integrated approach used in this study was found to model the energy interchange between the fluid and the structure accurately.
7) The agreement between the methods was found to be good only for the 0° inter-blade phase angle. In the case of the uncoupled analysis, the shape correction approximation produced somewhat different results from those obtained from the multi-passage analysis.
8) Significant frequency shifts were observed between the structural and aeroelastic modes of the rotor, especially for off-design conditions. The frequency shift could, in principle, be a key indicator for the type of analysis required in the sense the uncoupled may well be adequate in the case of small shifts. However, it is normally not possible to determine this frequency shift accurately without using a coupled analysis in the first place, unless the Gerolymos (1992b) technique is used.
9) The first two methods suffer from the limitation of being able to deal with one structural mode at a time. Therefore, a coupled analysis is more appropriate if the structural modes are likely to interact with each other. However, even the third method is limited to the analysis of one inter-blade phase angle per calculation and hence the coupling between the various nodal diameter modes cannot be taken into account. Ideally the whole annulus should be modelled, an approach that can also deal with blade mistuning and inlet distortions, as well as all the structural modes.
10) A possible flutter mechanism may exist for this blade, near stall, at around 2-3 nodal diameters, although the blade was stable on test.

Discussion

Thus the inference that can be drawn from these observations is that the presence of the fluid flow may shift the aeroelastic response frequency from the natural frequencies of the modes. Because of this fact the coupled method (3) stands a much better chance of accurately predicting flutter behaviour, as it is the only method which models this effect. However, it has been shown that the coupled method inherently cannot use a storage method such as shape correction to achieve the IBPA in a single-passage analysis. Thus method 2 is still a useful tool to have available.

The way in which the coupled analysis was employed in this study (multiple passages to achieve one IBPA at a time) is not the most efficient way of using this type of analysis. This method was used in order to give a back-to-back analysis of the 3 different methods, using identical grids etc., for each IBPA separately. However, the best way to make use of this technique is to do one calculation of the entire bladed assembly, so all the different possible IBPAs (or nodal diameter patterns) can be included at once. Then the system is free to respond to whichever modes are unstable, or indeed if the instability is caused by an interaction between them (a possibility which definitely cannot be predicted by the classical methods). This will be looked at in detail in Chapter 8.

A possible flutter mechanism at 2 to 3 nodal diameters would be in line with the understanding for compressors of this design. For low, forward travelling nodal diameter modes the destabilising effect comes from the change in incidence on to the vibrating blade as it moves which changes the loading. If the loading increases in the same direction as the blade is moving, which can happen if the neighbouring blades are moving with different phases to achieve this situation, then this is a destabilising effect. This may be counteracted by the stabilising effect of pure flap motion (in the absense of gross stall), and the IBPA will then change the trade-off between these opposing effects. The destabilising effect is likely to be larger at the near stall condition as the shock stands outside the passage, so small changes in incidence due to the blade motion are likely to lead to correspondingly larger changes in blade loading as the shock moves. Also the shock boundary-layer interaction is likely to exacerbate this effect further.

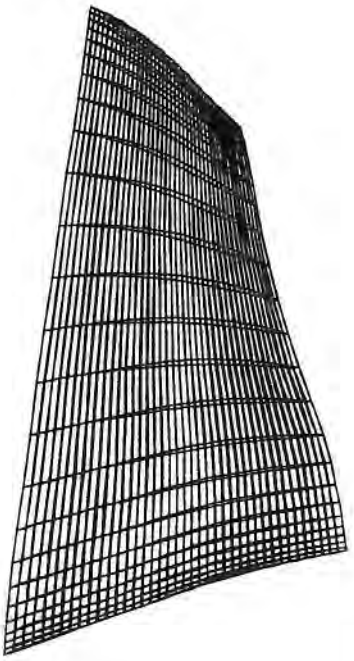

Fig. 7.1a Finite Element Mesh

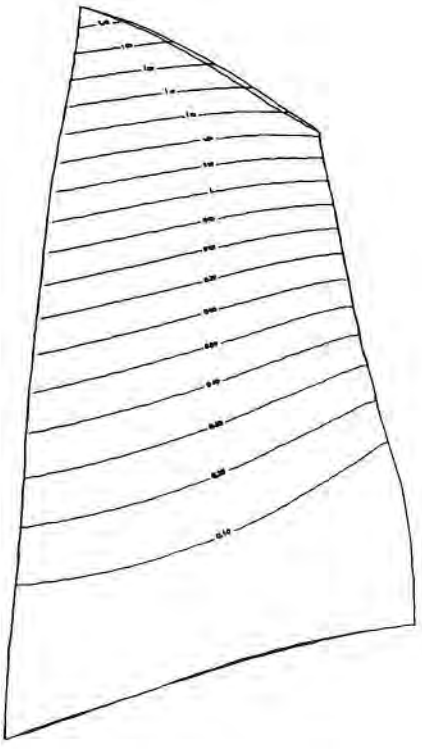

Fig. 7.1b Mode 1 (1st Flap)

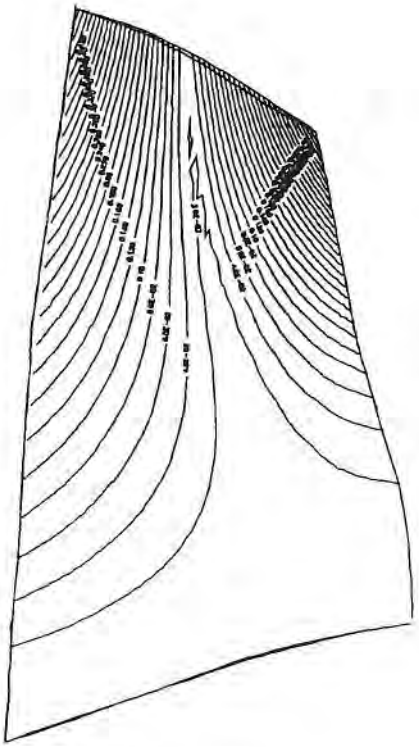

Fig 7.1c Mode 3 (1st Torsion)

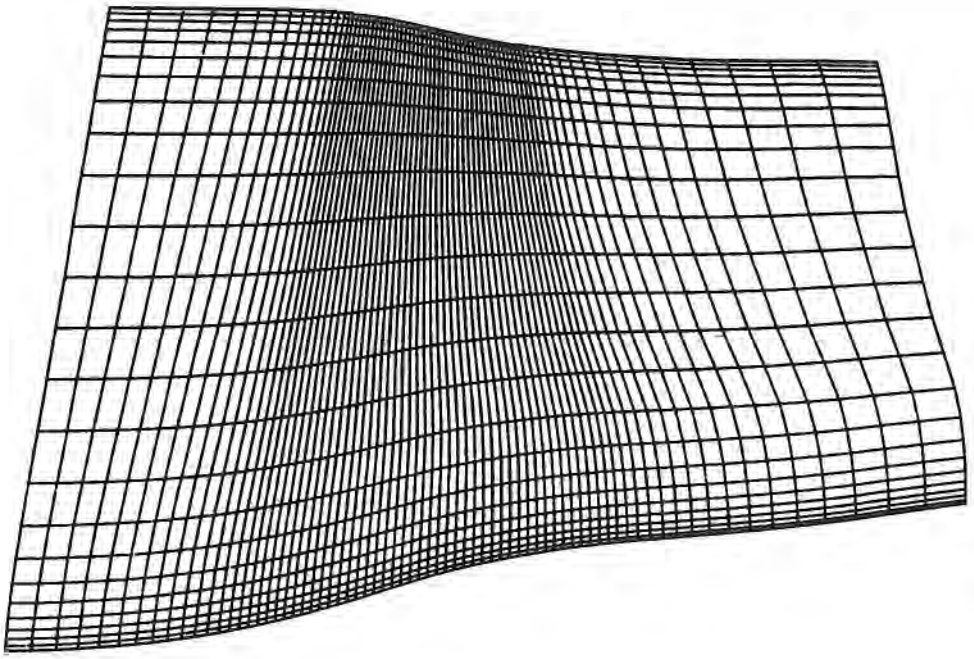

Fig. 7.2a Meridional view of Aerodynamic Mesh

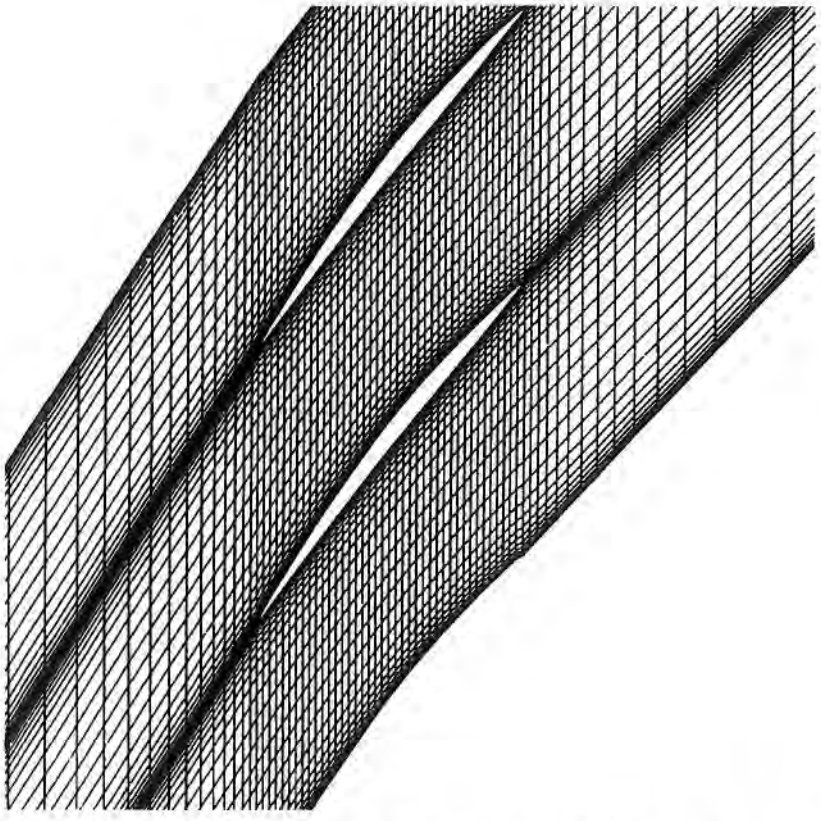

Fig. 7.2b Blade-to-Blade view of Aerodynamic Mesh (70% Height)

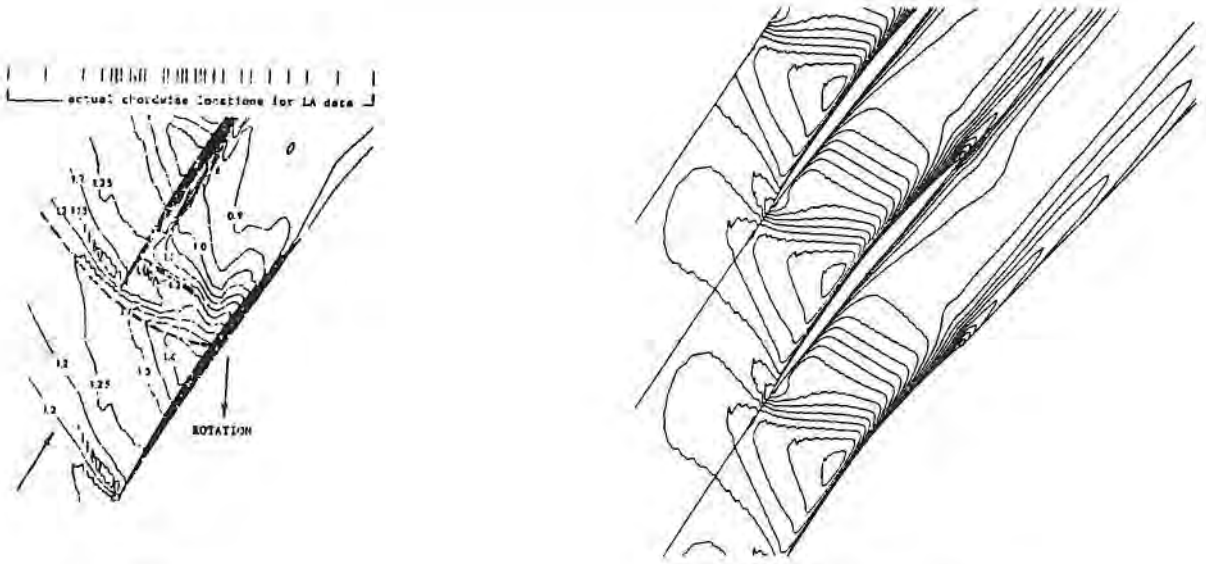

a) Experiment b) Computed

Fig. 7.3 Mach Number Contours PE (70% Height)

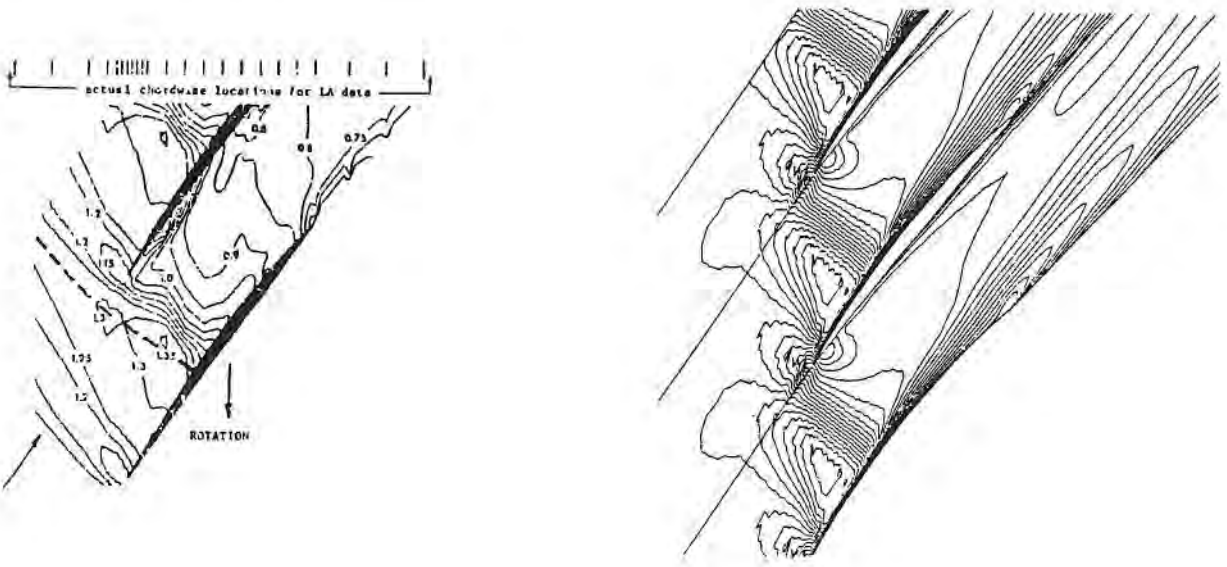

a) Experiment b) Computed

Fig. 7.4 Mach Number Contours NS (70% Height)

Peak Efficiency (PE) Near Stall (NS)

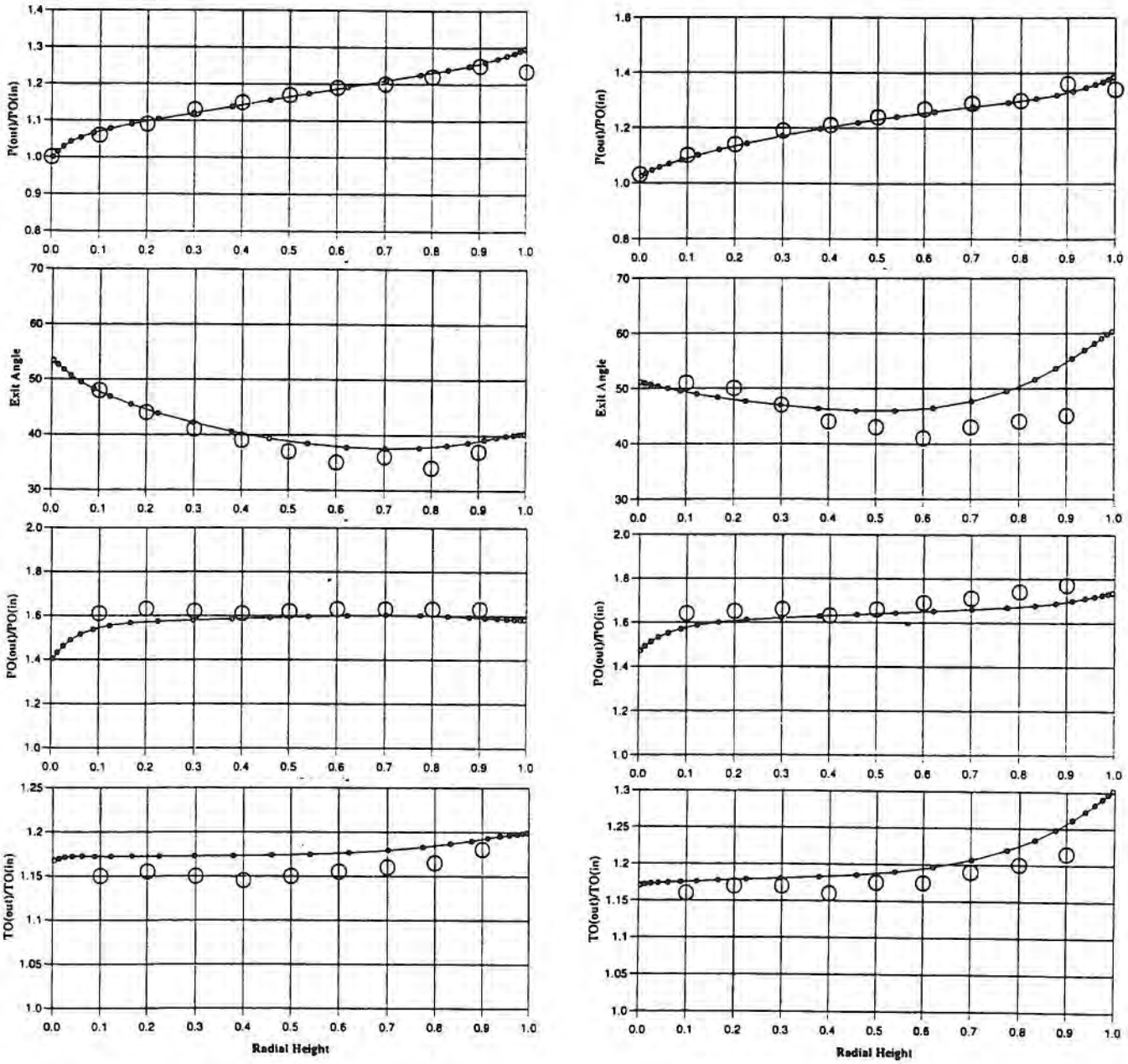

(a) Static Pressure, (b) Exit Angle, (c) Total Pressure & (d) Total Temperature

Fig. 7.5 Circumferentially Averaged Radial Profiles at Exit Fig. 7.6

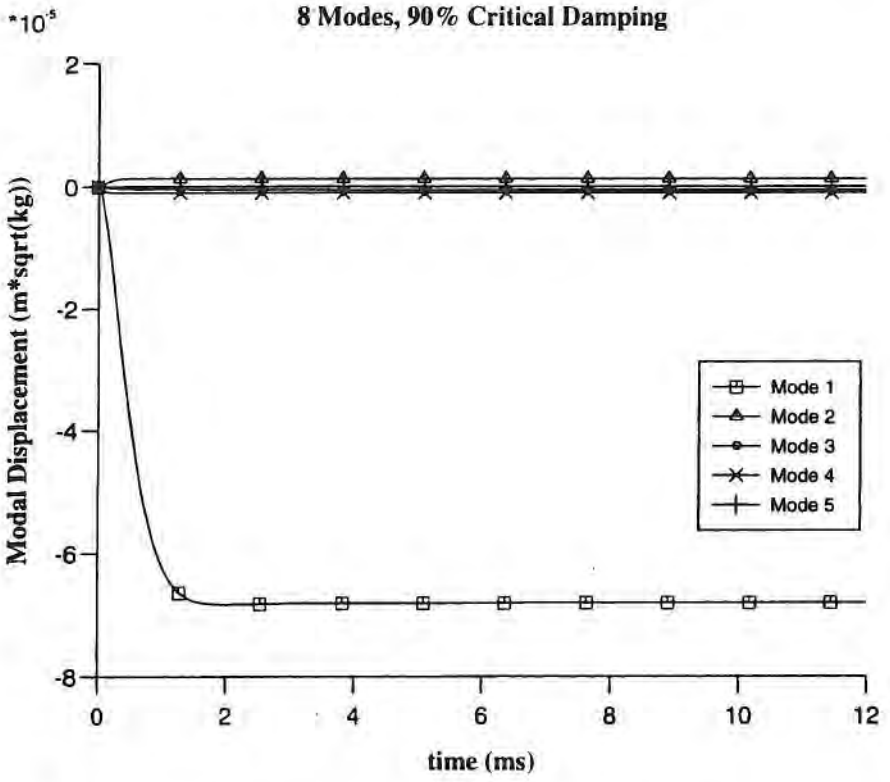

Fig. 7.7 Untwist Modal Displacement Time History (PE)

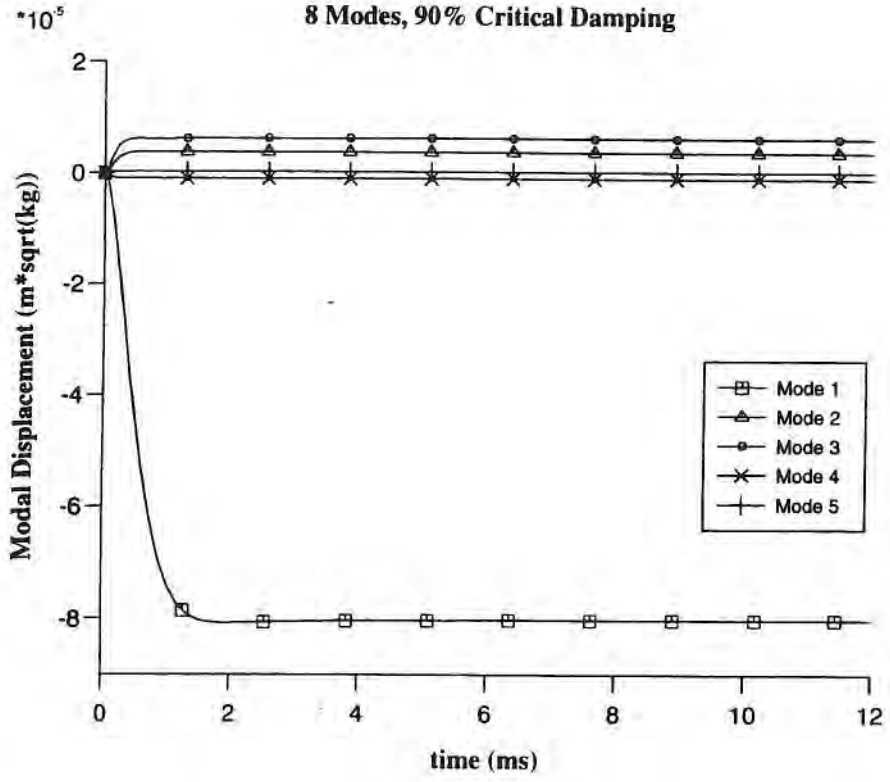

Fig. 7.8a Untwist Modal Displacement Time History (NS)

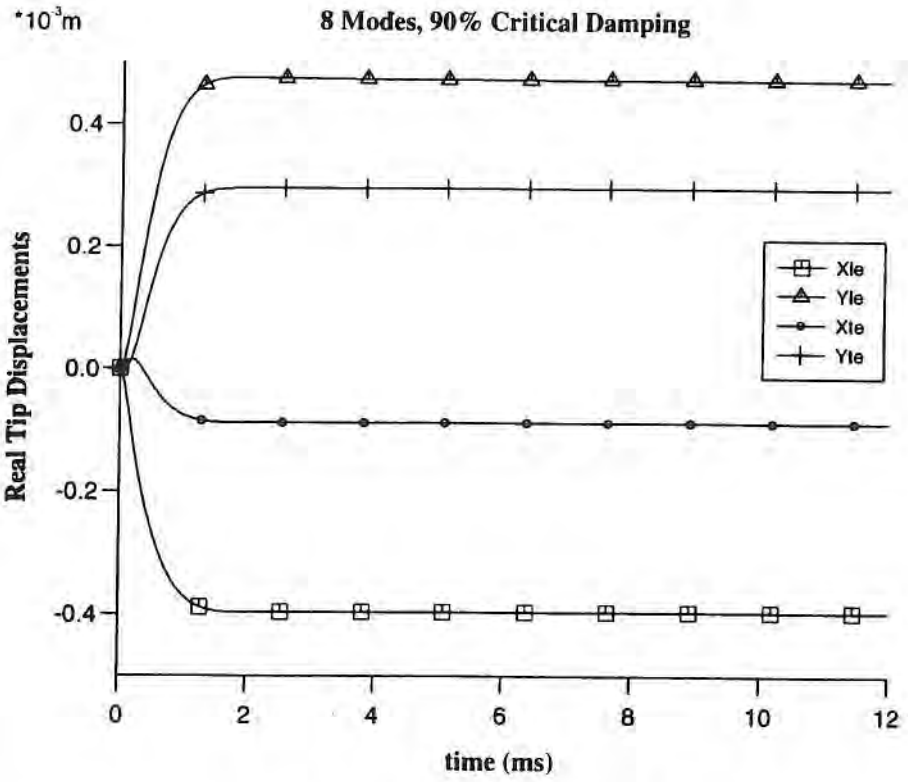

Fig. 7.8b Untwist Real Displacement Time History (NS)

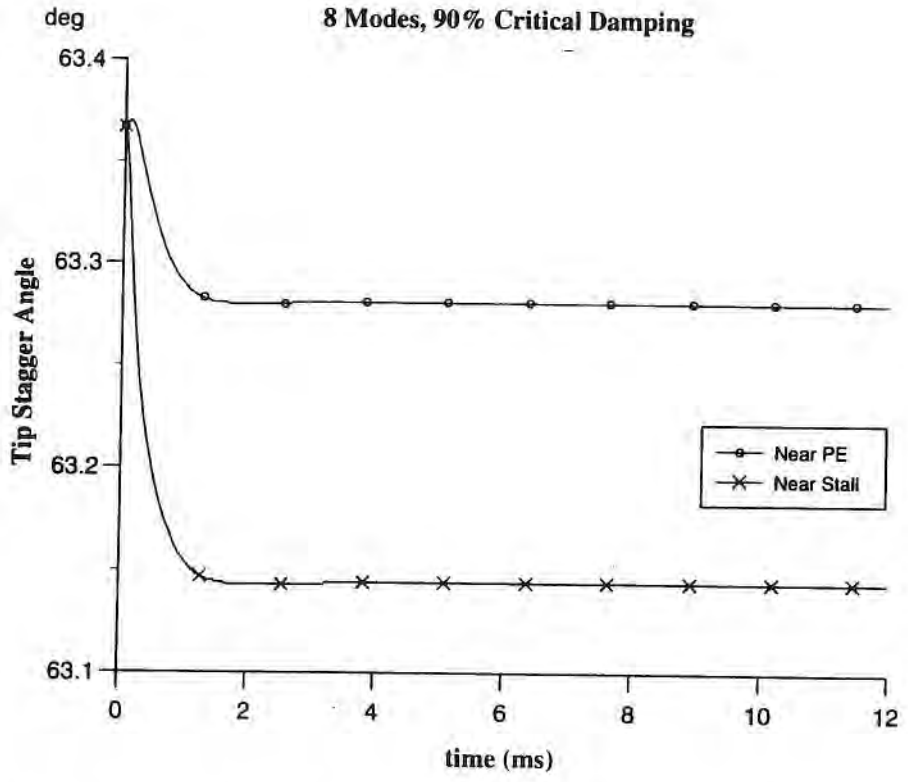

Fig. 7.9 Untwist Tip Stagger Time History (PE & NS)

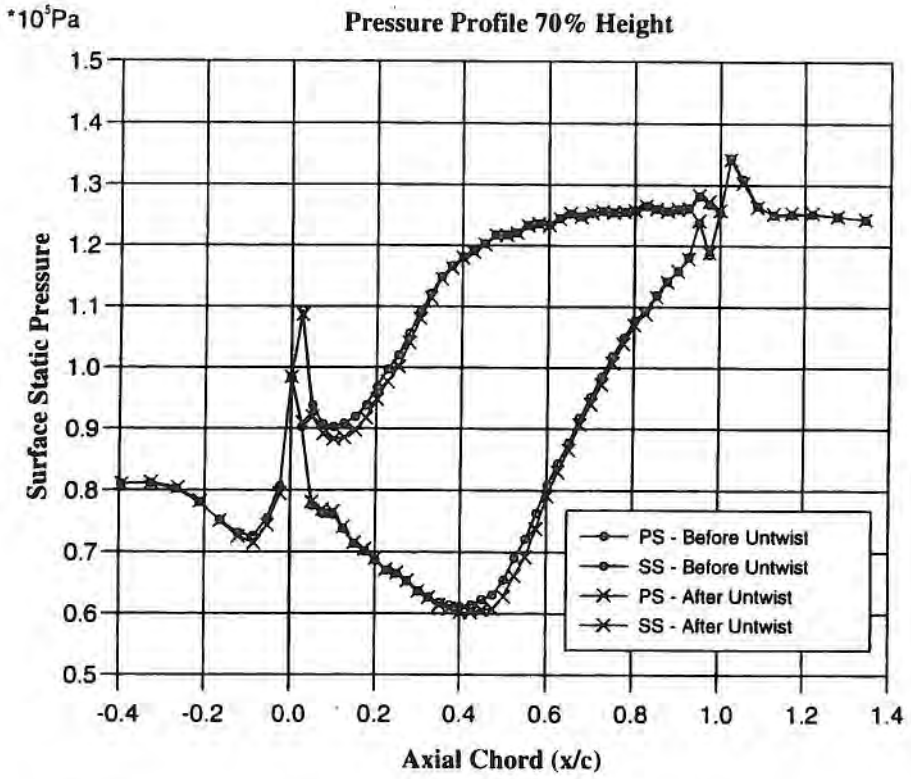

Fig. 7.10a Surface Static Pressure, 70% Height (PE)

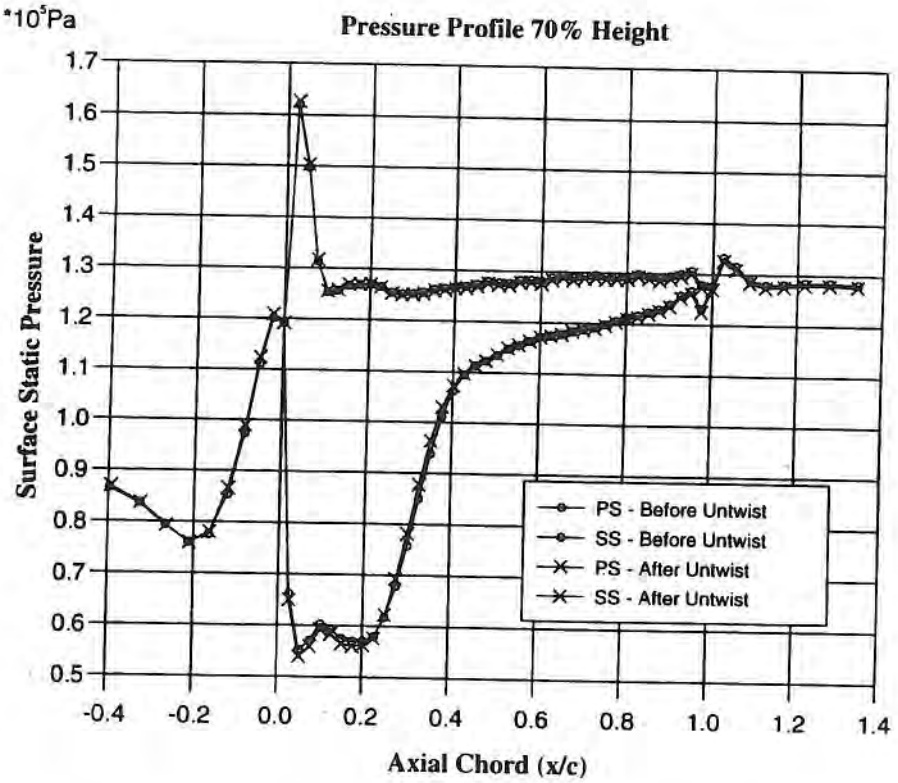

Fig. 7.10b Surface Static Pressure, 70% Height (NS)

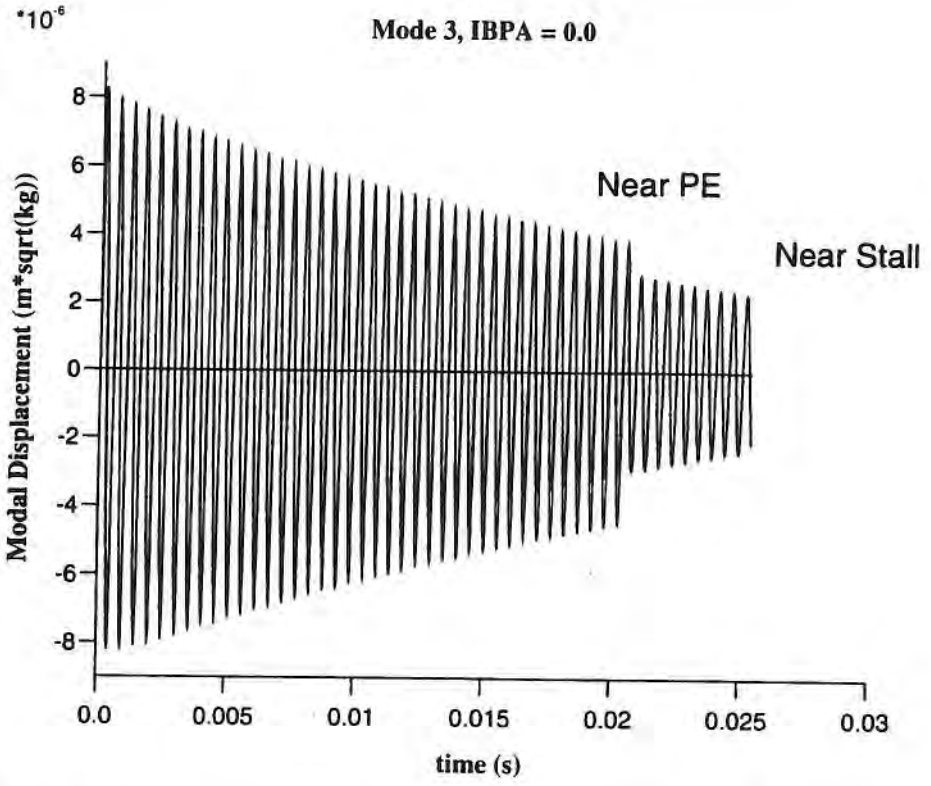

Fig. 7.11a Coupled Flutter Time History, Mode 3 Displacement

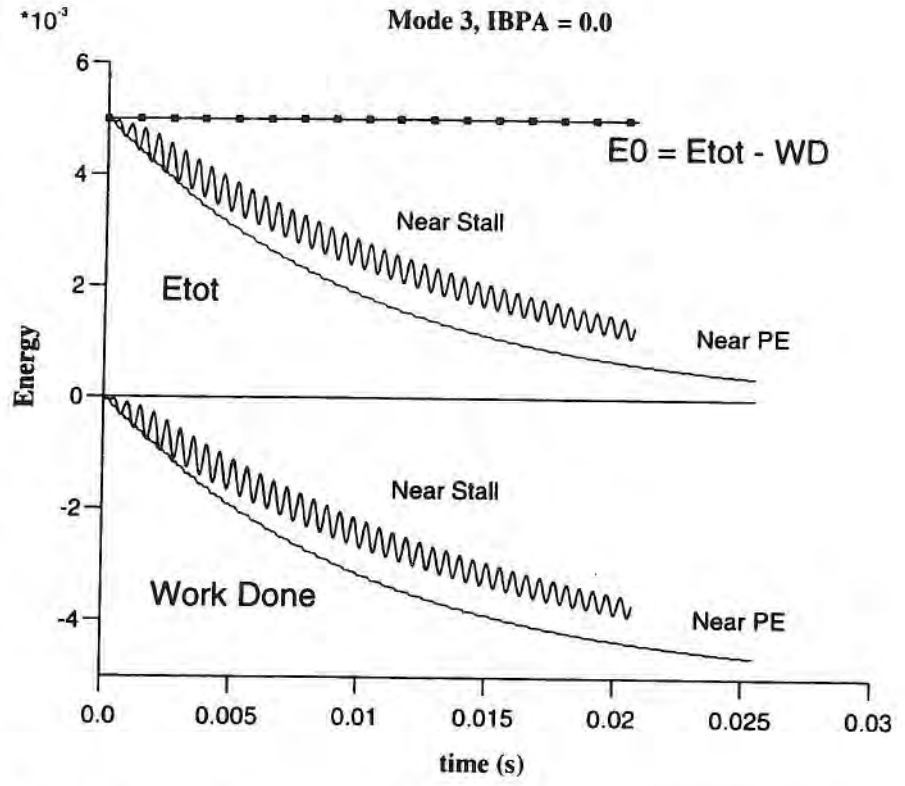

Fig. 7.11b Coupled Flutter Time History, Mode 3 Energy

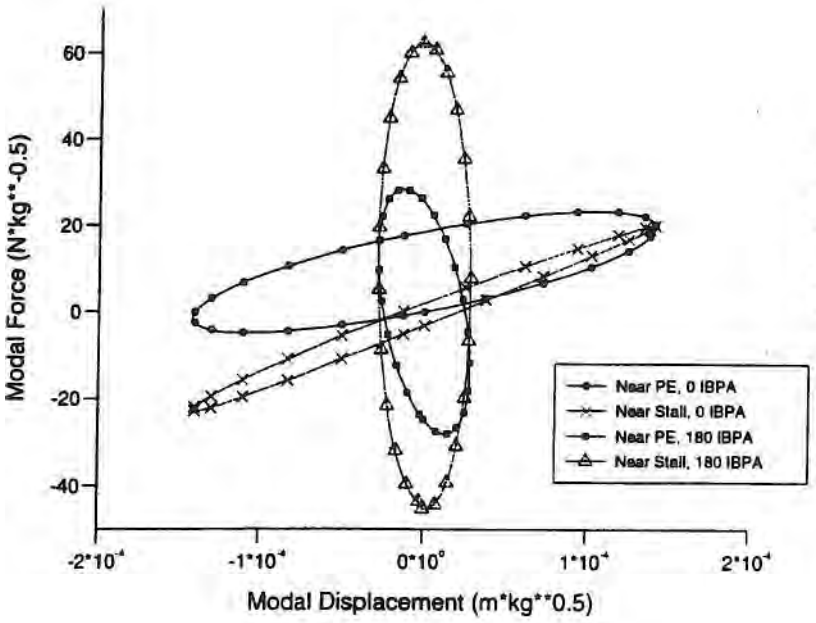

Fig. 7.12 Uncoupled Phase Plane (0 & 180 deg IBPA)

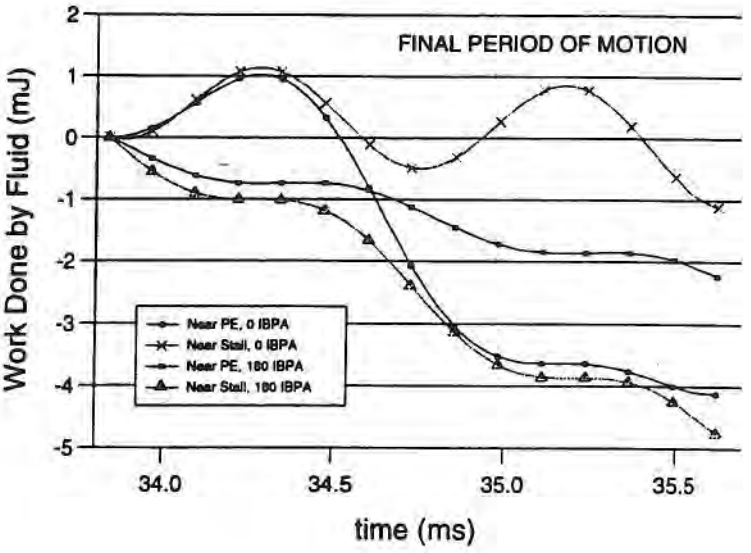

Fig. 7.13 Uncoupled Time History (0 & 180 deg IBPA)

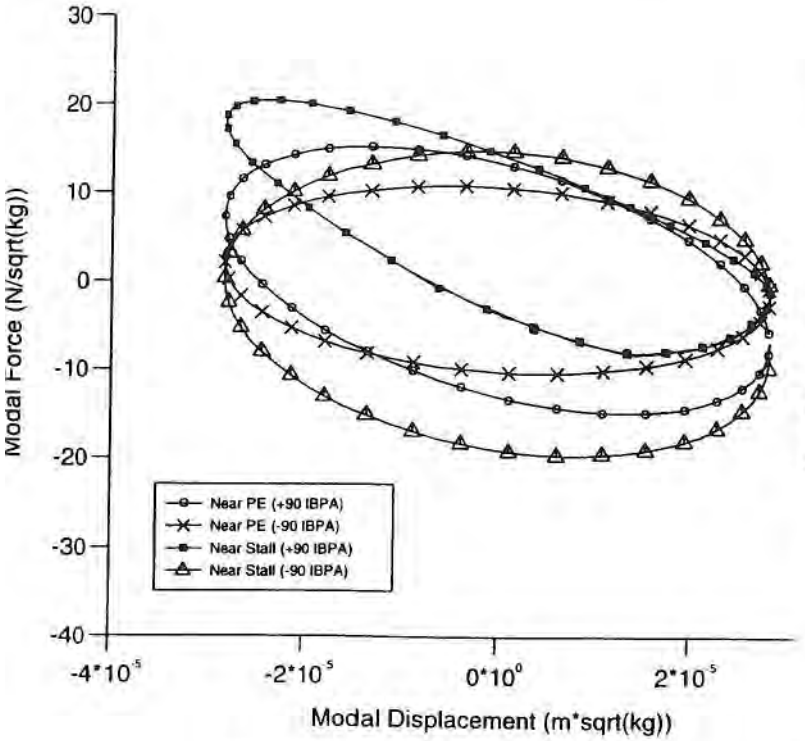

Fig. 7.14 Uncoupled Phase Plane (90 deg IBPA)

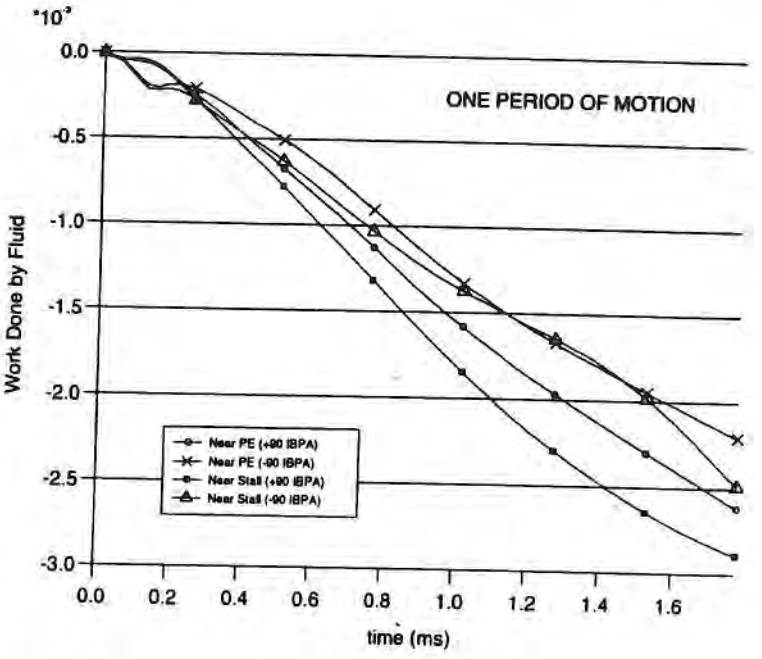

Fig. 7.15 Uncoupled Time History (90 deg IBPA)

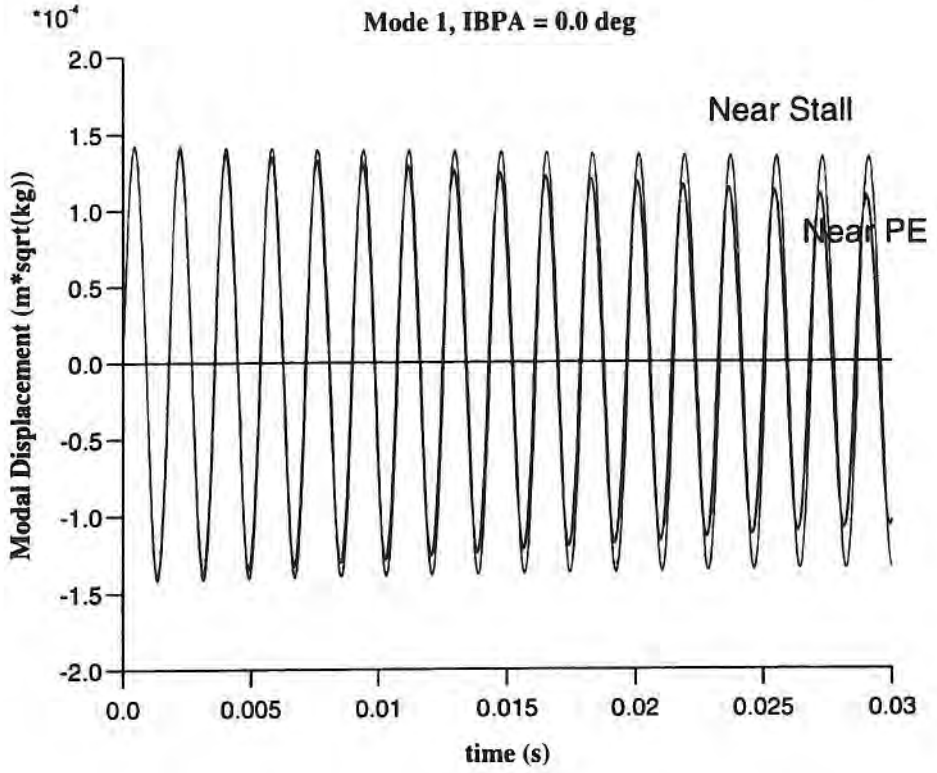

Fig. 7.16a Coupled Flutter Time History, Mode 1 Displacement (0 IBPA)

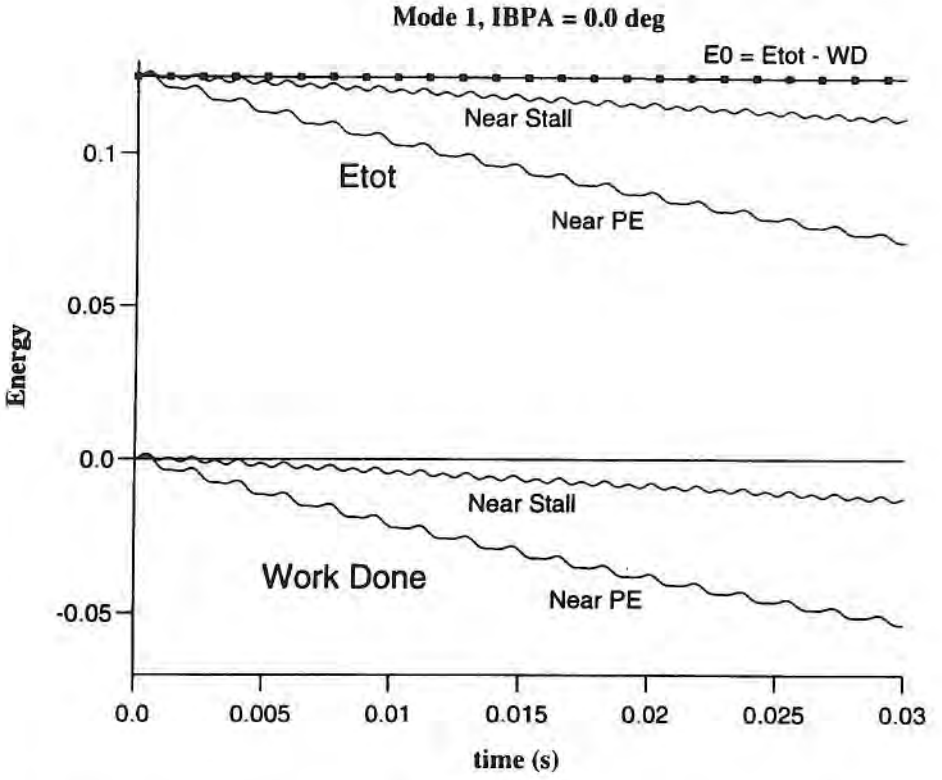

Fig. 7.16b Coupled Flutter Time History, Mode 1 Energy (0 IBPA)

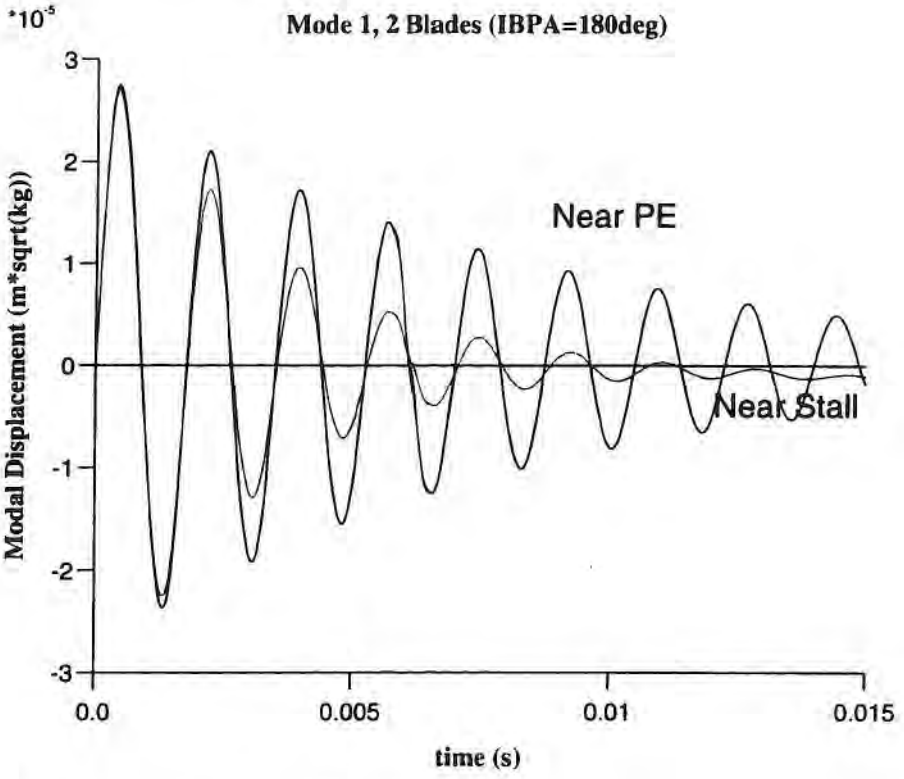

Fig. 7.17a Coupled Flutter Time History, Mode 1 Displacement (180 IBPA)

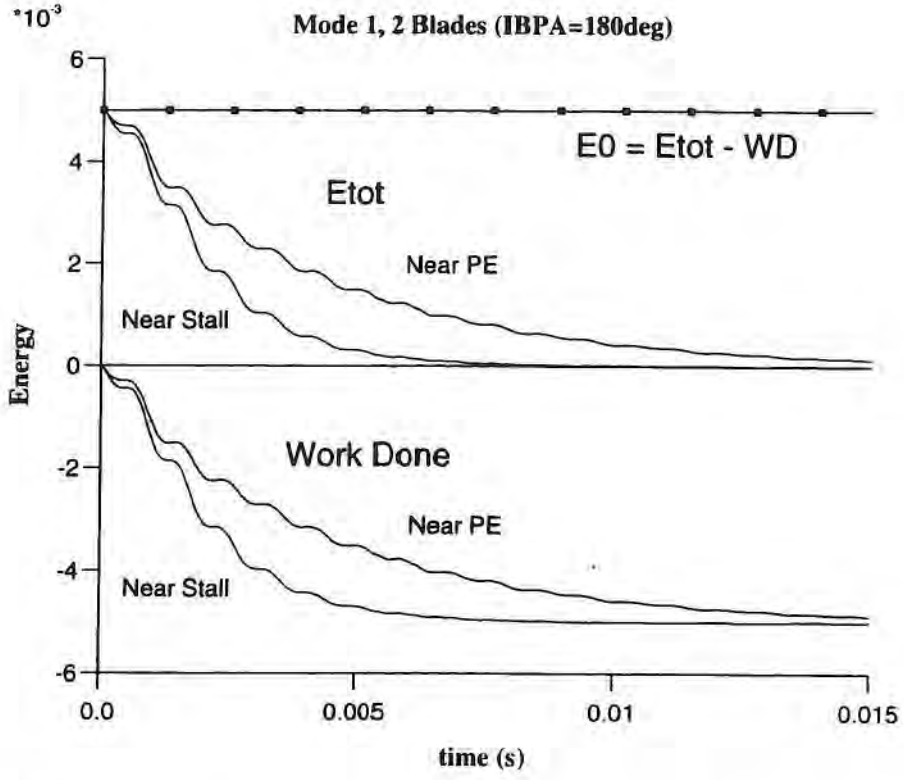

Fig. 7.17b Coupled Flutter Time History, Mode 1 Energy (180 IBPA)

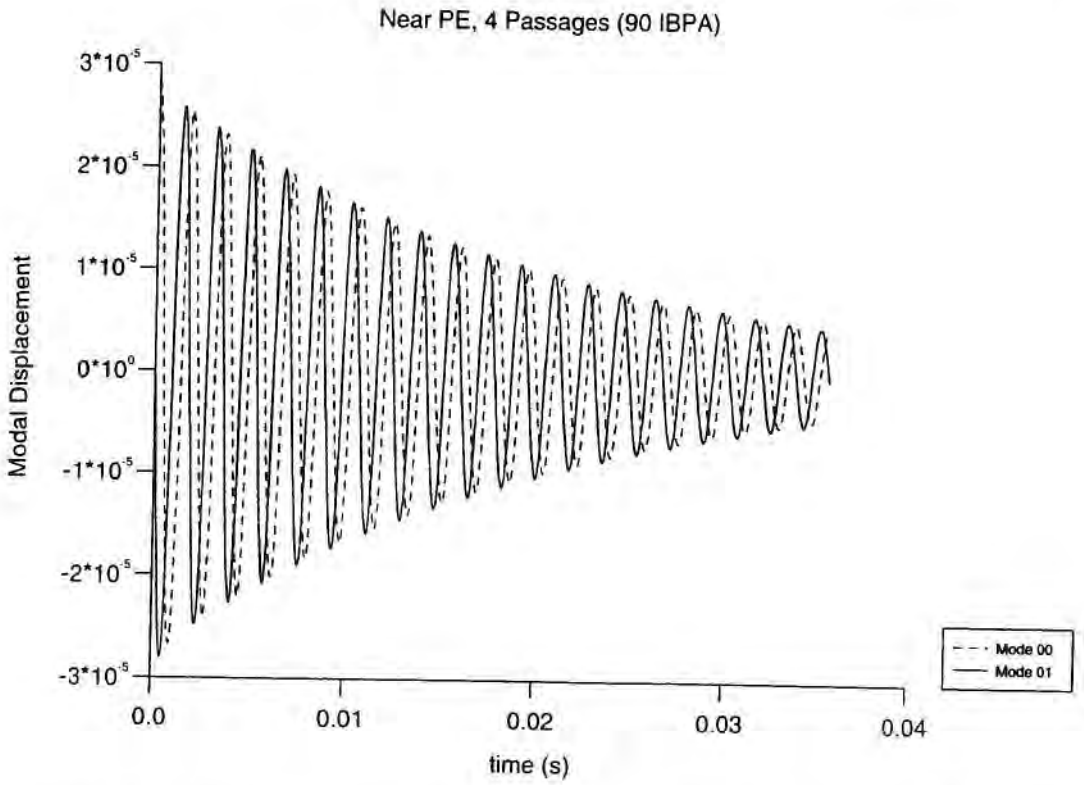

Fig. 7.18a Coupled Flutter Time History, Mode 1 Displacement (90 IBPA)

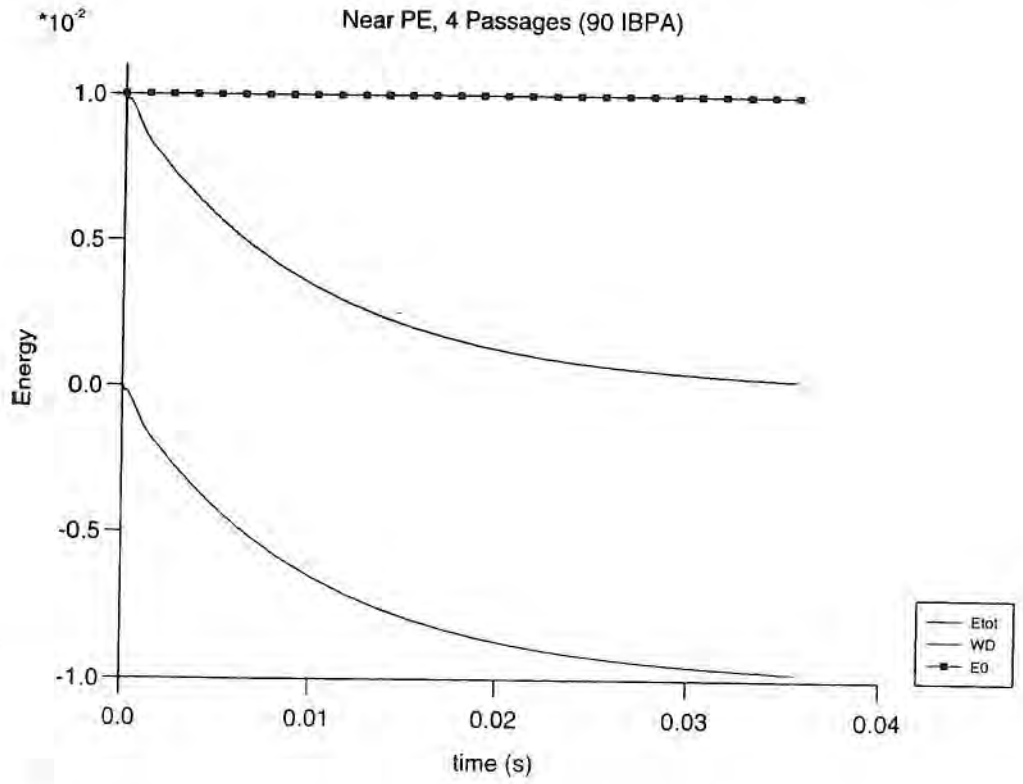

Fig. 7.18b Coupled Flutter Time History, Mode 1 Energy (90 IBPA)

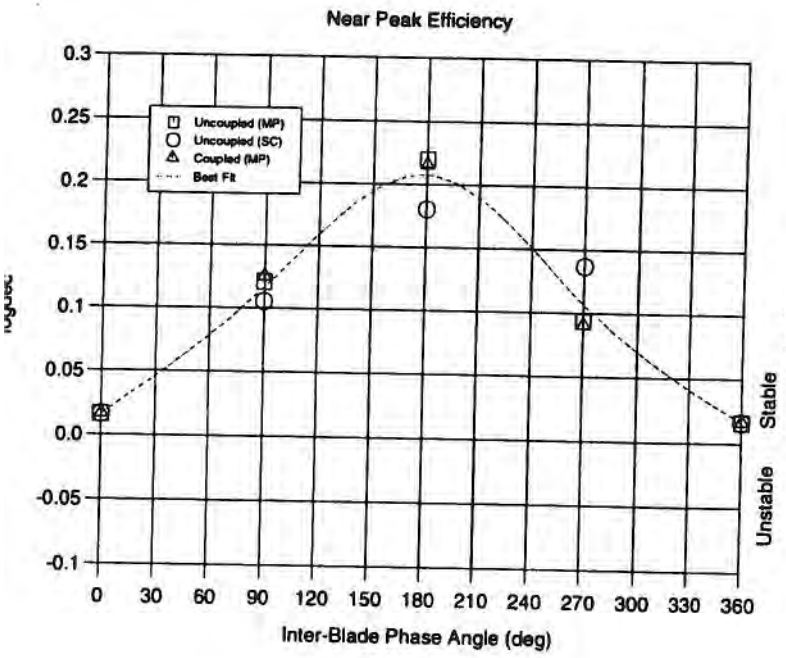

Fig. 7.19 Stability (PE)

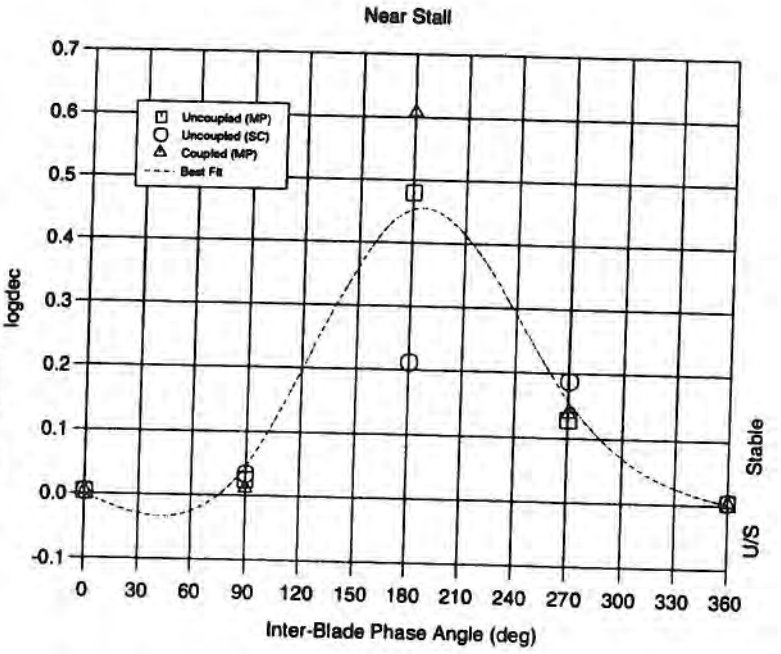

Fig. 7.20 Stability (NS)

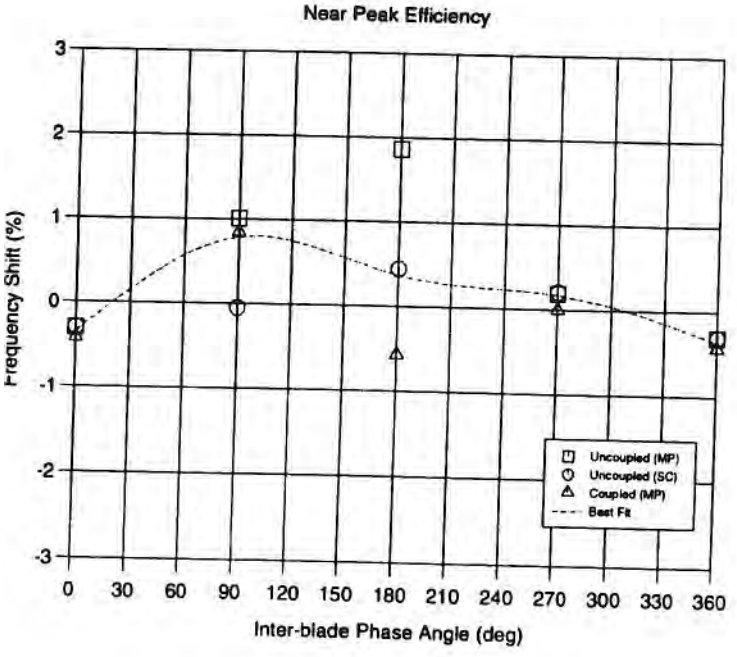

Fig. 7.21 Frequency Shift (PE)

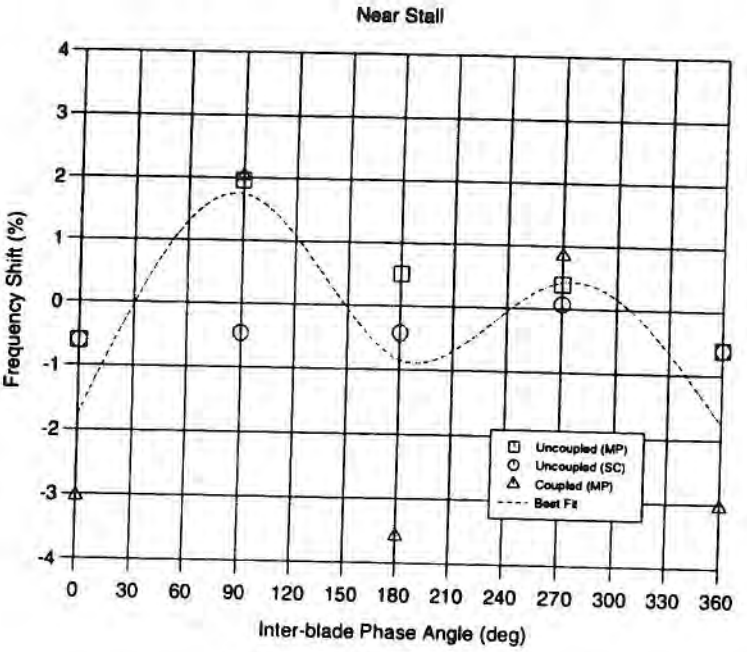

Fig. 7.22 Frequency Shift (NS)

Chapter 8

3D Bladed Assembly Flutter

8.0 About this Chapter

This chapter will concentrate on the flutter behaviour of the fan blade described in Chapter 6. First, the blade is analysed using an uncoupled single passage approach with 'shape correction' (method 2 of Chapter 7). This is used as a benchmark of the classical flutter analysis, against which to compare the new method. In this chapter a model of the whole bladed assembly is presented, using the coupled approach. In this way, instead of treating the IBPA as fixed and calculating the stability of each separately, all the possible IBPAs (or nodal diameter modes) can be included in one calculation. Thus, despite the fact that one huge calculation is required which may be very demanding on CPU time and memory, this approach may not need any more resources than the single passage approach overall (assuming the stability of most of the modes is required).

The test case used is the Low Speed case near stall. This fan assembly is known to flutter at or near this condition, and the position of the tested flutter boundary is known. This study is aimed at comparing the two approaches adopted, and at trying to obtain a better understanding of how flutter occurs at these conditions.

8.1 INTRODUCTION

The main difficulty with turbomachinery flutter prediction is the extra complication of having many interacting blades. Even if the effect of upstream and downstream rows is neglected, then the bladed disc may vibrate in different cicumferential patterns known as the inter-blade phase angles (IBPAs). In classical analyses spatial periodicity of vibration in the blade-row under consideration cannot be ignored. Thus, the IBPA is imposed on the calculation - but in reality this quantity is unknown for flutter, and should result from the prediction. This approach has been adopted in Chapter 7, both for the classical uncoupled methods, and for the coupled (PI) method. The uncoupled methods can only allow one mode to be examined at once, but the PI method can account for many blade modes simultaneously as demonstrated in the untwist calculations, albeit only at one IBPA.

But previous approaches, although valuable for trying to improve the understanding of particular flutter mechanisms, do not account for one final important effect. This is the possibility of different nodal diameter modes (IBPAs) interacting with each other - either in a transient manner, or to produce an unstable flutter mode. This may be particularly true of the forward and backward travelling modes of the same nodal diameter number which will have the same frequency in 'tuned' systems (in vacuo). Also, this effect may be even more pronounced in the case where mistuning is present, where the double modes split to two separate frequencies from a structural viewpoint.

To model such effects, every blade in the annulus must be included in the calculation, even though this is computationally very expensive. Although this approach may not be any more expensive than the single passage approach where a full flutter analysis is required (i.e. 1 calculation of N passages, must be compared against N calculations of 1 passage to cover all the possible IBPAs).

8.2 AEROELASTIC MODEL

The aerodynamic model of code AV3D is as described in Chapter 6. The flutter model described before in Chapter 7 uses single- or multiple-passage analysis with a *fixed* IBPA for each calculation. Therefore for a complete flutter analysis, the number of calculations necessary is equal to the number of blades (the number of possible IBPAs). So the fixed IBPA approach may take even more CPU time than one full annulus multi-passage run, if all the possible assembly modes are taken into account.

In this study the multi-passage version of AV3D will now be used. The only modification to the CFD code involves setting the variables of the upper periodic

boundary of one blade passage equal to the values on the lower boundary of the next passage. As the model now includes the whole annulus of blades, the first and last boundaries are also set to be equal.

The structural model is as described in previous chapters - normal vibration modes are obtained from an FE analysis of the blade static geometry, including the rotation effects. These modeshapes are then interpolated onto the aerodynamic grid surface points, and the structural motion is computed using the assumed modes method. The Newmark-β method is used to integrate the aeroelastic EOM in time. However in this case the modes are required for the entire rotor assembly (disk + blades).

To obtain the assembly modes, an FE model of the whole bladed disk could be used. However this would be an extremely inefficient way of obtaining the desired information, given some knowledge about bladed disk systems. Instead, the concept of cyclic symmetry can be employed in the FE analysis, enabling only one sector of the assembly (1 blade attached to a disk sector) to be calculated. The different possible nodal diameters are introduced through the boundary conditions on the periodic boundaries (a structural implementation of the IBPA). This is valid as a linear solution of normal modes is desired, and the only non-linear force considered (the centrifugal force due to rotation) is fixed as the calculation is done at fixed speed.

Note that this type of calculation produces the cyclic symmetry modes in terms of two components - symmetric (real) and anti-symmetric (imaginary) parts, for each possible nodal diameter pattern. The actual bladed assembly (N=26 in this case) will have double modes for all nodal diameters except 0 and 13 ($N/2$). Thus there are two modeshapes for each Fourier number (nodal diameter) which are the forward and backward travelling orthogonal modes which occur at the same frequency for the tuned system. These are referred to as mode n (forward travelling) and mode $-n$ [or sometimes $N-n$] (backward). For zero nodal diameters (analogous to treating the sector alone with no cyclic symmetry) the sine part is zero. For 13 ($N/2$) nodal diameters the two parts are the same. In this case 12 double modes plus 0 and 13 gives 26 (N) assembly modes in total for each blade mode. If there are r blade modes of interest, the analysis will then include $26r$ (Nr) structural modes. However, only the 1st flap blade mode has been considered here.

A further complication is that the modal mass of the full assembly must be recovered for the expanded modes. The procedure for obtaining the correct modal masses for the

assembly modes, for the particular finite element implementation used here, is as follows:

- mass normalise the sector modeshapes with respect to the mass of the sector model;
- for 0 and 13 ($N/2$) nodal diameters, divide the modeshape vectors by $\sqrt{26}$ ($\sqrt{N}$);
- for all other nodal diameters, divide the modeshape vectors by $\sqrt{13}$ ($\sqrt{(N/2)}$).

In simple terms, this factor of two comes about through energy considerations, as for all the nodal diameters apart from 0 and N/2, there are 2 possible modes, double modes having to split the energy between forward and backward travelling waves.

The full assembly modeshapes must be recovered by expanding the sector mode shapes. This process must be done in r-θ co-ordinates in order to preserve the symmetry. The expansion is as follows:

$$\begin{array}{lll} \text{Modeshapes of sector } j\text{:} & \text{mode } n & U_r\cos(2\pi jn/N) + U_i\sin(2\pi jn/N) \\ & \text{mode } -n & U_i\cos(2\pi jn/N) - U_r\sin(2\pi jn/N) \end{array} \qquad (8.1)$$

where U_r and U_i are the real and imaginary components of the modeshape vector, j is the sector (blade) number, and n is the Fourier number (nodal diameters).

Once the modeshapes have been normalised to the whole assembly modal mass, they are interpolated onto the fluid mesh, and remain fixed throughout the aeroelastic calculation.

8.3 CASE STUDY - TRANSONIC FANBLADE FLUTTER

The static aeroelasticity effects of a research transonic fanblade were examined in detail in Chapter 6. This study included a detailed look at the aerodynamics of this blade along a Low Speed characteristic. The same case will now be examined for flutter behaviour at these same conditions. In the static study a 25×81×25 mesh was used. This same mesh is used for single passage studies here. However this mesh is too fine to be able to model the entire annulus of 26 blades within the computational resources available. For the full assembly model, a 21×65×11 grid was used requiring only 115Mb of core memory, whilst still able to capture the (steady) viscous phenomena.

Experimental Flutter Results

At this Low speed, this fanblade was found to flutter at a normalised pressure ratio of 1.0254 and normalised mass flow rate of 0.8566 relative to the calculated peak efficiency point (7). This flutter point is shown as an asterisk on the compressor map (**Fig.8.2a**). The flutter frequency was 174 Hz (1F ω_n=185 Hz), and a phase difference of -66° was measured from blades 15 to 26. This corresponds to a IBPA of -6°. The possible IBPA for assembly modes on this 26 bladed-disc are: $\pm 13.85° \times n$ etc. Thus the tested IBPA of -6° does not correspond to any integer value of IBPA. Possible explanations for this are that the rotor assembly was not at a stable limit cycle flutter when the data point was taken; that the IBPA is not constant round the wheel at this flutter point; or possibly due to mistuning. However a more likely explanation is that due to the fact that only the phase between two blades was available, the possibility of extra $n \times 360°$ in the calculation of the blade to blade phase has been left out. Thus the possible IBPAs now become: -6.0°, 26.7°, 59.5° etc.; and the most likely of these would seem to correspond to 2 ND (27.7°).

This corrected value is now more in line with the accepted understanding that part-speed stall-flutter occurs in low positive numbers of nodal diameters (e.g. 2,3,4). The negative IBPAs (backward travelling waves) tend to be stable because the relative motion of the blades reduces the incidence of the fluid flow and thus becomes more stable.

Note that the flutter response frequency from the test is considerably lower than the natural frequency of first flap (by about 10Hz). This is presumably due to a combination of disc flexibility and aeroelastic effects. The coupled aeroelastic model is more appropriate here as it can take account of both these effects by modelling the whole bladed disc assembly.

8.3.1 Structural Model

The FE model has 210 elements and 1628 nodes to form the aerofoil, and 258 elements 1994 nodes in total, including the disc sector, - the model is shown in **Fig. 8.1**. This fan blade is solid, and is modelled using 20-node brick elements.

In order to model the assembly modes of the bladed disk, a disc sector was added to the root of the blade (see **Fig. 8.1**). For this fan blade, the disc can be considered to be relatively stiff compared to the blade, so large frequency reductions due to disc flexibility are not expected. To run the cyclic symmetry model, the multi-face boundary conditions were applied to the periodically repeating faces of the disc sector,

and a fixed condition was applied to the inner circumference of the disc. In the current FE implementation, the sector must be fixed in space in order to obtain the 1 nodal diameter modes; otherwise a rigid body mode would result. A solution was then obtained for the first six blade modes, for nodal diameter patterns from 0 to 13. The results for the first three blade modes families are shown in **Tab. 8.1** for the Low speed case.

Table 8.1: FE Sector Model Natural Frequencies (Low Speed)

Case (Nodal Diameters)	1st Mode Family Frequency (Hz)	2nd Mode Family Frequency (Hz)	3rd Mode Family Frequency (Hz)
0	184.86	388.11	711.16
1	184.87	388.13	711.20
2	184.87	388.17	711.28
3	184.89	388.19	711.32
4	184.89	388.19	711.33
5	184.89	388.19	711.30
6	184.89	388.19	711.27
7	184.90	388.20	711.25
8	184.90	388.21	711.23
9	184.90	388.22	711.22
10	184.91	388.23	711.21
11	184.91	388.25	711.21
12	184.91	388.26	711.21
13	184.91	388.26	711.21

It can be seen from these results that the assumption that the disc is very stiff was reasonable, as there is practically no variation in the assembly natural frequencies. However the cyclic symmetry procedure is important for obtaining the correct assembly modal mass, which is unknown if the blade alone modes are used to create derived assembly modes. Also, with the cyclic symmetry technique, the modes change smoothly in the circumferential direction over the sector, not in step changes (of $\Delta\theta=360/N$) as occurs if the blade alone modes are expanded.

8.3.2 Interpolation onto the Aerodynamic Mesh

The interpolation program (SLink) was used to transfer the structural data, including both the interpolation of static deflections (untwist due to centrifugal loads alone), and the mass-normalised mode shapes. The two aerodynamic grids had about 2050 and 1110 points on the two blade surfaces respectively. Care was taken to ensure that a good mapping had taken place, using the facility to plot the modeshape contours on both the structural and aerodynamic grids. Again the tip leading edge point was used as the reference location to line up the two meshes, as the displacements are likely to

be largest there, and small discrepancies around the hub do not matter as the modeshapes are near zero in magnitude in that region.

8.3.3 Steady Flow Results

The steady flow aerodynamics and untwist have been examined in Chapter 6 for this fanblade along the Low Speed characteristic using a 25×81×25 mesh. As well as this mesh, another mesh has been used here for the full assembly model. Results for this 21×65×11 mesh will be briefly presented here. This mesh was selected after some testing of various mesh densities to find the best compromise between modelling the steady flow aerodynamics adequately (primarily determined by shock position) and the memory required to include 26 blade passages. Given unlimited computational power, this would not be necessary, however this resource, although increasing rapidly with time, is not likely to become 'unlimited' as there is a tendency to model larger and larger problems as the resources improve.

The aerodynamic analysis on the 21×65×11 mesh was focussed on the near-stall condition, as this is where this blade was known to flutter. Three new points on the operating characteristic, including the effect of untwist, were computed. The overall performance results were as follows:

Table 8.2: Performance Along Low Speed Characteristic (21×65×11 mesh)

Case	Total Pressure Ratio (rel. to PE)	Inlet Mass Flow (rel. to PE)	Tip Untwist Angle (deg)
A	1.0155	0.8564	3.043
B	1.0183	0.8987	2.979
C	1.0176	0.9164	2.932

Calculations at these points can be compared with the results from the finer mesh given in **Tab. 6.2**. The fan performance characteristics for the new points are plotted with the finer mesh results in **Fig.8.2 a&b**, and the Mach no. contours at 70% height for case A, B & C are plotted in Figs. **8.3 b-d**. The surface static pressure distribution at 70% height for cases A, B & C are plotted in **Fig. 8.4a**, and a comparison of the coarse & fine pressure distributions is shown in **Fig. 8.4b**. It can be seen that the comparison is quite reasonable, considering that the operating condition is close to stall.

8.3.4 Single Blade Passage Uncoupled Flutter Analysis

The first flutter analysis of this fan was using the single-passage uncoupled method with shape correction as described as 'Method 2' in Chapter 7. This is in order to

provide a benchmark against which to compare the multi-passage results. This was done using the 25×81×25 mesh at points '1' and '2' on the fine mesh computed characteristic (see **Tab. 6.2 & 8.6**). Also an extra point, '0' has been used in this case, which lies in between 1 & 2 (see **Tab 8.6** and **Fig. 8.2**). The results are as shown in **Tables 8.3-5** below:

Table 8.3 Uncoupled Flutter Stability Low Speed, point '1'

Nodal Diameters	IBPA (deg)	Stability (logdec)	Frequency Shift (Hz) ω_n=186.0 Hz
0	0.00	0.0002	-1.46
1	13.85	-0.0033	-1.03
2	27.69	0.0023	-0.91

Table 8.4 Uncoupled Flutter Stability Low Speed, point '0'

Nodal Diameters	IBPA (deg)	Stability (logdec)	Frequency Shift (Hz) ω_n=186.0 Hz
0	0.00	0.0163	-1.08
1	13.85	0.0017	-1.35
2	27.69	0.0123	-1.07
3	41.45	0.0344	-0.80
6	83.08	0.1343	-0.02
13	180.00	0.2360	-2.97
-6 (20)	276.92	0.2700	-3.64

Table 8.5 Uncoupled Flutter Stability Low Speed, point '2'

Nodal Diameters	IBPA (deg)	Stability (logdec)	Frequency Shift (Hz) ω_n=186.0 Hz
0	0.00	0.0204	-1.58
1	13.85	0.0101	-1.79
2	27.69	0.0231	-1.32

These results are plotted in **Figs. 8.5** for stability (logdec) and **Fig 8.6** for frequency shift. It can be seen that the least stable area is around 1ND. The aerodynamic damping (logdec) varies with IBPA in a broadly sinusoidal fashion, as was found in the previous chapter. Also the trend along the characteristic is correctly predicted, in that at 0, 1 & 2 ND modes the fan is predicted to be less stable as stall is approached.

The trend in the predicted frequency shift is not so clear. However, as observed for the Rotor 67 fanblade, the shift is larger the more stable the case - thus here the shift is largest around 180° IBPA (2% of natural frequency). The overall trend also appears to be sinusoidal, however all the values are relatively small in this case - which supports the use of the modal approach for the structure. In cases with larger changes in

frequency the modeshapes also may change, which would invalidate the use of the assumed modes method.

8.3.5 Single Passage Coupled Flutter Analysis

The flutter stability along the Low Speed characteristic was investigated next using the coupled method for 0° IBPA only (single blade passage analysis). This IBPA was chosen as non-zero values of IBPA require a multi-passage approach, and these will be investigated using a full assembly model in the next section for a more limited number of points on the characteristic. The following studies were done using this approach:

- Flutter along Low Speed characteristic (single mode - 1F, zero IBPA only)
- Effect of higher modes (modes 1-5, zero IBPA only)
- Effect of starting conditions (zero IBPA only)

Flutter Stability along Characteristic

The flutter stability of the points on the Low Speed characteristic, as calculated in Chapter 6 was investigated using the same 25×81×25 mesh. An integrated aeroelastic computation for zero IBPA was started from a small modal velocity in mode 1 (1F). The results are tabulated below:

Table 8.6: Coupled Flutter Stability, Low Speed, IBPA=0°

Case	Total Pressure Ratio (rel.)	Inlet Mass Flow (rel.)	Tip Untwist Angle (deg)	Stability (logdec)	Response Frequency (Hz)
1 (NS)	1.016	0.840	3.07	-0.0148	185.1
0	1.016	0.868	2.98	0.0014	184.6
2	1.016	0.895	3.00	0.0136	184.2
3	1.013	0.924	2.95	0.0269	183.9
5	1.004	0.981	2.74	0.0575	183.2
7 (PE)	0.997	1.003	2.55	0.0652	183.0
20 (MF)	0.930	1.023	2.20	0.0557	183.6

A typical time history for the nearly stable case ('0') is plotted in **Fig. 8.7 a&b**. The variation of stability (logdec) and response frequency shift are plotted in **Figs. 8.8 & 8.9** respectively. These show that the aeroelastic response frequency varies quite markedly with operating condition, by about 2 Hz (1% of natural frequency) from the working line to flutter. Around the peak efficiency case '7', which is also the most stable case, the stability does not vary much. Also the frequency shift is largest here, for these most stable cases. However, from cases '5' onwards up the characteristic, the

stability appears to decrease almost linearly, until the last point computed is marginally unstable. This point corresponds to the highest back pressure that could sustain a stable steady untwist position. If the back pressure was raised any higher then the flow would 'stall' before equilibrium could be reached (i.e. the numerical model would break down). At these conditions the current fluid model (AV3D) is probably at the limits of its applicability, as the thin-layer viscous model is not designed for use with grossly stalled flow.

The fact that the point on the characteristic nearest stall yielded an unstable result does not necessarily indicate that this is the flutter mode. This is because only zero IBPA was investigated here - so it is quite likely that in the real case that other nodal diameters would flutter first - as was indicated in the uncoupled study in the previous section. However this study may be indicative of the general stability behaviour along the part-speed characteristic, with other modes having less or more stable stability lines. The mode that has the stability line cutting the axis of neutral stability (zero logdec) first will then be the flutter mode.

Effect of Starting Conditions & Higher Modes

For the zero IBPA cases it was possible to start the flutter analysis either by starting directly from steady flow about the untwisted blade, or by forcing the motion in that mode (1F) for 10 periods first, as is done for uncoupled analyses. Both of these options were tried, and it was found that virtually no difference resulted in the predicted frequency and logdec of response. However 0° IBPA may be a special case in that it is near neutral stability, so the effect of starting conditions may be less pronounced.

The possible effect of higher modes is of potential interest, in order to assess whether the assumption that only mode 1 (1F) is of importance in the flutter stability of this blade. To this end, a case was run with the first 5 modes kept in the aeroelastic analysis still at zero IBPA. Then the motion was begun with an impulse to mode 3 (1st torsion); the resulting motion of the first 3 modes in modal co-ordinates can be seen in **Fig. 8.10**. It can be seen that mode 3 (1st torsion at 704 Hz) is damped by the fluid and rapidly transfers its energy via the fluid into mode 1. Mode 1 gradually increases its amplitude, and its logdec was found to be almost exactly the same as for the case with mode 1 alone. It can be concluded that the higher modes do not play a significant role in flutter of this fan blade, although they are important in the calculation of untwist.

8.3.6 Multiple Blade Passage Coupled Analysis

The most complete analysis was performed next. A full annulus model was used, to determine the effect of all the assembly modes. As explained above, this model requires a large amount of memory and CPU time, so to make these calculations feasible a slightly coarser mesh was used - the whole annulus model mesh is shown in **Fig. 8.11**. The steady flow for this mesh was introduced in **Section 8.3.3**, and the points on the characteristic near the flutter boundary have been labelled A, B & C (see **Table 8.2**). These points must be related to the points computed on the finer mesh labelled '1', '2' etc. that have so far been analyses (see **Table 8.6**).

One of the most difficult issues with this model is how to start the flutter calculations. There are 26 assembly modes in this case (and this is only because we are restricting this study to the 1st flap mode) so there are many ways of starting the motion. One possibility would be to give one blade an impulse in the physical domain and convert this to initial velocities of the modes in the modal domain. However, it was found that this took too long for the pattern of motion to spread round the annulus due to the time-step limitations. Alternatively, one particular nodal diameter mode could be given an initial motion, but again this may take a while for the motion to settle into an identifiable pattern. It was found that the best way to identify the time-history resulting from an initial disturbance, was to give all the assembly modes the same initial motion (usually a small velocity, but a displacement could equally be used).

The energy approach is used to determine the overall stability. This is particularly important for the assembly model as it may no longer be easy to establish the stability from the time histories of motion either in the real domain or in the modal domain. This is due to the fact that the assembly modes are free to interact with one another through the fluid coupling. Thus a particular mode may appear to be transiently unstable, but it may be growing by taking energy from another mode, while the overall situation is stable.

Time histories for all the modes in the calculation for cases A, B & C are shown in **Figs. 8.12a, b & c**. Also, the energy plot is shown for Case A in **Fig. 8.13**, and the time histories of selected modes in Case B as shown in **Figs. 8.14 a-d**. It can be seen that Case A is considerably unstable - to the extent that after growing quite rapidly, the size of the displacements became such that the fluid code 'blew up'. The most rapidly growing modes were in the range 2-6 nodal diameters in this case. Case B is marginally unstable, with the least stable mode being 3 nodal diameters. In Case C, all the modes are stable, however the least stable modes are still in the low positive IBPA

range. These results are more clearly seen in **Figs. 8.15 & 8.16** where stability (logdec) and frequency shift are plotted for cases B & C. The actual values are determined by the initial response over the first few periods of motion. It was not really possible to process the data accurately for case A, but it is clear that this case was more unstable that the other two.

These results are in line with the shape correction method results on the finer grid (see **Figs. 8.5 & 8.6**). The multi-passage results seem to be showing the least stable nodal diameter in the range 2-4, with 3 most likely (around +40° IBPA), whereas the shape correction method gave 1 nodal diameter. Both results are also reasonably consistent with the available experimental data, which suggests 1 or 2 nodal diameters as the flutter mode.

Also the predicted position of the flutter boundary (between points B & C on the compressor map) would seem to be encouraging. This flutter point occurs before the tested point as one moves up the characteristic, however this is to be expected as there was no structural damping in the aeroelastic model, and also the model is perfectly tuned. Any mistuning in the real case (and there must have been some) would tend to delay the onset of flutter.

As described before, these whole annulus calculations were extremely CPU and memory intensive. The in core memory required was about 115 Mbytes, and each run took between 2-3 weeks of CPU time on an IBM RS6000-360 workstation (depending on how the flutter behaviour developed). These times are equivalent to about 40 hours CPU on a single Cray Y-MP processor. It should be noted, however, that these multi-passage calculations are ideal candidates for parallel computers, as the computational domain is already conveniently split into sections, which may be spread over the processors. The communication between the passages is only needed at the end of each time-step, which should be ideal for parallel efficiency. Thus, these types of calculation should be speeded up by orders of magnitude on parallel machines that are now becoming available.

8.4. CONCLUDING REMARKS

The flutter code has been shown to be successful in predicting some of the most important trends in flutter analysis, namely the variation in stability along the operating characteristic, i.e. the blade becoming less stable as the part-speed flutter boundary was approached. This raises the question of whether the part-speed flutter

boundary, usually known as the stall-flutter boundary, is a purely viscous mechanism or whether it can indeed be predicted by an inviscid mechanism (as seems to be the case in these predictions). The relative performance of viscous and inviscid methods needs to be evaluated further in order to understand the precise mechanisms of flutter.

In the case of the single passage analysis using AV3D a marked variation of stability with IBPA was demonstrated, although the accuracy of this method for non-zero IBPAs is somewhat unknown. The single passage version of the code needs to be tested against the multi-passage version of AV3D, which is now available, in order to determine the strengths and weaknesses of each method.

For the multi-passage analysis, the trend for relative stability of the different assembly modes was marked, the trend being broadly in line with the equivalent single-passage 'shape correction' results. Unfortunately the two grids used were not identical due to the huge computational requirement of the multi-passage calculations. In this case it would seem that the single passage results have given quite good results, however they have the major drawback of having to do many separate calculations. Thus not all the IBPAs were investigated, which would be dangerous to do in the general case - as one might miss the flutter regime entirely. The problem of many IBPAs to investigate becomes particularly difficult if there are more blades in the bladerow (say 50-100) which will lead to correspondingly more modes to investigate.

The analysis of this fan blade has shown that the modelling of the interactions between the different structural modes and the fluid may be vital to the correct prediction of flutter, in the general case. Although these interactions were not that strong in the case presented, for cases where flutter occurs by the fluid coupling together different blade modes the classical methods may miss the flutter regime entirely. Thus, the multi-passage approach will ultimately be preferred to the single passage flutter analysis. Also, the mechanism that determines the least stable IBPA is poorly understood in a wide range of aeroelastic phenomena that are not even touched on here, and this will be the subject of further research.

8.4.1 Flutter Prediction Methods

During this study some of the advantages and disadvantages of the two different approaches became clearer:

Advantages of Single Passage Analysis

- Less CPU time and core memory per case, so it is possible to use a much finer mesh;

- Need only investigate a particular mode, so easier to compare 2 designs for stability in that mode.

Disadvantages of Single Passage Analysis

- Response frequency of aeroelastic mode is strictly speaking, unknown, so an approximation must be made to determine the time delay across the boundaries;
- No interaction between modes through fluid coupling is possible as only one structural mode is used at a time - although the method of Gerolymos (1992b) addresses both these problems;
- The blade motion must be forced for a number of cycles first (usually 10-15 cycles) to establish the phase lag in the fluid flow;
- Overall CPU time may be more than that required for multi-passage analysis if a full stability analysis involving all IBPAs is required.

8.4.2 Flutter Behaviour of this Fanblade

From the studies described here, the following points were observed about the flutter behaviour of this fan blade:

1) Prediction of the untwist at off-design conditions along with the correct fluid flow is vital to the success of flutter analyses.
2) Only the first flap mode is thought to be important in the flutter of fan blade, as the higher modes (2-5) were very stable (at least at zero IBPA).
3) The maximum aeroelastic response frequency is about 1% lower than the blade natural frequency (no disc flexibility considered), and it varies slightly with IBPA and more strongly with fluid operating condition. The measured aeroelastic frequency was about 8% lower than the natural frequency possibly due to disc & root flexibility, and damping.
4) Stability in the first flap mode varies markedly with both IBPA and operating point.
5) Stability along the Low Speed characteristic is shown to decrease and ultimately become unstable as the tested flutter boundary is approached.
6) The least stable assembly mode is predicted to be 3 ND by the multi-passage approach and 1 ND by the single-passage approach with fixed IBPA for this Low Speed case. This compares to the experimental evidence which seems to indicate 1 or 2 ND with some possibility of some errors in this measurement.
7) In the multi-passage analysis, the coupling between the assembly modes via the fluid is found to be strong. This feature implies a non-linear behaviour.

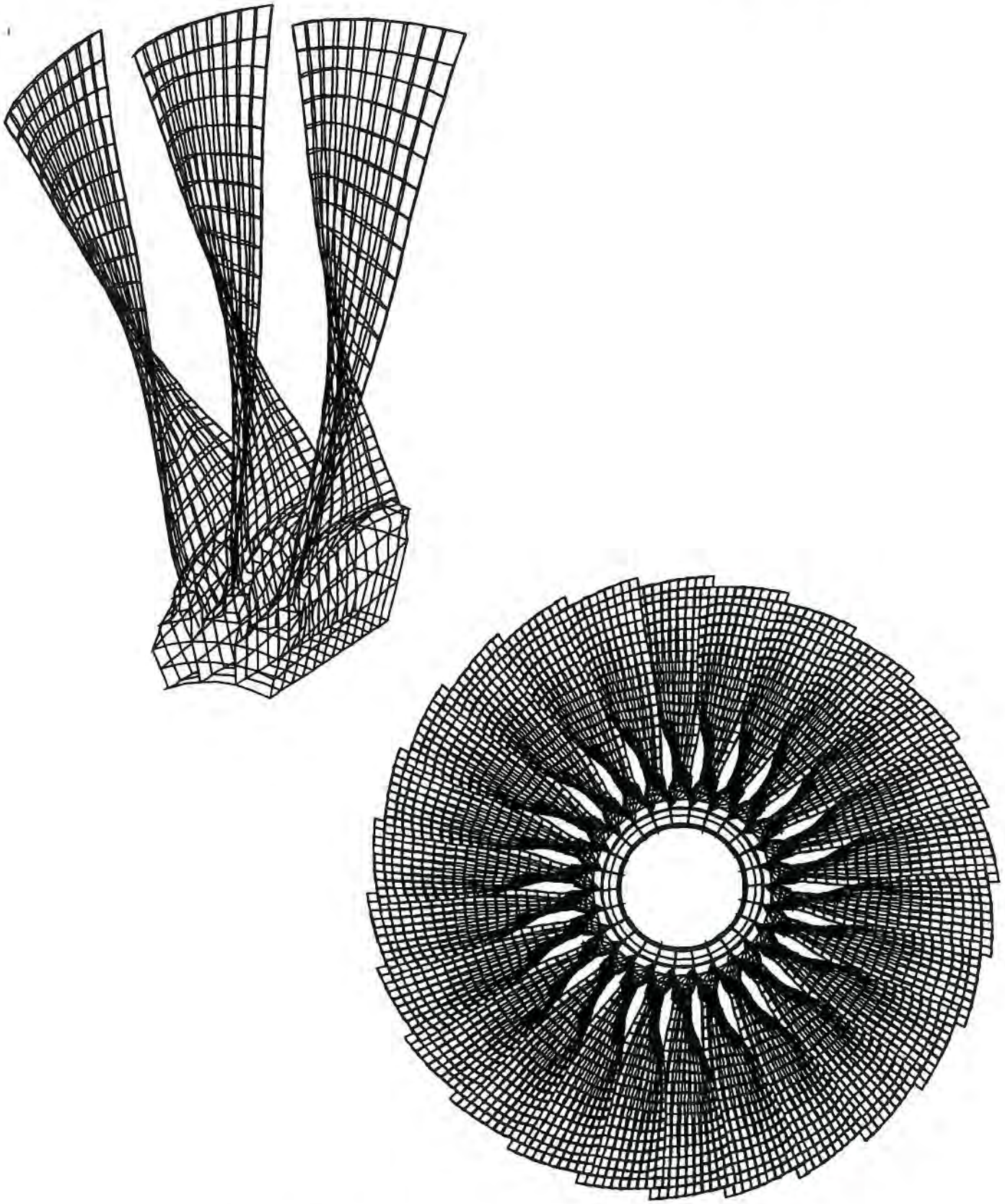

Fig. 8.1 FE Cyclic Symmetry Model Mesh

a) Rotor Pressure Ratio

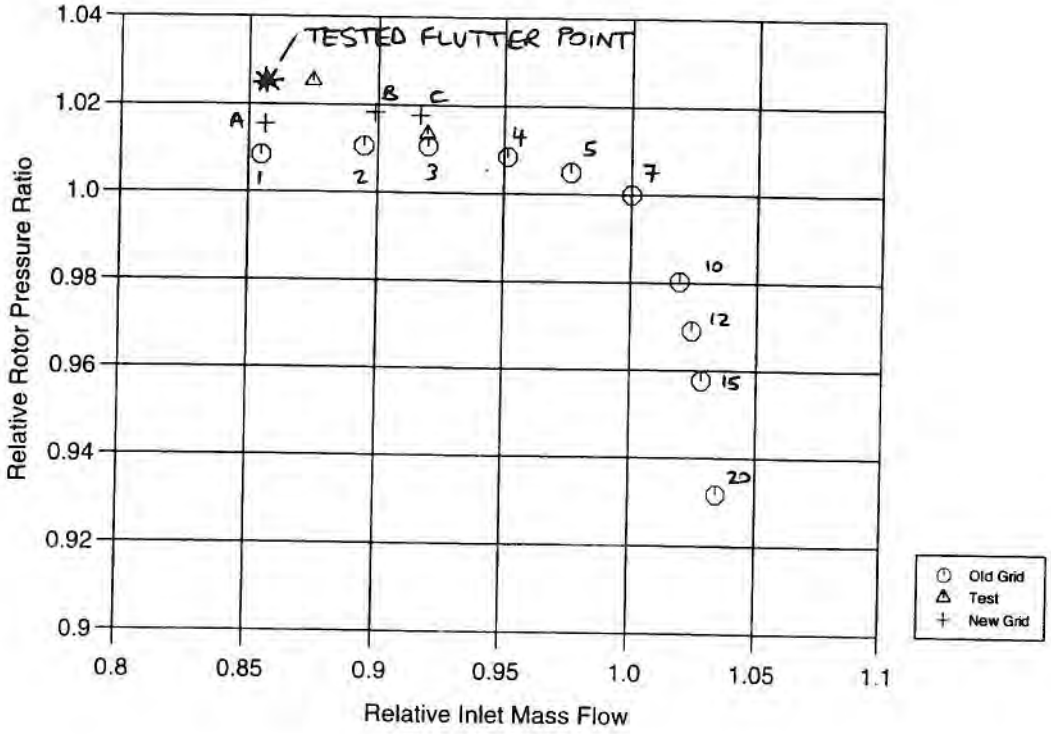

b) Tip Stagger

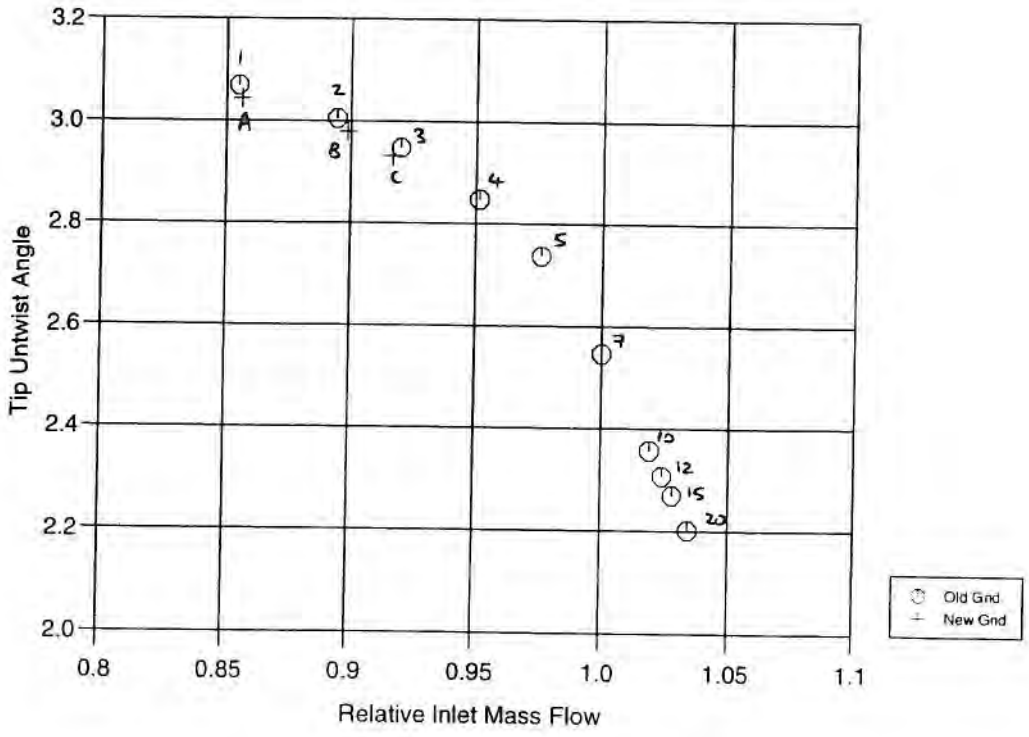

Fig. 8.2 Fan Performance Characteristics (Low Speed, new points)

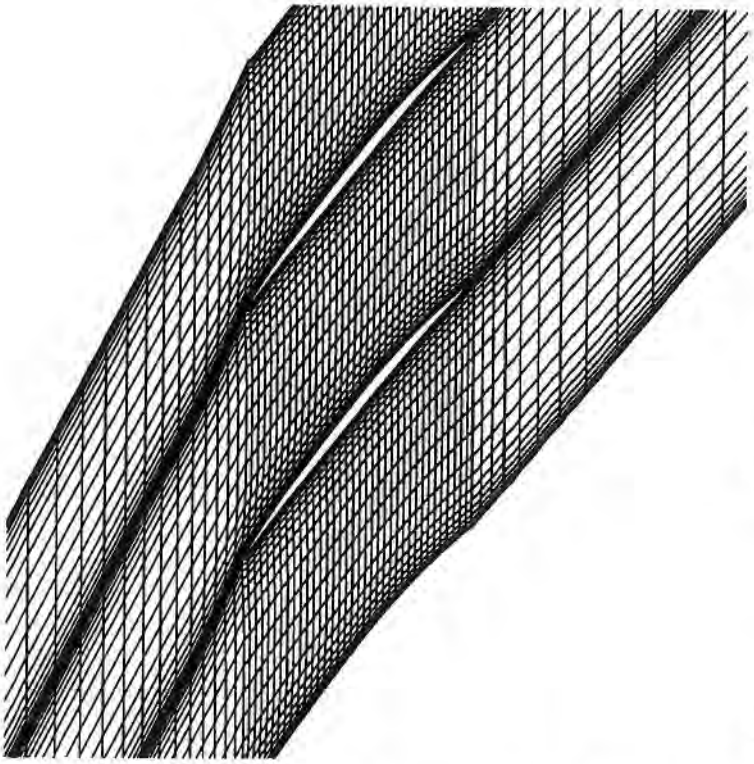

Fig. 8.3a Blade-to-blade Mesh

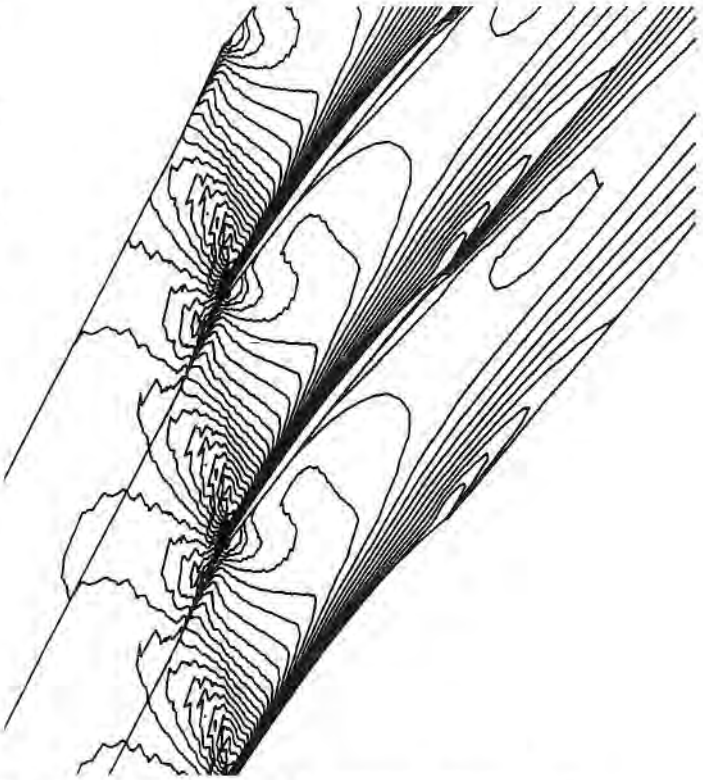

Fig. 8.3b Mach No. Contours (Point 'A')

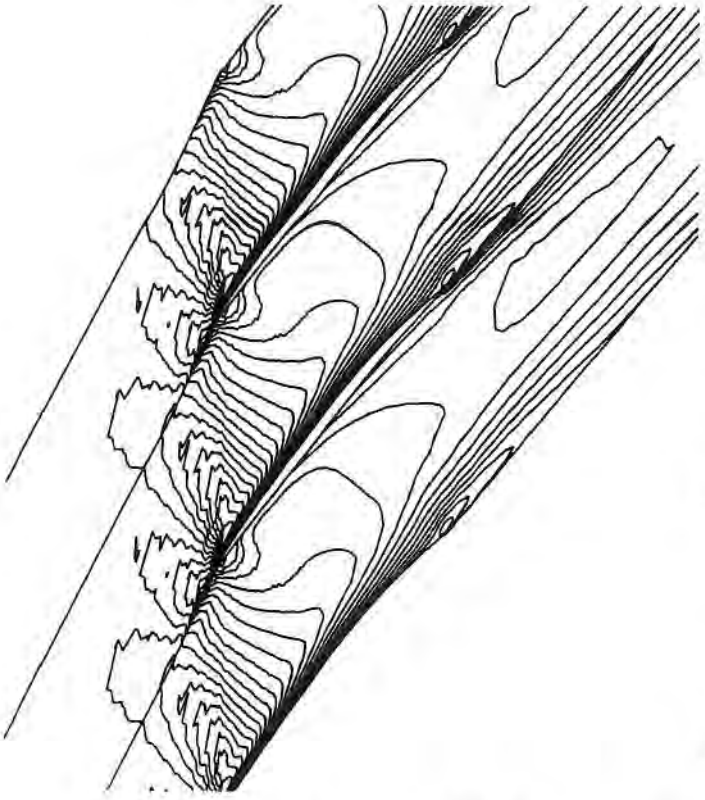

Fig. 8.3c Mach No. Cont. (Point 'B')

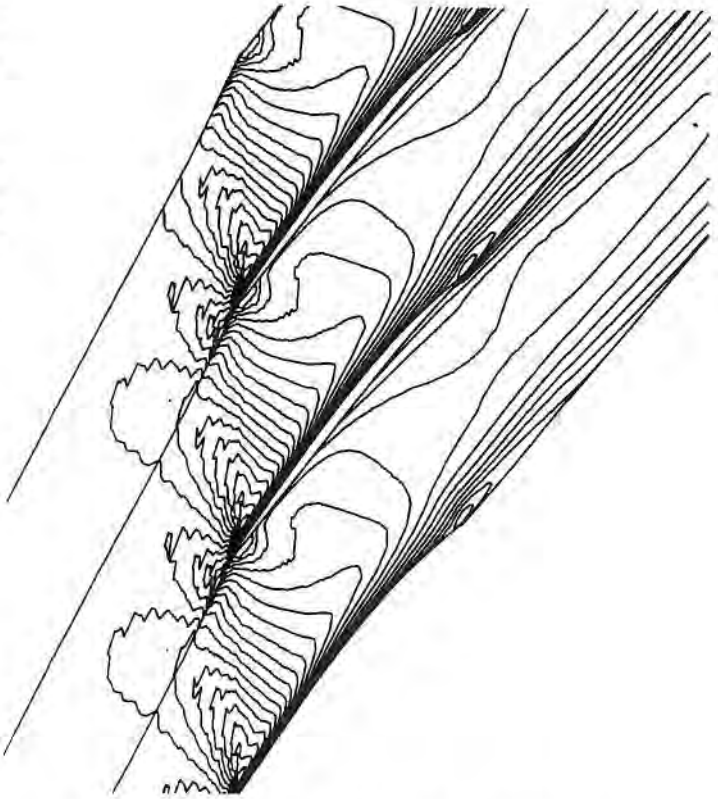

Fig. 8.3d Mach No. Cont. (Point 'C')

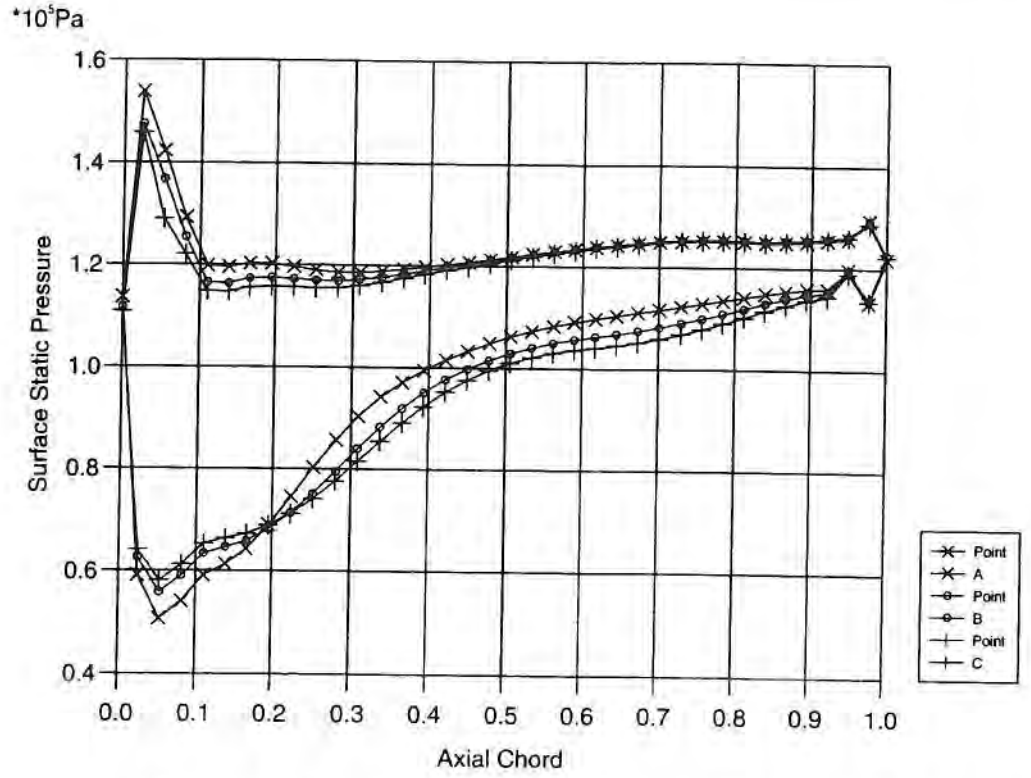

Fig. 8.4a Surface Static Pressure 70% Height (Points A, B & C)

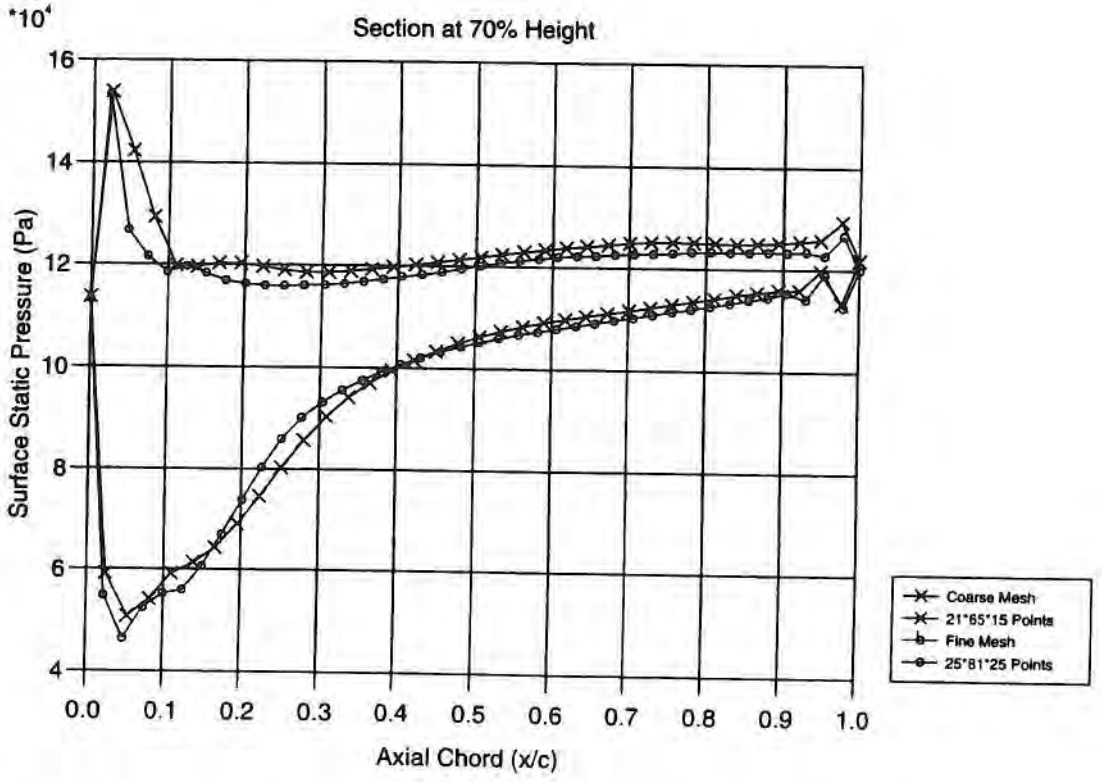

Fig. 8.4b Surface Static Pressure 70% Height (Coarse/Fine Grids)

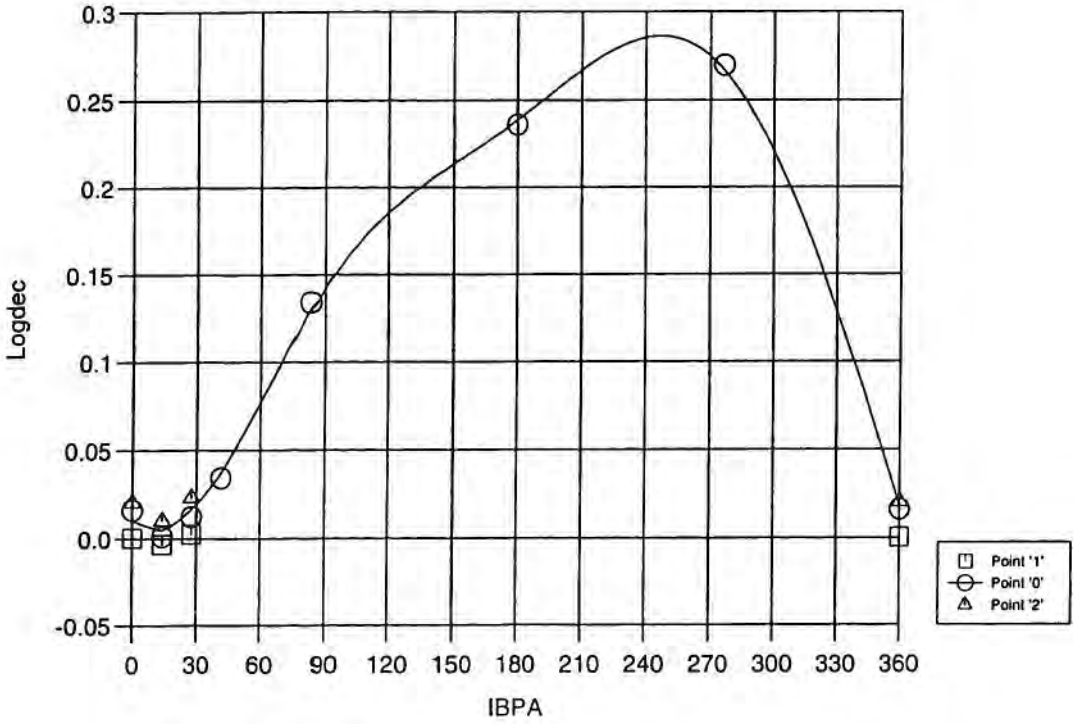

Fig. 8.5 Flutter Stability (logdec) - Points 1, 0 & 2)

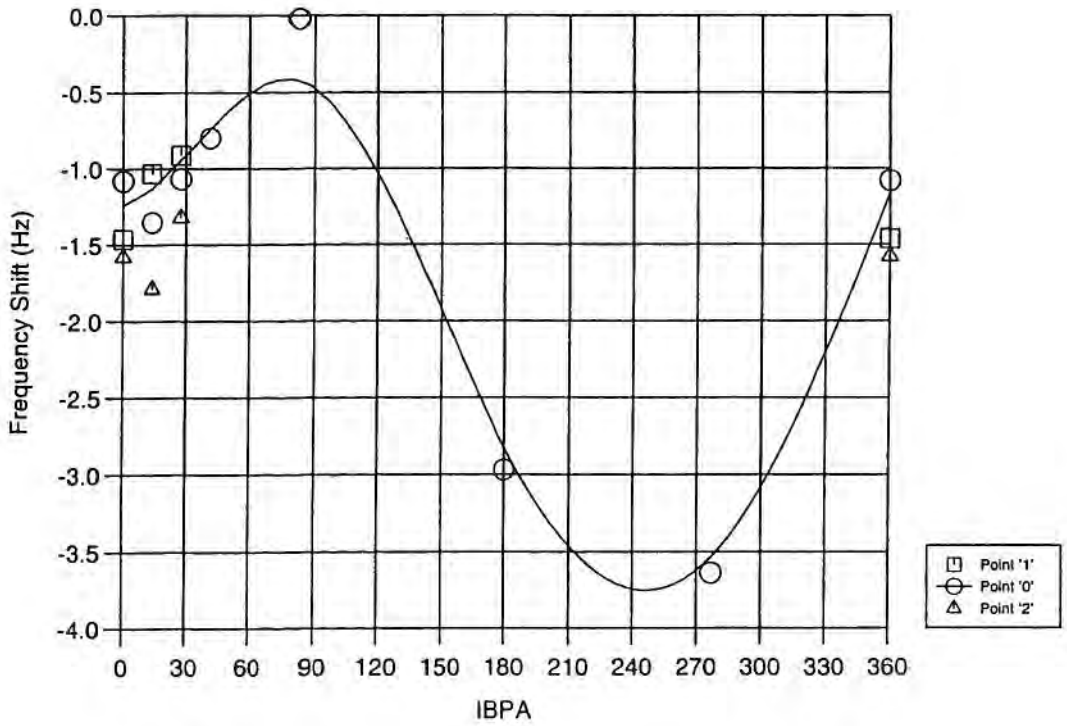

Fig. 8.6 Flutter Frequency Shift - Points 1, 0 & 2)

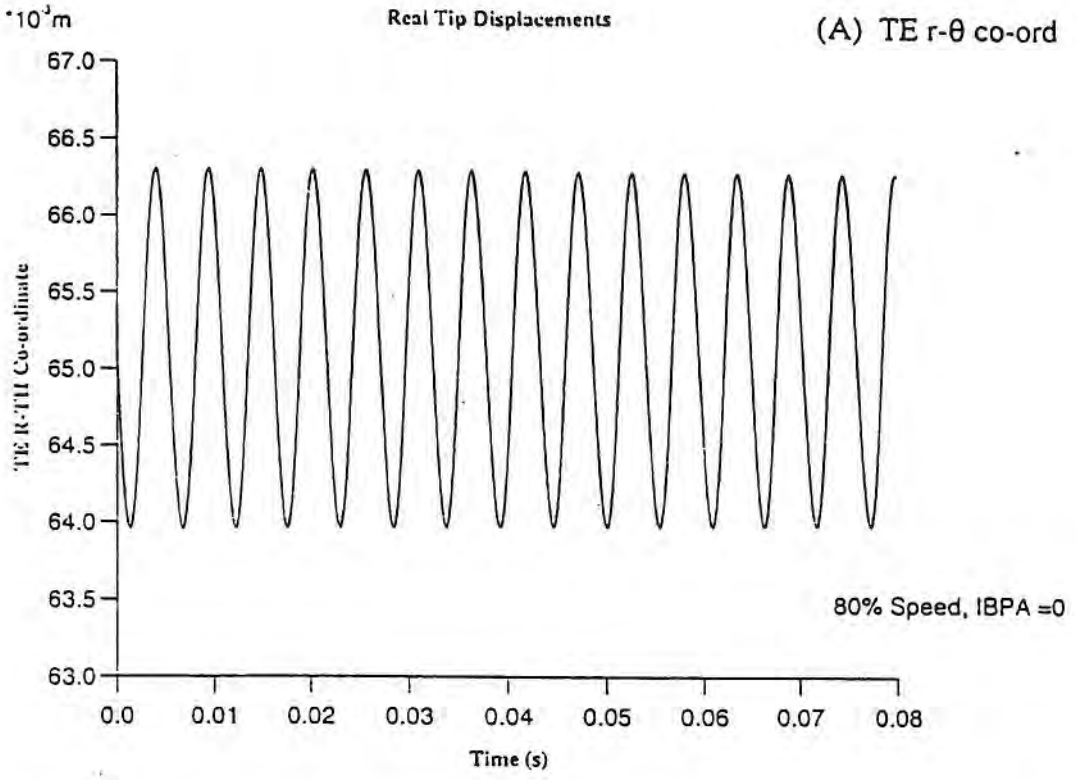

Fig. 8.7a Flutter Time History (TE Co-ord) - Low Speed, 0 IBPA, Point '0'

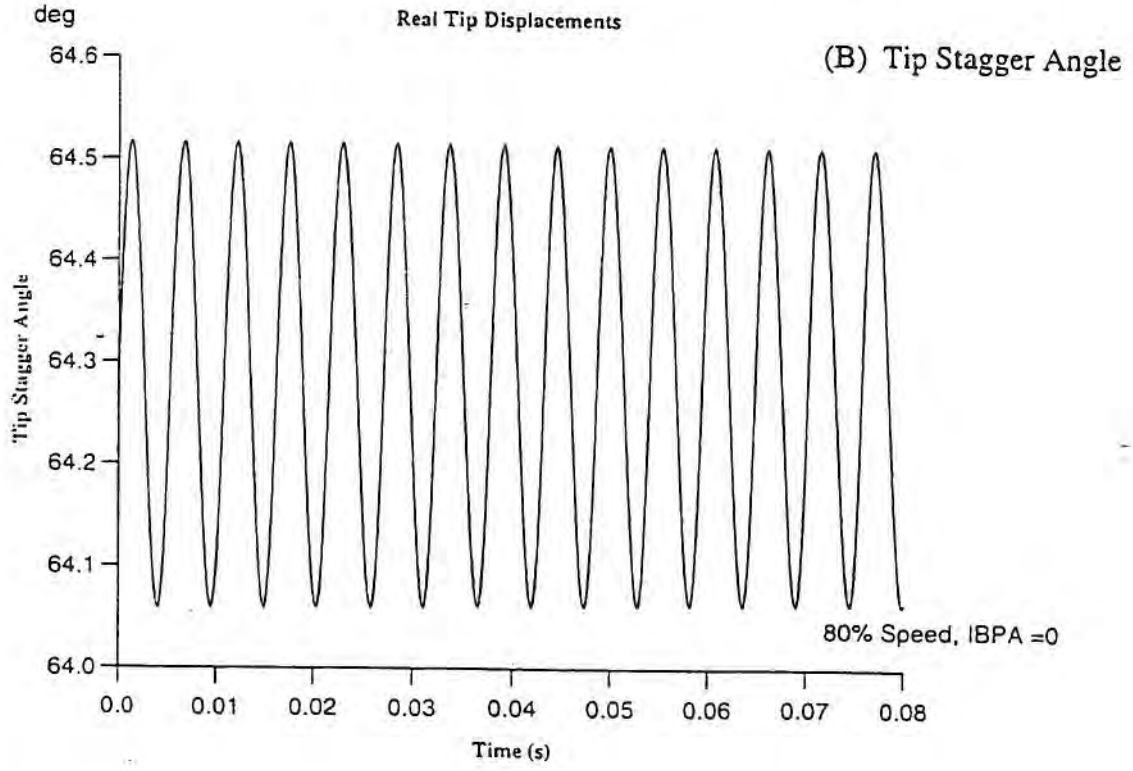

Fig. 8.7b Flutter Time History (Tip Stagger) - Low Speed, 0 IBPA, Point '0'

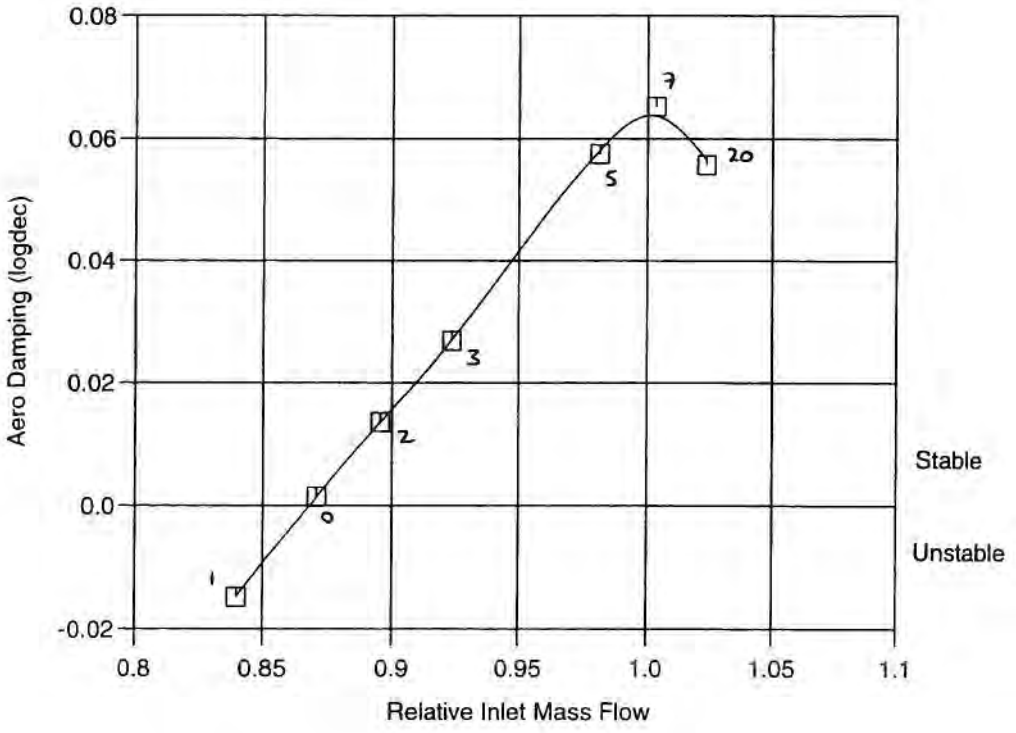

Fig. 8.8 Flutter Stability (logdec) - Along Low Speed Characteristic

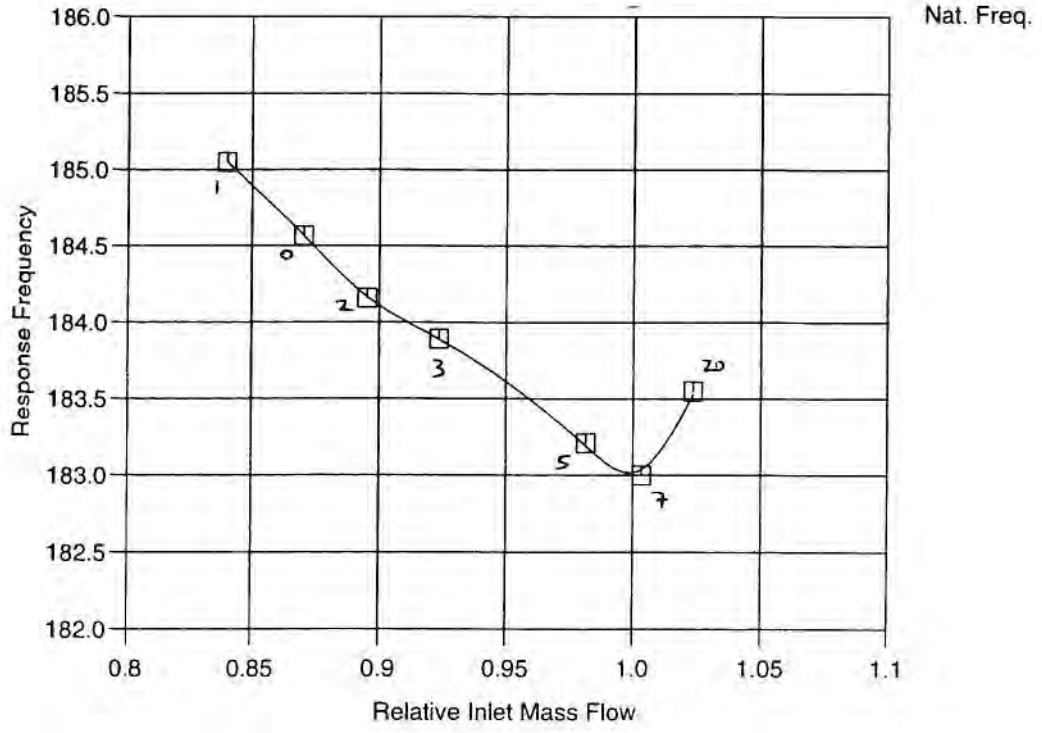

Fig. 8.9 Flutter Frequency Shift - Low Speed along Characteristic

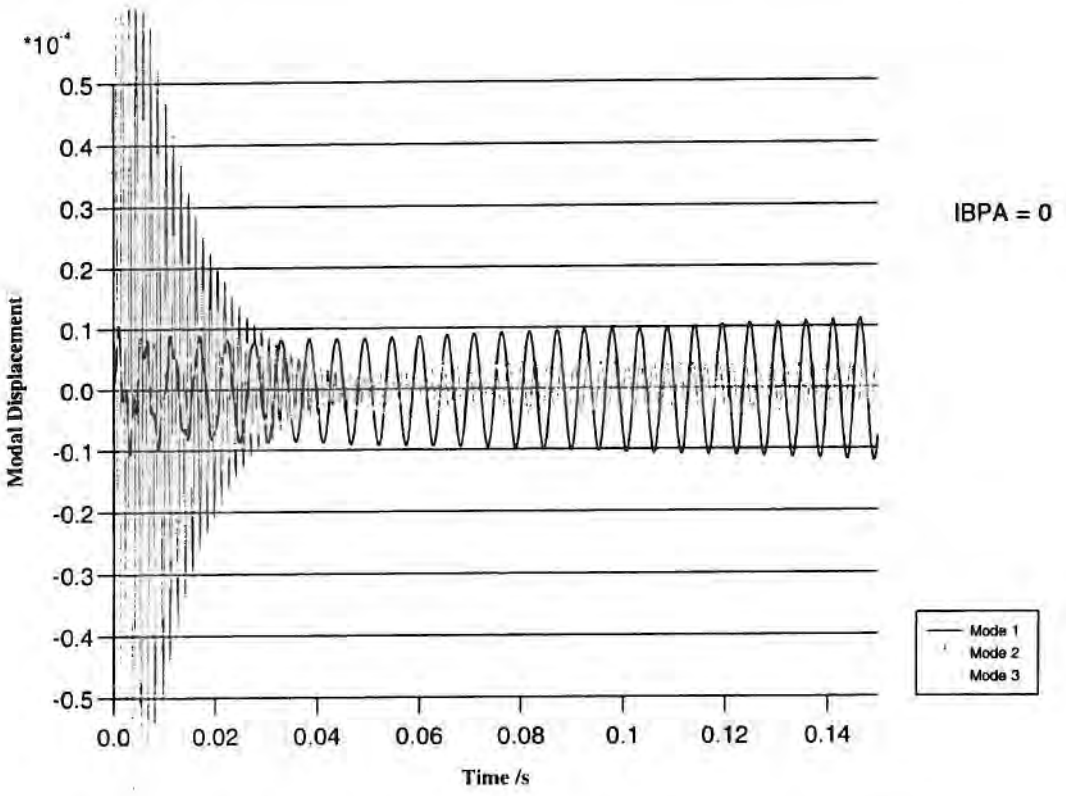

Fig. 8.10 Flutter Time History - 5 Modes, Low Speed, 0 IBPA

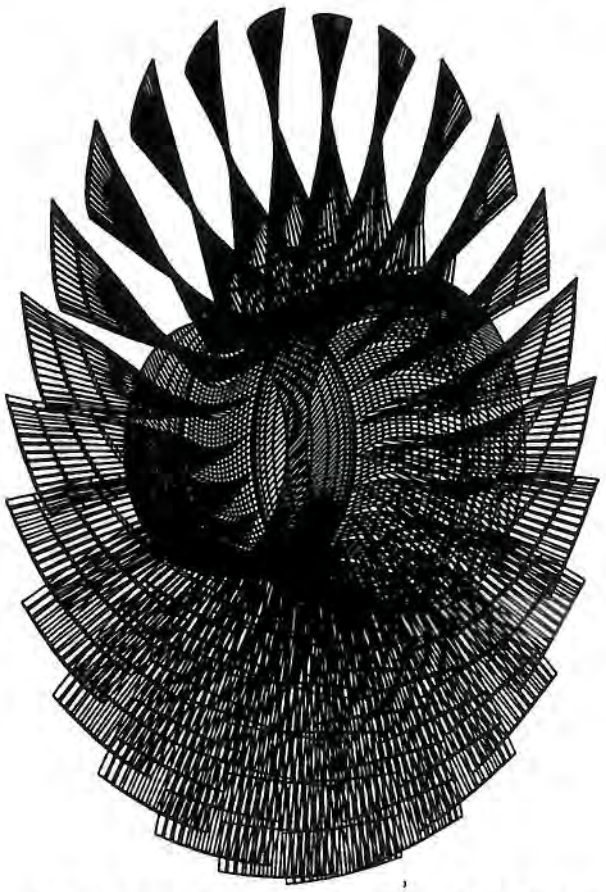

Fig. 8.11 AV3D Multiple Blade Passage Mesh (whole annulus)

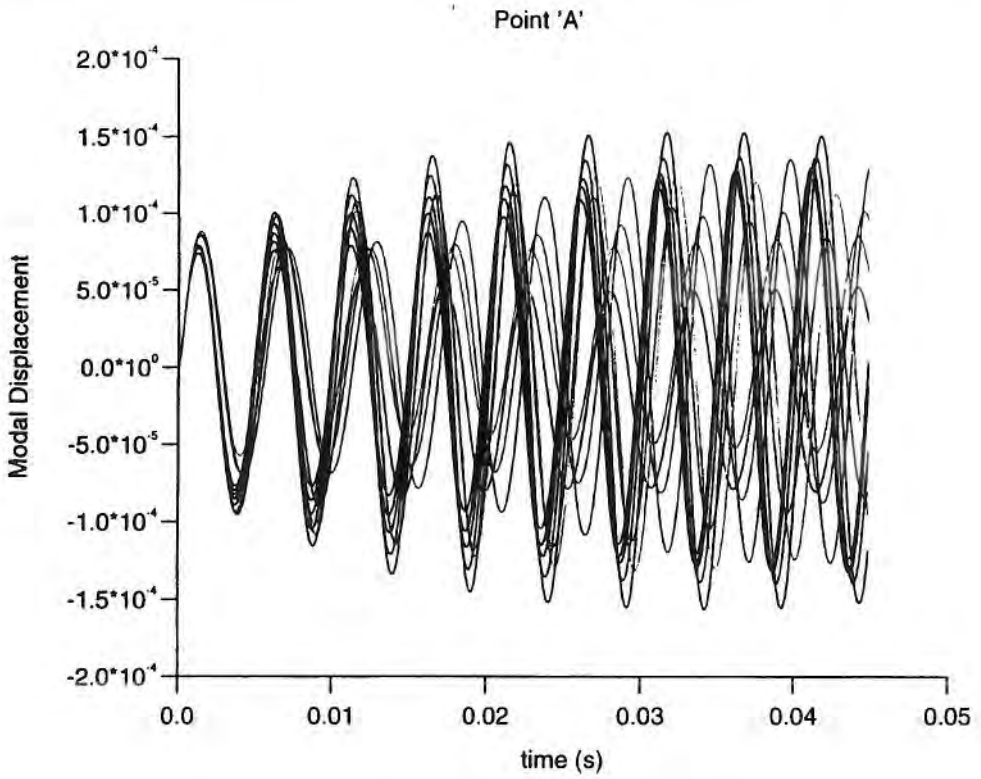

Fig. 8.12a Multi-passage Flutter Time History, Point 'A'

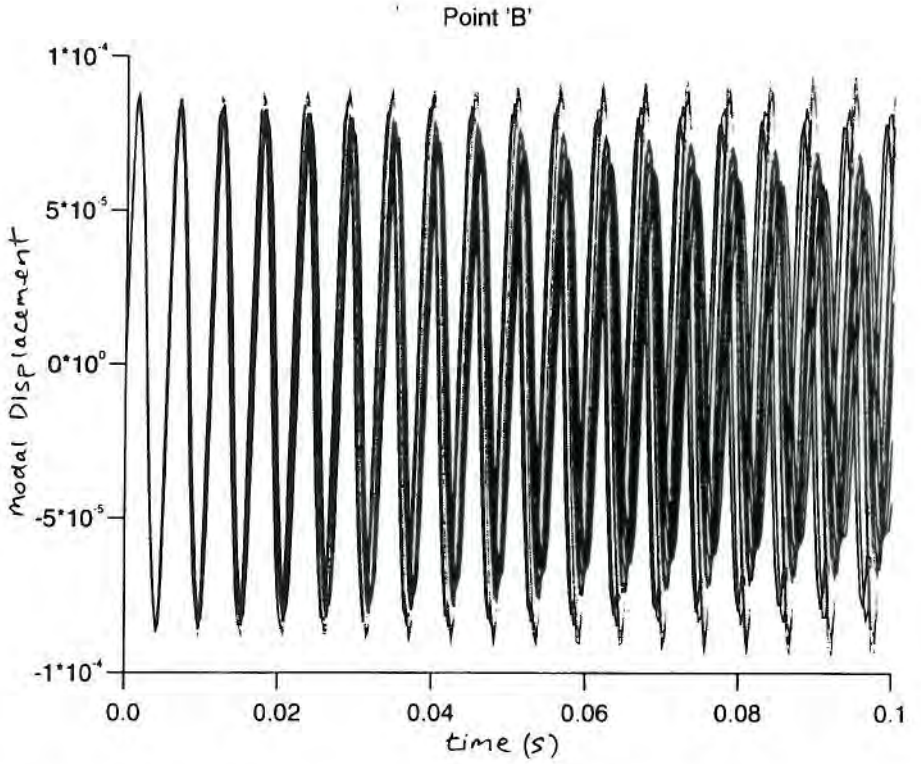

Fig. 8.12b Multi-passage Flutter Time History, Point 'B'

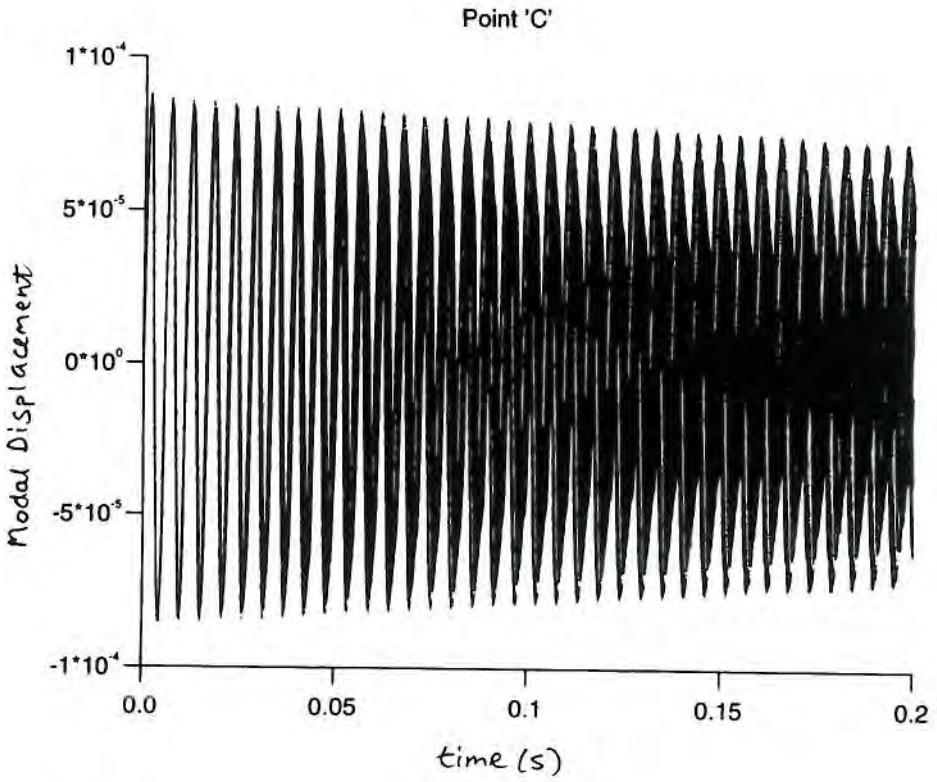

Fig. 8.12c Multi-passage Flutter Time History, Point 'C'

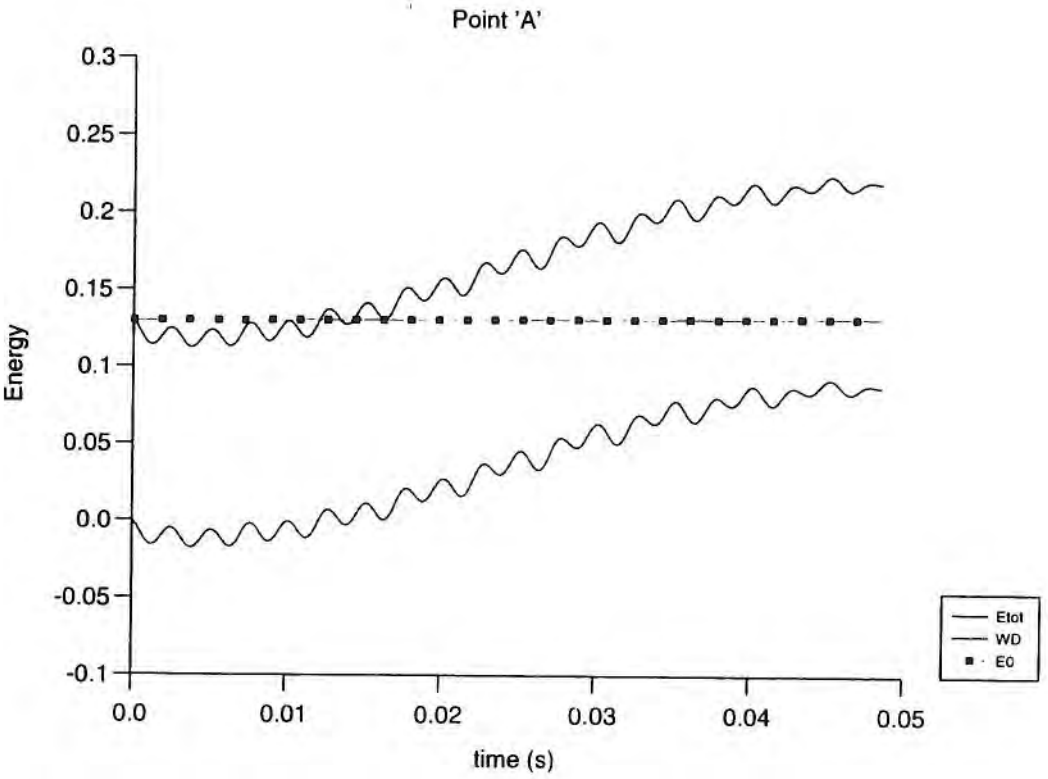

Fig. 8.13 Multi-passage Flutter Energy History, Point 'A'

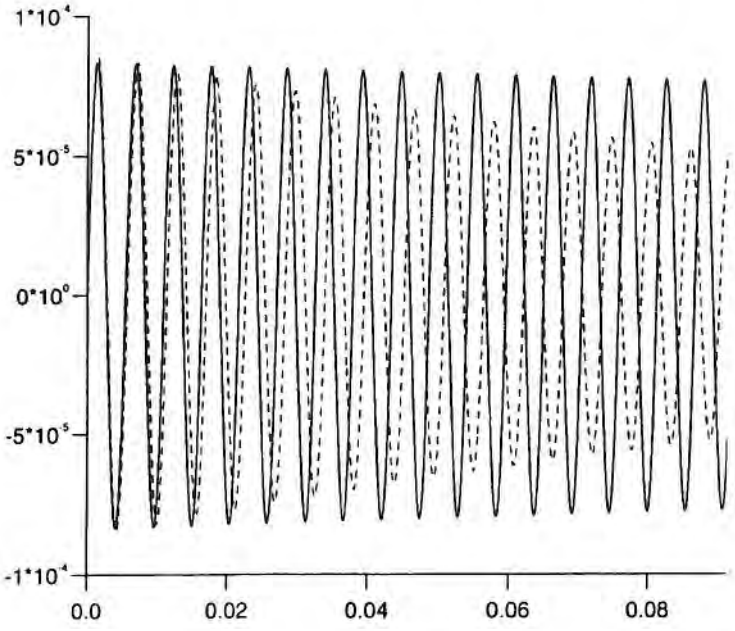

a) 0 & 13 Nodal Diameters

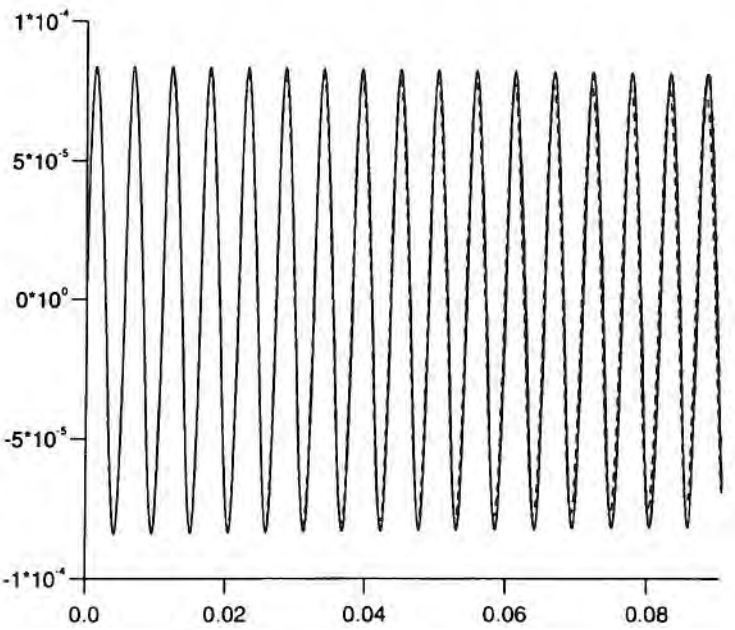

b) 1 & -1 Nodal Diameters

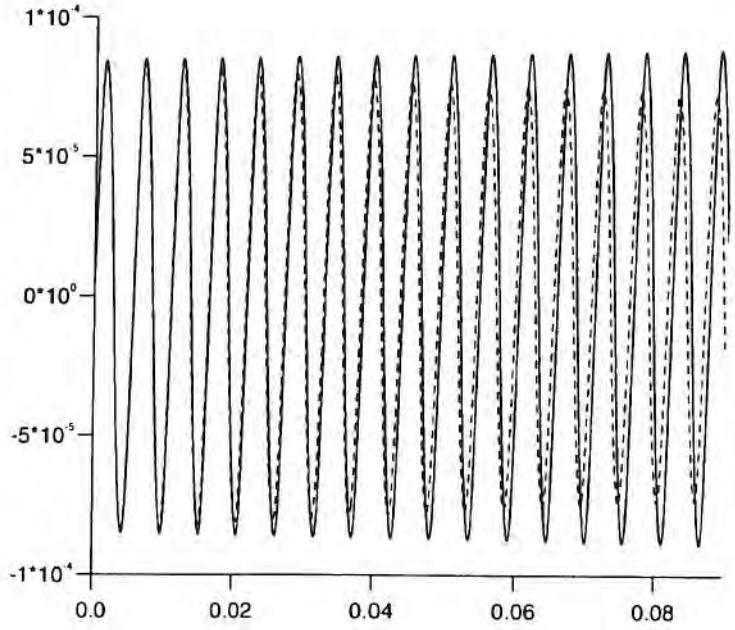

c) 2 & -2 Nodal Diameters

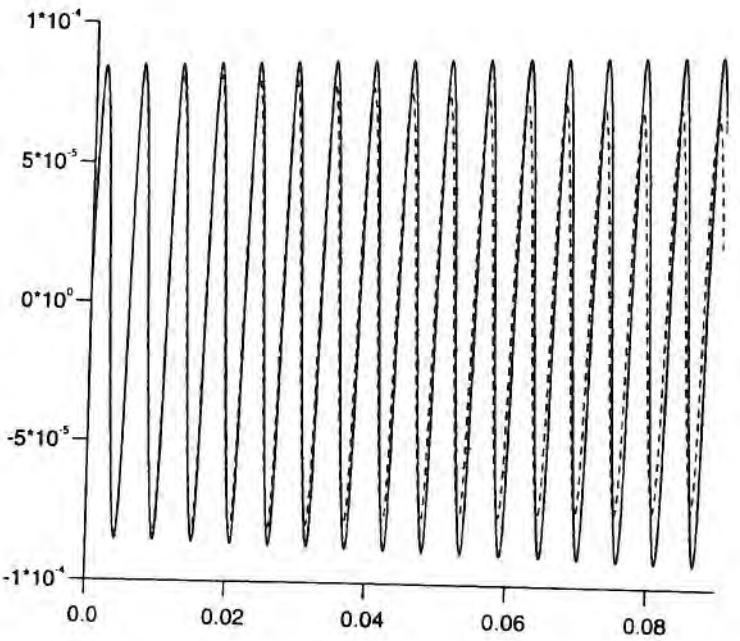

a) 3 & -3 Nodal Diameters

Fig. 8.14 Multi-passage Flutter Displacement History, Point 'B'

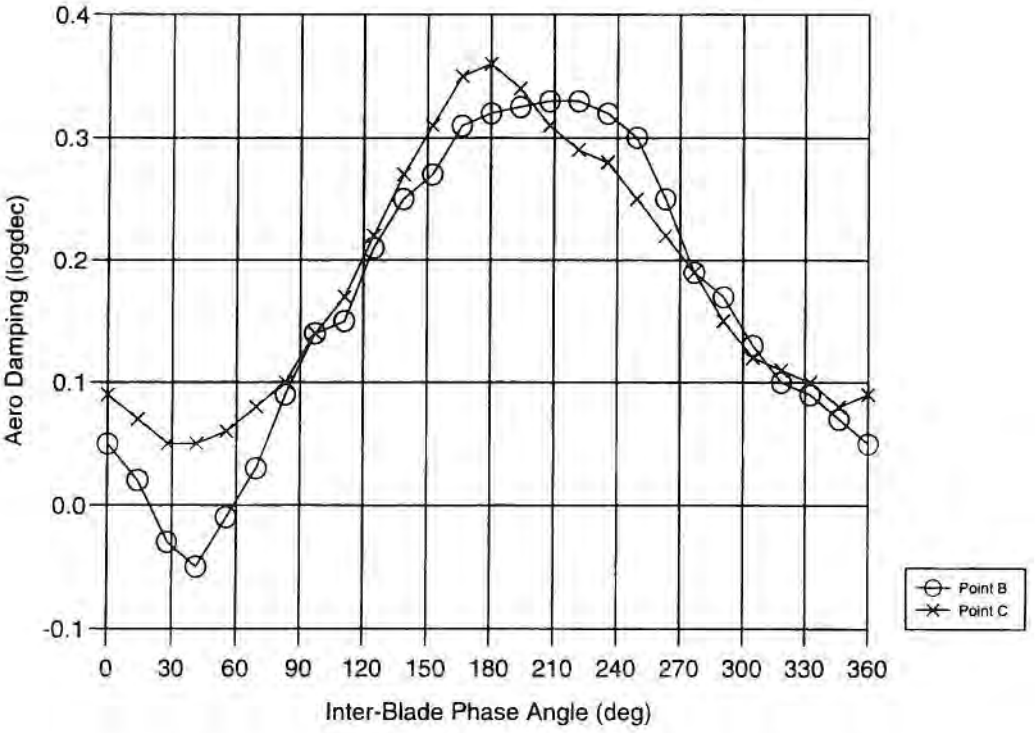

Fig. 8.15 Flutter Stability (logdec) Points 'B' & 'C'

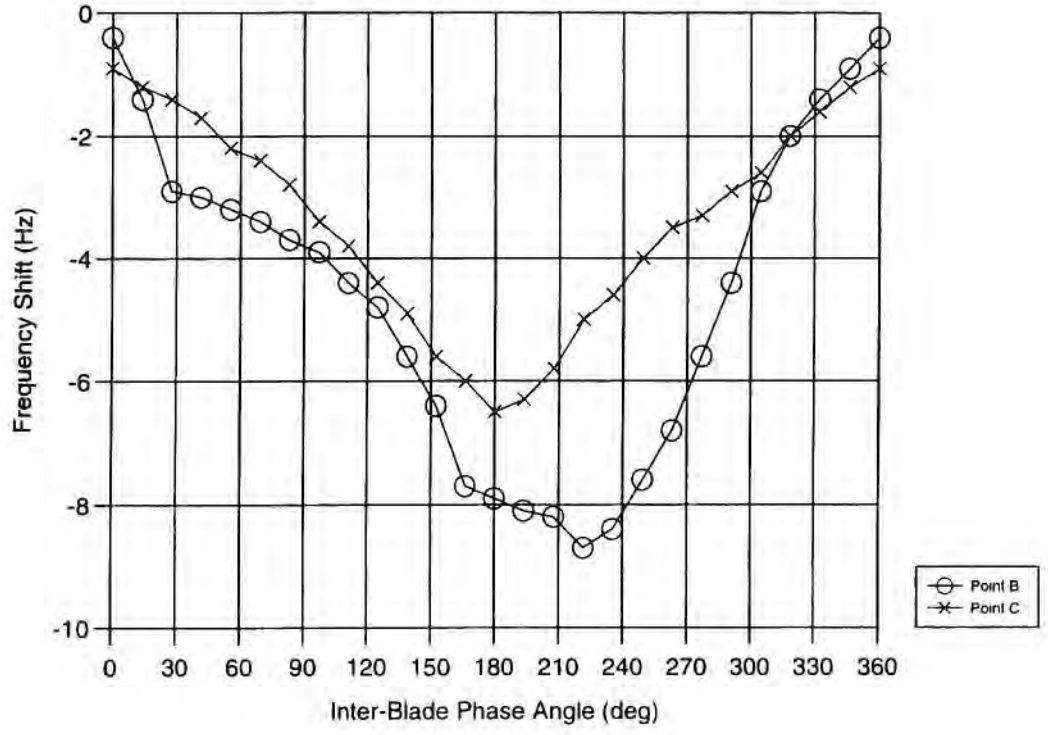

Fig. 8.16 Flutter Frequency Shift Points 'B' & 'C'

Chapter 9

Conclusions & Recommendations

9.0 About this Chapter

This chapter draws together the findings that have been presented in the preceding chapters. The results so far have been critically evaluated for suggesting the best way forward for flutter prediction methods. Finally, some recommendations for future research work are put forward.

9.1 INTEGRATED AEROELASTIC COUPLING

The primary aim of this work has been the presentation of an integrated aeroelasticity model, that did not necessarily rely on any one solution technique or solver. This method has been termed 'partially-integrated' to distinguish it from an alternative method that attempts to solve for the entire fluid/structure domain using one time-domain solver. The latter approach may have the advantage of modelling the coupling more accurately, especially in highly non-linear cases where the rate of energy transfer between the two domains is large. However, it has the limitations imposed by using the same solver for the two different domains for which some compromise has to be reached (i.e. use one more suited to the fluid, in which case it is not so good for the structure, and vice-versa). Also the choice of time step may be highly restrictive in using time-domain solvers for the structure.

The primary aim above has been reached, in that a general method has been presented, and applied to two different application areas (wings and compressor blades) using two different codes (UV2D & AV3D). The methodology can also be applied to a wide range of other problems (e.g. turbine blades, all types of external aerodynamic surfaces, or even civil engineering structures) provided that the fluid- and structural-dynamic solvers are capable of handling the specific type of problem.

Chapters 4 & 5 show the value of the integrated approach over the classical methods for the wing case where the mass ratio is relatively low, so that the flow is able to change the flutter frequency significantly from the structural natural frequencies such that the modes coalesce to form a coupled flutter mode. This phenomenon cannot be predicted by an uncoupled classical method unless the flutter mode is known in advance. This will inevitably lead to such a method failing to predict the transonic dip in the flutter boundary, which must be avoided in modern wing design.

Chapter 6 is a validation of the integrated model, at least in a static sense, since the correct blade position is predicted under gas and rotational loads from knowledge of the flow condition. Dynamic amplitudes are much more difficult to validate as no reliable experimental data exist, and factors such as mistuning and structural damping affect the results. So, for the numerical model to match the observed behaviour, one needs accurate estimates of the magnitude of these two effects and this is probably not yet possible with the present level of understanding and modelling of these phenomena.

Chapters 7 & 8 show that although reasonable results can be obtained using the classical (uncoupled) approach at fixed IBPA. However, the integrated model really comes into its own when a more representative model of the structure is introduced. This is the full assembly model where all the possible structural modes are allowed to interact with each other, rather than calculating their effects separately. The importance of using such integrated models will be discussed further in the next sections.

9.2 IMPORTANCE OF NON-LINEARITIES

The exact effect of non-linearities can be difficult to determine accurately; first it is necessary to review the various components of the model, and identify the non-linear ones. The fluid models are non-linear, modelling either Euler equations or thin-layer Navier-Stokes equations. Thus the fluid model reacts in a non-linear manner to motion of the flexible solid boundaries. The turbulence model used in the latter case is an additional source of non-linearity, but it is probably only valid in a quasi-steady manner (i.e. it gives the steady effect that the boundary layer has on shock position etc. but the unsteady effects are expected to be predominantly driven by the inviscid flow).

The structural model is linear, as it relies on a linear superposition of orthogonal modes. However, in the case of rotating blades, the modeshapes have been calculated including non-linear geometrical effects and rotational forces. The aeroelastic time integration which handles the coupling between the fluid and structure is capable of handling non-linearity, even though the structural model used is linear. The formulation of the current aeroelasticity model does not preclude a fully non-linear structural model i.e. direct integration of the mass and stiffness matrices. However, this approach was not adopted, not because it is not desirable but because it would require several orders of magnitude more computing power than is currently available. This is due to the restrictive time-step limits imposed on the structure, and the large amount of interpolation that would be required. Thus the main restriction in the current aeroelastic model is that the integrated model predicts the change in frequency due to presence of the fluid, but may predict the change in modeshape. This restriction is not thought to be a great problem for turbomachinery blading where the mass ratio is low, but the linearity assumption may need to be revisited for cases where aeroelastic frequency shifts are high (say above 10% of the corresponding natural frequency) or there are 2 modes which are close in frequency that are fluttering.

Also it should be remembered that the current model will only be valid as long as the structural displacements are small enough for the linearising assumption to be valid. This is not usually too much of a problem for flutter point prediction as small amplitudes may be used to assess the flutter onset. However, as models improve and are used to predict limit cycle or forced response amplitudes, this may need to be reassessed. The issue over initial conditions has been covered in Chapter 5 where a non-linear response was demonstrated. There different time histories of motion were produced for the same case when it was given different initial velocities. This was a stable case, however in unstable cases usually the same limit cycle or divergence is ultimately produced, but with a different transient response. These type of effects cannot be predicted with a linear model.

For the turbomachinery cases the 'direct store' implementation of the IBPA on a single passage using the shape correction technique is a linearising assumption. Thus not only is this method uncoupled, and can only handle one IBPA at a time, but it also linearises the passage-to-passage effect on the non-linear flow. In any case the method appears to have some merits, which would seem to suggest that the predominant effects for fan flutter are linear. However this method would probably perform considerably less well on cases where either the mass ratios were lower - leading to higher frequency shifts for the aeroelastic modes, or if two structural modes were close together in frequency. Here using an uncoupled approach of treating them separately and using the superposition principle may produce poor results - and might even miss the flutter altogether.

In the full assembly model it is more difficult to separate which effects are linear and which are non-linear. Certainly with a full analysis a different result is produced compared to the case of treating each assembly mode separately. Although the effect appears to be non-linear, the structural model is still a linear superposition of modes. Therefore, the interaction between the modes has to be non-linear in nature, with the source of the non-linearity coming from the unsteady fluid flow. Nevertheless, to resolve this problem fully, a fully non-linear structural model would have to be tried. If this produced similar results to the current model, the use of the assumed modes approach would be vindicated. However, such an approach would take a tremendous amount of computational power, and this is not currently practicable.

In conclusion, it is believed that the inclusion of the non-linear fluid model within the coupled aeroelasticity model is essential for flutter prediction in the general case,

however the linear structural model seems to be adequate for the turbomachinery blade problem, at least for the time being.

9.3 MULTIPLE PASSAGES FOR HANDLING THE IBPA

As highlighted in Chapter 7, two approaches have been used to handle the IBPA for the flutter analysis of bladed discs. The first is the shape correction implementation of the direct store technique. The second is using multiple blade passages to directly model the phase differences between the blades. In the first case, information about the primitive variables on the lower boundary are stored in time, and the values on the upper boundary can be determined from the values on the other boundary at a previous time (given a fixed IBPA and frequency). In the multi-passage method the periodic boundary condition is to simply set the variables on neighbouring passage boundaries, and on the first and last boundaries equal, as for steady flow. Thus the former method can only be used in a classical (uncoupled) fashion, as the results are only valid once the solution has converged to a periodically repeating state. In the latter method the solution remains accurate throughout the domain at all times, so the integrated (coupled) approach may be used, albeit at the expense of a larger calculation.

In Chapter 7 the multi-passage approach was used with fixed IBPA in order to directly compare with the uncoupled single passage results. However, the multi-passage method for the whole annulus has several advantages, especially if no a priori knowledge of the flutter behaviour is available.

1) In this case where all possible IBPAs have to be tried with the single passage uncoupled approach, this would require more CPU power, and a lot more user input that one large multi-passage job.
2) If there are 2 mode families that are close in frequency (or even cross over) at different nodal diameters. Here the approach of singling out individual IBPAs will almost certainly be invalid as flutter will be determined by modal interactions.
3) The multi-passage technique has the possibility of looking at the effect of mistuning, which has been shown to be important in some flutter problems.
4) If interaction with up/downstream bladerows or ducts is shown to be important for flutter. The neighbouring row is unlikely to have the same number of blades due to the forced response problems that would result and hence a full assembly approach is the most likely to succeed. This is also the case for acoustic interactions and forced response problems (see below).

In conclusion, the multiple blade passage approach is useful for validating single passage models, but it becomes invaluable when used in a full assembly mode in order to model increasingly complex problems (only one of which is flutter) in the turbomachinery environment.

9.4 AN INVISCID MECHANISM FOR FLUTTER?

Since the work reported here uses thin-layer Navier-Stokes equations, in theory the viscous terms have been modelled adequately, but, strictly speaking, the turbulence model used is only really valid for steady flow. It has been shown that it important to include the viscous effects, as without them there is no boundary-layer blockage and the shock will be predicted too far downstream if pure Euler calculations are performed. This means that flutter will not be predicted at the same mass flow and pressure ratio as in the test, which makes it difficult to compare the predictions.

It would be too much to claim that such a primitive turbulence model used in conjunction with relatively coarse meshes as used in these studies can model the unsteady shock boundary-layer interaction accurately. Modern CFD computations for *steady* flow are now routinely using 300,000 - 1,000,000 points per blade passage, in order to capture the viscous phenomena. Unsteady calculations on such grids would require prohibitive computer time, especially for multiple passages. But, despite the inadequacies of the viscous modelling used here, flutter has been predicted, and it is appropriate to discuss the significance of this result.

Classically, the type of flutter examined here at part-speed, above the working line, near the stall condition, has been termed 'stall flutter'. This was because it was believed that flutter generally occurred in two main ways: through coupling of modes, or through dynamic stall. Thus the type of wing flutter as see in Chapters 4 & 5 can be explained by the former, as could some types of flutter in old clappered fans (so called system mode instability). Flutter in wings can occur due to dynamic stalling at lower speeds and high angle of attack, as can happen in civil engineering structures. As the type of flutter presented in Chapters 7 & 8 occurs in a single mode, usually first flap, it has always been associated with stalling. The fact that flutter has been predicted with a predominately inviscid unsteady model (albeit viscous for the steady flow) and that no gross stalling is observed in the model as the blade flutters, would seem to refute this observation.

A simple explanation for this has been put forward by Freeman (1995). In addition to the stabilising effect that always occurs in first flap vibration, a destabilising force

exists due to the mean flow which is strongly dependent on IBPA. The relative motion between the blades tends to increase and decrease the blade spacing. In quasi-steady terms, increasing the blade pitches increases the loading (as each blade has to turn more flow). If the phase of the motion is compared with the phase of this force, it can be seen that to first order, the maximum peak destabilising force occurs at +90° IBPA, and becomes minimum at -90°. This explanation is in line with the observations, and the presence of higher order effects may explain why +90° is not always the least stable IBPA. Thus, this work provides more evidence that the mechanism for part-speed compressor flutter may be predominately driven by the inviscid main flow mechanism, and that the viscous effects, although important may be only a 'second order' effect.

9.5 OVERALL RECOMMENDATIONS FOR FLUTTER PREDICTION

Based on the findings in this work, it is now appropriate to recommend a best practice for flutter predictions in turbomachinery blading in general, and fans in particular. It may be recalled that fans were chosen for these studies as they tend to be the most critical component in modern high bypass ratio turbofans, both in terms of performance and safety. They have also been one of the most difficult components to obtain reliable flutter predictions in the past, due to the complex 3D flowfield. Thus it is hoped that the conclusions from these blades may be applied to other types of turbomachinery blading.

In general, the recommended method for a general aeroelastic analysis of a turbomachinery blade is as follows:

- Obtain the 3D steady viscous flow field at the desired operating conditions.
- Calculate the untwist at these conditions (to do this the CF-only geometry will be required for the starting conditions). The untwist may be particularly significant at off-design conditions where flutter is expected to occur.
- If the flutter mode is known from a test, it may be sufficient to investigate the blade mode and the IBPAs that are causing the problem using a single passage uncoupled approach; but at least some of the other modes and IBPAs should also be investigated as a minimum.
- If the bladerow has a large number of blades it may be necessary to obtain an equivalent solution on a coarser mesh to enable the full assembly calculations (untwist should be included on the new mesh).

- At least one full assembly calculation should be done, to determine the least stable mode(s). If the flutter mode is unknown at the start, it may be quicker and easier to do this calculation in preference to the single passage approach.
- If further insight is required into the flutter mechanism, then the multi-passage coupled approach at fixed IBPA could be used. This is because the multi-passage whole annulus model is the most representative model, however the results can be difficult to interpret, and the mechanism of flutter may not be clear.

If this approach is adopted then flutter predictions should be possible for most problems encountered in turbomachines. The only aspects that have been left out so far are discussed in the next section.

9.6 FUTURE DIRECTIONS

In spite of their very substantial computational requirements, integrated non-linear aeroelasticity methods will probably gain gradual acceptance in industrial applications as they can predict limit cycle behaviour, a phenomenon which is commonly observed in engine tests. However, major challenges will remain with the modelling of the various components and a number of possible improvements are discussed below.

9.6.1 Improved Structural Model

The structural representation has been so far provided in the form of a modal model obtained by a free vibration analysis. The mode shapes are then interpolated onto the aerodynamic grid on the blade surface and converted into principal co-ordinates. Although this approach does not compromise the integrity of the aeroelastic model vis-à-vis the fluid/structure coupling, it inherently assumes small amplitude vibration and linear structural behaviour (summation over a set of fixed modes). Although the structural analysis is probably one of the most accurate components of the aeroelasticity problem, an improved representation may be based on an elemental approach where the local mass and stiffness matrices are formed, and solved simultaneously with the same time-integrator as the fluid. This would allow geometric and other non-linear behaviour, and the modes of the structure would no longer be fixed, but allowed to change under the fluid loading. Although this approach has been advocated by Bendiksen (1991), it is difficult to implement a finite-volume type nodal model in 3D since the formulation is not directly compatible with the current well-established finite element techniques.

The alternative way of handling the structural model, without resorting to the modal approach, is to form global mass and stiffness matrices. These could be directly

integrated in time, however this would be computationally very expensive. The full model could be reduced by a condensation technique such as Guyan reduction, but it is debatable whether this would give a more accurate result than the modal approach. Also with these structural models, the 'trick' of interpolating the (fixed) modeshape onto the aerodynamic mesh cannot be used, so unless the surfaces meshes had coincident points (which is unlikely due to the different requirements of fluid & structural modelling) a large amount of interpolation at each timestep would be required. To compensate for this implicit timestepping could be used, in order to use large time-steps, or a hybrid scheme could be adopted where unequal timestep were taken in the fluid and structural domains.

The structural model in the general case could also include other localised non-linear features such as friction damping. The inclusion of such effects is of primary interest since manufacturers routinely use blade under platform dampers as a passive means of flutter control and the exact nature of the phenomenon is not fully understood. Similarly, non-linear behaviour also exists at shroud interfaces and it may be a crucial issue to understand and to model some of the aeroelastic instabilities.

However, the inclusion of such features may be very expensive in terms of CPU time since it will no longer be possible to describe the structural model in terms of its normal modes since the stiffness matrix will be time-dependent. Also, the higher modes will automatically be included and the required time step will be very small. Although there are numerical techniques to circumvent such problems, to conduct such general analyses with thousands of degrees of freedom in the time domain will probably require a computing power far beyond that is currently available today.

9.6.2 Mistuning

There are no reported cases of 3D aeroelasticity models with mistuning as most such approaches are based on single blade passage analyses. The introduction of mistuning would require the modelling of the whole annulus for flutter cases (when mistuning is believed to be beneficial) and at least two full bladerows for forced response (where mistuning is always causes higher vibration levels). In spite of obvious computational difficulties, such analyses will probably be reported within the next few years. The assembly modes model used in Chapter 8 would have to be adapted for mistuning studies. Either the mistuned assembly modes would have to be adopted, where it is believed that the modeshapes remain almost the same, but the double modes split to two different frequencies. Alternatively, in the case where disc coupling is weak, each blade could be treated as a cantilever with slightly different natural frequencies.

9.6.3 Aerodynamic Features

Of immediate interest are tip leakage and models capable of handling secondary flows, separation and such like. Also, improved representation for transition and turbulence (especially for unsteady flows) and mesh generation and quality for viscous models is extremely desirable. As available computer power may well continue to increase exponentially, it is important that aeroelasticity methods can take advantage of new developments in CFD as they become available. Although it is now possible to obtain complete vehicle solutions for external aerodynamics (Batina 1991), multi-stage multi-passage unsteady models for turbomachinery still remain a large problem, which are some way off from being used routinely.

9.6.4 Forced Response

The models that have been presented in this work are also capable of forced response analysis. The advantage of the integrated model in this case is that the blade motion is calculated directly as the unsteady forcing (from wakes or potential fields) affects the mean flow. Thus the amplitude of vibration is determine from both the unsteady pressures arising from the forcing, and the (stabilising) pressure forces arising from the blade motion. It can be assumed that the mean flow is stable to blade motion in this case, otherwise flutter would occur, not forced response. In classical models the unsteady pressures from the forcing, and the aerodynamic damping from the blade motion are usually calculated separately (and sometimes the aerodynamic damping is ignored altogether). There is no known example in the literature for such an integrated forced response calculation, and it is unknown by how much the blade motion affects the unsteady forcing and vice-versa.

The CFD model described above would need some modifications to enable this kind of calculation. In rotor only calculations, the inlet (or exit) boundary conditions need to be able to take account of potential fields or wakes coming from the upstream (or downstream) row. The boundary condition then rotates with respect to the rotor to give the unsteady forcing. In full stator-rotor interactions, the entire preceding blade row has to be modelled, and the rotating row moves past it with a sliding plane in-between, with an appropriate boundary condition.

In both cases, at least two periodicities result: one from the different blade numbers, and the other from the vibrating blade motion. These will need to be handled appropriately at the periodic boundaries, and could be done by a 'direct store' type of approach, however as more than one periodicity is involved (and possibly many due to different modes and nodal diameters being excited) it may well be easier, and more

accurate to model the entire annulus. There may be other difficulties as well, as modelling the wake accurately may require dynamic mesh adaptation, as the wake moves through the rotor row. If the mesh is too coarse, the wake will dissipate under the numerical smoothing, and a uniformly fine grid would be too expensive computationally. Such a model would, however, represent the ultimate forced response prediction, and could be used for friction damping and mistuning studies.

9.6.5 Acoustic Interactions

Another type of phenomena, related to aeroelasticity is acoustic interactions. It has been observed that some flutter phenomena may be accompanied by an acoustic resonance, that tends to exacerbate the flutter. In extreme cases it may lead to spontaneous self-destruction of the machine. The multi-passage multi-stage approach advocated for the forced response model above, could also be used to examine this phenomenon. The fluttering blade row could be modelled as described herein, and the up/downstream bladerow or duct in which the resonance occurs could also be included in the model. Then the difference between including or not including the other row in the model could be highlighted.

9.7 RECOMMENDATIONS FOR FURTHER RESEARCH

The recommendations for further research have been discussed above. They are summarised here.

Further Calculations

The method should be tested further on a wide range of cases to improve the understanding of how different types of flutter occur, as well as to validate the model. These should include real machine geometries, cascade tests, and tests against other codes and approaches. This should lead to greater understanding of both the phenomena involved, and of the best way to model each situation.

Structural Model

The structural model should be improved. This could then be used to test the limitations of the current linear model that has been adopted. This could be used to test the effect of the fluid loading on the modeshape, and also non-linear structural phenomena such as non-linear materials, or friction damping could be added. This approach would also relieve the current limitation in the untwist calculations that the change in rotational CF loads have not been recalculated when the blade moves due to the gas loads.

Mistuning

The effect of structural mistuning should be investigated. The use of the entire bladed disc annulus model is ideal to determine the effect of mistuning on flutter (or forced response). This would require a different model of the assembly modes to account for the mistuning - i.e. the double modes become split in frequency, and the modeshapes will change. This model could then be used to answer the question a to whether mistuning is indeed beneficial to the flutter margins, and what arrangements produce the greatest effect.

Improved aerodynamic model

The aerodynamic model should be improved. Use of the full Navier-Stokes model with more accurate turbulence model would lead to improved understanding of the effect of viscous phenomena such as shock boundary-layer interaction on flutter. In the first instance it may be necessary to revert to single passage calculations in order to capture such unsteady viscous phenomena using finer meshes. However, computer power may well advance to such an extent that very fine meshes may be used even for whole annulus calculations. Alternatively, detailed single passage calculations may help the understanding on these phenomena and may lead to improvements in the turbulence modelling for unsteady flow. Then improvements may be obtained even on the relatively coarse grids necessary to model many blades passages.

Multi-Row Calculations

Finally the multi-passage approach should be extended to also allow the calculation of multiple bladerows. Using this model forced response and the effect of other bladerows on flutter could be investigated. Such a multi-passage multi-stage approach should be adopted to enable unsteady flow and aeroelastic modelling of virtually any turbomachinery problem. In this way the possibility of flutter being strongly affected by the interaction with up- and downstream ducts or bladerows could be investigated.

REFERENCES

Abdel-Rahim, A., Sisto. F. & Thangam, S., 1991, Computational Study of Stall Flutter in Linear Cascades, *ASME Paper* 91-GT-5

Adamczyk, J.J. 1978, Analysis of Supersonic Stall Bending Flutter in Axial-Flow Compressor by Actuator Disk Theory, *NASA Technical Paper* No. NASA-TP-1345

Adamczyk, J.J., & Goldstein, M.E. 1978, Unsteady Flow in a Supersonic Cascade with Leading-Edge Locus, *AIAA Journal* **16**(12), 1248

Adamczyk, J.J., Stevans, W., and Jutras, R. 1982, Supersonic Stall Flutter of High-Speed Fans, *Journal of Engineering for Power* **104**(3) 675

Afolabi, D.H., 1988, Vibration Amplitude of Mistuned Blades, *ASME Journal of Turbomachinery,* **110** 535-545

AGARD Manual on Aeroelasticity in Axial-Flow Turbomachines, 1985, Volume 1 - Unsteady Turbomachinery Aerodynamics; Volume 2 - Structural Dynamics and Aeroelasticity, Ed. Platzer, M.F., & Carta, F.O., *AGARDograph* **298**

Armstrong, E.K, & Stevenson, M.A., 1960, Some Practical Aspects of Compressor Blade Vibration, *Journal of the Royal Aeronautical Society* **64** (591) 117-130

Armstrong, E.K., 1967, Recent Blade Vibration Techniques, *ASME Journal of Engineering for Power* **1** 437-444

Arnone, A., 1993, Viscous Analysis of Three-Dimensional Rotor Flow Using a Multigrid Method, *ASME Paper* 93-GT-19, IGTI Gas Turbine Conference, Cincinnati OH

Ashley, H., 1970, Aeroelasticity, *Applied Mechanics Reviews*

Aso, S. & Kumamoto, Y. 1994, Experimental and Computational Studies on Separated Flows around Oscillating Airfoil, *Proc. 7th Int. Symposium on Unsteady Aerodynamics & Turbomachines, Fukuoka*

Atassi, H., & Akai, T.J. 1978, Aerodynamic Force and Moment on Oscillating Airfoils in Cascade, *ASME Paper* 78-GT-181

Bakhle, M.A., Reddy, T.S.R., & Keith, T.G. 1992, Time Domain Flutter Analysis of Cascades Using a Full-Potential Solver, *AIAA Journal.* **30**(1) 163

Baldwin, B.S. & Lomax, H. 1978, Thin-Layer Approximation and Algebraic Model for Separated and Turbulent Flows, *AIAA Paper 78-257*

Baldwin, B.S. & Barth, T.J. 1990, A One-Equation Turbulence Transport Model for High Reynolds Number Wall-Bounded Flows, *NASA* TM 102847

Ballhaus, W.F., & Goorjian, P.M. 1977, Implicit Finite-Difference Computations of Unsteady Transonic Flows about Airfoils, *AIAA Journal* **15**(12) 1728

Ballhaus, W.F., & Goorjian, P.M. 1978, Computation of Unsteady Transonic Flows by the Indicial Method, *AIAA Journal* **16**(2) 117

Batina, J.T., & Yang, T.Y. 1984, Application of Transonic Codes to Aeroelastic Modelling of Airfoils Including Active Controls, *Journal of Aircraft* **21**(8) 623

Batina, J.T. 1988, Efficient Algorithm for Solution of the Unsteady Transonic Small-Disturbance Equation, *Journal of Aircraft* **25**(7) 598

Batina, J.T. 1989, Unsteady Aerodynamics Methods for Transonic Aeroelastic Analysis, *Proc. of European Forum on Aeroelasticity and Structural Dynamics,* Paper 89-002

Batina, J.T., 1990, Unsteady Euler Airfoil Solutions Using Unstructured Dynamic Meshes, *AIAA Journal* **28**(8) 1381

Batina, J.T. 1991, Unsteady Euler Algorithm with Unstructured Dynamic Mesh for Complex Aircraft Configuration, *AIAA Journal* **29**(3) 327

Beam, R.M., & Warming, R.F. 1978, Implicit Factured Schemes for the Compressible Navier-Stokes Equations, *AIAA Journal* **14**(4) 393

Bendiksen, O.O., & Friedmann, P.P. 1982, The Effect of Bending-Torsion Coupling on Fan and Compressor Blade Flutter, *Journal of Engineering for Power* **104** 617

Bendiksen, O.O., 1984, Flutter of Mistuned Turbomachinery Rotors, *ASME Journal of Engineering for Gas Turbines and Power* **106** 25-33

Bendiksen, O.O. 1986, Rôle of Shocks in Transonic/Supersonic Compressor Rotor Flutter, *AIAA Journal* **24**(7) 1179

Bendiksen, O.O., & Kousen, K.A. 1987, Transonic Flutter Analysis Using the Euler Equations, *AIAA Paper* 87-0911-CP, Dynamics Specialists Conference, Monterey, CA

Bendiksen, O.O. 1988, Recent Developments in Flutter Suppression Techniques for Turbomachinery Rotors, *Journal of Propulsion* **4**(2) 164

Bendiksen, O.O. 1991, A New Approach to Computational Aeroelasticity, *AIAA Paper* 91-0939, 31st Structural Dynamics and Materials Conference, Baltimore, MD

Bendiksen, O.O. 1993, Aeroelastic Problems in Turbomachines Flight-Vehicle Materials, Structures and Dynamics, Assessment and Future Directions: *ASME Publications* **5** 00241-297

Berry, H.M., Batina, J.T., & Yang,T.Y. 1986, Viscous Effects on Transonic Airfoil Stability and Response, *Journal of Aircraft* **23**(5) 361

Bert, C.W. & Stricklin, J.D., 1988, Comparitive Evaluations of Six Different Numerical Integration Methods for Non-Linear Dynamic Systems, *Journal of Sound and Vibration* **127** (2) 221

Bishop, R.E.D. & Johnson, D.C., 1960, Mechanics of Vibration, *Cambridge University Press, UK*

Bisplinghoff, R.L., Ashley, H., & Halfman, R.L. 1955, Aeroelasticity, *Addison Wesley Publishing Co.*

Bisplinghoff, R.L., & Ashley, H. 1962, Principles of Aeroelasticity, *John Wiley & Sons, New York*

Borland, C.J., & Rizzetta, D.P. 1982, Nonlinear Transonic Flutter Analysis, *AIAA Journal* **20**(11) 1606

Bölcs, A., & Fransson, T.H. 1986, Aeroelasticity in Turbomachines - Comparison of Theoretical and Experimental Cascade Results, *EPFL Communication* No. 13

Brase, L.O., & Eversman, W. 1988, Application of Transient Aerodynamics to the Structural Nonlinear Flutter Problem, *Journal of Aircraft* **25**(11) 1060

Brenneis, A., & Eberle, A. 1990, Application of an Implicit Relaxation Method Solving the Euler Equations for Time-Accurate Unsteady Problems, *Journal of Fluids Engineering* **112** 510

Campbell, W., 1924, The Protection of Steam Turbine Wheels from Axial Vibration, *ASME* **46** 31-160

Carta, F.O., 1967, Coupled Blade-Disc-Shroud Flutter Instabilities in Turbojet Engine Rotors, *ASME Journal of Engineering for Power* **89** 419

Cebeci, T. & Smith A.M. 1974, Analysis of Turbulent Boundary Layers, *Academic Press, New York*

Cebeci, T., Platzer, M.F., Jang, H.M., & Chen, H.H., 1992, An Inviscid-Viscous Interaction Approach to the Calculation of Dynamic Stall Initiation on Airfoils, *ASME Paper* 92-GT-128

Celi, R., & Friedmann, P.P. 1988, Rotor Blade Aeroelasticity in Forward Flight with an Implicit Aerodynamic Formulation, *AIAA Journal* **26**(12) 1425

Chaderjian, N.M., & Guruswamy, G.P. 1992, Transonic Navier-Stokes Computations for an Oscillating Wing Using Zonal Grids, *Journal of Aircraft* **29**(3) 326

Chi, R.M., & Srinivasan, A.V. 1985, Some Recent Advances in the Understanding and Prediction of Turbomachine Subsonic Stall Flutter, *ASME Journal of Engineering for Gas Turbines and Power* **107** 408 (Paper 84-GT-151)

Chiang, H.D., & Kielb, R.E. 1992, An Analysis System for Blade Forced Response, *ASME Paper* 92-GT-172

Chow, L.J., Pulliam, T.H., & Steger, J.L. 1984, A General Perturbation Approach for Computational Fluid Dynamics, *AIAA Journal* **22**(12) 1749

Cohen, H., Rogers, G.F.C. & Saravanamuttoo, H.I.H, 1987, Gas Turbine Theory, *Longman Scientific & Technical, Third Edition*

Collar, A.R., 1947, The Expanding Domain of Aeroelasticity, *Journal of the Royal Aeronautical Society* **51** 1

Collar, A.R., 1978, The First Fifty Years of Aeroelasticity, *Aerospace* **5** 12

Cottney, D.J. & Ewins, D.J., 1975, On Predicting the Natural Frequencies of Shrouded Bladed Disks, *ASME Paper* 75-DET-113

Crawley, E.F. & Hall, K.C., 1985, Optimization and Mechanism of Mistuning in Cascades, *ASME Journal of Engineering for Power* **107** 418-426

Crawley, E.F. & Ducharme, E.H. 1990, Parametric Trends in the Flutter of Advanced Turboprops, *ASME Journal of Turbomachinery* **112** 741

Craig, R.R. & Bampton, M.C.C., 1968, Coupling of Substructures for Dynamic Analysis, *AIAA Journal* **6** (7) 1313-1321

Curtiss, H. C., Scanlan, R. H. & Sisto, F. , Ed. Dowell, E. H. 1989, A Modern Course in Aeroelasticity, *Kluwer Academic Publishers*

Cunningham, H.J., Batina, J.T., & Bennett, R.M., 1988 Modern Wing Flutter Analysis by Computational Fluid Dynamics Methods, *Journal of Aircraft* **25**(10) 962

Davies, M.R.D., & Bryanston-Cross, P.J. 1985, Holographic Measurements and Theoretical Predictions of the Unsteady Flow in a Transonic Annular Cascade, *ASME Journal of Engineering for Gas Turbines and Power* **107** 450

Dawes, W.N. 1987, A Numerical Analysis of the Three-Dimensional Viscous Flow in a Transonic Compressor Rotor and Comparison with Experiment, *ASME Journal of Turbomachinery* **109** 83

Denton, J.D. 1975, A Time Marching Method for Two- and Three-Dimensional Blade to Blade Flows, *A.R.C., R & M.* No. 3775

Denton, J.D. 1983, An Improved Time-Marching Method for Turbomachinery Flow Calculation, *Journal of Engineering for Power* **105** 514

Donea, J., Giuliani, S., & Halleux, J.P. 1982, An Arbitary Lagrangian-Eulerian Finite Element Method for Transient Dynamic Fluid-Structure Interactions, *Computer Methods in Applied Mechanics and Engineering* **33** 689

Dunn, P., & Dugundji, J. 1992, Nonlinear Stall Flutter and Divergence Analysis of Cantilevered Graphite/Epoxy Wings, *AIAA Journal* **30**(1) 153

Dye, R. C. & Henry, T. A., 1969, Vibration of Compressor Blades Resulting from Scatter in Blade Natural Frequencies, *Journal of Engineering for Power* 182-187

Edwards, J.W., Bennett, R.M., Whitlow, W., & Seidel, D.A. 1983, Time-Marching Transonic Flutter Solutions Including Angle-of -Attack Effects, *Journal of Aircraft* **20**(11) 899

Ekaterinaris, J.A., & Platzer., M.F. 1994, Progress in the Analysis of Blade Stall Flutter, *Proc. 7th Int. Symposium on Unsteady Aerodynamics & Turbomachines, Fukuoka*

Erdos, J.I., Alzner, E., & McNally, W. 1977, Numerical Solution of Periodic Transonic Flow through a Fan Stage, *AIAA Journal* **15**(11) 1559

Ewins, D.J. 1973, Vibration Characteristics of Bladed Disc Assemblies, *Journal of Mechanical Engineering Sciences* **15**(3)

Ewins, D.J. 1976, Vibration Modes of Mistuned Bladed Disks, *ASME Journal of Engineering for Power* 349

Ewins, D.J. 1991, The Effects of Mistuning on Vibration Response, *IFToMM Conference, Prague*

Ewins, D. J. & Han Z. S. 1984, Resonant Vibration Levels of a Mistuned Disk, *Journal of Vibration, Acoustics and, Sress and Reliability in Design* **106** 211-217

Farhat, C., Lesoinne, M. & Maman, N., 1995, Mixed Explicit / Implicit Time Integration of Coupled Aeroelastic Problems - 3-Field Formulation, Geometric Conservation and Distributed Solution, *International Journal for Numerical Methods in Fluids* **21** (10) 807-835

Ferrand, P., & Aubert, S. 1994, Study of Unsteady Transonic Flow with a New Mixed Van Leer Flux Splitting Method, *Proc. 7th Int. Symposium on Unsteady Aerodynamics & Turbomachines, Fukuoka*

Fleeter, S. 1979, Aeroelasticity Research for Turbomachine Applications, *Journal of Aircraft* **16**(5) 320

Ford, R.A.J., & Foord, C.A. 1979, An Analysis of Aeroengine Fan Flutter using Twin Orthogonal Vibration Modes, *ASME Paper* 79-GT-126

Forsching, H. W. 1974, Fundamentals of Aeroelasticity, *Springer-Verlag, Berlin*

Fransson, T., & Pandolfi, M. 1986, Numerical Investigation of Unsteady Subsonic Compressible Flows Through an Oscillating Cascade, *ASME Paper* 86-GT-304

Freeman, C., 1995, Private Communication

Friedmann, P., & Yuan, C. 1977, Effect of Modified Aerodynamic Strip Theories on Rotor Blade Aeroelastic Stability, *AIAA Journal* **15**(7) 932

Friedmann, P.P. 1987, Recent Trends in Rotary Wing Aeroelasticity, *Vertica* **11**(1) 139

Gallman, J.W., Batina, J.T., & Yang, T.Y. 1988, Computational Transonic Flutter Boundary Tracking Procedure, *Journal of Aircraft* **25**(3) 263

Garrick, I.E. 1976, Aeroelasticity - Frontiers and Beyond, 13th Von Karman Lecture, *Journal of Aircraft* **13**(9) 641

Garrick, I.E., & Reed, W. H. 1981, Historical Development of Aircraft Flutter, *Journal of Aircraft* **18**(11) 897

Gea, L.M., Chow, C.Y., & Chang, I.C. 1992, Transonic Aeroelasticity Analysis for Rotor Blades, *Journal of Aircraft* **29**(3) 477

Gerolymos, G. A. 1988, Numerical Integration of the Blade-to-Blade Surface Euler Equations in Vibrating Cascades, *AIAA Journal* **26**(12) 1483

Gerolymos, G.A. 1992a, Advances in the Numerical Integration of the 3-D Euler Equations in Vibrating Cascades, *ASME Paper* 92-GT-170

Gerolymos, G. A. 1992b, Coupled 3-D Aeroelastic Stability Analysis of Bladed Disks, *ASME Paper* 92-GT-171

Giles, M.B. 1988, Calculation of Unsteady Wake/Rotor Interaction, *AIAA Journal of Propulsion* **4**(4) 356

Giles, M.B. 1990a, Stator/Rotor Interaction in a Transonic Turbine, *AIAA Journal of Propulsion* **6**(5) 621

Giles, M.B. 1990b, Non-Reflecting Boundary Conditions for Euler Equation Calculations, *AIAA Journal* **28**(12) 2050-2058

Giles, M.B., & Haimes, R. 1991, Validation of a Numerical Method for Unsteady Flow Calculations, *ASME Paper* 91-GT-271

Giles, M.B. 1992, An Approach for Multi-Stage Calculations Incorporating Unsteadiness, *ASME Paper* 92-GT-282

Giles, M.B. 1994, Stability of Aeroelastic Coupling Schemes, *Private Communication*

Greenhalgh, S., Curtiss, H.C., & Smith, B. 1984, Aerodynamic Properties of a Two-Dimensional Inextensible Flexible Airfoil, *AIAA Journal* **22**(7) 865

Guruswamy, G.P., & Yang, T.Y. 1981, Aeroelastic Time Response Analysis of Thin Airfoils by Transonic Code LTRAN2, *Computers and Fluids* **9**(4) 409

Guruswamy, G.P., & Goorjian, P.M. 1984, Effects of Viscosity on Transonic Aerodynamic & Aeroelastic Characteristics of Oscillating Airfoils, *Journal of Aircraft* **21**(9) 700

Guruswamy, G.P., & Goorjian, P.M. 1985, Efficient Algorithm for Unsteady Transonic Aerodynamics of Low-Aspect Ratio Wings, *Journal of Aircraft* **22**(3) 193

Guruswamy, G.P., & Goorjian, P.M. 1987, Transonic Aeroelasticity of Wings with Active Control Surfaces, *AIAA Paper* 87-0709

Guruswamy, G.P., & Goorjian, P.M. 1988, Unsteady Transonic Aerodynamics and Aeroelastic Calculations at Low Supersonic Freestreams, *Journal of Aircraft* **25**(10) 955

Guruswamy, G.P. 1989, Integrated Approach for Active Coupling of Structures and Fluids, *AIAA Journal* **27**(6) 788

Guruswamy, G.P. 1990, Unsteady Aerodynamic and Aeroelastic Calculations for Wings Using Euler Equations, *AIAA Journal* **28**(3) 461

Guruswamy, G.P., 1992, Navier-Stokes Computations on Swept-Tapered Wings, Including Flexibility, *AIAA Journal of Aircraft* **29** (4) 588

Guyan, R. J. 1965, Reduction of Mass and Stiffnes Matrices, *AIAA Journal* **3**(2) 380

Halliwell, D.G., Newton, S.G., & Lit, K.S. 1984, A Study of Unsteady Pressures Near the Tip of a Transonic Fan in Unstalled Supersonic Flutter, *Journal of Vibration, Acoustics, Stress, and Reliability in Design* **106** 198

Hall, K.C., & Crawley, E.F. 1989, Calculation of Unsteady Flows in Turbomachinery Using the Linearised Euler Equations, *AIAA Journal* **27**(6) 777

Hall, K.C., & Clark, W.S. 1991, Calculation of Unsteady Linearized Euler Flows in Cascades using Harmonically Deforming Grids, *Proc. 6th International Symposium on UAATP, Notre Dame*

Hall, K.C., & Lorence, C.B. 1992, Calculation of Three-Dimensional Unsteady Flows in Turbomachinery Using the Linearized Harmonic Euler Equations, *ASME Paper* 92-GT-136

He, L. 1990, An Euler Solution for Unsteady Flows Around Oscillating Blades, *Journal of Turbomachinery* **112** 714

He, L., & Denton, J.D. 1991a, Inviscid-Viscous Coupled Solution for Unsteady Flows Through Vibrating Blades: Parts 1 & 2, *ASME Papers* 91-GT-125 & 126

He, L., & Denton, J.D. 1991b, An Experiment on Unsteady Flow Over an Oscillating *Airfoil ASME Paper* 91-GT-181

He, L. 1992, Method of Simulating Unsteady Turbomachinery Flows with Multiple Perturbations, *AIAA Journal* **30**(11) 2730

He, L. 1993a, New Two-Grid Acceleration Method for Unsteady Navier-Stokes Calculations, *AIAA Journal of Propulsion and Power* **9**(2) 272

He, L. 1993b, Three-Dimensional Time-Marching Inviscid and Viscous Solutions for Unsteady Flows around Vibrating Blades, *ASME Paper* 93-GT-92

Henke, H., Müller, U.R., & Schulze, B. 1991, A Viscous Inviscid Interaction Method for use in Transonic Flutter Analysis, *Proc. Int. Forum on Aeroel. & Struc. Dyn., Aachen,* Paper 91-064

Hirt, C.W., Amsden, A.A. & Cook, J.L. 1974, An Arbitary Lagrangian-Eulerian Computing Method for all Flow Speeds, *Journal of Computational Physics* **14**

Hodson, H.P. 1984, An Inviscid Blade to Blade Prediction of a Wake Generated Unsteady Flow, *ASME Paper* 84-GT-43

Holmes, D.G., & Chuang, H.A. 1991, Two Dimensional Linearized Harmonic Euler Flow Analysis for Flutter and Forced Reponse, *Proceedings of 6th UAATP, Notre Dame*

Hoyniak, D. & Fleeter, S., 1986, Aerodynamic and Structural Detuning of Supersonic Turbomachinery Rotors, *AIAA Journal of Propulsion and Power* **2** (2) 161-167

Huff, D.L., Swafford, T.W., & Reddy, T.S.R. 1991, Euler Flow Predictions for an Oscillating Cascade Using a High Resolution Wave-Split Scheme, *ASME Paper* 91-GT-198

Hughes, T.J.R., Lin, W.K. & Zimmerman, T.K., 1981, Lagrangian-Eulerian Finite Element Formulation for Incompressible Viscous Flows, *Computer Methods in Applied Mechanics and Engineering* **29** 329-349

Imregun, M., & Ewins, D.J. 1984, Aeroelastic Vibration Analysis of Tuned and Mistuned Bladed Systems, *Proc. 2nd Symp. on UAATP, Cambridge*

Imregun M. 1994, Prediction of Flutter Stability Using Aeroelastic Response Functions, *Journal of Fluids and Structures* (In print)

Irretier, H. 1979, Coupled Vibrations of Blades in Bending-Bending-Torsion and Disks in Out-of-Plane and In-Plane Motion, *ASME Paper* 79-DET-90, 7th ASME Conf. on Mechanical Vibrations and Noise

Irretier, H. 1982, Mistuned Bladed Disks - Dynamical Behaviour and Computation, *IFTOMM Rotordynamics Problems in Powerplant, Rome*

Irretier, H. 1988, Free and Forced Vibrations of Turbine Blades, CISM Course No. 297 'Rotordynamics 2 - Problems in Turbomachinery' p.397, *Springer-Verlag*

Jameson, A. 1974, Iterative Solution of Transonic Flows over Airfoils and Wings Incliding Flows at Mach 1, *Comm. Pure & Applied Maths* **27** 283

Jameson, A., Schmidt, W., & Turkel, E. 1981, Numerical Solutions of the Euler Equations by Finite Volume Methods Using Runge-Kutta Time-Stepping Schemes, *AIAA Paper* No. 81-1259

Jameson, A. 1983a, The Evolution of Computational Methods in Aerodynamics, *Journal of Applied Mechanics* **50**(4) 1052

Jameson, A., & Baker, T.J. 1983b, Solution of the Euler Equations for Complex Configurations, *AIAA Paper* 83-1929

Johnson, D.A. & King, L.S. 1985, A Mathematically Simple Turbulence Closure Model for Attached and Separated Turbulent Boundary Layers, *AIAA Journal* **23** 1684

Jones, W.P. & Launder, B.E. 1973, The Calculation of Low-Reynolds-Number-Phenomena with a Two-Equation Model of Turbulence, *International Journal of Heat and Mass Transfer* **16** 1119

Karpel, M. 1982, Design for Active Flutter Suppression and Gust Alleviation Using State-Space Aeroelastic Modelling, *Journal of Aircraft* **19**(3) 221 1982

Kaza, K.R.V., & Kielb, R.E. 1982, Flutter and Response of a Mistuned Cascade in Incompressible Flow, *AIAA Journal* **20**(8) 1120

Kaza, K.R.V., & Kielb, R.E. 1985, Vibration and Flutter of Mistuned Bladed Disk Assemblies, *AIAA Journal of Propulsion and Power* **1**(5) 336

Kaza, K.R.V. 1988, Development of Aeroelastic Analysis Methods for Turborotors and Propfans - Including Mistuning, *Lewis Structures Technology , Vol. 1, Proc. NASA Lewis Research Center*

Kielb, R.E., & Kaza, K.R. 1985, Flutter of Swept Fan Blades, *Journal of Turbomachinery* **107** 395

Kielb, R.E., & Ramsey, J.K. 1989, Flutter of a Fan Blade in Supersonic Axial Flow, *Journal of Turbomachinery* **111** 462

Klose, A.H. 1992, Advanced Ducted Engines: Impact of Unsteady Aerodynamics on Fan Vibration Properties, *ASME Paper* 92-GT-228

Korakianitis, T. 1992, On the Prediction of Unsteady Forces on Gas Turbine Blades: Parts 1 & 2, *Journal of Turbomachinery* **114** 114

Kousen, K.A., & Bendiksen, O.O. 1988, Nonlinear Aspects of the Transonic Aeroelastic Stability Problem, *AIAA Paper* 88-2306

Kousen, K.A., & Bendiksen, O.O. 1989, Limit Cycle Phenomena in Computational Transonic Aeroelasticity, *AIAA Paper* 89-1185-CP

Kovats, Z. 1980, Interferometrically Measured Aerodynamic Forces on a Vibrating Turbine Blade Group, *Journal of Enginering for Power* **102** 638

Lalanne, M. 1985, Vibration Problems in Jet Engines, *Shock and Vibration Digest* **17**(3) 19

Lane, F. 1956, System Mode Shapes in the Flutter of Compressor Blade Rows, *Journal of Aeronautical Sciences* **23** 1

Lee, C.L. 1986, An Iterative Proceedure for Nonlinear Flutter Analysis, *AIAA Journal* **24**(5) 833

Leishman, J.G., & Nguyen, K.Q. 1990, State-Space Representation of Unsteady Airfoil Behaviour, *AIAA Journal* **28**(5) 836

MacCormack, R.W. 1976, An Efficient Numerical Method for Solving the Time-Dependent Compressible Navier-Stokes Equations at High Reynolds Number, *NASA Technical Memorandum*, TM-X-73129

Malone, J.B., & Sankar, N.L. 1984, Numerical Simulation of Two-Dimensional Unsteady Transonic Flows Using the Full-Potential Equation, *AIAA Journal* **22**(8) 1035

Manwaring, S.R., & Wisler, D.C. 1992, Unsteady Aerodynamics and Gust Response in Compressors and Turbines, *ASME Paper* 92-GT-422

Mehmed, O. & Murthy, D.V., 1991, Experimental Investigation of Propfan Aeroelastic Response in Off-Axis Flow with Mistuning, *AIAA Journal of Propulsion and Power* 7 (1) 90-98

Meirovitch, L., 1980, Computational Methods in Structural Dynamics, *Sijthoff & Noordhoff*

Mikolajczak, A.A,, Arnoldi, R.A., Snyder, L.E., & Stargardter, H. 1975, Advances in Fan and Compressor Blade Flutter Analysis and Predictions, *AIAA Journal of Aircraft* **12**(4) 325

Namba, M. 1972, Lifting Surface Theory for a Rotating Subsonic or Transonic Blade Row, *A.R.C. R & M.* No. 3740

Namba, M., & Toshimitsu, K. 1993, Unsteady Aerodynamic Response of Two-Dimensional Subsonic and Supersonic Oscillating Cascades with Chordwise Displacement and Flexible Deformation, *Journal of Sound and Vibration* **162**(3) 503

Nagashima, T., & Whitehead, D.S. 1977, Linearized Supersonic Unsteady Flow in Cascades, *A.R.C. R & M.* No. 3811

Newland, D.E., 1989, Mechanical Vibration Analysis and Computation, *Longman Group UK Ltd.*

Ni, R.H., & Sisto, F. 1976, Numerical Computations of Nonstationary Aerodynamics of Flat Plate Cascades in Compressible Flow, *ASME Journal of Engineering for Gas Turbines and Power* **98** 165

Ni, R.H. 1981, A Multiple Grid Scheme for Solving the Euler Equations, *AIAA Paper* No. 81-1025

Obayashi, S., Guruswamy, G.P., & Goorjian, P.M. 1991, Streamwise Upwind Algorithm for Computing Unsteady Transonic Flows Past Oscillating Wings, *AIAA Journal* **29**(10) 1668

Peraire, J., Peiro, J., Morgan, K., Vahdati, M., & Molina, R.C., 1985, Hypersonic Flow Computations around Re-Entry Vehicles, *AGARD Paper from Conference Proceedings* 514

Pierzga, M.J. & Wood, J.R. 1985, Investigation of the Three-Dimensional Flow Field Within a Transonic Fan Rotor: Experiment and Analysis, *ASME Journal of Engineering for Gas Turbines and Power* **107** 436

Platzer, M.F. 1975, Transonic Blade Flutter: A Survey, *Shock and Vibration Digest* 7(7) 97-106

Platzer, M.F. 1977, Unsteady Flows in Turbomachines - A Review of Current Developments, *AGARD* -CP-227 Unsteady Aerodynamics

Platzer, M.F. 1978, Transonic Blade Flutter: A Survey of New Developments, *Shock and Vibration Digest* **10**(9) 11-20

Platzer, M.F. 1982, Transonic Blade Flutter: A Survey of New Developments, *Shock and Vibration Digest* **14**(7) 3-8

Rai, M. 1987, Unsteady 3D Navier-Stokes Simulations of Turbine Rotor-Stator Interaction, *AIAA Paper* 87-2038

Rao, J.S. 1977, Turbine Blading Excitation and Vibration, *The Shock and Vibration Digest* **9** 15

Rao, J.S. 1980, Turbomachine Blade Vibration, *The Shock and Vibration Digest* **12** 12

Rao, J.S. 1983a, Turbomachine Blade Vibration, *The Shock and Vibration Digest* **15** 3

Rao, J.S. 1983b, Free and Forced Vibrations of Turbine Blades, *ASME Vibrations of Blades and Bladed Disk Assembies* p.11

Rao, J.S. 1987, Turbomachine Blade Vibration, *The Shock and Vibration Digest* **19** 3

Rausch, R.D., Batina, J.T., & Yang, H.T.Y. 1990, Euler Flutter Analysis of Airfoils Using Unstructured Dynamic Meshes, *Journal of Aircraft* **27**(5) 436

Rizzetta, D.P. 1979, Time Dependent Response of a Two-Dimensional Airfoil in Transonic Flow, *AIAA Journal* **17**(1) 26

Robinson, B.A., Batina, J.T., & Yang, H.T.Y. 1991, Aeroelastic Analysis of Wings Using the Euler Eqution with a Deforming Mesh, *Journal of Aircraft* **28**(11) 781

Samolovich, G. 1967, Resonance Phenomena in Sub- and Supersonic Flow Through an Aerodynamic Cascade, *Mekhanika Zhidkosti Gaza* **2**(3) 143-144.

Sankar, N.L., & Tang, W. 1985, Numerical Solution of Unsteady Viscous Flow Past Rotor Sections, *AIAA Paper* 85-0129

Sankar, N.L., Wake, B.E., & Lekoudis, S.G. 1986, Solution of the Unsteady Euler Equations for Fixed and Rotor Wing Configurations, *Journal of Aircraft* **23**(4) 283

Sanliturk, K. Y, Imregun, M & Ewins, D. J. 1992, Statistical Analysis of Random Mistuning of Bladed Assemblies, *IMechE Proceedings of the 5th Int Conf. on Vibrations of Rot. Machinery*, Paper C432/110

Scalzo. A. J., Allen, J. M & Antos, R. J 1986, The Analysis and Solution of a Non-synchronous vibration Problem in the Last Row Turbine Blade of a Large Industrial Combustion Turbine, *ASME Paper* 86-GT-230

Scott, J.N., & Hankley, W.L. 1986, Navier-Stokes Solutions of Unsteady Flow in a Compressor Rotor, *Journal of Turbomachinery* **108** 206

Sharma, O.P., Pickett, G.F., & Ni, R.H. 1992, Assessment of Unsteady Flows in Turbines, *Journal of Turbomachinery* **114** 79

Shaw, L.M., Boldman, D.R., Buggele, A.E., & Buffum, D.H. 1986, Unsteady Pressure Measurements on a Biconvex Airfoil in a Transonic Oscillating Cascade, *Journal of Engineering for Gas Turbines and Power* **108** 53

Siden, L.D.G. 1991, Numerical Simulation of Unsteady Viscous Compressible Flows Applied to Blade Flutter Analysis, *ASME Paper* 91-GT-203

Sinha, A. 1986, Calculating the Statistics of Forced Response of a Mistuned Bladed Disk Assembly, *AIAA Journal* **20**(7) 1001-1008

Sisto, F. 1953, Stall Flutter in Cascades, *Journal of the Aeronautical Sciences* **20**(9) 598

Sisto, F. and Ni, R. 1972, Quasi-Static Moment Measurements for Airfoils in an Annular Cascade, *AAIA Journal of Aircraft* **9**(4) 298-305.

Sisto, F., Wu, W., Thangam, S., & Jonnavithulas, S. 1989, Computational Aerodynamics of Oscillating Cascades with the Evolution of Stall, *AIAA Journal* **27**(4) 462

Sisto, F., Thangam, S., & Abdel-Rahim, A. 1991, Computational Prediction of Stall Flutter in Cascaded Airfoils, *AIAA Journal* **29**(7) 1161

Smith, T.E., & Kadambi, J.R. 1991, The Effect of Steady Aerodynamic Loading on the Flutter Stability of Turbomachinery Blading, *ASME Paper* 91-GT-130

Snyder, L.E. & Commerford, G.L. 1974, Supersonic Unstalled Flutter in Fan Rotor: Analytical and Experimental Results, *ASME Paper* 74-GT-40

Srinivasan, A.V. (Ed.) 1976, Structural Dynamic Aspects of Bladed Disk Assemblies, *Proc. ASME Winter Annual Meeting, New York*

Srinivasan, A.V., & Fabunmi, J.A. 1984, Cascade Flutter Analysis of Cantilevered Blades, *Journal of Engineering for Gas Turbines and Power* **106** 34

Srinivasan, A.V., & Cutts, D.G. 1985, Aerodynamically Excited Vibrations of a Part-Span Shrouded Fan, *Journal of Engineering for Gas Turbines and Power* **107** 399

Srivastava, R., Sankar, L.N., Reddy, T.S.R., & Huff, D.L. 1991, Application of an Efficient Hybrid Scheme for Aeroelastic Analysis of Advanced Propellors, *Journal of Propulsion* 7(5) 767

Stark, V.J.E. 1984, General Equations of Motion for an Elastic Wing and Methods of Solution, *AIAA Journal* **22**(8) 1146

Stratizar, A.J. & Powell, A.J. 1985, Investigation of the Three-Dimensional Flow within a Transonic Fan Rotor: Experiment and Analysis, *ASME Journal of Engineering for Gas Turbines and Power* **107** 436-445

Su, J. 1992, Time Marching Integral Equation Method for Unsteady Transonic Flows Around Airfoils, *Int. Journal for Numerical Methods in Eng* **34** 455

Surampudi, S.P., & Adamczyk, J.J. 1986, Unsteady Transonic Flow over Cascade Blades, *AIAA Journal* 24(2) 293

Tadros, R.N., & Botman, M. 1981, Dynamic Response of Blades and Vanes to Wakes in Axial Turbomachinery, *ASME Paper* 81-DET-33

Takahara, S., Adachi, T., & Kadoya, Y. 1980, On the Numerical Analysis of Stall Flutter in Turbine Cascades, *Proceedings of the 2nd Int. Symp. on Aeroelasticity in Turbomachines*

Tanida, Y. and Okazaki, T. 1963, Stall Flutter in Cascade (Translatory Vibration of Cascade Blades as Treated by Semi-Actuator Disc Methods, Parts 1 & 2, *JSME* **6**(4) 744-758

Tatum, K.E., & Giles, G.L. 1988, Integrating Nonlinear Aerodynamic and Structural Analysis for a Complete Fighter Configuration, *Journal of Aircraft* **25**(12) 1150

Theodorsen, T. 1935, General Theory of Aerodynamic Instability and mechanism of Flutter, *NACA Report* 496

Thomas R.M. & Gladwell, I., 1988, Variable-Order Variable-Step Algorithms for Second-Order Systems Parts I&II, *International Journal for Numerical Methods in Engineering* **26** 39-80

Thomson, W.T., 1950, Matrix Solution for the Vibration of Non-Uniform Beams, *ASME Journal of Applied Mechanics,* pp337-339

Trépanier, J.Y., Reggio, M., Zhang, H., & Camarero, R. 1991, A Finite-Volume Method for the Euler Equations on Arbitary Lagrangian-Eulerian Grids, *Computers & Fluids* **20** 399

Tse, F.S., Morse, I.E., & Hinkle, R.T. 1978, Mechanical Vibrations - Theory and Applications, *Allyn and Bacon, second edition*

Turner M.G. & Jennions, I.K. 1992, An Investigationof Turbulence Modelling in Transonic Fans Including a Novel Implementation of an Implicit κ-ε Turbulence Model, *ASME Paper* 92-GT-308

Ueda, T., & Dowell, E.H. 1984, Flutter Analysis Using Nonlinear Aerodynamic Forces, *Journal of Aircraft* **21**(2) 101

Usab, W.J., & Verdon, J.M. 1986, On the Application of a Linearised Unsteady Potential-Flow Analysis to Fan-Tip Cascades, *Journal of Turbomachinery* **108** 59

Usab, W.J., & Verdon, J.M. 1991, Advances in the Numerical Analysis of Linearised Unsteady Cascade Flows, *Journal of Turbomachinery* **113** 633

Vahdati, M. and Imregun, M. 1994, Non-Linear Aeroelastic Analyses Using Unstructured Dynamic Meshes, *Proc of the 7th Int Symp. on Unsteady Aerodynamics and Aeroelasticity of Turbomachines, Fukuoka*

Venkatakrishnan, V., & Jameson, A. 1988, Computation of Unsteady Transonic Flows by Solution of the Euler Equations, *AIAA Journal* **26**(8) 974

Verdon, J. M. Analysis of Unsteady Supersonic Cascades, *ASME Papers* 77-GT-44 & 77-GT-45

Verdon, J.M. 1993, Review of Unsteady Aerodynamic Methods for Turbomachinery Aeroelastic and Aeroacoustic Applications, *AIAA Journal* **31**(2) 235

Verdon, J.M. & Caspar, J.R. 1984, A Linearized Unsteady Aerodynamic Analysis for Transonic Cascades, *Journal of Fluid Mechanics* **149** 403

Visbal, M.R., & Shang, J.S., J.M. 1989, Investigation of the Flow Structure Around a Rapidly Pitching Airfoil, *AIAA Journal* **27**(7) 1044

Wei, S. T. and Pierre, C. 1990, Statistical Analysis of the Forced Response of Mistuned Cyclic Assemblies, *AIAA Journal* **28**(5) 861-868

Whitehead, D. S. 1959, The Vibration of Cascade Blades Treated by Actuator Disk Methods, *Proc. IMechE* **173** 555

Whitehead, D.S. 1960, Force and Moment Coefficients for Vibrating Aerofoils in Cascade, *A.R.C., R & M.* No. 3254

Whitehead, D.S. 1966a, Bending Flutter of Unstalled Cascade Blades at Finite Deflection, *A.R.C. R & M.* No. 3429

Whitehead, D.S. 1966b, Torsional Flutter of Unstalled Cascade Blades at Zero Deflection, *A.R.C. R & M.* No. 3429

Whitehead, D.S. 1966c, Aerodynamic Aspects of Blade Vibration, Applied Mechanic Convention, *Proc IMechE* **180** Part 3I

Whitehead, D.S. 1970, Vibration and Sound Generation in a Cascade of Flat Plates in Subsonic Flow, *A.R.C. R & M.* No. 3865

Whitehead, D.S. 1990, A Finite Element Solution of Unsteady Two-Dimensional Flow in Cascades, *International Journal for Numerical Methods in Fluids* **10** 13

Williams, M.H., Cho, J., & Dalton, W.N. 1991, Unsteady Aerodynamic Analysis of Ducted Fans, *Journal of Propulsion* 7(5) 800

Wu, J., Kaza, K.R., & Sankar, L.N. 1987, A Technique for the Prediction of Airfoil Flutter Characteristics in Separated Flow, *AIAA Paper* 87-0910-CP

Yamamoto, K., & Tanida, Y. 1990, Self-Excited Oscillation of Transonic Flow Around an Airfoil in Two-Dimensional Channels, *Journal of Turbomachinery* **112** 723

Yamamoto, O., & August, R. 1992, Structural and Aerodynamic Analysis of a Large-Scale Advanced Propellor Blade, *Journal of Propulsion* **8**(2) 367

Yang, T.Y., Guruswamy, G.P., & Stritz, A.G. 1980, Flutter Analysis of a NACA 64A006 Airfoil in Small Disturbance Transonic Flow, *Journal of Aircraft* **17**(4) 225

Yang, T.Y., Guruswamy, G.P., & Stritz, A.G. 1982, Application of Transonic Codes to Flutter Analysis of Conventional and Supercritical Airfoils, *Journal of Aircraft* **19**(3) 211

Yang, T.Y., & Batina, J.T. 1983, Transonic Time-Response Analysis of 3-Degree-of-Freedom Conventional and Supercritical Airfoils, *Journal of Aircraft* **20**(8) 703

Yang, Z.C., & Zhao, L.C. 1988, Analysis of Limit Cycle Flutter of an Airfoil in Incompressible Flow, *Journal of Sound and Vibration* **123**(1) 1

Yiu, H., 1995, Vibration Characteristics of Mistuned Bladed Disc Assemblies, *PhD Thesis, Imperial College, University of London*

Zienkiewicz, O.C. and Taylor, R.L., 1989, The Finite Element Method Vol. 1&2, *Fourth Edition, McGraw-Hill Book Company*